Enzymes impliqués dans la production des formes réactives de l'oxygène dans les membranes plasmiques, les mitochrondries et les chloroplastes

Eiri Heyno



UNIVERSITÉ PARIS-SUD XI − FACULTÉ DES SCIENCES D'ORSAY

ECOLE DOCTORALE SCIENCES DU VÉGÉTAL

THÈSE

présentée pour obtenir le grade de
Docteur en Sciences de l'Université Paris Sud XI

Discipline : Biologie − Spécialité : Sciences du végétal

par

Eiri Heyno

Enzymes impliqués dans la production des formes réactives de l'oxygène dans les membranes plasmiques, les mitochondries et les chloroplastes

Production of reactive oxygen species
in plasma membranes, mitochondria and chloroplasts

Thèse soutenue le 9 décembre 2009 devant le jury composé de :

M. MICHEL DRON, Professeur, Orsay	(PRÉSIDENT)
M. CHRISTOPHE BAILLY, Professeur, UPMC, Paris	(RAPPORTEUR)
M. PAOLO TROST, Professeur, Università di Bologna	(RAPPORTEUR)
M. GERHARD LEUBNER, Professeur, Universität Freiburg	(EXAMINATEUR)
M. SÉBASTIEN THOMINE, Directeur de recherche, CNRS Gif sur Yvette	(EXAMINATEUR)
MME. ANJA LISZKAY, Chargée de recherche CNRS, CEA Saclay	(DIRECTRICE DE THÈSE)

Table of content

2. Results

Thank you to

First of all, I thank dr. Anja Krieger-Liszkay, my supervisor, for getting me in France, taking care of all kinds of official and unofficial things that encounter a PhD student. I have learned a lot of science and how it all turns over at the bench and with people in general. I couldn't have had a better supervisor.

Next I would like to thank dr. Sun Un who has tried hard to keep me on the main road, not getting too much lost in the millions of side paths, but focusing on the light at the end of the tunnel. It wasn't a truck after all.

I am grateful for Prof. Peter Schopfer for stimulating discussions and correspondance during the thesis. I thank also the group of Prof. Peter Beyer, dr. Susanne Bolte, dr. Éva Hideg, dr. Winfried Leibl, dr. Bill Rutherford and dr. Sébastien Thomine for discussions, revisions and teaching me new methods.

I am grateful to all my old friends and the ones I made during the thesis, for sharing the highs, the lows and the everyday. I think you recognise yourselves here without me listing all the names... A special thanks to my house mates and fellow doctorantes Agnès and Clémence. It can all be concentrated to this small remark made at the breakfast table on a very cold November morning, 2008 (06.57 a.m.): "We are dependent of our experiments".

Merci MICHEL DRON, for arranging me the grant and always being so encouraging. Merci Maryelle Fradin for keeping me up to date about all the running things, deadlines, courses etc. I also would like to thank the administration in CEA, which has made things run smoothly.

There are so many people involved in this thesis, I haven't forgotten you although you might not be mentioned here.

Last but not least I thank my mother for endless support, conversation and supply of black bread and sweets.

1. Introduction

Formation of reactive oxygen species in biological systems

Formation of reactive oxygen species (ROS) is unavoidable in life in the present oxygen-rich environment. All cellular organisms derive energy from electron transfer reactions in photosynthetic and/or respiratory membranes which are susceptible to leakage of electrons to O_2. O_2 can be reduced to several forms of ROS, some of which are very reactive towards cellular compounds. ROS play a dual role in life. On one hand, ROS are deleterious compounds which, when produced uncontrolled, lead to the oxidation of proteins and DNA, and consequently to mutations, and to lipid peroxidation (Fridovich, 1978). On the other hand there are enzymes deliberately producing ROS, such as the plasma membrane NADPH oxidase (Morel et al. 1991). Now it is considered that ROS, unavoidably or deliberately produced, are necessary molecules in many cellular responses and that it is crucial to have a balance between ROS-producing and detoxifying reactions in the cell (Mittler et al., 2004).

What are reactive oxygen species?

The term reactive oxygen species is very wide and comprises both radical and non-radical forms of oxygen which are formed in the course of the reduction of O_2 to H_2O. Hypochlorous acid (OHCl) and peroxynitrite ($ONOO^-$) are also called ROS, as well as singlet oxygen ($^1O_2$) and ozone (O_3). In this work the species resulting from the reduction of O_2 are discussed. Superoxide ($O_2^{\bullet-}$) is formed when O_2 receives one electron (Eq 1.). $O_2^{\bullet-}$ gets rapidly protonated to $HO_2^{\bullet}$ at acidic pH (pK=4.8) which leads to its spontaneous dismutation to hydrogen peroxide (H_2O_2) and O_2 (Eq 2.). SOD catalyses this reaction making it efficient also at higher pH. There are several enzymes that produce H_2O_2 as a side product, such as amine oxidases and the glycolate oxidase (Cona et al., 2006; Buchanan et al., 2000). Neither $O_2^{\bullet-}$ nor H_2O_2 are very reactive towards cellular components, but they facilitate the formation of the extremely reactive hydroxyl radical ($^{\bullet}OH$). $^{\bullet}OH$ can be formed from H_2O_2 in the presence of reduced transition metals like Fe^{2+} or Cu^+, which is also called the Fenton reaction (Eq. 3.). In the Fenton reaction the transition metal is oxidised. Re-reduction of the transition metal can be achieved by $O_2^{\bullet-}$ or ascorbate (Eq. 4.).

$$O_2 + e^- \rightarrow O_2^{\bullet-} \qquad \text{Eq. 1.}$$

$$2O_2^{\bullet-} + 2H^+ \rightarrow H_2O_2 + O_2 \qquad \text{Eq. 2.}$$

$$H_2O_2 + Fe^{2+}/Cu^+ \rightarrow {}^{\bullet}OH + {}^{-}OH + Fe^{3+}/Cu^{2+} \qquad \text{Eq. 3.}$$

$$Fe^{3+}/Cu^{2+} + O_2^{\bullet-}/\text{ascorbate} \rightarrow Fe^{2+}/Cu^+ + O_2/\text{ascorbate}^{\bullet} \qquad \text{Eq.4.}$$

The coupled reaction of equations 3. and 4. is called the iron-catalysed Haber-Weiss reaction in which the re-reduction of the transition metal by ascorbate or $O_2^{\bullet-}$ facilitates a sustained generation of $^{\bullet}OH$.

Because $^{\bullet}OH$ is so destructive, its formation is avoided by limiting the amounts of its precursors through the action of antioxidative enzymes, such as superoxide dismutase (SOD), catalase and peroxidases. Antioxidative enzymes are so efficient that direct 1- and 2-electron reactions producing $O_2^{\bullet-}$ and H_2O_2 are not harmful in normal metabolism.

1.1 ROS production in the plasma membrane.

The plasma membrane (PM) is the outermost membrane of the cell and separates the cytoplasm from the environment. It controls the traffic of ions and other solutes in and out of the cell, senses the exterior, starts signalling cascades in response to environmental stimuli, catalyses the formation and deposit of cellulose to the cell wall etc.. Biochemical studies on plant PMs have revealed several redox enzymes which are involved in reduction of nitrate, iron, iron chelates, monodehydroascorbate, quinones and oxygen (reviewed by Bérczi and Møller, 2000; Lüthje, 2008). The identities of the latter activities are presently not well understood.

PMs contain both NADH- and NADPH-dependent $O_2^{\bullet-}$-producing activities but the molecular identity of these activities have remained unsolved. From a genetic point of view, a mammalian phagocyte-type NADPH oxidase (NOX) is known to be present. An NADPH-dependent $O_2^{\bullet-}$-producing enzyme was purified from bean PMs which contained an FMN (Van Gestelen et al., 1997; 1998). However, no cytochrome b, characteristic for the NOX, was detected in by these authors. Yet NOXs have been detected in the PMs by antibodies that were raised against peptides of plant NOX sequences (Keller et al., 1996; Sagi and Fluhr, 2001) and GFP-tagged NOX proteins were shown to be localised in the PM (Kobayashi et al., 2007). The isolation and biochemical characterisation of the plant NOX is yet to be accomplished.

Other enzymes, such as quinone reductases (QRs) and peroxidases (PRXs), may also participate in PM $O_2^{\bullet-}$ production. QRs are found in PMs and their activity is often followed via reduction of tetrazolium dyes and cytochrome c, both of are reduced by $O_2^{\bullet-}$. However, the mechanism of $O_2^{\bullet-}$ by QRs has not been studied further. PRXs can produce ROS in addition to their reactions reducing H_2O_2 to H_2O (the mechanisms are presented in detail in chapter 1.1.3). Therefore, they may also take part in PM ROS production. In the following subchapters ROS-producing activities in the PM are introduced giving special focus on the NOX and QR. Last, PRXs are presented and and their participation in cell wall modifications.

1.1.1 NADPH oxidases (NOXs)

NOXs are PM enzymes which reduce extracellular O_2 to $O_2^{\bullet-}$ using cytosolic NADPH as the source of electrons. They were first discovered in mammalian phagocytes which are responsible for killing and digesting invading pathogens. In 1932 Baldridge and Gerard reported an increased oxygen uptake during phagocytosis, now known as the respiratory burst. The mitochondrion was ruled out as the compartment responsible for the respiratory burst and the pentosephosphate pathway was shown to be the source of energy for the burst (Sbarra and Karnovsky, 1959). At the end of the 60ies it was clear that H_2O_2 is produced by phagocytes in response to pathogens and that the myeloperoxidases of the phagocytes are important in killing the invading pathogens (Paul et al., 1970, and the references therein). $O_2^{\bullet-}$ generation by the phagocytes was shown by Babior et al. (1973). The NOX was discovered in the next decade. Phagocytes from X-linked chronic granulomatous disease (CGD) patients were found to lack a cytochrome b distinct from mitochondrial cytochromes (Segal, 1983), the mutated gene in X-linked CGD was found (Royer-Pokora 1986) and shown to encode one subunit of the NADPH oxidase complex (Teahan et al., 1987; Dinauer et al. 1987). Today this subunit is called the catalytic subunit $gp91^{phox}$/Nox2 for its glycosylated molecular weight of 91 kDa (unglycosylated mw is 65 kDa). NOXs are present in vast majority of eukaryotes. Because of the importance of the phagocytic NOX2 in human health, it is the most studied enzyme of the NOX family. There are seven different NOX systems in animals which are encoded in different tissues and have different roles in physiology. Some of them have additional motifs in the catalytic subunit (NOX5 and DUOX1-2) and others additional subunits (NOXs 1-4) (Sumimoto, 2008).

In plants respiratory burst in response to pathogens was first reported by Doke (1983). Genes encoding NOXs were found in the 90ies. In *Arabidopsis thaliana* 10 genes encode NOXs (Torres and Dangl, 2005) and they were named respiratory burst oxidase homologs (*AtrbohA-J*). Rboh genes show approximately 30 % identity with the catalytic subunit $gp91^{phox}$ of human phagocyte NOX (Groom et al., 1996; Keller et al., 1998; Torres et al., 1998).

1.1.1.1 Structure and reaction mechanism of NOX

NOXs are intrinsic membrane proteins with six transmembrane α-helices containing two completely conserved pairs of His residues involved in heme binding and binding sites for NADPH and a flavin in the cytosolic C-terminus (Fig. 1.1). The first heme is thought to be coordinated near the flavin (lower heme) and the second heme near the extracellular side (upper heme) based on models from the $gp91^{phox}$ (Cross and Segal, 2004; Sumimoto, 2008). The sequences of *Rboh* genes predict proteins of about 100 kDa because of the additional two N-

terminal Ca^{2+}-binding EF hands which are not present in the $gp91^{phox}$ (Torres and Dangl, 2005). In mammalian NOX5 there are also four EF-hands in the N-terminus, and the mammalian DUOX1 and 2 contain two cytosolic EF-hands, an extra α-helix and an extracellular peroxidase motif (Fig. 1.1). The phagocytic NOX2 is a multisubunit enzyme containing the membrane proteins $gp91^{phox}$ and $p22^{phox}$ and four cytosolic subunits $p47^{phox}$, $p67^{phox}$, $p40^{phox}$ and a Rac GTPase (Sumimoto, 2008). Of these, only the cytosolic GTPases are involved in the regulation of plant NOXs while the other subunits are not found in plant genomes (Tenhaken and Rübel, 1999).

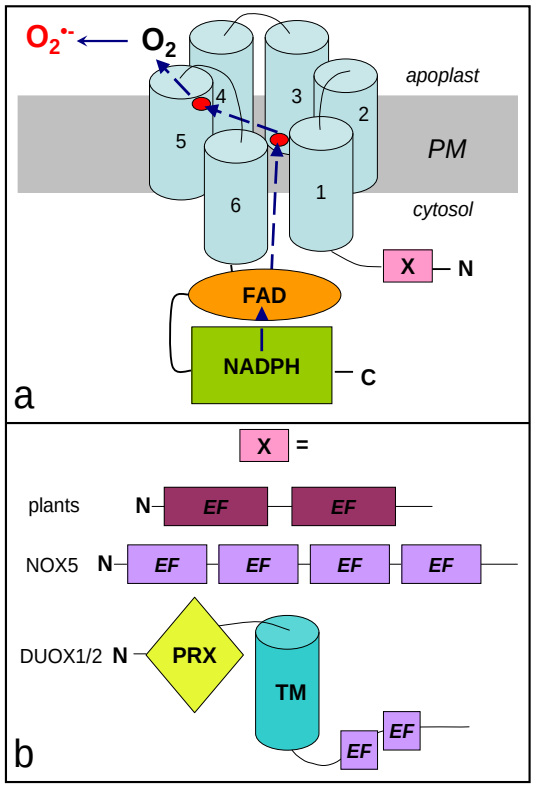

Figure 1.1 Structure of the NADPH oxidase. a) Predicted domains of the catalytic subunit of the NOX proteins. Binding sites for NADPH and FAD are cytosolic, the two hemes are coordinated in the histidine residues of two membrane-spanning α-helices (no°s 3 and 5). The transfer of electrons from NADPH to O_2 is depicted by blue dashed arrows. b) Additional motifs (X) is present in some NOXs. This motif can include cytosolic Ca^{2+}-binding EF-hands or an extra α-helix fused to an extracellular peroxidase.

A single turnover of the phagocytic NOX involves several electron transfer steps. In the first step two electrons from NADPH are transferred to the flavin to form $FADH_2$. Subsequently the lower heme is reduced, followed by the reduction of the upper heme and, finally, the reduction of O_2. There are two models suggesting either one or two $gp91^{phox}$ units involved in a turnover (Cross and Segal, 2004; Vignais, 2002). O_2 is required to facilitate rapid turnover of the NOX since in anaerobic conditions the reduction rate of the flavin and the hemes is one order of magnitude lower than in aerobic condition. A reason for this might be the unusual midpoint potentials of the two hemes, the E_m of the lower heme being -225 mV and that of the higher heme -265 mV. In this situation O_2 is able to act as an electron acceptor (E_m $O_2/O_2^{\bullet-}$ = -160 mV). The cytosolic subunits have been shown necessary to allow full activity of the phagocytic enzyme (Morel et al., 1991).

1.1.1.2 Biological functions of and regulation of plant NOXs

The ten *Atrboh* genes are expressed differentially, some throughout the plant body but some tissue-specifically, suggesting multiple roles for NOXs in plant life (Sagi and Fluhr, 2006). Many functions of plant NOXs have been revealed by using knock-out mutants, plant-

pathogen interactions being the most studied phenomenon. Plant response to pathogen challenge is characterized by two successive ROS bursts (Lamb and Dixon, 1997) and different Rbohs are needed for each burst (Yoshioka et al, 2003; Kobayashi et al., 2007). AtrbohD and F are both involved in pathogen defence, but their roles are different and depend on the invading pathogen species (Torres et al., 2002; 2005). NOXs role in defense is, in addition to the production of antimicrobicidal ROS, involved in complex signaling networks. These include the stress hormones salicylic acid and jasmonic acid that regulate the hypersensitive response (Torres and Dangl., 2005). NOX activity is regulated by phosphorylation (Benschop et al., 2007; Kobayashi et al., 2007, Nühse et al., 2007), GTPases and Calcium (Torres and Dangl., 2005; Sagi and Fluhr, 2006)

AtrbohD- and F-derived H_2O_2 is important in stomatal closure (Kwak et al., 2003). H_2O_2 is produced down-stream of ABA-signal transduction which is mediated by kinases (Mustilli et al., 2002; Sirichandra et al., 2009). AtrbohD- and F-derived H_2O_2 is required for NO accumulation mediating the stomatal closure (Bright et al., 2006). These two NOXs are also involved in ABA-regulated inhibition of seed germination (Kwak et al., 2003). AtrbohB was shown to be obligatory for seed after-ripening (Müller et al., 2009).

AtrbohC is involved in root hair development (Foreman et al., 2003) and AtrbohI and J are involved in pollen tube growth (Potocký et al., 2007). The polarized growth of these cell types is brought about by oscillations in Ca^{2+} concentrations, pH and ROS (Cárdenas, 2009).

PM $O_2^{\bullet-}$ production is involved in the ROS-mediated cell wall modification. This leads to either growth (loosening of the cell wall) or arrest of growth (stiffening of the cell wall). NOXs, or PM ROS production, are involved in the growth of roots of *A. thaliana* (Renew et al., 2005), maize shoots (Liszkay et al., 2003; Dunand et al., 2007) and maize leaves (Rodríguez et al., 2002). Conversely ROS is also involved in lignification of cell wall in the stems of *Zinnia elegans* (Barcelo, 2005) and cell cultures if *Picea abis* (Kärkönen et al., 2009).

1.1.2 Quinone reductases (QRs)

QRs catalyse the reduction of quinones to quinoles by using NAD(P)H as electron donor. A QR was first discovered by Ernster and Navazio (1958) in the soluble cytoplasmic fraction from animal tissues and it was named DT-diaphorase and later vitamin K reductase (Maerki and Martius, 1961). Now it is known that QRs reduce several kinds of ring-containing substrates, including quinones, nitro-aromatic compounds, chromate and ferric iron (Deller et al., 2008).

The first characterization of cytosolic QRs in plants was performed by Spitsberg and Coscia in 1982. Subsequently more QRs were found in several plant species both in the

cytosolic fraction (Sparla et al., 1996; 1998; 1999; Trost et al., 1995) and in plasma membrane (Guerrini et al., 1987; Luster and Buckhout, 1989; Pupillo et al., 1986; Serrano et al., 1994; Schopfer et al., 2008 [this work]).

1.1.2.1 Structure and reaction mechanism of quinone reductases

The structure and reaction mechanisms of animal, bacterial and yeast QRs is known in detail (Deller et al., 2008). QRs have a similar structure to bacterial flavodoxins, which is also called the flavodoxin fold. It contains a twisted central cluster of β-parallel sheets surrounded by α helices (Fig. 1.2). The flavin cofactor is FAD in mammals, FMN in plants and fungi, and either or in bacteria. The flavin is non-covalently bound. Bacterial flavodoxins are monomers, human quinone reductase, QR1, is a dimer, some bacterial and all the plant quinone reductases reported so far are tetramers (Deller et al., 2008). The size of the monomer varies between 18-30 kDa. Crystal structures obtained from bacterial and mammalian QRs suggest that each subunit is an independent catalytic subunit (Andrade et al., 2007; Li et al., 1995). QRs are clearly soluble enzymes but seem to have an affinity to membranes (Carey et al., 2007; Jonas et al., 2006).

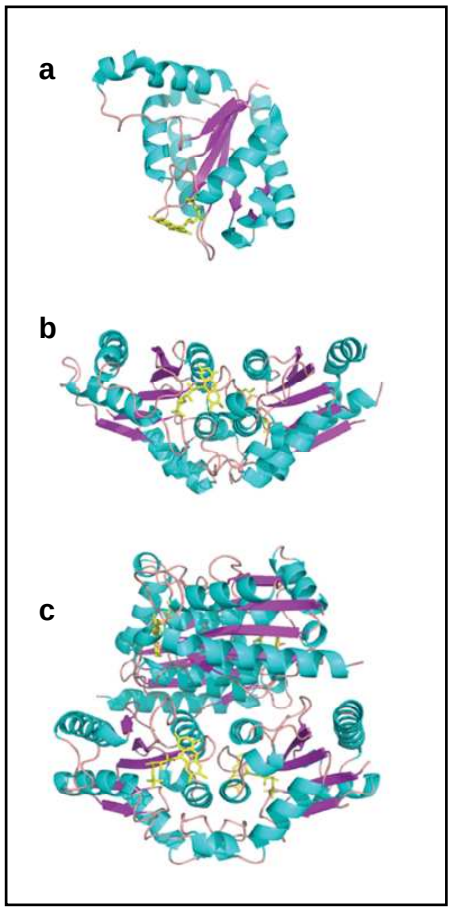

Figure 1.2 Structure of quinone reductases. a) *E. coli* flavodoxin b) Lot6p from S. cerevisiae. C) YhdA from *B. subtilis*. QR1 and Lot6p form dimers in solution whereas YhdA is a tetramer. The α helices are shown in blue and the β-sheets in purple. The flavin cofactor is shown in yellow. Figures are from Deller et al., (2008).

All the described QRs of the flavodoxin family have a characteristic ping-pong reaction mechanism (Sollner et al., 2008). First NAD(P)H binds to the active site and the subsequent transfer of a hydride ion to the flavin forms a dihydroflavin. After $NAD(P)^+$ has left the active site, the quinone binds to the same site and receives in a single step the hydride ion, and a proton originating from water, and leaves the site as quinol. No flavin semiquinone species have been detected in this reaction (Iyanagi and Yamazaki, 1970). Therefore, quinone reductases are considered as enzymes catalysing obligatory two-electron reactions.

1.1.2.2 Biological functions of QRs

QRs are involved in many aspects of physiology. In animals QRs function as vitamin K reductases involved in blood clotting reactions (Gong et al., 2008). Both in plants and animals they are conscidered as PM electron transfer enzymes (Döring and Lüthje, 1996; Morré, 2004).

QRs seem to be involved both in antioxidative and prooxidative reactions. Quinols produced by QRs can be removed from the active quinone pool by conjugation to glucuronic acid or sulphate (Shangari et al., 2005). Also a futile redox cycling of quinones by a QR and a quinol monooxygenase was reported in *E. coli* (Adams and Jia, 2004; 2006). These reactions are important because quinones can be reduced also to the semiquinone radical form which reacts readily with O_2 forming ROS (Iyanaki and Yamazaki, 1969). A fungal QR functions in the detoxification of quinones derived from fungal break-down of lignin (Brock et al., 2005; Brock and Gold, 1996). Mammalian and bacterial QRs metabolise a number of toxic compounds such as benzene and azodyes, (Smith, 1999; Deller et al., 2008). However, it has been reported that both plant and animal QRs produce $O_2^{\bullet-}$ in reactions involving NAD(P)H and quinones (Ernster et al., 1962; Spitsberg and Coscia, 1982).

In plants QRs are up-regulated in response to salt-stress and pathogens (Nohzadeh Malakshah et al., 2007; Jiang et al., 2007; Greenshields et al., 2005). The exact role and mode of action of QRs in these responses is not known. Additionally, the FQR1 is encoded by an early auxin-responsive gene (Laskowski et al., 2002) which links QRs to hormone signalling.

1.1.3 Peroxidases

There is evidence on low abundancies of PM-bound PRXs (Mika and Lüthje, 2003; Mika et al., 2008). Microscopic analysis of plant tissues show PRXs mainly in the cell wall (Passardi et al., 2006) and intracellular sites such as vacuoles (Hall and Sexton., 1972).

PRXs are a large class of enzymes comprising both highly substrate-selective and non-specific members. The substrate-specific PRX (class I PRXs e.g. ascorbate and glutathione PRX) reduce H_2O_2 to H_2O and are considered as antioxidative enzymes. The non-specific PRXs (class III PRXs) are present only in plants and are secreted to the cell wall. They catalyse the reduction of H_2O_2 by acceptiong electrons from a wide range of phenolic substrates (SH_2). This reaction has three steps as depicted in the following equations:

$$\text{PRX } [Fe^{3+}] + H_2O_2 \rightarrow \text{compound I } [Fe^{4+} = O \cdots por^{\bullet+}] + H_2O$$

$$\text{compound I} + SH_2 \rightarrow SH^{\bullet} + \text{compound II } [Fe^{4+} = O \cdots por]$$

$$\text{compound II} + SH_2 \rightarrow SH^{\bullet} + \text{PRX}\,[Fe^{3+}] + H_2O$$

The initial electrons to reduce H_2O_2 originate from the heme iron and the porphyrin ring. The arising end products ($SH^{\bullet}$) are radicals and may react with each other to start polymerization reactions, as is the case with phenolic substrates targeted to lignin and suberin biosynthesis (Halliwell and Gutteridge, 2006). Also NADH serves as a PRX substrate to form $NAD^{\bullet}$ which reacts readily with O_2 to form $O_2^{\bullet-}$. $O_2^{\bullet-}$ can combine with the PRX heme iron converting it into the labile perferryl form (Fe^{2+}-O_2/Fe^{3+}-$O_2^{\bullet-}$), also designated as Compound III. This form is able to catalyse a reaction resembling the Fenton reaction (Chen and Schopfer, 1999):

$$\text{Compound III} + H_2O_2 \rightarrow \text{PRX} + O_2 + {}^{\bullet}OH + {}^{-}OH$$

There is evidence that $^{\bullet}$OH plays an important role in cell extension by attacking and breaking the load-bearing bonds in the cell wall. Characteristic xyloglucan fingerprints are detected in cell walls where $^{\bullet}$OH was formed chemically (Miller and Fry, 2001, Schopfer, 2001) and in cell walls of ripening fruit (Fry et al., 2001) and elongating seedlings (Müller et al., 2009). $^{\bullet}$OH can be formed in the cell wall by the PRX-mediated Fenton reaction.

1.1.4 Objectives of the PhD thesis with respect to ROS production in the plasma membrane

In this thesis the identities and biochemistry of PM ROS-producing enzymes were studied with the help of specific inhibitors. Different spectroscopic methods were used for detecting different forms of ROS. The following following studies were performed:

- NADPH-binding enzymes in PMs were isolated by chromatographic methods and a $O_2^{\bullet-}$-producing QR was identified (chapter 2.1).
- QR knock-out insertion lines of *A. thaliana* were characterised to reveal the biological role of QRs in plants (chapter 2.4)
- Cadmium was tested as a potential inhibitor of the NOX activity (chapter 2.2).
- Regulation of the NOX by $O_2^{\bullet-}$ (end-product inhibition) and phosphorylation was studied in isolated PMs (chapter 2.3)

1.2 ROS formation in mitochondria

The mitochondrion is the energy factory of the cell. In its soluble matrix reside the Krebs cycle enzymes (also called citric acid or tricarboxylic acid cycle) by which pyruvate and

a number of other organic acids are oxidised and decarboxylated to form NADH, $FADH_2$ in and CO_2. The respiratory electron transfer chain is composed of four respiratory complexes and an ATP synthase. Figure 1.3. shows a simplified respiratory electron transfer chain that oxidises NADH and succinate.

In mitochondria most ROS formation occurs at the level of respiratory complex I (NADH: ubiquinone oxidoreductase) and complex III. $O_2^{\bullet-}$ can be formed at the FMN site or the quinone-binding site of the complex I via reverse electron transport from ubiquinol. Alternatively, a high NADH/NAD^+ ratio can lead to $O_2^{\bullet-}$ production at the FMN site (Murphy, 2009). Complex III can be partially inhibited by the fungal toxin antimycin A (AA) which leads to the stabilization of the semiquinone radical in the bifurcated reaction cycle and subsequently to $O_2^{\bullet-}$ generation (Slater, 1973; Cape et al., 2007, Zhang et al., 2007). There is evidence that certain metals, such as Zn^{2+} and Cd^{2+} bind to complex III between heme b_{low} and $cytc_1$ (Link and von Jagow, 1995) having a similar effect as AA in mammalian mitochondria (Wang et al., 2004).

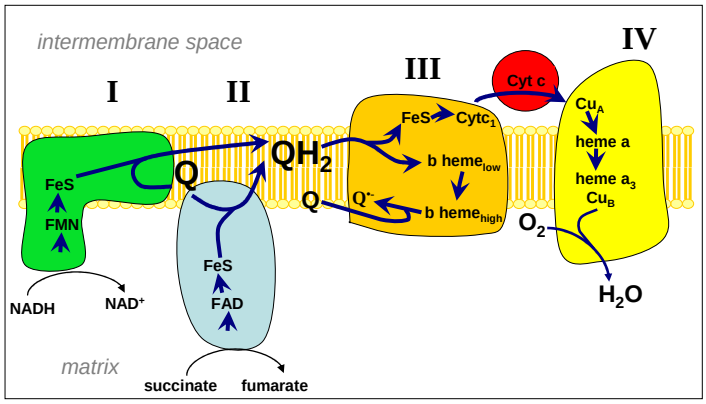

Figure 1.3. Respiratory electron transfer chain in the mitochondrion. The first two complexes transfer electrons to the ubiquinone pool in the membrane. Complex I, the NADH:ubiquinone oxidoreductase, passes electrons from NADH via FMN and 8-10 FeS clusters, at the last of which ubiquinone is reduced to QH_2. Complex II, the succinate:ubiquinone oxidoreductase, passes electrons from succinate via FAD and three FeS clusters reducing ubiquinone to QH_2. QH_2 diffuses from the complexes to the membrane and further to complex III, the cytochrome bc_1, which passes the electrons on by the bifurcated reaction. One e^- is passed via the FeS cluster and cyt_f to the soluble cyt c, which donates the electrons to complex IV, the cytochrome oxidase. The other e^- is passed on via two hemes to a quinone, which binds at a specific site, forming a semiquinone. A second bifurcated reaction passes again one e^- to the cyt c and one e^- to the semiquinone forming a QH_2 (not shown), which enters the ubiquinone pool. Complex IV passes the electrons via two copper ions (Cu_A), heme a and a CuFe center (heme a3 and Cu_B) to O_2 forming 2 H_2O after the transfer of four electrons. Protons are transported by complexes I, II and IV to the intermembrane space creating a proton gradient that is used in and ATP synthesis (not shown).

1.2.1 Objectives of the PhD thesis with respect to ROS production in mitochondria

In this thesis the toxicity of Cd^{2+} was investigated with respect to its potential inhibition of the PM NOX (chapter 2.2). As Cd^{2+} generally increases cellular ROS production (Schützendübel and Polle, 2002), it was investigated if Cd^{2+} leads to increased ROS production

also in plant mitochondria and if the increased ROS production in response to Cd^{2+} *in vivo* can be explained by this source.

1.3 ROS formation in chloroplasts

In photosynthesis the energy from light-driven reactions is used to assimilate CO_2 (dark reactions). In this work some aspects of the light reactions leading to ROS production are addressed. Figure 1.4. shows a simplified scheme of the electron transfer reactions of the two photosystems, PSII and PSI, the cytochrome b_6f complex ($cytb_6f$) and plastocyanin in the thylakoid membranes residing in the chloroplast. Under high light conditions, more light energy is captured by the photosystems than can be used by the sinks of reducing power, the Calvin cycle and nitrate reduction. This leads to over-reduction of the NADP pool and the plastoquinone pool. If the plastoquinone pool is completely reduced, the lack of an acceptor in the secondary quinone (Q_B) site will prevent the forward electron transport from Q_A to Q_B leading to the charge recombination reaction of the primary pair (P_{680}^+ $Pheo^-$). $^1O_2$ can be generated via the triplet chlorophyll ($^3P_{680}$) formed in the charge recombination reaction (Krieger-Liszkay et al. 2008). Over-reduction of the NADP pool is caused by the limitations in CO_2 assimilation or other sinks of NADPH and leads to the use of O_2 as an alternative electron acceptor at the acceptor side of PSI. This reaction produces $O_2^{\bullet-}$ (Badger et al., 2000). Also other sites of ROS production, although less pronounced, have been found in the electron transfer chain, e.g. PSII (Pospíšil, 2009),

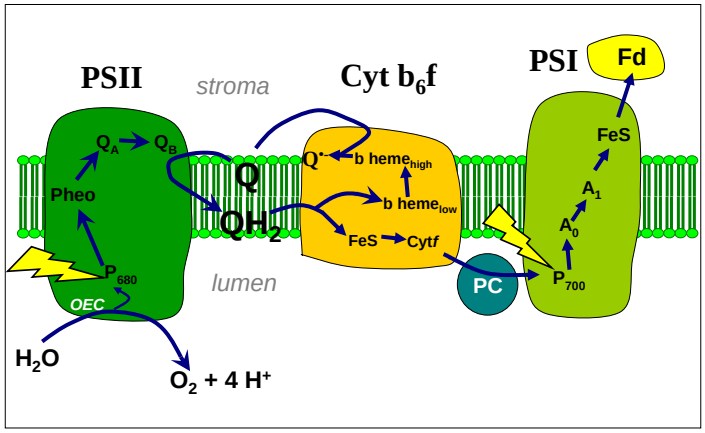

Figure 1.4. Photosynthetic electron transfer chain. The central chlorophyll of PSII (P_{680}) is excited by light. Charge separation takes place and the pheophytin (Pheo) is reduced. Next the electron is passed on via a bound quinone (Q_A) to a loosely bound quinone Q_B which, after accepting two electrons, leaves PSII and diffuses to the plastoquinone pool. Electrons which reduce the P_{680}^+ are derived from H_2O, catalysed by the oxygen evolving complex (OEC) of PSII. The electrons of the QH_2 are passed on by the bifurcated reaction of the $cytb_6f$ complex. One e^- reduces the FeS cluster and cyt_f and finally the soluble plastocyanin, which donates the electrons to PSI. The other e^- is passed on via two hemes to a quinone, which binds at a specific site, forming a semiquinone. A second bifurcated reaction passes again one e^- to the plastocyanin and one e- to the semiquinone forming a QH_2 (not shown), which enters the plastoquinone pool. The central chlorophyll of PSI (P700) is excited by light. Charge separation takes place and the following acceptors are subsequently reduced: A chlorophyll molecule (A_0), then a VitK (A_1), and finally the electron is passed through a series of FeS clusters to the soluble ferredoxin (Fd). From Fd finally $NADP^+$ is reduced via the ferredoxin-$NADP^+$-reductase (not shown). The water splitting and the cyt b_6f transporting protons from the stroma to the thylakoid lumen create a proton gradient that is used in ATP synthesis (not shown).

plastosemiquinones in the thylakoid membranes (Ivanov et al., 2007) and the $cytb_6f$ complex (Suh et al., 2000). Plants can adjust the amount of incoming exitation energy by several means such as tuning the ratio of PSII and PSI exitation and/or energy dissipation processes in the light-harvesting antenna. Excess energy can also be dissipated to heat (Horton et al., 1996) or used to run the water-water cycle (Asada, 1999) and photorespiration (Kozaki and Takeba, 1996). The water-water cycle and photorespiration involve the production of ROS followed by its detoxification by the antioxidative enzymes of chloroplast and peroxisomes, respectively. It can thus be seen that protection of the photosynthetic machinery can be brought about via ROS when an efficient antioxidant system is at hand.

PTOX is a plastoquinol:oxygen oxidoreductase located in the stromal lamellae and is thought to produce H_2O by the oxidation of two plastoquinol molecules (Carol and Kunz, 2001). This is interpreted as an adjustive mechanism that keeps the quinone pool relatively oxidised. The proposed role for PTOX is controversial in many aspects. Evidence against the protective role was provided by Rosso et al. (2006) who observed no difference in the oxidation state of the plastoquinone pool in the WT and PTOX knock-out lines or PTOX-overexpressing *A. thaliana*, respectively. Yet PTOX is up-regulated in response to abiotic stresses (Streb et al., 2005; Díaz et al., 2007; Stepien et al., 2008).

1.3.1 Objectives of the PhD thesis with respect to ROS production in the chloroplast

Given that the mechanism of O_2 reduction by PTOX is not known and that is has been proposed to produce $O_2^{\bullet -}$ in a side reaction (Affourtit et al., 2002), it was investigated whether PTOX produces ROS (chapter 2.5). Additionally its role as a photoprotective enzyme in low and high light stress was clarified.

2.Results

2.1. Naphthoquinone-dependent generation of superoxide radicals by quinone reductase isolated from the plasma membrane of soybean

Manuscript presented with publishers permission

Naphthoquinone-Dependent Generation of Superoxide Radicals by Quinone Reductase Isolated from the Plasma Membrane of Soybean[W]

Peter Schopfer, Eiri Heyno, Friedel Drepper, and Anja Krieger-Liszkay*

Universität Freiburg, Institut für Biologie II, D–79104 Freiburg, Germany (P.S., F.D.); and Commissariat à l'Energie Atomique, Institut de Biologie et Technologies de Saclay, CNRS Unité de Recherche Associée 2096, Service de Bioénergétique Biologie Structurale et Mécanisme, F–91191 Gif-sur-Yvette cedex, France (E.H., A.K.-L.)

Using a tetrazolium-based assay, a NAD(P)H oxidoreductase was purified from plasma membranes prepared from soybean (*Glycine max*) hypocotyls. The enzyme, a tetramer of 85 kD, produces $O_2^{\cdot-}$ by a reaction that depended on menadione or several other 1,4-naphthoquinones, in apparent agreement with a classification as a one-electron-transferring flavoenzyme producing semiquinone radicals. However, the enzyme displayed catalytic and molecular properties of obligatory two-electron-transferring quinone reductases of the DT-diaphorase type, including insensitivity to inhibition by diphenyleneiodonium. This apparent discrepancy was clarified by investigating the pH-dependent reactivity of menadionehydroquinone toward O_2 and identifying the protein by mass spectrometry and immunological techniques. The enzyme turned out to be a classical NAD(P)H:quinone-acceptor oxidoreductase (EC 1.6.5.2, formerly 1.6.99.2) that reduces menadione to menadionehydroquinone and subsequently undergoes autoxidation at pH $\geq$ 6.5. Autoxidation involves the production of the semiquinone as an intermediate, creating the conditions for one-electron reduction of O_2. The possible function of this enzyme in the generation of $O_2^{\cdot-}$ and H_2O_2 at the plasma membrane of plants in vivo is discussed.

The plasma membrane of plant cells displays transmembrane electron transport from cytoplasmic NAD(P)H to various external electron acceptors, which is accompanied by depolarization of the membrane potential and secretion of H^+ into the apoplast (Bérczi and Møller, 2000; Vuletić et al., 2005; Lüthje, 2007). Peculiar properties of this redox system, which can be demonstrated in right-side-out plasma membrane vesicles (Menckhoff and Lüthje, 2004), are as follows: (1) use of both NADH and NADPH as electron donors; (2) use of artificial substrates such as ferricyanide (FeCN), dichlorophenoleindophenole (DCPIP), or quinones as electron acceptors; and (3) insensitivity to KCN. The molecular composition and biochemical function of this so-called ''standard system'' (Bienfait and Lüttge, 1988) found in monocotyledonous and dicotyledonous plants are not well understood at present, despite numerous attempts to isolate and characterize potentially related enzyme activities from solubilized plasma membranes. The artificial electron acceptors generally used for assaying these activities provide no hints to the natural electron transfer reaction catalyzed by this system in the plasma membrane in vivo. The various operationally defined names coined for these enzymes from their ill-characterized catalytic activities, such as NAD(P)H dehydrogenase, NAD(P)H oxidase, NAD(P)H-FeCN reductase, NAD(P)H-duroquinone reductase, and NAD(P)H-superoxide synthase, obscure the fact that there are obviously several enzymes with overlapping substrate specificities that have not yet been properly disentangled.

In this context, it is of particular interest to know whether the plasma membrane redox system is capable of transferring electrons from NAD(P)H to O_2 and whether such an activity is involved in the generation of reactive oxygen species at the outer membrane face (Murphy and Auh, 1996; van Gestelen et al., 1997; Vuletić et al., 2003). Based on molecular genetic studies, this capacity is generally attributed to the ''respiratory burst oxidase'' homologues (RBOHs; i.e. plant equivalents to the NADPH oxidase [NOX] of mammalian phagocytes) that catalyze a transmembrane electron transport from NADPH to O_2 via FAD and cytochrome (Cyt) b_{558}, resulting in the formation of superoxide radicals ($O_2^{\cdot-}$; Sumimoto et al., 2005). So far, the expression of RBOH genes in plants has been studied mainly at the level of transcription. Moreover, Arabidopsis (*Arabidopsis thaliana*) mutants defective in one or another member of the RBOH family have been characterized (Torres and Dangl, 2005; Gapper and Dolan, 2006). Using antibodies raised against RBOH peptides, RBOH proteins have been identified by immunoblotting in plasma membranes from several

* Corresponding author; e-mail anja.krieger-liszkay@cea.fr.

The author responsible for distribution of materials integral to the findings presented in this article in accordance with the policy described in the Instructions for Authors (www.plantphysiol.org) is: Anja Krieger-Liszkay (anja.krieger-liszkay@cea.fr.).

[W] The online version of this article contains Web-only data.

www.plantphysiol.org/cgi/doi/10.1104/pp.108.118745

plant species (Keller et al., 1998; Sagi and Fluhr, 2001; Simon-Plas et al., 2002) and by in situ imaging of GFP-RBOH fusion protein (Kobayashi et al., 2006). However, RBOH proteins have not yet been isolated from plants, and their catalytic properties and cofactor requirements are still largely unknown. The ability of diphenylene iodonium (DPI) to inhibit mammalian NOX at low concentrations (<10 μM; Doussiere and Vignais, 1992) has often been used as a diagnostic feature for NOX activity in plant cells or cell fractions, although DPI also inhibits other flavin- or heme-containing enzymes, especially at higher concentrations (≥10 μM; Frahry and Schopfer, 1998; Doussiere et al., 1999); therefore, it is no suitable tool to unequivocally identify NOX enzymes.

Attempts to isolate proteins with $O_2^{\cdot-}$ synthase activity from plasma membranes by biochemical methods have not yet led to homogeneous results. van Gestelen et al. (1997) separated an $O_2^{\cdot-}$-producing, FMN-containing protein fraction from FeCN/DCPIP oxidoreductases in solubilized *Phaseolus* plasma membranes. No cytochrome was detected. $O_2^{\cdot-}$ generation was much higher with NADPH than with NADH and could be inhibited by DPI, although only at high concentrations (60 μM for 50% inhibition). The $O_2^{\cdot-}$-producing activity of plasma membrane vesicles was strongly elevated by 1,4-naphthoquinones (NQs) such as juglone, and the active proteins could be divided by ion exchange chromatography into a NADPH-specific, NQ-independent fraction and three NQ-dependent fractions (van Gestelen et al., 1998). The main NQ-dependent fraction showed high specificity for NADH compared with NADPH. The plasma membrane reduced Cyt *c* at pH 6 in a juglone-stimulated manner, leading to the conclusion that semiquinones are involved in the catalytic cycle.

Using *Rosa* cells as a source of plasma membranes, Murphy et al. (2000) partly purified an $O_2^{\cdot-}$-producing enzyme activity that showed apparent specificity for either NADH or NADPH, depending on whether lucigenin luminescence or Cyt *c* reduction was used to assay $O_2^{\cdot-}$ formation. Spectroscopic evidence indicated the presence of pterin rather than flavin in the preparation. The activity was stimulated by NQ (menadione [MD]) and strongly inhibited by DPI (≤0.5 μM for 50% inhibition) and NaN_3 but not by KCN.

Taken together, this fragmentary experimental evidence illustrates that the enzymatic mechanism(s) for $O_2^{\cdot-}$ generation in the plant plasma membrane may be more complex than suggested by the concept modeled on phagocyte NOX. In an attempt to elucidate this complex picture, we are investigating the molecular and catalytic properties of NAD(P)H-oxidizing enzymes that are potentially involved in $O_2^{\cdot-}$ generation by plasma membranes isolated from soybean (*Glycine max*) hypocotyls. In this article, we describe an enzyme

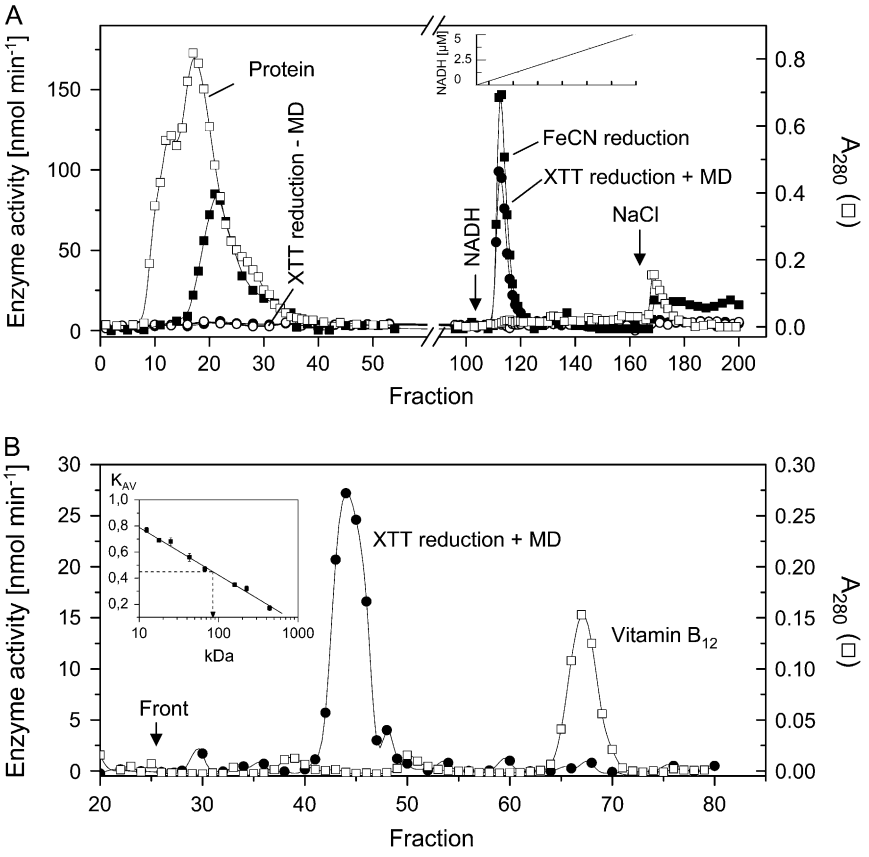

Figure 1. Purification of a MD-dependent NAD(P)H oxidoreductase activity by chromatography on Blue Sepharose (A) and Superdex (B). A, A sample of 5 mL of solubilized plasma membrane extract was applied to a 16- × 1-cm column of Blue Sepharose Fast Flow equilibrated with 10 mM HEPES (pH 8.0) containing 0.2% (w/w) Tween 20. The column was washed (0.5 mL min^{-1}) with 100 mL of the same buffer (fractions 0–107), followed by gradient elution (0–5 μM NADH; fractions 108–167) and 1 M NaCl (fractions 168–200) in the same buffer. B, A sample of 0.7 mL of enzyme purified as shown above (fractions 110–120) together with a small amount of vitamin B_{12} was applied to a Superdex 200 HR 10/30 column, eluted (6 mL h^{-1}) with 10 mM HEPES (pH 8.0), and collected in 300-μL fractions. The column was calibrated with Cyt *c* (12.4 kD), myoglobin (17.8 kD), chymotrypsin (25 kD), ovalbumin (43 kD), bovine serum albumin (67 kD), aldolase (160 kD), catalase (230 kD), and ferritin (440 kD) as shown in the inset. The position of the oxidoreductase is indicated by dashed lines.

Table I. *Redox activities of solubilized plasma membranes and the purified enzyme fraction eluted with NADH from the Blue Sepharose column*

Activities were measured in the absence (−MD) or presence (+MD) of 100 μM MD at pH 7.5. Protein concentrations were 1.5 ± 0.5 mg mL^{-1} (solubilized proteins) and 6.4 ± 0.4 μg mL^{-1} (purified enzyme). XTT concentration was 500 μM. Ratio = (specific activity + MD)/(specific activity − MD); yield = (specific activity in the purified enzyme fraction/specific activity in the solubilized protein fraction).

Assay Reaction	Specific Activity						Yield	
	Solubilized Protein Fraction			Purified Enzyme Fraction			−MD	+MD
	−MD	+MD	Ratio	−MD	+MD	Ratio		
	μmol min^{-1} mg^{-1} protein						%	
NADPH oxidation	0.0016 ± 0.0004	0.15 ± 0.01	94	<0.1[a]	29 ± 1	>290	–	83
NADH oxidation	0.0018 ± 0.0020	0.16 ± 0.01	89	<0.1[a]	30 ± 1	>300	–	79
XTT reduction with NADPH	0.0038 ± 0.0001	0.10 ± 0.002	26	<0.1[a]	22 ± 0.1	>220	–	92
XTT reduction with NADH	0.025 ± 0.002	0.10 ± 0.005	4	<0.1[a]	19 ± 1	>190	–	80
Cyt *c* reduction with NADPH	0.009 ± 0.001	0.30 ± 0.01	33	0.16 ± 0.04	60 ± 6	380	7	86
Cyt *c* reduction with NADH	0.017 ± 0.003	0.31 ± 0.01	18	0.11 ± 0.05	63 ± 4	570	3	87
FeCN reduction with NADPH	0.21 ± 0.01	0.38 ± 0.02	1.8	25 ± 1	54 ± 1	2.2	50	61
FeCN reduction with NADH	0.39 ± 0.01	0.53 ± 0.03	1.4	25 ± 2	52 ± 2	2.1	27	42
DCPIP reduction with NADPH	0.029 ± 0.003	0.032 ± 0.001	1.1	3.0 ± 0.2	3.3 ± 0.2	1.1	43	43
DCPIP reduction with NADH	0.028 ± 0.003	0.031 ± 0.003	1.1	2.2 ± 0.2	2.2 ± 0.2	1.0	33	30

[a]Below detection limit.

that is responsible for the NQ-stimulated production of $O_2^{\cdot-}$ in these membranes. $O_2^{\cdot-}$-producing activity was measured using the tetrazolium compound Na,3′-(1-[phenylamino-carbonyl]-3,4-tetrazolium)-bis(4-methoxy-6-nitro)benzenesulfonic acid hydrate (XTT), which can be reduced by $O_2^{\cdot-}$ to a photometrically detectable formazan (Able et al., 1998). To analyze the reaction mechanism of $O_2^{\cdot-}$ generation, we developed spectrophotometric methods enabling the measurements of concentration changes of NAD(P)H, quinones, and XTT in the same reaction mixture.

RESULTS AND DISCUSSION

Purification of a NAD(P)H Oxidoreductase Activity from Solubilized Plasma Membranes

A plasma membrane fraction showing NADH-dependent XTT reduction in the presence of MD and detergent was isolated from the upper hypocotyl region of dark-grown soybean seedlings by established techniques and checked for contaminating proteins (see "Materials and Methods"). Extensive washing of the membranes with 1.5 M NaCl or $CaCl_2$ did not affect this activity (data not shown). The proteins solubilized from these membranes by Tween 20 were subjected to affinity chromatography on a Blue Sepharose column. Extensive washing with buffer removed the bulk of the nonbound proteins, including a FeCN reductase, from the bound XTT-reducing fraction that could be eluted from the column with 1 μM NADH (Fig. 1A). The protein concentration of the active enzyme fraction was very low (4–8 μg mL^{-1}). The elution profile obtained with the active enzyme fraction after chromatography on a calibrated Superdex 200 column revealed a single peak of an apparent molecular mass of approximately 85 kD (Fig. 1B). Redox activities of this enzyme fraction in the absence and presence of MD in comparison with the solubilized plasma membrane are summarized in Table I.

The reaction catalyzed by the purified enzyme in the presence of NAD(P)H and MD consumed O_2. The addition of XTT suppressed the O_2 consumption, and this suppression could be partially counteracted by adding superoxide dismutase (SOD; Fig. 2). These

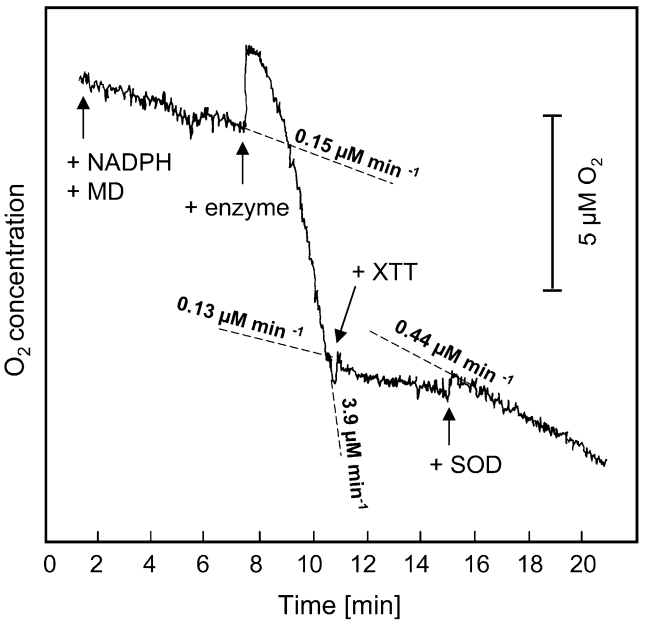

Figure 2. Consumption of O_2 by the NAD(P)H oxidoreductase, its suppression by XTT, and the partial reversion of the suppression by SOD (pH 7.5). The addition of NADPH (200 μM), MD (100 μM), enzyme, XTT (100 μM), and SOD (100 μg mL^{-1}) is indicated by arrows. The measurements were performed in a 2-mL total volume containing 1.3 μg mL^{-1} purified enzyme.

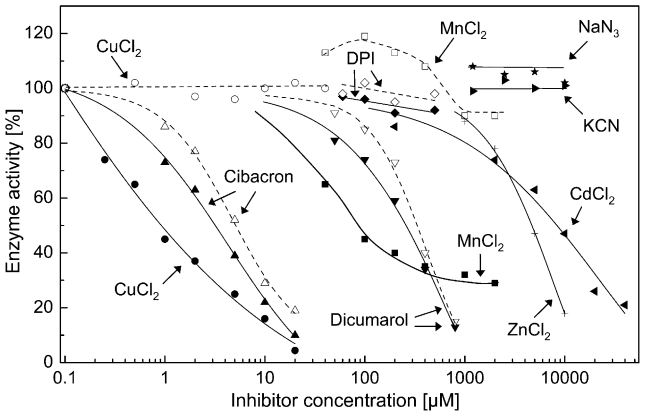

Figure 3. Effects of various inhibitors on the NAD(P)H oxidoreductase activity, measured either as oxidation of NADPH (200 μM; white symbols, dashed lines) or reduction of XTT (100 μM; black symbols) in the presence of MD (100 μM) at pH 7.5. NADPH oxidation was measured in the absence of XTT. Reaction mixtures with dicumarol and DPI contained up to 2% dimethyl sulfoxide, which had no effect on enzyme activity (100% = 4 μM min^{-1} produced by 1.3 μg mL^{-1} purified enzyme).

results are in agreement with a reaction mechanism involving the reduction of O_2 to $O_2^{\cdot -}$ that subsequently reduces XTT to $XTTH_2$, whereby O_2 is regenerated according to:

$$2\,O_2^{\cdot -} + 2\,H^+ + XTT \rightarrow 2\,O_2 + XTTH_2$$

This reaction is suppressed by the disproportionation of $O_2^{\cdot -}$ with SOD.

A number of conclusions can be drawn from these data. (1) Utilizing adsorption to Blue Sepharose followed by desorption with NADH resulted in an at least 200-fold increase in specific activity of an 85-kD NAD(P)H oxidoreductase isolated from solubilized plasma membranes in a single purification step. A closely related protocol was used by Luster and Buckhout (1989) to purify an "electron transport protein" with similar properties from maize (*Zea mays*) plasma membranes. (2) Our purified enzyme consumes O_2 and reduces XTT and Cyt *c* in a MD-dependent reaction. Its ability to reduce FeCN is slightly stimulated by MD, while DCPIP is independent of MD. NADH and NADPH are oxidized at similar rates in the presence of MD. (3) In the absence of an electron acceptor except O_2, the NAD(P)H-oxidizing activity is very low in the solubilized membrane fraction and not detectable in the purified enzyme fraction. No NOX-type activity could be detected in the elution profile of the Blue Sepharose column (Fig. 1A), although the solubilized membrane fraction does contain measurable amounts of MD-independent XTT- and Cyt *c*-reducing activity. (4) The purified enzyme accounts for 80% to 90% of the NAD(P)H oxidoreductase activity detected by the XTT assay in the presence of MD and about 50% of the FeCN/DCPIP reductase activity present in the solubilized membrane fraction.

Peroxidase Activity of the Purified Plasma Membranes

The formation and decomposition of reactive oxygen species is affected by peroxidases. Moreover, hydroquinones can be converted into semiquinones by these enzymes (Ohnishi et al., 1969). Plasma membranes isolated from maize roots were reported to contain at least two tightly bound guaiacol peroxidases (Mika and Lüthje, 2003). We tested aliquots (50 μg of protein) of our solubilized plasma membrane fraction with the assay used by these authors and found no detectable peroxidase activity. Using a tetramethylbenzidine-based assay with increased sensitivity revealed a peroxidase activity of 12 nmol min^{-1} mL^{-1} (6 nmol min^{-1} mg^{-1} protein), corresponding to 1.7 ng of horseradish peroxidase equivalents per milligram of protein estimated from a standard curve with pure horseradish peroxidase. The peroxidase activity solubilized from the plasma membrane accounted for 0.06% of the soluble peroxidase activity in the tissue homogenate, indicating that significant amounts of peroxidases appear not to be obligatory components of plant plasma membranes.

Effects of Oxidoreductase Inhibitors

We investigated the effect of several diagnostic inhibitors on the NAD(P)H-oxidizing and XTT-reducing activities of the enzyme purified from plasma membranes to compare them with known classes of oxidoreductases. The data summarized in Figure 3 demonstrate that: (1) KCN and NaN_3 ($\leq$10 mM) had no effect on XTT reduction; (2) Zn^{2+} and Cd^{2+} inhibited XTT reduction only at very high concentrations (50% inhibitory concentration [I_{50}] = 2 mM and 5 mM, respectively); (3) DPI ($\leq$500 μM) had no effect on both assay reactions; (4) Cibacron Blue and dicumarol inhibited both assay reactions (I_{50} = 3–5 μM and 300 μM, respectively); and (5) Cu^{2+} and Mn^{2+} inhibited XTT reduction but not NADPH oxidation (I_{50} = 1 μM and 100 μM, respectively), indicating that these redox-active ions interfered with the electron transfer from

Table II. *K_m and V_{max} values for various steps of the reaction system catalyzed by the NAD(P)H oxidoreductase at pH 7.5*

K_m and V_{max} values were obtained from linear Lineweaver-Burk plots using equal amounts of purified enzyme. NAD(P)H (30–200 μM) oxidation was determined from the decrease in A_{340} in the presence of 100 μM MD. XTT (12–100 μM) reduction was determined from the increase in A_{470} in the presence of 200 μM NADPH and 100 μM MD. MD (20–200 μM) reduction was determined from the consumption of NADPH (200 μM) in the absence of XTT.

Reaction	K_m	V_{max}
	μM	μM min^{-1}
NADPH oxidation	90[a]	4.1
NADH oxidation	200[a]	5.6
XTT reduction	14	3.6
MD reduction	70	7.1

[a]Equivalent values were obtained by measuring the reduction of XTT (500 μM) under similar conditions.

the reduced MD to XTT rather than with the initial catalytic activity of the enzyme.

The following compounds exhibited no effect on XTT reduction: rotenone (10 μM), piericidin A (100 μM), nitrofurantoin (100 μM), quinacrine (100 μM), $CaCl_2$ (2 mM), $MgCl_2$ (2 mM), EDTA (4 mM), *N*-ethylmaleimide (10 mM), 4-chloromercuribenzoate (400 μM), FMN (10 μM), and FAD (10 μM; data not shown).

An important result emerging from this list deserves further consideration, namely the insensitivity of the enzyme to DPI, an inhibitor inactivating many flavoenzymes, including NOX-type enzymes at less than 10 μM (Cross, 1987; Doussiere and Vignais, 1992). DPI binds to, and thereby inactivates, the catalytic center of these enzymes only after its reduction to the phenyl radical (O'Donnell et al., 1994); therefore, it attacks specifically one-electron-transferring flavoenzymes such as NOX (Cross, 1987) or mitochondrial NADH: ubiquinone reductase (Ragan and Bloxham, 1977). As a consequence, flavoenzymes transferring two electrons in one step from NAD(P)H to various acceptors are not subject to inhibition by DPI (Cross, 1987). Examples of this class are the NAD(P)H:quinone-acceptor oxidoreductases known as DT-diaphorases in animals (Lind et al., 1990; Ross, 1997). Functionally related flavoenzymes have also been found in plants (Spitsberg and Coscia, 1982; Luster and Buckhout, 1989; Valenti et al., 1990; Serrano et al., 1994; Rescigno et al., 1995; Trost et al., 1995, 1997; Sparla et al., 1996, 1998). These enzymes catalyze the transfer of a hydride atom to various benzoquinones and naphthoquinones, directly forming the corresponding hydroquinones and thus avoiding the intermediate semiquinone radical that can reduce O_2 to $O_2^{\cdot-}$ (Iyanagi and Yamazaki, 1970; Lind et al., 1990; Sparla et al., 1996; Ross, 1997). A purified quinone oxidoreductase investigated by Trost et al. (1997) was shown to be insensitive to DPI. A further remarkable feature of this group of enzymes is that they can be inhibited by Cibacron Blue (Prestera et al., 1992) and dicumarol (Lüthje et al., 1994; Rescigno et al., 1995).

Evidently, the enzyme isolated from soybean plasma membranes shares some important properties with two-electron-transferring quinone reductases. Therefore, the basic problem is to explain the ability of this enzyme to elicit one-electron transfer from NAD(P)H, presumably via quinone intermediates, to O_2, a property that appears to be incompatible with the reaction mechanism of DPI-insensitive NAD(P)H oxidoreductases.

Catalytic Properties of NAD(P)H Oxidoreductase

The following experiments were conducted with the purified enzyme fraction eluted from Blue Sepharose by NADH (Fig. 1A). Table II shows the kinetic parameters for the substrates involved in the O_2-reducing reaction measured by the XTT assay. In order to elucidate the role of quinones, we examined the ability of several NQs and 1,4-benzoquinones (BQs) to replace MD in this reaction (Table III). Unsubstituted NQ, 5-hydroxy-NQ, and 5-hydroxy,2-methyl-NQ supported XTT reduction similar to MD. The enzyme was inactive with 2-hydroxy- and 2-methoxy-substituted

Table III. *Quinone substrate specificity of the NAD(P)H oxidoreductase determined as NADPH oxidation, hydroquinone accumulation, or XTT reduction with or without SOD*

Enzyme activity was measured at pH 7.5 with 200 μM NADH, 100 μM quinone, 100 μM XTT with or without 100 μg mL^{-1} SOD (in the case of XTT reduction), and 0.13 μg mL^{-1} purified enzyme. The percentage of the normalized activity is given in parentheses (the value for NADPH oxidation or XTT reduction without SOD is set to 100%).

Sample	Enzyme Activity			
	NADPH Oxidation	Hydroquinone Accumulation	XTT Reduction without SOD	XTT Reduction with SOD
	$\mu M\ min^{-1}$			
NQ	6.9 ± 0.4 (100)	1.1 ± 0.1 (16)	4.9 ± 0.4 (100)	1.0 ± 0.1 (20)
2-Methyl-NQ (MD, vitamin K_3)	4.5 ± 0.2 (100)	2.0 ± 0.1 (44)	4.0 ± 0.1 (100)	1.9 ± 0.1 (48)
5-Hydroxy-NQ (juglone)	5.7 ± 0.4 (100)	0.01 ± 0.05 (<1)	4.1 ± 0.3 (100)	0.5 ± 0.1 (12)
5-Hydroxy,2-methyl-NQ (plumbagin)	3.5 ± 0.1 (100)	0.4 ± 0.1 (11)	2.5 ± 0.1 (100)	1.4 ± 0.2 (56)
2-Hydroxy-NQ (lawsone)	<0.1	<0.1	<0.1	–
2-Methoxy-NQ	<0.1	<0.1	<0.1	–
2,3-Dimethoxy-NQ	0.1 ± 0.2	<0.1	0.2 ± 0.1	–
2-Methyl,3-phythyl-NQ (phylloquinone, vitamin K_1)	0.4 ± 0.5	<0.1	<0.1	–
Menaquinone-4 (vitamin K_2)	<0.1	0.4 ± 0.2	<0.1	–
BQ	4.3 ± 0.3 (100)	4.8 ± 1.0 (112)	0.02 ± 0.02	–
2-Methyl-BQ (toluquinone)	6.1 ± 1.0 (100)	5.9 ± 0.8 (97)	0.01 ± 0.02	–
2,5-Dimethyl-BQ (xyloquinone)	6.3 ± 0.9 (100)	5.2 ± 0.7 (83)	0.08 ± 0.02	–
2,6-Dimethyl-BQ	6.8 ± 1.0 (100)	4.8 ± 0.9 (71)	0.01 ± 0.02	–
2,3-Dimethoxy,5-methyl-BQ (ubiquinone 0)	5.0 ± 0.2 (100)	4.7 ± 0.2 (94)	0.04 ± 0.02	–
Tetramethyl-BQ (duroquinone)	0.3 ± 0.1	0.4 ± 0.3	<0.01	–
2,6-Dimethoxy-BQ	<0.1	<0.1	<0.2	–
2,5-Dihydroxy-BQ	<0.1	<0.2	<0.02	–
Tetrahydroxy-BQ	<0.1	<0.1	<0.2	–

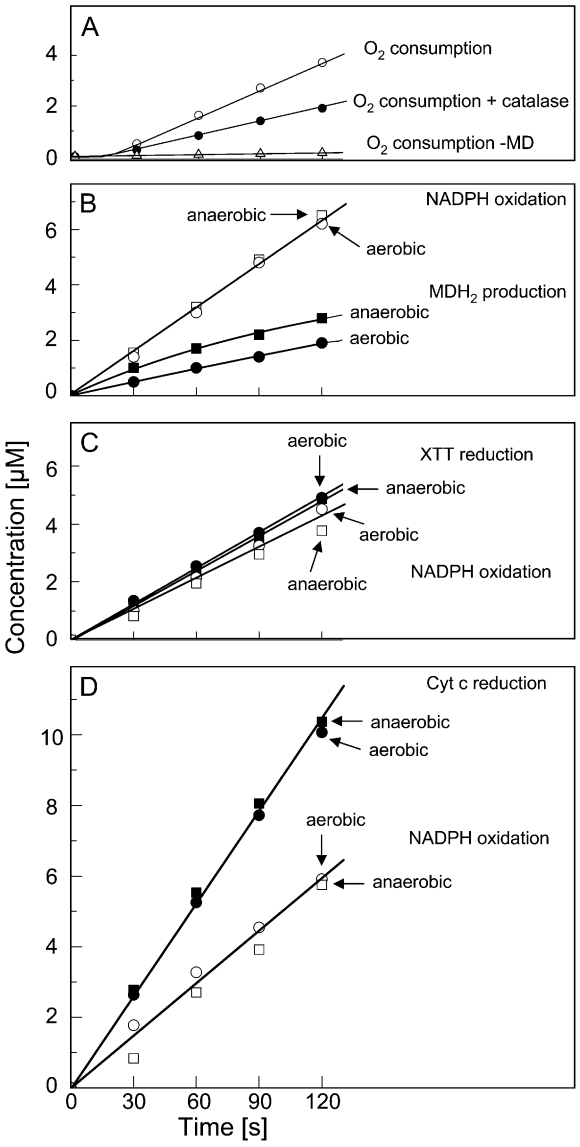

Figure 4. Concentration changes of various substrates involved in the transfer of electrons from NADPH to XTT or Cyt *c* in the reaction catalyzed by the NAD(P)H oxidoreductase (200 μM NADPH and 100 μM MD, pH 7.5). A, O_2 consumption with and without catalase (200 μg mL^{-1}). B, MD reduction and simultaneously measured NADPH oxidation at 260 μM O_2 (aerobic) or about 10 μM O_2 (anaerobic). C, Reduction of added XTT (100 μM) and simultaneously measured NADPH oxidation under aerobic or anaerobic conditions. D, Reduction of added Cyt *c* (50 μM) and simultaneously measured NADPH oxidation under aerobic or anaerobic conditions.

NQs as well as phylloquinone and menaquinone-4. Only those NQs that can be reduced by NADPH to the respective hydroquinones supported XTT reduction. However, the accumulation of hydroquinones fell short of NADPH consumption to an extent depending on the type of NQ. XTT reduction in the presence of active NQs could only partially be inhibited by removing $O_2^{\cdot-}$ with a saturating amount of SOD, and again this depended on the particular NQ. None of the tested BQs supported XTT reduction, although several of them were reduced by NADPH to the corresponding hydroquinones that accumulated in stoichiometric amounts. This result is in conflict with the reaction catalyzed by one-electron-transferring reductases that includes the intermediary formation of semiquinone.

Taken together, these results indicate that the enzyme is capable of utilizing several NQs and BQs as electron acceptors, but only certain NQs can mediate electron transfer to XTT. This situation is highly reminiscent of the findings of Ernster et al. (1962) that DT-diaphorase catalyzes the reduction of Cyt *c* in the presence of some NQs but not in the presence of BQs. It also appears from our data that the reduction of XTT in the presence of active NQs can only in part be attributed to the formation of $O_2^{\cdot-}$.

In order to clarify the connections between NADPH oxidation and $O_2^{\cdot-}$ production, we examined the stoichiometries between NADPH oxidation, O_2 consumption, and XTT reduction in the MD-mediated reaction system (Fig. 4). If all electrons delivered by NADPH are utilized for the reduction of O_2 to $O_2^{\cdot-}$ (NADPH + 2 O_2 → $NADP^+$ + H^+ + 2 $O_2^{\cdot-}$), the molar ratio of NADPH oxidation to O_2 consumption would be 1:2. If the disproportionation of $O_2^{\cdot-}$ into H_2O_2 (2 $O_2^{\cdot-}$ + 2 H^+ → H_2O_2 + O_2) is taken into account, the ratio will be 1:1. Figure 4, A and B, shows that after a lag of about 20 s, the steady-state rates of these changes show a ratio of 1:0.7, indicating that at the air-saturated O_2 concentration (260 μM) about two-thirds of the electrons removed from NADPH are utilized for reducing O_2. The O_2 consumption could be reduced by half with catalase, indicating that H_2O_2 is produced that decomposes according to H_2O_2 → H_2O + ½ O_2 (Fig. 4A). About one-third of the electrons removed from NADPH are utilized for accumulating menadionehydroquinone (MDH_2). This portion can be significantly increased by reducing the O_2 concentration in the reaction mixture from 260 μM to about 10 μM (Fig. 4B), suggesting that MDH_2 accumulation competes with O_2 reduction for electrons. (For technical reasons, it was not possible to establish O_2 concentrations lower than 10 μM during the reaction.) If XTT was added to the reaction mixture, it captured the electrons removed

Table IV. *Effects of SOD (100 μg mL^{-1}) on various steps involved in the transfer of electrons from NADPH to XTT in the reaction catalyzed by the NAD(P)H oxidoreductase*

Experimental details are as described for Figure 4. Inhibition of the XTT reduction by SOD was saturated at ≥1 μg mL^{-1}. SOD (50 μg mL^{-1}) inhibited XTT reduction by >95% if the enzyme was replaced by a similarly active concentration (50 nM) of methoxyphenazine methosulfate catalyzing the univalent reduction of O_2 by NAD(P)H.

Reaction	Reaction Rate	
	−SOD	+SOD
	$\mu M\ min^{-1}$	
O_2 consumption	1.9 ± 0.3	1.7 ± 0.3
NADPH consumption	3.3 ± 0.5	3.4 ± 0.1
MDH_2 accumulation	1.2 ± 0.3	1.1 ± 0.2
XTT reduction	2.5 ± 0.3	1.3 ± 0.1

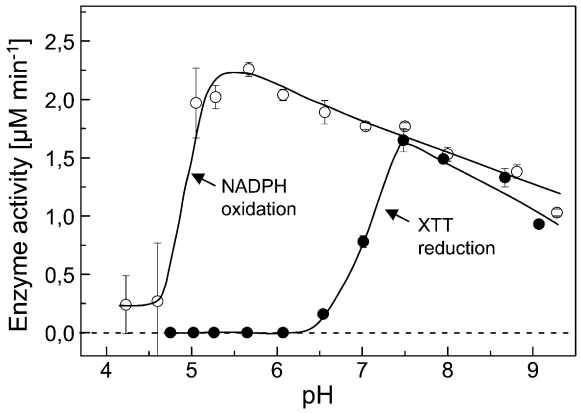

Figure 5. pH dependence of NADPH oxidation and XTT reduction affected by the NAD(P)H oxidoreductase in the presence of MD. Experimental details are as described for Figure 4, except that the pH was adjusted by mixing 20 mM HEPES and 20 mM MES. NADPH oxidation was measured in the absence of XTT; however, similar results were obtained in the presence of XTT.

from NADPH with a molar ratio that varied between 1:1 and 1:0.7 in different experiments at both air-saturated and reduced O_2 concentrations (Fig. 4C). This correlation presumably reflects a variable contribution of MDH_2 accumulation that in turn is influenced by the rate of the enzyme reaction. Similar to XTT, Cyt *c* was able to capture most of the electrons removed from NADPH (molar ratio of 1:1.7, in good agreement with NADPH + 2 Cyt $c_{oxidized} \rightarrow NADP^+ + H^+ + 2$ Cyt $c_{reduced}$; Fig. 4D).

It can be concluded from these results that the electron transfer from NADPH can be accounted for by the accumulation of MDH_2 and, after a lag phase, the consumption of O_2. In the presence of XTT or Cyt *c*, the electron transfer to these acceptors is essentially complete and can occur via two competing routes, only one of which involves the reduction of O_2. This conclusion is further supported by the finding that SOD at saturating concentrations inhibits XTT reduction by 50% without affecting O_2 reduction, NADPH oxidation, or MDH_2 accumulation (Table IV).

Another interesting property of the reaction system catalyzed by the oxidoreductase emerged from the investigation of the pH dependence of the NADPH-oxidizing and the XTT-reducing activities (Fig. 5). NADPH oxidation displays a broad asymmetric peak between pH 4.5 and >9.0, with an optimum at pH 5.5. However, XTT reduction covers only the high pH range (pH > 6) of this curve, with an apparent optimum at pH 7.5. Hence, in the range of pH 5 to 6, NADPH oxidation takes place at a high rate, but the electrons cannot be utilized for the reduction of XTT. Figure 6 shows that under these conditions, no O_2 consumption can be observed and the NADH oxidation is accompanied by MDH_2 accumulation with a molar ratio of 1:1. Obviously, at pH 6, $O_2^{\cdot-}$ production is completely shut down in favor of the accumulation of MDH_2.

Molecular Properties of the NAD(P)H Oxidoreductase

Two genetically unrelated families of two-electron-transferring NAD(P)H:quinone-acceptor oxidoreductases have been identified in plants. Both contain FMN and are based on subunits of similar size. The enzyme cloned from Arabidopsis, AtNQR [for Arabidopsis NAD(P)H:quinone-acceptor oxidoreductase], by Sparla et al. (1999) belongs to a family of tetrameric flavoproteins composed of 21- to 22-kD subunits (Trost et al., 1995, 1997; Sparla et al., 1998). The NAD(P)H:quinone-acceptor reductase cloned from Arabidopsis, AtFQR1, by Laskowski et al. (2002) belongs to the WrbA family of flavoproteins that show sequence similarities to flavodoxins and other prokaryotic and fungal proteins. These enzymes are dimers or tetramers of 21-kD subunits (Patridge and Ferry, 2006).

To test whether the NAD(P)H oxidoreductase purified from soybean plasma membranes was related to one of these families, we examined its affinity to antibodies raised against recombinant AtNQR and AtFQR1. Native PAGE of cytosolic proteins, solubilized plasma membranes, and purified oxidoreductase revealed similar bands for MD-dependent $O_2^{\cdot-}$-producing activity using nitroblue tetrazolium chloride (NBT) in-gel staining (Fig. 7A). Immunoblots of these gels demonstrated that the activity purified from the plasma membranes can be attributed to NQR (Fig. 7B), while the activity in the cytosolic fraction can be attributed to FQR1 (Fig. 7C). For unknown reasons, the activity in the plasma membrane fraction showed only a very weak signal with the NQR antibody. When similar samples were subjected to SDS-PAGE, no clear protein bands could be detected by silver staining in the purified enzyme preparation (Fig. 8). Only faint bands at 60, 80 to 90, and 110 kD became visible,

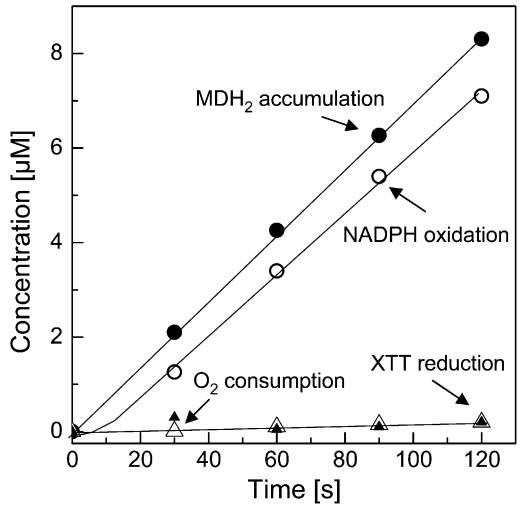

Figure 6. NADPH oxidation, MDH_2 accumulation, O_2 consumption, and XTT reduction affected by the NAD(P)H oxidoreductase at pH 6. Experimental details are as described for Figure 4, except that the reaction mixture was adjusted to pH 6.0 with MES.

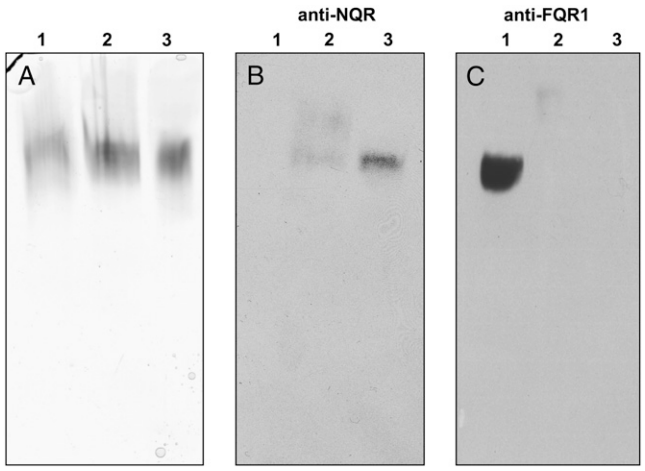

Figure 7. Native PAGE and immunoblot analysis of protein fractions containing cytosolic proteins (lane 1), solubilized plasma membrane proteins (lane 2), and purified NAD(P)H oxidoreductase protein (lane 3). Amounts of samples giving the same activity of XTT reduction (10 nmol $XTTH_2$ min^{-1} for A and 30 nmol $XTTH_2$ min^{-1} for B and C) were loaded on the gel. A, The gel was stained for enzyme activity using the NBT assay. B and C, Immunoblots were decorated with antibodies directed against NQR and FQR1.

indicating the presence of impurities. NQRs are characterized by an extraordinarily high specific activity and, as such, the protein associated with the catalytic activity has been reported to be difficult to detect (Trost et al., 1997). Immunoblots of the SDS gels showed a single band at approximately 22 kD, similar to recombinant AtNQR, with the antibody against NQR but not with the antibody against FQR1 in the purified oxidoreductase preparation. On the other hand, the FQR1 antibody gave a positive reaction with a cytosolic antigen of very similar size (Fig. 8).

Given the molecular mass of approximately 85 kD for the native oxidoreductase purified from plasma membranes (Fig. 1B), these data are in agreement with the finding that plant NQRs are homotetramers of 21.5-kD subunits (Sparla et al., 1996, 1999). Beyond that, the enzyme demonstrates an immunological relationship to AtNQR identified by Sparla et al. (1999) rather than to AtFQR1 identified by Laskowski et al. (2002). FQR1 appears to be at least in part responsible for the quinone reductase activity in the cytosolic fraction.

Mass spectrometry (MS) analysis performed with the proteins extracted from the NBT-stained band obtained with the purified plasma membrane enzyme (Fig. 7A, lane 3) confirmed the homology with the NAD(P)H:quinone-acceptor oxidoreductase NQR (EC 1.6.5.2, formerly EC 1.6.99.2). Table V summarizes the peptides that identify a translation of the assembled EST Glycine_max-35276 being homologous with AtNQR (see also the sequence alignment provided as Supplemental Table S1). Interestingly, the NQR contains a FMN-binding site that was first identified in a FMN reductase of *Pseudomonas aeruginosa* by x-ray crystallography and that is clearly distinguishable from the flavodoxin key fingerprint motif (Agarwal et al., 2006). This FMN reductase shows high sequence homology with NQR. The largest quantity of the NQR peptides coincided with the center of the NBT-stained gel bands. Most of the peptides identified in the stained region of the gel were from lipoxygenase-4 (swissprot identifier P38417), which was not responsible for the NBT reduction. Other peptides detected were mainly from soybean ESTs, which were homologous with the fasciclin-like arabinogalactan proteins 1 and 2 from Arabidopsis (swissprot identifiers Q9FM65 and Q9SU13). However, the profiles of these signals did not match the profile of the NBT-staining signal (data not shown). Two weak signals in the MS spectra identify peptides of a FQR1 homolog (EST Glycine_max-394114201), but their integrated intensity was more than 30-fold smaller than that of peptides from NQR. If significant, these signals are likely due to a minor contamination with soluble proteins.

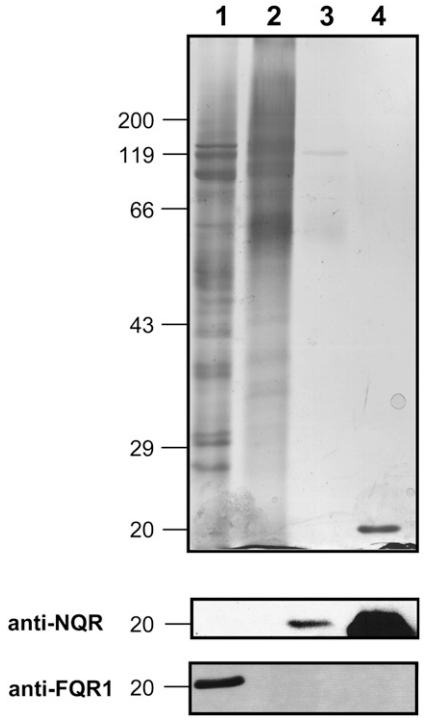

Figure 8. Silver-stained SDS-PAGE (8%) and immunoblot analysis of protein fractions containing cytosolic proteins (lane 1), solubilized plasma membrane proteins (lane 2), purified NAD(P)H oxidoreductase protein (lane 3), and recombinant AtNQR (1 μg; lane 4). Samples with the following activities were loaded onto the gel for silver staining: 8 nmol $XTTH_2$ min^{-1} (15 μg; lanes 1 and 2) and 140 nmol $XTTH_2$ min^{-1} (7.5 μg; lane 3); samples with the following activities were loaded onto the gel for blotting: 30 nmol $XTTH_2$ min^{-1} (lanes 1 and 2) and 140 nmol $XTTH_2$ min^{-1} (lane 3). Marker positions (kilodaltons) are given on the left side. Immunoblots were decorated with antibodies directed against NQR and FQR1. The amount of NQR protein in the plasma membrane protein fraction (lane 2) was insufficient for detectable NQR antibody binding.

Table V. *Mass spectrometric identification of soybean NQR following in-gel digestion by trypsin of the NBT-stained band from native gel electrophoresis (Fig. 7A, lane 3)*

Peptide[a]	Retention Time[b]	M_r(obs)[c]	z[d]	M_r(cal)	Difference	E Value[e]	Sequence (Modification)
16–27	38.4	1,101.6039	2	1,101.6029	0.0010	1.7E-10	M.AAVAGASSSVIK.V (acetylated N terminus)
28–36	33.5	872.5078	2	872.5079	−0.0001	2.7E-04	K.VAALSGSLR.K
47–55	30.9	959.5034	2	959.5036	−0.0002	1.4E-03	R.SAIELSQGR.V
56–90	56.7	3,928.0185	3	3,928.0145	0.0040	5.9E-10	R.VEGLQIEYVDISPLPLLNTDLEVN-GTYPPQVEAFR.Q
93–115	55.2	2,468.2830	2	2,468.2838	−0.0008	1.4E-11	K.ILAADSILFASPEYNYSVASPLK.N
93–115	55.2	2,468.2842	3	2,468.2838	0.0004	4.7E-15	K.ILAADSILFASPEYNYSVASPLK.N
132–146	36.1	1,272.6573	2	1,272.6574	−0.0001	3.2E-12	K.PAAIVSAGGGFGGGR.S

[a]Sequence numbering is for PlantGDB-assembled EST PUT-161a-Glycine_max-35276. [b]Retention time (minutes) from reverse-phase HPLC. [c]Relative molecular mass determined from mass/charge ratio and charge. [d]Charge determined from isotope distribution observed. [e]Expected number of random hits having an equal or better score (probability scoring by the OMSSA program).

From the sequence data (Supplemental Table S1), it is clear that NQR lacks all diagnostic features of an integral membrane protein with membrane-spanning helices. However, in agreement with previous investigators (Luster and Buckhout, 1989; Valenti et al., 1990; Serrano et al., 1994; Trost et al., 1997; van Gestelen et al., 1997, 1998), we conclude that NQR can be present as a peripheral membrane protein tightly bound to the plasma membrane based on the following criteria: (1) the enzyme can be liberated from the plasma membrane by detergent but not by high salt (1.5 M $CaCl_2$ or NaCl), and (2) soluble proteins present in the homogenate, such as peroxidase, Glc-6-P dehydrogenase, and FQR, were undetectable, or detectable only in traces, in the solubilized membrane fraction. The other proteins, identified as impurities in our NQR preparation by mass spectrometry, show membrane association domains. The lipoxygenase contains a polycystin/lipoxygenase/α-toxin domain that may be involved in protein-lipid interaction (Bateman and Sandford, 1999) and the fasciclin-like arabinogalactan-protein A glycosylphosphatidylinositol anchor. The presence of membrane-associated proteins in the purified plasma membrane protein preparation may be taken as a further indication of the membrane-associating nature of NQR. Further studies are needed to clarify whether NQR is attached to the inner or outer surface of the plasma membrane (Bérczi and Møller, 1998).

Redox Properties of MDH_2

The results reported to date indicate that the purified NQR shares many features with the two-electron-transferring DT-diaphorases of mammals (Märki and Martius, 1960; Ernster et al., 1962; Lind et al., 1990; Ross, 1997) and certain quinone reductases of plants (Luster and Buckhout, 1989; Trost et al., 1995; Sparla et al., 1999), with the notable exception of the ability to reduce O_2 to $O_2^{\cdot -}$ at pH $\geq$ 6.5. This reaction implies the formation of a semiquinone intermediate and the capacity for one-electron-transferring reaction (van Gestelen et al., 1998). A key to explain this seemingly disparate property emerged when we investigated the stability of MDH_2 as a function of pH. When added to buffered water containing 260 μM O_2, MDH_2 was stable at acidic pH. However, autoxidation increased steeply when the pH was raised to $\geq$6.5 (Fig. 9A). XTT reduction was inhibited by SOD by only 50% (Fig. 9B). The molar ratios (1:1 in the case of O_2 and XTT, 1:2 in the case of Cyt *c*) showed that the electron transfer from MDH_2 to these acceptors was complete (Fig. 10). Net O_2 consumption was prevented when XTT was present (Fig. 10A), similar to the enzyme-catalyzed reaction (Fig. 2). Moreover, in agreement with the results shown in Table IV, SOD reduced the molar ratio of MDH_2 oxidation/XTT reduction from 1:1 to 1:0.5, indicating that 50% of the electrons provided by MDH_2 could be diverted to XTT without the participation of $O_2^{\cdot -}$ (Fig. 10B). In the case of Cyt *c*, this fraction increased to 70% (Fig. 10C).

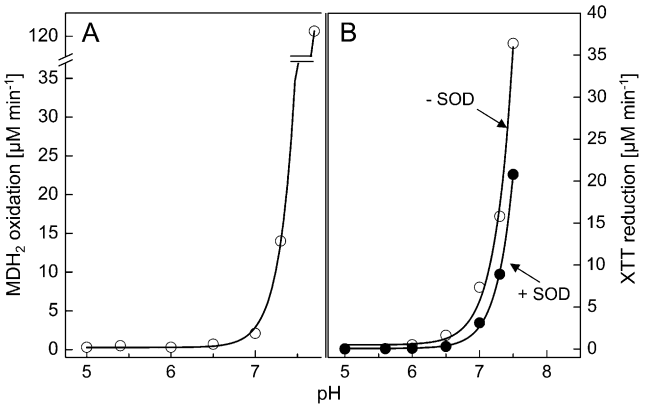

Figure 9. MDH_2 autoxidation (A) and accompanying XTT reduction in the absence and presence of SOD (B) as a function of pH. A, MDH_2 (100 μM) from a freshly prepared 5 mM stock solution in ethanol was added to HEPES (20 mM) adjusted to pH 5.0 to 7.7. The decrease of A_{290} due to the conversion of MDH_2 to MD was recorded for $\leq$1 min. At pH $>$ 7.5, the rates were too rapid to be followed accurately. B, Similar measurements recording the reduction of XTT (100 μM) with or without SOD (100 μg mL^{-1}) in the presence of MDH_2 (100 μM).

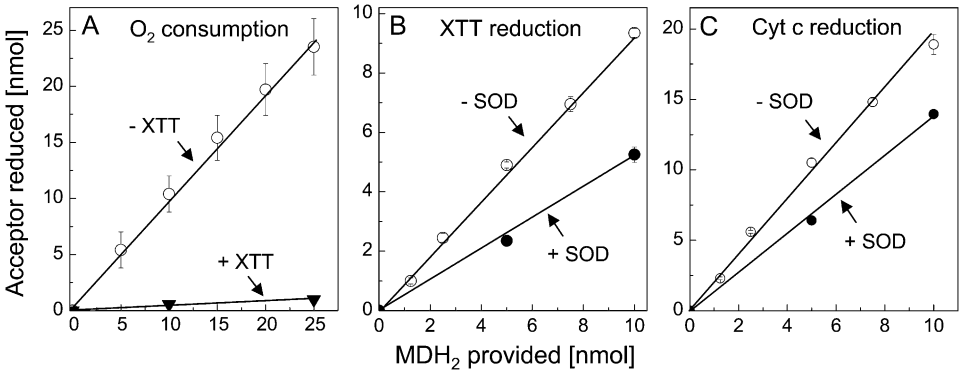

Figure 10. Molar relations in the electron transfer from MDH_2 to O_2 (A), XTT (B), or Cyt *c* (C) at pH 7.5. A, Various amounts of MDH_2 dissolved in ethanol were added to HEPES in the absence or presence of XTT (100 μM). The amounts of O_2 consumed were measured when the reaction was completed (after 6–10 min). B and C, Reduction of XTT (100 μM; B) or Cyt *c* (100 μM; C) in the absence or presence of SOD (100 μg mL^{-1}) measured after completion of the reaction (after 1–2 min).

The kinetics of MDH_2 autoxidation, concomitant O_2 uptake, and reduction of added XTT or Cyt *c* at pH 7.5 revealed that XTT and Cyt *c* are more potent acceptors than O_2 for electrons provided by MDH_2 (Fig. 11). Reducing the O_2 concentration to about 10 μM strongly reduced MDH_2 autoxidation (Fig. 11A) but affected XTT reduction only slightly (Fig. 11C) and Cyt *c* reduction not at all (Fig. 11D). Hence, electron transfer from MDH_2 to XTT or Cyt *c* also can take place without the intermediary formation of $O_2^{\cdot-}$. Moreover, aerobic MDH_2 oxidation was slowed by SOD, indicating that this reaction depends in part on the formation of $O_2^{\cdot-}$ (Fig. 11A).

In summary, basic features observed in the redox reaction catalyzed by the isolated oxidoreductase are also found in the nonenzymatic reactions of MDH_2 in neutral or alkaline solutions. The enzyme functions as a bona fide NQR that catalyzes an obligate two-electron reduction of certain quinones and is consequently insensitive to inhibition by DPI. However, some naphthohydroquinones produced by the enzyme, such as MDH_2, can act as converters from two-electron- to one-electron-transferring reactions, depending on their propensity to undergo autoxidation after activation at high pH (compare with Table III). During the reaction, intermediates are produced that can react either with O_2-forming $O_2^{\cdot-}$ or with artificial one-electron acceptors such as XTT or Cyt *c*. In retrospect, it is interesting that an NQR assay has been developed based on this principle (Prochaska and Santamaria, 1988). The differing susceptibility to autoxidation of various naphthohydroquinones produced by DT-diaphorase has been described by Buffinton et al. (1989). Lind et al. (1982) noted that MDH_2 was stable at pH $\leq$ 6.5 but underwent autoxidation at pH 7.5.

Reaction Mechanisms Involved in the Oxidation of MDH_2 by O_2 or XTT

The ability of redox-labile hydroquinones to form semiquinones in alkaline solution (i.e. in their anionic

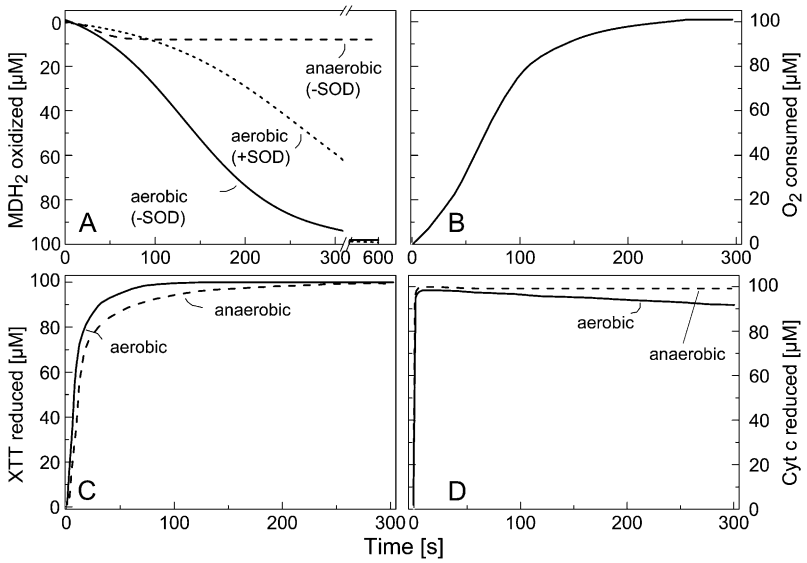

Figure 11. Kinetics of the autoxidation of MDH_2 (A), concomitant uptake of O_2 (B), and reduction of added XTT (C) or Cyt *c* (D) at pH 7.5. A, Oxidation of MDH_2 (100 μM) was followed (A_{290}) in 260 μM O_2 (aerobic) and about 10 μM O_2 (anaerobic) in the absence or presence of SOD (100 μg mL^{-1}). B, Decrease of O_2 concentration during the oxidation of MDH_2. C and D, Reduction of XTT (200 μM; C) or Cyt *c* (200 μM; D) added to 100 μM MDH_2 aerobically or anaerobically.

form) is well known in chemistry (Brunmark and Cadenas, 1989). A general scheme illustrating the reactions involved in MDH_2 autoxidation via the semiquinone ($MD^{\cdot-}$) intermediate state is depicted in Figure 12. MDH_2 produced by NQR (reaction 1) and activated by deprotonation at pH ≥ 6.5 (reaction 2) can undergo conversion to MD via two routes (A and B) involving three one-electron-transferring reactions (Cadenas, 1995):

$$MD^{2-} + O_2 \rightarrow MD^{\cdot-} + O_2^{\cdot-} \quad (3)$$

$$MD^{2-} + O_2^{\cdot-} + 2H^+ \rightarrow MD^{\cdot-} + H_2O_2 \quad (4)$$

$$MD^{\cdot-} + O_2 \rightarrow MD + O_2^{\cdot-} \quad (5)$$

After initiation by reaction 3, autoxidation can be propagated through the redox cycle of route B, reaching a steady-state rate after overcoming a lag phase (compare with. Figs. 4A and 11, A and B). If present, XTT reacts with $O_2^{\cdot-}$ according to:

$$O_2^{\cdot-} + \tfrac{1}{2}XTT + H^+ \rightarrow O_2 + \tfrac{1}{2}XTTH_2 \quad (6)$$

Moreover, the data from Figures 10 and 11 demonstrate that XTT can replace O_2 by reacting either with MD^{2-} or with $MD^{\cdot-}$:

$$MD^{2-} + H^+ + \tfrac{1}{2}XTT \rightarrow MD^{\cdot-} + \tfrac{1}{2}XTTH_2 \quad (7)$$

or

$$MD^{\cdot-} + H^+ + \tfrac{1}{2}XTT \rightarrow MD + \tfrac{1}{2}XTTH_2 \quad (8)$$

Because of the negative standard redox potential of the $MD^{\cdot-}$/MD couple (−203 mV) compared with the $MD^{2-}/MD^{\cdot-}$ couple (+193 mV; Öllinger et al., 1990), reaction 8 will be thermodynamically strongly favored over reaction 7. However, in either case, only 50% of the XTT will be reduced via $O_2^{\cdot-}$ (reaction 6) and route B will be shut off due to the lack of $O_2^{\cdot-}$. This explains the finding that the overall reaction can be inhibited by 50% with SOD (compare with Table IV; Figs. 9B and 10B). The lower inhibitory effect of SOD in the case of Cyt *c* (Fig. 10C) could be due to the ability of this acceptor to react to some extent with both MD^{2-} and $MD^{\cdot-}$. Evidently, XTT and Cyt *c* reduction specifically detect $O_2^{\cdot-}$ production only to the extent that can be inhibited by SOD.

The autoxidation of the hydroquinones is affected by SOD in various ways (Öllinger et al., 1990). As shown in Figure 11A, SOD causes a partial inhibition of the O_2-limited MDH_2 oxidation. The removal of $O_2^{\cdot-}$ eliminated electron flow through route B. No effect of SOD on NADPH oxidation, MDH_2 accumulation, and O_2 consumption was detected in the much slower autoxidation reaction limited by the enzymatic production of MDH_2 (Table IV), suggesting that $O_2^{\cdot-}$ had no major influence on autoxidation under these conditions.

Similar to SOD, electron acceptors such as XTT or Cyt *c* will decrease the concentration of $O_2^{\cdot-}$ in the reaction system, shutting down route B. Nevertheless, electron flow is strongly enhanced even at very low O_2 concentrations (Fig. 11, C and D). These results show that route A is sufficient to mediate rapid electron flow provided that suitable sinks are available to remove $O_2^{\cdot-}$ and $MD^{\cdot-}$.

Potential Function of NQR in the Plasma Membrane of Intact Cells

Based on their biochemical properties, quinones and their reduced forms can exhibit both antioxidant and prooxidant activities. For example, linoleic acid autoxidation can be inhibited by phylloquinone and enhanced by phyllohydroquinone (Canfield et al., 1985). With respect to their biological functions in animal cells, cytosolic two-electron-transferring quinone reductases are often considered to act as antioxidant enzymes, protecting the cell against the harmful accumulation of quinones that can produce toxic radicals upon reduction by one-electron-transferring reductases (Lind et al., 1982; Cadenas, 1995; Ross, 1997). In plants, an antioxidant function of two-electron-transferring quinone reductases was recently supported by the observation that the expression of these enzymes can be upregulated in vivo under stress conditions that involve the formation of toxic oxidants (Matvienko et al., 2001; Greenshields et al., 2005). On the other hand, the supposition that these enzymes generally serve as antioxidant tools to protect against quinone toxicity has been challenged on the ground that redox-labile hydroquinones can autoxidize in vivo with the

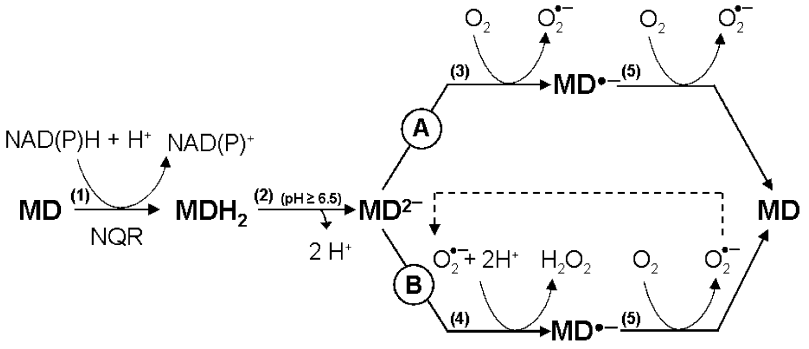

Figure 12. Redox chemistry involved in the MD-mediated univalent reduction of O_2 by route A and route B. Reaction 1, Divalent enzymatic reduction of MD to MDH_2 by NQR; reaction 2, activation of MDH_2 by deprotonation; reaction 3, univalent oxidation of MD^{2-}, producing $MD^{\cdot-}$ (semiquinone) by reducing O_2 to $O_2^{\cdot-}$; reaction 4, univalent oxidation of MD^{2-}, producing $MD^{\cdot-}$ by reducing $O_2^{\cdot-}$ to H_2O_2; reaction 5, oxidation of $MD^{\cdot-}$ by reducing O_2 to $O_2^{\cdot-}$.

formation of reactive oxygen species, including hydroxyl radicals (Nutter et al., 1992; Dicker and Cederbaum, 1993; Cadenas, 1995). The plasma membrane plays an important role as a site of $O_2^{\cdot -}$ and H_2O_2 generation, serving functions such as cell wall expansion or pathogen defense. Although this performance is often ascribed to NOX-type enzymes (Gapper and Dolan, 2006), alternative sources of reactive oxygen species cannot be excluded. This is especially true in those cases in which $O_2^{\cdot -}$ production cannot be inhibited by even high concentrations of DPI and in which a significant part of XTT or Cyt *c* reduction is resistant to inhibition by SOD. Examples of striking DPI insensitivity of $O_2^{\cdot -}$ production or transmembrane electron transport by plasma membrane vesicles have been reported (Menckhoff and Lüthje, 2004; Mojović et al., 2004). As shown here, the NQR purified from plasma membranes has a potential to elicit $O_2^{\cdot -}$ production, unaffected by DPI, if supplied with a quinone substrate such as MD. Autoxidation of the hydroquinone produced in this way can lead directly to $O_2^{\cdot -}$ and H_2O_2 formation. Alternatively, coupling of $O_2^{\cdot -}$ generation to hydroquinone oxidation could be accomplished by peroxidase at the apoplastic side of the plasma membrane. Ohnishi et al. (1969) have shown that horseradish peroxidase catalyzes the conversion of hydroquinones to semiquinone radicals in the presence of H_2O_2, even at acidic pH not permitting autoxidation. In both cases, a low-potential cytochrome as a one-electron donor for the reduction of O_2 would be unnecessary. A low-potential *b*-type cytochrome is an essential component of NOX enzymes but in fact has never been detected in plasma membranes of plants (Bérczi and Møller, 2000). Quinones such as ubiquinone or plastoquinone function as lipid-soluble, mobile electron carriers in mitochondrial or thylakoid membranes, suggesting a similar condition in the plasma membrane (Barr et al., 1992). Specifically, this property could be utilized to mediate an electron transport from NAD(P)H oxidation by NQR at the cytoplasmic face to O_2 reduction at the apoplastic face of the plasma membrane. In this case, only catalytic amounts of quinone would be required, which undergo redox cycling and thereby transport electrons (and protons) across the membrane, in agreement with the net equation describing the reaction catalyzed by NOX:

$$\mathrm{NAD(P)H} + 2\,\mathrm{O_2} \rightarrow \mathrm{NAD(P)^+} + \mathrm{H^+} + 2\,\mathrm{O_2^{\cdot -}}$$

Basic questions arising in this context concern the access to substrates and the environmental conditions for the activity of NQR in or at the plasma membrane in vivo. These questions are still wide open. Nevertheless, several findings have been reported hinting at a redox-mediating function of quinones also in the plasma membrane (e.g. the inhibition of electron transport processes by ''vitamin K antagonists'' such as dicumarol; Döring et al., 1992; Lüthje et al., 1994). Although MD (vitamin K_3) is not a normal constituent of the plasma membrane, a substance with the chromatographic and spectroscopic properties of phylloquinone (menadione with a phytyl side chain, vitamin K_1) has been isolated from plasma membrane preparations of maize roots (Lüthje et al., 1998; Lochner et al., 2003). Phylloquinone serves as an electron transfer component in PSI of photosynthesis (Brettel, 1997). Unfortunately, the solubility of phylloquinone in water is extremely low, preventing a direct test of its activity as a substrate for NQR in aqueous solution (compare with Table III). The reactivity of the prenylmenadione derivatives (vitamin K series) with DT-diaphorase in aqueous solution decreases with the length of their prenyl side chain and parallel to their insolubility in water (Märki and Martius, 1960). This suggests that in lipophilic surroundings, phylloquinone can act as a substrate for NQR. It has indeed been demonstrated that phylloquinone is easily reduced by the DT-diaphorase if it is incorporated into the membrane of liposomes and thus can transport electrons from the outside to the inside of this vesicle (Martius et al., 1975).

MATERIALS AND METHODS

Materials

Seedlings of soybean (*Glycine max* 'Jutro') were grown on wet vermiculite in darkness for 4.5 d at 25°C. The top 2 cm of the hypocotyl was excised and used for plasma membrane preparation.

Chemicals were obtained from Merck (polyethylene glycol 6000), Sigma or Aldrich (quinones, horseradish peroxidase, Cibacron 3G-A, dicumarol, DPI, nitrofurantoin, rotenone, piericidin A, *N*-ethylmaleimide, 4-chloromercuribenzoate, quinacrine, and bicinchoninic acid), Amersham Bioscience (Blue Sepharose 6 Fast Flow), Pharmacia (Superdex 200 HR 10/30 column), Roche Biochemicals (Cyt *c*, Cu/Zn-SOD, and catalase), and Polyscience (XTT).

MDH_2 was synthesized after Fieser et al. (1939) and purified by silica gel chromatography.

Quinone stock solutions (100 mM) were prepared in dimethyl sulfoxide or ethanol (vitamins K_1 and K_2), diluted with assay buffer to 1 mM, and used within the next 2 h. Juglone solutions had to be kept in darkness to prevent disintegration. MDH_2 was dissolved in water-free ethanol and added directly to the reaction medium.

Preparation and Solubilization of Plasma Membranes

The procedure devised by Thein and Michalke (1988) was adopted with some modifications. Batches (100 g) of hypocotyl segments were homogenized with a blender in 400 mL of cold medium containing 10 mM Tris-HCl (pH 8.0), 20 mM Na_2EDTA, 300 mM NaCl, 0.5 mM phenylmethylsulfonyl fluoride, and 1 g L^{-1} bovine serum albumin. After filtering the slurry through nylon cloth, a membrane fraction was isolated by differential centrifugation (30 min at 1,500*g*, 45 min at 100,000*g*, 4°C) and resuspended in 180 mL of medium (without phenylmethylsulfonyl fluoride and albumin). Intracellular membranes were precipitated by adding 0.043 g mL^{-1} polyethylene glycol 6000 and stirring for 30 min on ice. After removing the precipitate by centrifugation (30 min at 1,500*g*, 4°C), the plasma membranes contained in the supernatant were pelleted (45 min at 100,000*g*, 4°C), resuspended in 3 mL of 20 mM HEPES (pH 7.8) containing 20 mM Na_2EDTA and 250 mM Suc, and stored at −70°C.

The purity of the isolated membrane fraction was ascertained by separating the proteins of the different fractions by SDS-PAGE followed by semidry blotting on polyvinylidene difluoride membranes and decoration of the membranes with specific polyclonal antibodies directed against the Rieske protein (mitochondria) and the plasma membrane P-ATPase. The plasma membrane fraction showed the strongest signal with the anti-P-ATPase antibodies and no signal with the anti-Rieske antibodies, indicating that there

was no detectable contamination by mitochondrial membranes (Supplemental Fig. S1). Conventional two-phase partitioning (Larsson et al., 1994) of microsomes resulted in a plasma membrane fraction with very similar properties if tested according to these criteria.

The cytosolic protein fraction was prepared from the homogenate by removing insoluble material by centrifugation (45 min at 100,000*g*, 4°C).

Membrane localization of the oxidoreductase activity was tested by incubating plasma membranes in 1.5 M $CaCl_2$ or 1.5 M NaCl for 1 h at 4°C in 20 mM HEPES (pH 7.8), followed by washing three times with the same buffer.

Plasma membrane suspensions were solubilized by adding an equal volume of 4% (w/v) Tween 20 and incubating for 30 min at 30°C. After clearing by centrifugation (15 min at 12,000*g*), the enzyme solution could be stored at −70°C without loss of activity for several months. The contamination of the solubilized plasma membrane fraction with soluble proteins was estimated by measuring the activity of the cytosolic marker enzyme Glc-6-P dehydrogenase. The concentration of the Glc-6-P dehydrogenase in the membrane fraction was about 5% of the concentration expected if the membrane vesicles contained the same concentration as the cytosolic tissue fraction.

Protein Determination

The protein contents of enzyme extracts were estimated with the bicinchoninic acid procedure as described by Kaushal and Barnes (1986) using bovine serum albumin as a standard. This method provides reliable results in the presence of detergents such as Tween 20 at protein concentrations of ≥ 1 μg mL^{-1}.

Enzyme Assays

Photometric measurements of reaction rates at specific wavelengths allowed the determination of XTT reduction, NAD(P)H oxidation, and hydroquinone accumulation in mixtures of these components. The standard assay mixture contained 200 μM NADPH, 100 μM MD, 100 μM XTT, and enzyme extract (start of reaction) in 20 mM HEPES (pH 7.5) in a total volume of 500 μL (25°C). XTT reduction was measured at 470 nm (ε_{470} = 24.2 mM^{-1} cm^{-1}) or 550 nm (ε_{550} = 9.8 mM^{-1} cm^{-1}) for 1 to 2 min. NADPH oxidation was measured at 340 nm (ε_{340} = 6.21 mM^{-1} cm^{-1}) and corrected for absorbance changes caused by XTT reduction (ε_{340} = 5.4 mM^{-1} cm^{-1}). Absorbance changes due to MD reduction at 340 nm (ε_{340} = −0.09 mM^{-1} cm^{-1}) are negligible. Because of overlapping absorbance spectra, the determination of coupled NADPH oxidation and MDH_2 accumulation (in the absence of XTT) required measurements at two wavelengths (290 and 340 nm) and mathematical separation of the two partial reactions using the following formulas (1-cm cuvette):

$$\Delta C_{NADPH} = -0.160\,\Delta A_{340} - 0.0066\,\Delta A_{290}$$

$$\Delta C_{MDH2} = 0.456\,\Delta A_{290} - 0.0675\,\Delta A_{340}$$

Suitable wavelengths pairs and extinction coefficients for corresponding measurements with other quinones were determined from difference spectra (oxidized → reduced) as outlined in Supplemental Appendix S1. Modifications of the standard assays are described in the figure legends.

FeCN (500 μM) reduction was measured at 420 nm (ε_{420} = 1.02 mM^{-1} cm^{-1}). DCPIP (30 μM) reduction was measured at 600 nm (ε_{600} = 22.0 mM^{-1} cm^{-1}). Cyt *c* (50 μM) reduction was measured at 550 nm (ε_{550} = 21.0 mM^{-1} cm^{-1}).

Anaerobic conditions during the enzyme reaction were obtained by evacuating the reaction mixture followed by gassing with argon. This lowered the O_2 concentration by about 96% (10 μM).

Peroxidase activity was measured at 25°C either with 8.3 mM guaiacol and 8.8 mM H_2O_2 in 50 mM citrate-NaOH at pH 5.0 (470 nm, ε_{470} = 26.6 mM^{-1} cm^{-1}; Mika and Lüthje, 2003) or with 100 μM 3,3′,5,5′-tetramethylbenzidine and 5 mM H_2O_2 in the same buffer at pH 4.5 (654 nm, ε_{654} = 39 mM^{-1} cm^{-1}; Imberty et al., 1984). Tested with horseradish peroxidase (Sigma type VI; 300 purpurogallin units mg^{-1} protein), the detection limits of these assays were 1 ng and 10 pg, respectively, in 1 mL of reaction mixture.

Oxygen consumption was measured with a Clark-type oxygen electrode using 2 mL of standard assay mixture (25°C).

PAGE and Western Blotting

SDS-PAGE was carried out in 8% polyacrylamide. Proteins were visualized by silver staining. Native PAGE was carried out using 0.1% CHAPS instead of SDS. The sample buffer contained 40 mM Tris-HCl (pH 7.8), 0.1% CHAPS, 10% glycerol, and 0.002% bromphenol blue. Samples were mixed with sample buffer in a 2:1 ratio. The running buffer contained 25 mM Tris, 1.44% Gly, and no detergent. Gels were incubated for 20 min in 50 mM Tris-HCl (pH 7.4), 0.2 mM NBT, 0.1 mM $MgCl_2$, and 1 mM $CaCl_2$ in the dark. The reaction was started after 20 min of preincubation by adding 0.2 mM NADH and 0.1 mM MD and continued for approximately 15 min.

Proteins were transferred onto nitrocellulose (SDS-PAGE) or polyvinylidene difluoride (native PAGE) membranes by semidry blotting using a Multiphor II Novablot unit (Amersham Bioscience). For detection, the ECL system (Amersham Bioscience) was used according to the manufacturer's protocol.

Protein Identification by HPLC-Electrospray Mass Spectrometry

The NBT-stained region of a native PAGE gel derived from a sample of purified plasma membrane oxidoreductase (Fig. 7A, lane 3) was cut into 10 horizontal 2-mm strips that were processed individually to establish abundance profiles of the identified peptides. After destaining the gel slices and reduction of proteins by 10 mM 1,4-dithiothreitol, Cys residues were modified by iodoacetamide at a final concentration of 55 mM for 30 min at room temperature. After washing in 5 mM NH_4HCO_3 and dehydration by ethanol, 0.25 μg of trypsin (Promega) in 5 mM NH_4HCO_3 was added to each sample and incubated on ice for 20 min. The buffer was exchanged to 5 mM NH_4HCO_3, and digestion was done overnight at 37°C. Peptides were extracted successively with 0.1% formic acid and acetonitrile, dried, and resuspended in 3% acetonitrile and 0.1% formic acid.

Peptide mixtures were separated for nano-LC-electrospray ionization-MS/MS using a FAMOS autosampler (Dionex), an Ultimate inert HPLC system (Dionex), and an Agilent HPLC 1100 pump connected to the nano-electrospray ionization source of a Finnigan LTQ-FT (Thermo Electron Corporation) for online mass detection. Peptides were first collected on a trap column (0.1 × 15 mm, Zorbax Eclipse XDB-C18, 5 μm; Agilent Technology) for desalting and concentrating followed by separation on an analytical column made up by fused silica emitters (0.075 × 105 mm, 6 μm; Proxeon Biosystems) filled with Hydrosphere C18, 3 μm (YMC). Peptides were eluted during a 60-min gradient using 97% water, 3% acetonitrile, and 0.1% formic acid as solvent A and 80% acetonitrile, 20% water, and 0.1% formic acid as solvent B at a flow rate of 0.15 μL min^{-1}.

Mass spectrometric detection consisted of full scans at a resolution of 25,000 followed by data-dependent selected ion scans at a resolution of 50,000 and low-resolution MS/MS scans using a dynamic exclusion of parent ion masses for 60 s.

The MS and MS/MS spectra were searched against the soybean EST assembly from PlantGDB (Dong et al., 2005; release October 2007, based on GenBank release 161) and soybean and Arabidopsis (*Arabidopsis thaliana*) proteins from the uniprot database (release 12.4, October 2007) using an in-house installation of the program OMSSA (Geer et al., 2004; version 2.1). Search results were filtered and sorted using in-house-written software (F. Drepper, unpublished data). Peptide hits were considered significant if the precursor and product ion masses matched within 2 ppm and 0.5 relative mass units, respectively, and if the E-value was below 0.01.

Statistics

Data represent means or representative examples from measurements repeated three to six times. Typical SE values are shown in Figure 5 and Tables I, III, and IV but omitted in other figures for the sake of clarity.

Supplemental Data

The following materials are available in the online version of this article.

Supplemental Figure S1. Comparison of two methods of plasma membrane preparation.

Supplemental Table S1. NQR sequence alignment.

Supplemental Appendix S1. Formulas and extinction coefficients used for the determination of NAD(P)H oxidation and quinone reduction in NADPH/quinone mixtures.

ACKNOWLEDGMENTS

We are grateful to K. Kienzler and B. Knapp (both Universität Freiburg) for excellent technical assistance; Dr. W. Seiche (Universität Freiburg) for synthesizing menadionehydroquinone; Drs. F. Sparla and P. Trost (Università di Bologna) for stimulating discussions and provision of NQR antibodies and AtNQR recombinant protein; and Dr. M. Laskowski (Oberlin College), Dr. W. Michalke (Universität Freiburg), and Dr. U. Schulte (Universität Düsseldorf) for providing antibodies directed against FQR1, P-ATPase, and Rieske protein, respectively. Special thanks are due to Dr. W. Haehnel (Universität Freiburg) for placing his mass spectrometry facilities at our disposal.

Received March 5, 2008; accepted April 8, 2008; published April 11, 2008.

LITERATURE CITED

Able AJ, Guest DI, Sutherland MW (1998) Use of a new tetrazolium-based assay to study the production of superoxide radicals by tobacco cell cultures challenged with avirulent zoospores of *Phytophthora parasitica* var *nicotinae*. Plant Physiol **117:** 491–499

Agarwal R, Bonanno JB, Burley SK, Swaminathan S (2006) Structure determination of an FMN reductase from Pseudomonas aeruginosa PA01 using sulphur anomalous signal. Acta Crystallogr D Biol Crystallogr **62:** 383–391

Barr R, Pan RS, Crane FL, Brightman AO, Morré DJ (1992) Destruction of vitamin K_1 of cultured carrot cells by ultraviolet radiation and its effect on plasma membrane electron transport reactions. Biochem Int **27:** 449–456

Bateman A, Sandford R (1999) The PLAT domain: a new piece in the PKD1 puzzle. Curr Biol **9:** 588–590

Bérczi A, Møller IM (1998) NADH-monodehydroascorbate oxidoreductase is one of the redox enzymes in spinach leaf plasma membranes. Plant Physiol **116:** 1029–1036

Bérczi A, Møller IM (2000) Redox enzymes in the plant plasma membrane and their possible roles. Plant Cell Environ **23:** 1287–1302

Bienfait F, Lüttge U (1988) On the function of two systems that can transfer electrons across the plasma membrane. Plant Physiol Biochem **26:** 665–671

Brettel K (1997) Electron transfer and arrangement of the redox cofactors in photosystem I. Biochim Biophys Acta **1318:** 322–373

Brunmark A, Cadenas E (1989) Redox and addition chemistry of quinoid compounds and its biological implications. Free Radic Biol Med **7:** 435–477

Buffinton GD, Öllinger K, Brunmark A, Cadenas E (1989) DT-diaphorase-catalysed reduction of 1,4-naphthoquinone derivatives and glutathionyl-quinone conjugates: effect of substituents on autoxidation rates. Biochem J **257:** 561–571

Cadenas E (1995) Autoxidant and prooxidant functions of DT-diaphorase in quinone metabolism. Biochem Pharmacol **49:** 127–140

Canfield LM, Davy LA, Thomas GL (1985) Anti-oxidant/pro-oxidant reactions of vitamin K. Biochem Biophys Res Commun **128:** 211–219

Cross AR (1987) The inhibitory effects of some iodonium compounds on the superoxide generating system of neutrophils and their failure to inhibit diaphorase activity. Biochem Pharmacol **36:** 489–493

Dicker E, Cederbaum AI (1993) Requirement for iron for the production of hydroxyl radicals by rat liver quinone reductase. J Pharmacol Exp Ther **266:** 1282–1290

Döring O, Lüthje S, Böttger M (1992) Inhibitors of the plasma membrane redox system of *Zea mays* L. roots: the vitamin K antagonists dicumarol and warfarin. Biochim Biophys Acta **1110:** 235–238

Dong Q, Lawrence CJ, Schlueter SD, Wilkerson MD, Kurtz S, Lushbough C, Brendel V (2005) Comparative plant genomics resources at PlantGDB. Plant Physiol **139:** 610–618

Doussiere J, Gaillard J, Vignais PV (1999) The heme component of the neutrophil NADPH oxidase complex is a target for aryliodonium compounds. Biochemistry **38:** 3694–3703

Doussiere J, Vignais PV (1992) Diphenylene iodonium as an inhibitor of the NADPH oxidase complex of bovine neutrophils. Factors controlling the inhibitory potency of diphenylene iodonium in a cell-free system of oxidase activation. Eur J Biochem **208:** 61–71

Ernster L, Danielson L, Ljunggren M (1962) DT diaphorase. I. Purification from the soluble fraction of rat liver cytoplasm, and properties. Biochim Biophys Acta **58:** 171–188

Fieser LF, Campbell WP, Fry EM, Gates MD (1939) Naphthoquinones of the vitamin K_1 type of structure. J Am Chem Soc **61:** 3216–3223

Frahry G, Schopfer P (1998) Inhibition of O_2-reducing activity of horseradish peroxidase by diphenyleneiodonium. Phytochemistry **48:** 223–227

Gapper C, Dolan L (2006) Control of plant development by reactive oxygen species. Plant Physiol **141:** 341–345

Geer LY, Markey SP, Kowalak JA, Wagner L, Xu M, Maynard DM, Yang X, Shi W, Bryant SH (2004) Open mass spectrometry search algorithm. J Proteome Res **3:** 958–964

Greenshields DL, Liu G, Selvaray GLG, Wei Y (2005) Differential regulation of wheat quinone reductases in response to powdery mildew infection. Planta **222:** 867–875

Imberty A, Goldberg R, Catesson AM (1984) Tetramethylbenzidine and *p*-phenylenediamine-pyrocatechol for peroxidase histochemistry and biochemistry: two new, non-carcinogenic chromogens for investigating lignification processes. Plant Sci Lett **35:** 103–108

Iyanagi T, Yamazaki I (1970) One-electron-transfer reactions in biological systems. V. Difference in the mechanism of quinone reduction by the NADH dehydrogenase and the NAD(P)H dehydrogenase (DT-diaphorase). Biochim Biophys Acta **216:** 282–294

Kaushal V, Barnes LD (1986) Effect of zwitterionic buffers on measurements of small masses of protein with bicinchoninic acid. Anal Biochem **157:** 291–294

Keller T, Damude HG, Werner D, Doerner P, Dixon RA, Lamb C (1998) A plant homolog of the neutrophil NADPH oxidase $gp91^{phox}$ subunit gene encodes a plasma membrane protein with Ca^{2+} binding motifs. Plant Cell **10:** 255–266

Kobayashi M, Kawakita K, Maeshima M, Doke N, Yoshioka H (2006) Subcellular localization of Strboh proteins and NADPH-dependent O_2^--generating activity in potato tissues. J Exp Bot **57:** 1373–1379

Larsson C, Sommarin M, Widell S (1994) Isolation of highly purified plant plasma membranes and separation of inside-out and right-side-out vesicles. Methods Enzymol **228:** 451–469

Laskowski MJ, Dreher KA, Gehring MA, Abel S, Gensler AL, Sussex IM (2002) *FQR1*, a novel primary auxin-response gene, encodes a flavin mononucleotide-binding quinone reductase. Plant Physiol **128:** 578–590

Lind C, Cadenas E, Hochstein P, Ernster L (1990) DT-diaphorase: purification, properties, and function. Methods Enzymol **186:** 287–301

Lind C, Hochstein P, Ernster L (1982) DT-diaphorase as a quinone reductase: a cellular device against semiquinone and superoxide radical formation. Arch Biochem Biophys **216:** 178–185

Lochner K, Döring O, Böttger M (2003) Phylloquinone, what can we learn from plants? Biofactors **18:** 73–78

Luster DG, Buckhout TJ (1989) Purification and identification of a plasma membrane associated electron transport protein from maize (*Zea mays* L.) roots. Plant Physiol **91:** 1014–1019

Lüthje S (2007) Plasma membrane redox systems: lipid rafts and protein assemblies. Prog Bot **69:** 169–200

Lüthje S, González-Reyes JA, Navas P, Döring O, Böttger M (1994) Inhibition of maize (*Zea mays* L.) root plasma membrane-bound redox activities by coumarins. Z Naturforsch **49c: 447–452**

Lüthje S, van Gestelen P, Córdoba-Pedregosa MC, González-Reyes JA, Asard H, Villalba JM, Böttger M (1998) Quinones in plant plasma membranes: a missing link? Protoplasma **205:** 43–51

Märki F, Martius C (1960) Vitamin K-Reduktase, Darstellung und Eigenschaften. Biochem Z **333:** 111–135

Martius C, Ganser R, Viviani A (1975) The enzymatic reduction of K-vitamins incorporated in the membrane of liposomes. FEBS Lett **59:** 13–14

Matvienko M, Wojtowicz A, Wrobel R, Jamison D, Goldwasser Y, Yoder JI (2001) Quinone oxidoreductase message levels are differentially regulated in parasitic and non-parasitic plants exposed to allelopathic quinones. Plant J **25:** 375–387

Menckhoff M, Lüthje S (2004) Transmembrane electron transport in sealed and NAD(P)H-loaded right-side-out plasma membrane vesicles isolated form maize (*Zea mays* L.) roots. J Exp Bot **55:** 1343–1349

Mika A, Lüthje S (2003) Properties of guaiacol peroxidase activities isolated from corn root plasma membranes. Plant Physiol **132:** 1489–1498

Mojović M, Vuletić M, Bačić GG, Vučinić Z (2004) Oxygen radicals produced by plant plasma membranes: an EPR spin-trap study. J Exp Bot **55:** 2523–2531

Murphy TM, Auh CK (1996) The superoxide synthases of plasma membrane preparations from cultured rose cells. Plant Physiol **110:** 621–629

Murphy TM, Vu H, Nguyen T, Woo CH (2000) Diphenylene iodonium sensitivity of a solubilized membrane enzyme from rose cells. Protoplasma **213:** 228–234

Nutter LM, Ngo EO, Fisher GR, Gutierrez PL (1992) DNA strand scission and free radical production in menadione-treated cells. Correlation with cytotoxicity and role of NADPH quinone acceptor oxidoreductase. J Biol Chem **267:** 2474–2479

O'Donnell VB, Smith GCM, Jones OTG (1994) Involvement of phenyl radicals in iodonium compound inhibition of flavoenzymes. Mol Pharmacol **46:** 778–785

Ohnishi T, Yamazaki H, Iyanagi T, Nakamura T, Yamazaki I (1969) One-electron-transfer reactions in biochemical systems. II. The reaction of free radicals formed in the enzymic oxidation. Biochim Biophys Acta **172:** 357–369

Öllinger K, Buffinton GD, Ernster L, Cadenas E (1990) Effect of superoxide dismutase on the autoxidation of substituted hydro- and seminaphthoquinones. Chem Biol Interact **73:** 53–76

Patridge EV, Ferry JG (2006) WrbA from *Escherichia coli* and *Archaeoglobus fulgidus* is an NAD(P)H:quinone oxidoreductase. J Bacteriol **188:** 3498–3506

Prestera T, Prochaska HJ, Talalay P (1992) Inhibition of NAD(P)H:(quinone-acceptor) oxidoreductase by Cibacron blue and related anthraquinone dyes: a structure-activity study. Biochemistry **31:** 824–833

Prochaska HJ, Santamaria AB (1988) Direct measurement of NAD(P)H: quinone reductase from cells cultured in microtiter wells: a screening assay for anticarcinogenic enzyme inducers. Anal Biochem **169:** 328–336

Ragan CI, Bloxham DP (1977) Specific labelling of a constituent polypeptide of bovine heart mitochondrial reduced nicotinamide-adenine-dinucleotide-ubiquinone reductase by the inhibitor diphenyleneiodonium. Biochem J **163:** 605–615

Rescigno A, Sollai F, Masala S, Porcu MC, Sanjust E, Rinaldi AC, Curreli N, Grifi D, Rinaldi A (1995) Purification and characterization of an NAD(P)H:quinone oxidoreductase from *Glycine max* seedlings. Prep Biochem **25:** 57–67

Ross D (1997) Quinone reductases. *In* FP Guengrich, ed, Comprehensive Toxicology, Vol 3. Pergamon Press, New York, pp 179–197

Sagi M, Fluhr R (2001) Superoxide production by plant homologues of the gp91^{phox} NADPH oxidase: modulation of activity by calcium and by tobacco mosaic virus infection. Plant Physiol **126:** 1281–1290

Serrano A, Córdoba F, González-Reyes JA, Navas P, Villalba JM (1994) Purification and characterization of two distinct NAD(P)H dehydrogenases from onion (*Allium cepa* L.) root plasma membrane. Plant Physiol **106:** 87–96

Simon-Plas F, Elmayan T, Blein J-P (2002) The plasma membrane oxidase NtrbohD is responsible for AOS production in elicited tobacco cells. Plant J **31:** 137–147

Sparla F, Tedeschi G, Pupillo P, Trost P (1998) Molecular characterization of NAD(P)H:quinone oxidoreductase of tobacco leaves. Protoplasma **205:** 52–58

Sparla F, Tedeschi G, Pupillo P, Trost P (1999) Cloning and heterologous expression of NAD(P)H:quinone reductase of *Arabidopsis thaliana*, a functional homologue of animal DT-diaphorase. FEBS Lett **463:** 382–386

Sparla F, Tedeschi G, Trost P (1996) NAD(P)H:(quinone acceptor) oxidoreductase of tobacco leaves is a flavin mononucleotide-containing flavoenzyme. Plant Physiol **112:** 249–258

Spitsberg VL, Coscia CJ (1982) Quinone reductases of higher plants. Eur J Biochem **127:** 67–70

Strain HH, Svec WA (1966) Extraction, separation, estimation and isolation of the chlorophylls. *In* LP Vernon, GR Seely, eds, The Chlorophylls. Academic Press, New York, pp 21–66

Sumimoto H, Miyano K, Takeya R (2005) Molecular composition and regulation of the Nox family NAD(P)H oxidases. Biochem Biophys Res Commun **338:** 677–686

Thein M, Michalke W (1988) Bisulfite interacts with binding sites of the auxin-transport inhibitor N-1-napthylphtalamic acid. Planta **176:** 343–350

Torres MA, Dangl JL (2005) Functions of the respiratory burst oxidase in biotic interactions, abiotic stress and development. Curr Opin Plant Biol **8:** 397–403

Trost P, Bonora P, Scagliarini S, Pupillo P (1995) Purification and properties of NAD(P)H:(quinone acceptor) oxidoreductase of sugarbeet cells. Eur J Biochem **234:** 452–458

Trost P, Foscarini S, Preger V, Bonora P, Vitale L, Pupillo P (1997) Dissecting the diphenylene iodonium-sensitive NAD(P)H:quinone oxidoreductase of zucchini plasma membrane. Plant Physiol **114:** 737–746

Valenti V, Guerrini F, Pupillo P (1990) NAD(P)H-duroquinone reductase in the plant plasma membrane. J Exp Bot **41:** 183–192

van Gestelen P, Asard H, Caubergs RJ (1997) Solubilization and separation of a plant plasma membrane NADPH-O_2^- synthase from other NAD(P)H oxidoreductases. Plant Physiol **115:** 543–550

van Gestelen P, Asard H, Horemans N, Caubergs RJ (1998) Superoxide-producing NAD(P)H oxidases in plasma membrane vesicles from elicitor responsive bean plants. Physiol Plant **104:** 653–660

Vuletić M, Šukalović VHT, Vučinić Ž (2003) Superoxide synthase and dismutase activity of plasma membranes from maize roots. Protoplasma **221:** 73–77

Vuletić M, Šukalović VHT, Vučinić Ž (2005) The coexistence of the oxidative and reductive systems in roots: the role of plasma membranes. Ann N Y Acad Sci **1048:** 244–258

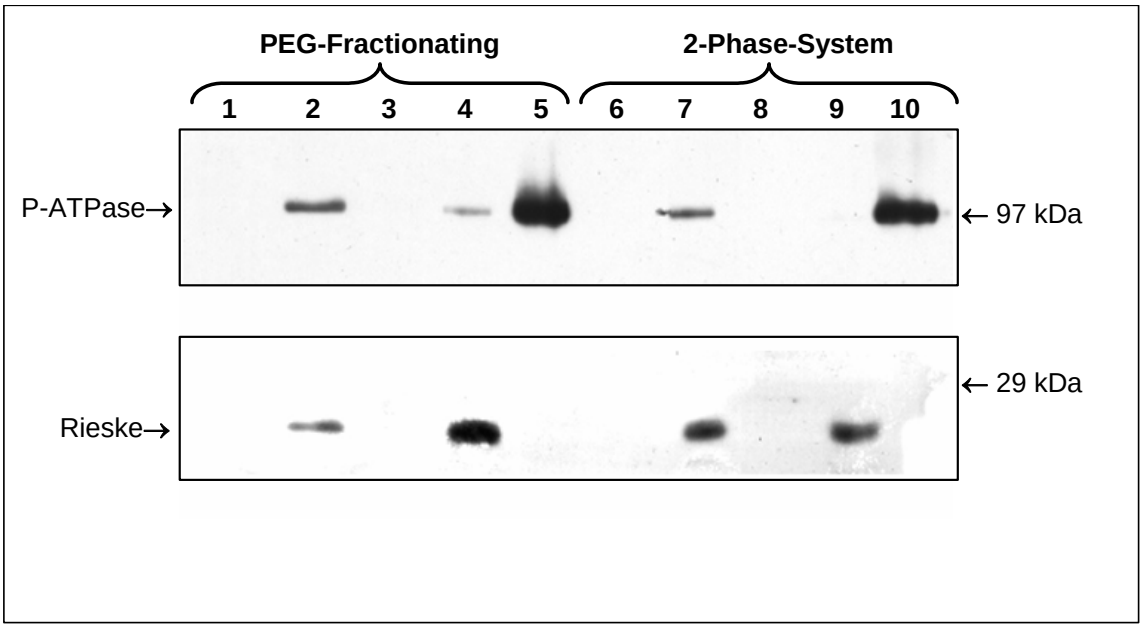

Fig. S1. Comparison of two methods of plasma membrane preparation.
Immunoblots of protein fractions prepared by PEG-fractionation according to Thein and Michalke (1988) or by dextran-PEG 2-phase system according to Larsson et al. (1994). Homogenate (1, 6), microsome fraction (2, 7), soluble protein fraction (3, 8), intracellular membrane vesicles (4, 9), plasma membrane fraction (5, 10). Samples containing 20 µg protein were loaded on the gel. Immunoblots were decorated with antibodies directed against P-ATPase and Rieske protein. Marker positions [kDa] are given on the right side.

Table S1

Multiple sequence alignment (CLUSTAL W 1.83) of plant NQR sequences from *Arabidopsis*, *Vitis vinifera* (Grape), *Glycine max* (soybean), *Solanum tuberosum* (potato) and *Oryza sativa* (rice). Peptides from the predicted soybean NQR identified by mass spectrometry are underlined. The FMN binding motif is shown in gray.

```
                                          ←  FMN  →
Q9LK88|NQR_ARATH                1 MEAVTAIKP-LIRVAALSGSLRKTSFHTGLLRAAIDLTKESVPGLQIEYI 49
A5AS03|A5AS03_VITVI             1 MAAAIEVQP-VIKVAALCGSLRKASFNRGLIRSAIKISKEAINGMEIEYV 49
PUT-161a-Glycine_max-35276     15 MAAVAGASSSVIKVAALSGSLRKGSYNRALIRSAIELSQGRVEGLQIEYV 64
Q8H9D2|NQR_SOLTU                1 ----MAAQP-VIKVAGLCGSLRKGSYNRGLLNAAMEICKDSITGMEIEYV 45
Q941Z0|NQR1_ORYSJ               1 --MEAAAARPVIRVAAICGSLRKASYNGGLLRAAAGVCEESIPGLRVDHV 48
Q941Y8|NQR2_ORYSJ               1 --MEGSTSPKALRVAAISGSLRRGSANTGLIRAAKEICEESIPGMVIDHV 48
                                            ::**.:.****: * : .*:.:*  : :  : *: ::::

Q9LK88|NQR_ARATH                  DISPLPLINTDLEVNGT-YPPVVEAFRQKILEADSILFASPEYNFSVSAP 98
A5AS03|A5AS03_VITVI               DIAPLPMLNTDLEVDGT-YPPAVEAFRQKILEADSILFASPEYNYSVTAP 98
PUT-161a-Glycine_max-35276        DISPLPLLNTDLEVNGT-YPPQVEAFRQKILAADSILFASPEYNYSVASP 113
Q8H9D2|NQR_SOLTU                  DISPLPFLNTDLEVNGT-YPPVVEAFRKKIEEADCFLFASPEYNYSITGP 94
Q941Z0|NQR1_ORYSJ                 DISGLPLLNTDLETADGGFPPAVEAFRDKVRQADCFLFGSPEYNYSIATP 98
Q941Y8|NQR2_ORYSJ                 DIPDLPLLNTDMEVDDG-FPPAVEAFRASVRAADCFLFASPEYNYSISGP 97
                                  **. **::***:*. .  :** ***** .:  **.:**.*****:*:: *

Q9LK88|NQR_ARATH                  LKNALDWASRPPNVWADKPAAIISTGGGFGGGRSQYHLRQIGVFLDLHFI 148
A5AS03|A5AS03_VITVI               LKNAIDWASRPPNVWADKPAAIISTGGGFGGGLSQYHLRQIGVYLDLHFI 148
PUT-161a-Glycine_max-35276        LKNALDWASRAPNVWAGKPAAIVSAGGGFGGGRSQYHLRQIGVFLDLHFI 163
Q8H9D2|NQR_SOLTU                  LKNAIDWASRPPNVWADKAAAMVSAGGGFGGGRSQYHLRQIGVFLDLHFI 144
Q941Z0|NQR1_ORYSJ                 LKNALDWASRGQNCWADKPAAIVSAGGGFGGGRSQYHLRQVGVFLDLHFI 148
Q941Y8|NQR2_ORYSJ                 LKNALDWGSRPPNCWADRAAAIVSASGGSGGGSRSMYHIRQVGVFLDIHFI 147
                                  ****:**.**  * **.:.**::*:.** **. * **:**:**:**:***

Q9LK88|NQR_ARATH                  NKPEFTLNAFQPPQKFDAEGNLVDEVTKERLKQVLLSLQAFTLRLQGK-- 196
A5AS03|A5AS03_VITVI               NKPEFFLNAFQPPAKFDAEGNLIDEDAKKRIKEVILSLQAFTRRLQGK-- 196
PUT-161a-Glycine_max-35276        NKPEFFLNAFQPPAKFNNDGDLIDEDAKNRLKDVLLSLKEFTLRLQGKN- 212
Q8H9D2|NQR_SOLTU                  NKPEFFLNAFQQPPKFDSDGVLTDEETKQRLRAVLLALQALALKLKGKCE 194
Q941Z0|NQR1_ORYSJ                 NKPELAVKAFEQPPKFDSDGNLIDAQIRERIKQVLLSLQAFTLRLQKKD- 197
Q941Y8|NQR2_ORYSJ                 NKPEVFIKAHQPPKKFDSDGNLIDPEIKEELKDMLLSLQAFALRLQGKPA 197
                                  ****. ::*.: * **: :* * *   ::.:: ::*:*: :: :*: *

Q9LK88|NQR_ARATH                  ------
A5AS03|A5AS03_VITVI               ------
PUT-161a-Glycine_max-35276        ------
Q8H9D2|NQR_SOLTU                  ------
Q941Z0|NQR1_ORYSJ                 ------
Q941Y8|NQR2_ORYSJ                 NSKHAA 203
```

Appendix

Formulas and extinction coefficients used for the determination of NAD(P)H oxidation and quinone reduction (hydroquinone accumulation) in NADPH/quinone mixtures. Suitable wavelengths pairs (λ_1, λ_2) were selected from absorbance (A) spectra of the quinones (100 μM) dissolved in 20 mM HEPES, pH 7.5, with 0.1% DMSO (0.1% ethanol + 2% Tween 20 in the case of vitamins k_1 and k_2) before and after exhaustive reduction with solid $NaBH_4$. NAD(P)H was oxidized with catalytic amounts of methoxyphenazine methosulfate. Disregarding possible impurities of the commercially obtained quinones, differential (ox → red) extinction coefficients ($\varepsilon_{\lambda 1}$, $\varepsilon_{\lambda 2}$) were calculated and used for the estimation of concentration changes (Δc_a, Δc_b, measured in a 1-cm cuvette) in a mixture of components a, b according to the general formulas:

$$\Delta c_a = \frac{\varepsilon^b_{\lambda 2}}{x}\Delta A_1 - \frac{\varepsilon^b_{\lambda 1}}{x}\Delta A_2 \text{, and } \Delta c_b = \frac{\varepsilon^a_{\lambda 1}}{x}\Delta A_2 - \frac{\varepsilon^a_{\lambda 2}}{x}\Delta A_1 ,$$

whereby ΔA_1 = measured absorbance change at λ_1, ΔA_2 = measured absorbance change at λ_2 and $x = \varepsilon^b_{\lambda 2} \cdot \varepsilon^a_{\lambda 1} - \varepsilon^b_{\lambda 1} \cdot \varepsilon^a_{\lambda 2}$. Δc_b, $\varepsilon^b_{\lambda 1}$, $\varepsilon^b_{\lambda 2}$ refer to NAD(P)H →$NAD(P)^+$.

These formulas can be derived from the principle that the concentrations of the two pigments a, b in a mixture of these pigments can be calculated from the absorbance spectrum at two wavelengths (λ_1, λ_2) demonstrating large differences in ε_λ. From $A_1 = \varepsilon^a_{\lambda 1} \cdot c_a + \varepsilon^b_{\lambda 1} \cdot c_b$, and $A_2 = \varepsilon^b_{\lambda 2} \cdot c_b + \varepsilon^a_{\lambda 2} \cdot c_a$, the equations defining c_a and c_b can be derived by mutual substitution and rearrangement. This procedure has been exemplified in detail for the estimation of chlorophylls *a* and *b* in plant extracts (Strain HH, Svec WA, 1966).

Component a (ox→red)	λ_1 [nm]	λ_2 [nm]	$\varepsilon^a_{\lambda 1}$ [$mM^{-1}cm^{-1}$]	$\varepsilon^a_{\lambda 2}$ [$mM^{-1}cm^{-1}$]	$\varepsilon^b_{\lambda 1}$ [$mM^{-1}cm^{-1}$]	$\varepsilon^b_{\lambda 2}$ [$mM^{-1}cm^{-1}$]
NQ	290	340	2.23	-0.35	-0.92	-6.21
2-Methyl-NQ	290	340	2.18	-0.085	-0.92	-6.21
5-Hydroxy-NQ	366	425	-0.98	-3.15	-3.38	0.00
5-Hydroxy,2-methyl-NQ	420	366	-3.79	-1.41	0.00	-3.38
2-Hydroxy-NQ	450	366	-2.92	1.52	0.00	-3.38
2-Methoxy-NQ	282.3	340	-14.1	0.86	0.00	-6.21
2,3-Dimethoxy-NQ	282.3	340	-8.16	-0.16	0.00	-6.21

Vitamin k_1	282.3	366	-1.24	-0.32	0.00	-3.38
Vitamin k_2	282.3	366	-1.24	-0.32	0.00	-3.38
BQ	290	340	1.41	-0.008	-0.92	-6.21
2-Methyl-BQ	282.3	340	2.61	-0.38	0.00	-6.21
2,5-Dimethyl-BQ	282.3	340	3.11	-0.075	0.00	-6.21
2,6-Dimethyl-BQ	282.3	340	2.54	-0.26	0.00	-6.21
Ubiquinone 0	290	340	0.70	-0.25	-0.92	-6.21
Tetramethyl-BQ	290	340	1.22	-0.17	-0.92	-6.21
2,6-Dimethoxy-BQ	282.3	340	-11.2	-0.31	0.00	-6.21
2,5-Dihydroxy-BQ	290	366	3.14	-0.31	-0.92	-3.38
Tetrahyxdroxy-BQ	483	340	-16.9	-0.22	0.00	-6.21

(NQ=1,4-naphthoquinone, BQ=1,4-benzoquinone)

2.2. Origin of cadmium-induced reactive oxygen species production: mitochondrial electron transfer versus plasma membrane NADPH oxidase

Manuscript presented with publishers permission

Origin of cadmium-induced reactive oxygen species production: mitochondrial electron transfer versus plasma membrane NADPH oxidase

Eiri Heyno[1], Cornelia Klose[2] and Anja Krieger-Liszkay[1]

[1]CEA, iBiTecS, CNRS URA 2096, Service de Bioénergétique Biologie Structurale et Mécanisme, 91191 Gif-sur-Yvette Cedex, France; [2]Institut für Biologie II, Universität Freiburg, Schänzlestr. 1, 79104 Freiburg, Germany

Author for correspondence:
Anja Krieger-Liszkay
Tel: +33 1 6908 1803
Fax: +33 1 6908 8717
Email: anja.krieger-liszkay@cea.fr

Received: *25 March 2008*
Accepted: *16 April 2008*

Summary

• Cadmium (Cd^{2+}) is an environmental pollutant that causes increased reactive oxygen species (ROS) production. To determine the site of ROS production, the effect of Cd^{2+} on ROS production was studied in isolated soybean (*Glycine max*) plasma membranes, potato (*Solanum tuberosum*) tuber mitochondria and roots of intact seedlings of soybean or cucumber (*Cucumis sativus*).

• The effects of Cd^{2+} on the kinetics of superoxide ($O_2^{\bullet-}$), hydrogen peroxide (H_2O_2) and hydroxyl radical ($^{\bullet}OH$) generation were followed using absorption, fluorescence and spin-trapping electron paramagnetic resonance spectroscopy.

• In isolated plasma membranes, Cd^{2+} inhibited $O_2^{\bullet-}$ production. This inhibition was reversed by calcium (Ca^{2+}) and magnesium (Mg^{2+}). In isolated mitochondria, Cd^{2+} increased $O_2^{\bullet-}$ and H_2O_2 production. In intact roots, Cd^{2+} stimulated H_2O_2 production whereas it inhibited $O_2^{\bullet-}$ and $^{\bullet}OH$ production in a Ca^{2+}-reversible manner.

• Cd^{2+} can be used to distinguish between ROS originating from mitochondria and from the plasma membrane. This is achieved by measuring different ROS individually. The immediate (≤ 1 h) consequence of exposure to Cd^{2+} *in vivo* is stimulation of ROS production in the mitochondrial electron transfer chain and inhibition of NADPH oxidase activity in the plasma membrane.

Key words: cadmium (Cd), calcium (Ca), mitochondrial electron transport chain, NADPH oxidase, plasma membrane, reactive oxygen species (ROS).

New Phytologist (2008) **179**: 687–699

doi: 10.1111/j.1469-8137.2008.02512.x

Introduction

Life in an oxygen-rich atmosphere has to deal with the danger of oxidative stress. Reactive oxygen species (ROS), such as superoxide ($O_2^{\bullet-}$), hydrogen peroxide (H_2O_2) and hydroxyl radicals ($^{\bullet}OH$), are produced during normal cell metabolism but their production is drastically enhanced when plants are exposed to natural abiotic stresses such as high light, low temperatures and drought, and to biotic stresses such as attack by pathogens or wounding (e.g. Scandalios, 2002). Environmental pollutants such as heavy metal ions, for example cadmium (Cd^{2+}), are also known to induce oxidative stress (Schützendübel & Polle, 2002). Although ROS are considered to be damaging molecules, it is recognized that they play a major role in defense against pathogens, cellular signaling pathways and regulation of gene expression in a wide range of organisms, including plants (e.g. Apel & Hirt, 2004).

ROS are generated in a variety of reactions. These include the respiratory and photosynthetic electron transport chains and side reactions of enzymes such as peroxidases. In addition, specialized enzymes such as superoxide dismutases, xanthine oxidase and NADPH oxidases (NOXs) produce ROS (Halliwell & Gutteridge, 1999). ROS are not only produced in many different reactions but also in different compartments of the cell, including mitochondria, chloroplasts, peroxisomes, the cytosol and the apoplast.

Plant plasma membranes produce $O_2^{\bullet-}$ to the apoplastic side in response to different stimuli. This activity has been widely accepted to originate from plasma membrane-localized NOXs that reduce external O_2 using cytoplasmic NADPH as the electron source, although other plasma membrane-localized or -associated enzymes may also contribute to $O_2^{\bullet-}$ production. Ten genes encode NOXs in *Arabidopsis thaliana*. These genes are termed respiratory burst oxidase homologs A to J (*RbohA–J*) because of their homology to the catalytic subunit $gp91^{phox}$ (Nox2) of the NOX complex of mammalian phagocytes (Torres & Dangl, 2005). The plant NADPH oxidases are predicted to have six transmembrane helices with two heme-binding sites, cytoplasmic binding sites for NADPH and FAD at the C-terminus and two calcium (Ca^{2+})-binding EF-hand motifs at the N-terminus (Torres & Dangl, 2005), a similarity with the NOX5 NADPH oxidase in mammals (Banfi *et al.*, 2004). NOX-encoding genes are present in all plant species investigated so far, and they have distinctive expression patterns. Although the involvement of NOXs in important physiological processes has been demonstrated in plants (e.g. Foreman *et al.*, 2003; Kwak *et al.*, 2003; Potocký *et al.*, 2007), their enzymatic properties have rarely been studied. It has been shown that the EF-hand motifs in plant NOXs bind $^{45}Ca^{2+}$ (Keller *et al.*, 1998) and that Ca^{2+} stimulates the NOX activity of isolated plasma membranes (Sagi & Fluhr, 2001). The activation of mammalian NOX5 by Ca^{2+} in a cell-free system is in the micromolar range (Banfi *et al.*, 2004). Hence, in the plant plasma membrane micromolar Ca^{2+} concentrations can also be expected to lead to enhanced $O_2^{\bullet-}$ production.

Ca^{2+}-binding sites can be probed by other metals such as lanthanides and cadmium. Cd^{2+} has been shown to block cysteine groups in enzymes, leading to their inactivation (Van Assche & Clijsters, 1990; Kabała *et al.*, 2008), and to bind as a competitive inhibitor to Ca^{2+}-binding motifs such as radish calmodulin (Rivetta *et al.*, 1997) and the water-splitting complex of photosystem II (Faller *et al.*, 2005). Cd^{2+} is also known to block proton transport in $gp91^{phox}$ (Henderson *et al.*, 1988) and in complex III of the mitochondrial electron transport chain (Link & von Jagow, 1995). In addition, it has been reported that Cd^{2+} leads to increased $O_2^{\bullet-}$ production at complex III (Wang *et al.*, 2004). It has been known for more than 30 yr that mitochondrial electron transport can lead to $O_2^{\bullet-}/H_2O_2$ formation via the reaction of semiquinones with oxygen (e.g. Boveris & Chance, 1973; Cape *et al.*, 2007; Zhang *et al.*, 2007).

It has also been proposed that the plasma membrane NOXs may be implicated in the Cd^{2+}-induced ROS production after short-term exposure to the metal (Olmos *et al.*, 2003; Garnier *et al.*, 2006). Long-term exposure of plants to Cd^{2+} in micromolar concentrations has been widely studied and the symptoms (e.g. increased ROS production caused by the failure of the cellular antioxidant system, cell death and growth defects) are well characterized (Romero-Puertas *et al.*, 2004; Rodriguez-Serrano *et al.*, 2006). In long-term exposure of plants to Cd^{2+}, the molecular mechanism leading to increased $O_2^{\bullet-}$ production at the plasma membrane seems to require signaling pathways involving kinases, Ca^{2+} fluxes and *de novo* synthesis of NOX (Romero-Puertas *et al.*, 2004; Rodriguez-Serrano *et al.*, 2006; Van Belleghem, 2007).

In most biological systems it is difficult to determine the site of ROS production *in vivo*. In most studies only H_2O_2 has been measured. H_2O_2 is the only ROS that can diffuse easily through aquaporins in the membranes and over larger distances within the cell (Bienert *et al.*, 2007). In this work we used Cd^{2+} ions as a biochemical tool to distinguish between H_2O_2 originating from $O_2^{\bullet-}$ formed by the mitochondria and that originating from $O_2^{\bullet-}$ formed by the plasma membrane NOX using dyes and electron paramagnetic resonance (EPR) spin traps specific for $O_2^{\bullet-}$, H_2O_2 and $^{\bullet}OH$. Ca^{2+} was used as an indicator of NOX activity and a potential competitor for Cd^{2+}. To link the *in vitro* data to the *in vivo* situation, we studied the effect of short-term exposure to Cd^{2+} on ROS production with intact roots of cucumber (*Cucumis sativus*) and soybean (*Glycine max*) seedlings by measuring $O_2^{\bullet-}$, H_2O_2 and $^{\bullet}OH$ production.

Materials and Methods

Plant material

Different plant species were chosen for isolation of plasma membranes (soybean) and mitochondria (potato) and for *in vivo* (cucumber) experiments to obtain material with optimal activity in reasonable quantities. Soybean (*Glycine max* (L.) Jutro) seedlings were grown in the dark at 25°C in vermiculite for 4 d for plasma membrane preparation. Cucumber (*Cucumis sativus* L.) and soybean seedlings were grown between damp paper towels in a vertical position (root apex downwards) in rectangular Petri dishes at 25°C for 3 d (soybean) or 4 d (cucumber) in dim white light for in vivo measurements. Under these conditions, seedlings with straight roots of 40–60 mm length were obtained. *Arabidopsis thaliana* (L.) (background Columbia) wild type and *rbohC* and *D* mutants were grown for 20 d in a vertical position on rectangular plates (1% Phytagel and 4.3 g l^{-1} Murashige–Skoog basal medium without hormones) in short-day conditions.

Potato (*Solanum tuberosum* L.) tubers were purchased from the local market.

Isolation and solubilization of plasma membrane vesicles

Plasma membrane vesicles from etiolated soybean hypocotyls were isolated according to Michalke & Schmieder (1979). The top 1 cm of the hypocotyls was excised and incubated for 10 min in a fourfold volume (fresh weight/volume) of isolation buffer (10 mM Tris/HCl, pH 8.0, 20 mM Na_2EDTA and 300 mM NaCl) to which 0.1% bovine serum albumin (BSA) and 0.5 mM phenylmethylsulfonyl fluoride (PMSF) were added just before use. The hypocotyls were homogenized

in a blender (Waring, Torrington, CT, USA) and filtered through a nylon cloth, and the filtrate was centrifuged (30 min at 1300 ***g*** and 4°C). The supernatant (raw fraction) was again centrifuged (45 min at 91 000 ***g*** and 4°C) to separate soluble proteins and membranes. The pellet was resuspended in isolation buffer and homogenized in a glass potter. The homogenate was diluted twofold (fresh weight/volume) with isolation buffer. Polyethylene glycol (PEG) 6000 was added (4.3 g per 100 ml), and the mixture was stirred on ice for 30 min, followed by centrifugation (30 min at 1300 ***g*** and 4°C) to separate the intracellular membranes from plasma membranes. The supernatant, containing the plasma membranes, was centrifuged (45 min at 91 000 ***g*** and 4°C). The pellet was resuspended in isolation buffer without Na_2EDTA and homogenized in a glass potter. This method resulted in plasma membrane preparations containing 1.5–2 mg protein ml^{-1}.

Plasma membranes were solubilized with 2% Tween-20 (weight/volume) for 30 min at 45°C. The supernatant obtained after centrifugation (12 000 ***g*** in a bench centrifuge for 5 min) was stored at –70°C until use.

Isolation of mitochondria from potato tubers

Mitochondria were isolated according to Douce *et al.* (1987). Peeled tubers were macerated with a Moulinex (type 750) vegetable juice machine. The juice (*c.* 500 ml) was made up to 1000 ml with cold isolation buffer (0.5 M sorbitol, 8 mM Na_2EDTA and 80 mM 3-[N-morpholino] propane-sulfonic acid (MOPS), pH 7.5, with 0.4% BSA, 0.5% polyvinylpyrolidone and 8 mM cysteine added just before use), filtered through a nylon cloth and centrifuged (10 min at 370 ***g*** and 4°C). The supernatant was filtered again through a nylon cloth and centrifuged (15 min at 1000 ***g*** and 4°C). The supernatant was centrifuged (20 min at 11 700 ***g*** and 4°C) and the pellet was resuspended in 40 ml of cold Percoll-gradient buffer (25% Percoll, 0.4 M sorbitol and 100 mM MOPS, pH 6.9) and centrifuged (45 min at 30 000 ***g*** and 4°C). The white layer containing the mitochondria was collected and mixed with 8 volumes of cold wash buffer (0.4 M sorbitol and 10 mM MOPS, pH 7.2, and freshly added 0.1% BSA). After centrifugation (20 min at 8000 ***g*** and 4°C), the pelleted mitochondria were resuspended in measuring buffer (0.4 M sucrose, 5 mM $MgCl_2$, 30 mM KCl and 20 mM HEPES, pH 7.3) and used for measurements or frozen as droplets in liquid nitrogen and stored at –70°C. The droplets were rapidly thawed in a thin glass tube in 90°C water and immediately cooled in ice-water. This method resulted in basal respiratory activity of 41 ± 7 nmol O_2 mg^{-1} protein min^{-1} in the presence of 5 mM succinate, resembling the rates reported in Ravanel *et al.* (1984).

Determination of protein concentration

The protein concentration of the samples was determined with the Bradford assay (Bradford, 1976). In the presence of detergents the Amido black assay was used instead (Schaffner & Weissmann, 1973).

Ca^{2+} depletion by Chelex 100

Solubilized plasma membranes were depleted of Ca^{2+} by incubation with Chelex 100 beads (50–100 dry mesh; Sigma-Aldrich, St. Quertin Fallavier, France) according to Kashino *et al.* (1986). Membranes (0.5 ml, corresponding to *c.* 0.75 mg protein ml^{-1}) were incubated in 0.1–0.3 g Chelex 100 for 6 min at room temperature. During the incubation the mixture was vortexed for 10 s every 1 min. The Chelex-free samples were collected using a pipette.

SDS-PAGE and western blotting

Sodium dodecyl sulfate–polyacrylamide gel electrophoresis (SDS-PAGE) was carried out in 8–12% gradient polyacrylamide gels stained with silver. Western blotting was performed using a Multiphor II Novablot unit (Amersham Bioscience, Piscataway, NJ, USA). For detection, the enhanced chemoluminescence (ECL) system (Amersham Bioscience) was used according to the manufacturer's protocol.

Determination of NADH and NADPH oxidation

The kinetics of NADH and NADPH oxidation by solubilized plasma membranes were measured photometrically for 10 min as the decrease in absorbance at 340 nm at 25°C using the molar extinction coefficient $\varepsilon_{340} = 6.2 \times 10^3$ M^{-1} cm^{-1}. The reaction mixture (1 ml) contained 25 μg of plasma membrane protein and 200 μM NADH or NADPH in 20 mM HEPES, pH 7.8.

Detection of $O_2^{\bullet-}$ by XTT reduction or cytochrome c reduction

The kinetics of $O_2^{\bullet-}$ production was measured photometrically as the increase in absorbance of Na, 3′-(1-(phenylaminocarbonyl)-3,4-tetrazolium)-bis(4-methoxy-6-nitro)benzenesulfonic acid hydrate (XTT) at 470 nm. $O_2^{\bullet-}$ production was calculated using the molar extinction coefficient $\varepsilon_{470} = 21.6$ mM^{-1} cm^{-1} (Sutherland & Learmonth, 1997) according to the equation:

$$XTT + 2O_2^{\bullet-} + 2H^+ \rightarrow XTTH_2 + 2O_2$$

$O_2^{\bullet-}$ production of solubilized plasma membranes was measured in 20 mM phosphate buffer, pH 7.8. Measurements with $CdCl_2$ were performed in 20 mM HEPES buffer, pH 7.8, to avoid the formation of precipitates. The reaction mixture (1 ml) contained 0.5 mM XTT and 25 μg of solubilized membrane protein and was incubated for 5 min in darkness at 25°C. The reaction was started by adding 200 μM NADH. $O_2^{\bullet-}$ production of roots was measured in 10 mM MES buffer, pH 6.5, containing 0.5 mM XTT. The roots of four intact

cucumber seedlings were placed in 5 ml of reaction mixture. Samples (1 ml) were measured at the indicated times. The reaction mixture was bubbled with air during the incubation.

Alternatively, cytochrome c (cyt c) reduction was measured at 550 nm in the presence of 50 μM cyt c (ε_{550} = 21.0 mM^{-1} cm^{-1}).

Determination of H_2O_2 production by scopoletin oxidation

The kinetics of H_2O_2 production were measured as the decrease in scopoletin fluorescence at 25°C at 350 nm (excitation) and 460 nm (emission) (Staniek & Nohl, 1999). A standard curve with known H_2O_2 concentrations was determined for 5 μM scopoletin in the measuring buffer. H_2O_2 production in mitochondria was measured after 30 min of incubation (1 mg protein ml^{-1}) in the measuring buffer (see isolation of mitochondria) containing 5 μM scopoletin, 10 U horseradish peroxidase (HRP), 0.5 mM succinate and 2 μM mesoxalonitrile 3-chlorophenylhydrazone (CCCP) as an uncoupler. To avoid perturbations of the fluorescence, mitochondria were sedimented by centrifugation (5 min at 9000 ***g*** and 25°C) before measuring the fluorescence of the supernatant. All results were in the linear region of the standard curve.

H_2O_2 production in roots was measured in 10 mM MES, pH 6.5, containing 5 μM scopoletin. The roots of four intact cucumber seedlings or of three soybean seedlings were placed in 5 ml of assay medium. In case of *A. thaliana*, 20 seedlings were incubated in 1.5 ml of assay medium. Samples (1 ml) were measured at the indicated times. The assay medium was bubbled with air during the incubation.

EPR measurements

EPR spectra were recorded at room temperature with a Bruker 300 X-band spectrometer at 9.69 GHz microwave frequency, 63 mW microwave power and 100 kHz modulation frequency. For $O_2^{\bullet-}$ detection in solubilized plasma membranes, 200 μg ml^{-1} protein was incubated for 10 min in 10 mM phosphate buffer, pH 7.5, containing 200 μM NADH and 25 mM 2-ethoxycarbonyl-2-methyl-3,4-dihydro-2H-pyrrole-1-oxide (EMPO) (Olive *et al.*, 2000) in the presence of 50 μg ml^{-1} superoxide dismutase (SOD) or 1 mM KCN, respectively. For $O_2^{\bullet-}$ detection in isolated mitochondria, 1 mg protein ml^{-1} was incubated for 5 min in measuring buffer (see isolation of mitochondria) containing 25 mM EMPO, 0.5 mM succinate, 2 μM CCCP and, if indicated, 30 μM $CdCl_2$ or 2 μM antimycin A. The pure adducts of EMPO were obtained by dissolving KO_2 in 10 mM phosphate buffer, pH 7.5 ($O_2^{\bullet-}$ adduct), and by the Fenton reaction using 10 μM $FeSO_4$ + 100 μM H_2O_2 ($^{\bullet}OH$ adduct).

For $^{\bullet}OH$ detection in roots, four intact cucumber or soybean seedlings were incubated for 1 h in 10 mM MES buffer, pH 6.5, 50 mM N-tert-butyl-α-(4-pyridyl)nitrone N′-oxide (4-POBN) and 4% ethanol (Janzen *et al.*, 1978).

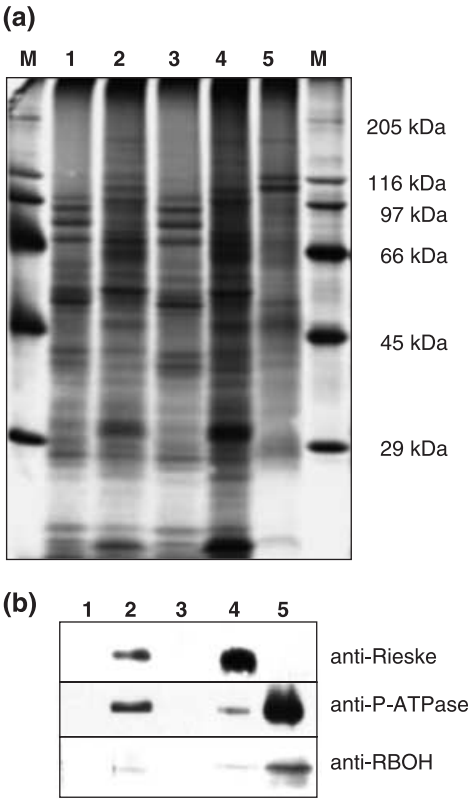

Fig. 1 Sodium dodecyl sulfate–polyacrylamide gel electrophoresis (SDS-PAGE) (a) and immunoblots (b) of protein fractions obtained from plasma membranes isolated from soybean. Lane 1, raw fraction; lane 2, total membranes; lane 3, soluble proteins; lane 4, intracellular membranes, and lane 5, plasma membranes. The immunoblot was decorated with polyclonal antibodies directed against the ATPase of the plasma membrane, Rieske protein and NADPH oxidase. In each lane, 20 μg of protein was loaded. The SDS gel was stained with silver.

Statistics

The data represent means or representative examples from measurements repeated 3–6 times. Typical standard errors are shown in Figs 4(a) and 6, and in tables, but omitted in other figures for the sake of clarity.

Results

Isolation of plasma membranes from soybean hypocotyls

Plasma membranes were isolated from soybean hypocotyls using a PEG-based membrane fractionation protocol (Michalke & Schmieder, 1979). Proteins at different isolation steps were separated by SDS gel electrophoresis and blotted (Fig. 1). To verify the separation of plasma membranes from other cellular membranes by PEG sedimentation, immunodetection was performed with antibodies directed against mitochondrial

Table 1 Activity of solubilized plasma membranes of soybean

	Specific activity (nmol mg^{-1} protein min^{-1})	
Assay reaction	–SOD	+SOD
NADH oxidation	2.9 ± 0.20	26.9 ± 0.22
XTT reduction	31.0 ± 1.01	1.03 ± 0.02
Cyt c reduction	34.0 ± 0.16	0

Activities were measured in the absence or presence of 50 μg ml^{-1} superoxide dismutase (SOD). The reaction assay contained 25 μg protein ml^{-1}, 200 μM NADH and either 500 μM Na,3′-(1-(phenylaminocarbonyl)-3,4-tetrazolium)-bis(4-methoxy-6-nitro)benzenesulfonic (XTT) or 50 μM cytochrome c (Cyt c).

Rieske protein and plasma membrane P-ATPase. The Rieske protein was detected only in the total membrane and the intracellular membrane fractions. P-ATPase was detected in the total membrane, weakly in the intracellular membrane and strongly in the plasma membrane fractions. Plasma membrane isolation using a two-phase separation protocol (Larsson *et al.*, 1994) resulted in similar protein compositions (data not shown). The presence of a NOX protein in the plasma membrane fraction was shown by immunodetection using anti-NtrbohD antibodies (Simon-Plas *et al.*, 2002). A weak signal was detected in total membrane and intracellular membrane fractions while a strong signal was found in the plasma membrane fraction.

$O_2^{\bullet-}$ production in solubilized plasma membranes

Solubilized plasma membranes produced $O_2^{\bullet-}$ when the electron donor NADH or NADPH was present. Solubilization was necessary to allow access to the substrates. Nonsolubilized membranes produced only 10% of the $O_2^{\bullet-}$ generated by the solubilized membranes. The activity was measured photometrically as NADH oxidation or reduction of either XTT or cytochrome c (Table 1). When NADPH instead of NADH was used as substrate, similar rates for the oxidation were obtained. The activities, measured in the absence of SOD, resembled those reported for plasma membrane preparations in the literature (Brightman *et al.*, 1988; DeHahn *et al.*, 1997; Van Gestelen *et al.*, 1997). In the presence of SOD, the NADH reduction was stimulated almost tenfold, indicating that $O_2^{\bullet-}$ inhibits NAD(P)H reduction when it is not removed.

The stoichiometry of NADH oxidation (measured in the presence of SOD) to XTT reduction was almost 1 : 1 (both are two-electron reactions), while the reduction of cyt c (one-electron acceptor) was lower than the theoretically expected 1 : 2 stoichiometry. This might be a result of the relatively low concentration of cyt c used in the assay. Addition of SOD to the XTT or cytochrome c reduction assay inhibited the reduction of the electron acceptors almost completely. Therefore these assays can be used to determine $O_2^{\bullet-}$ production.

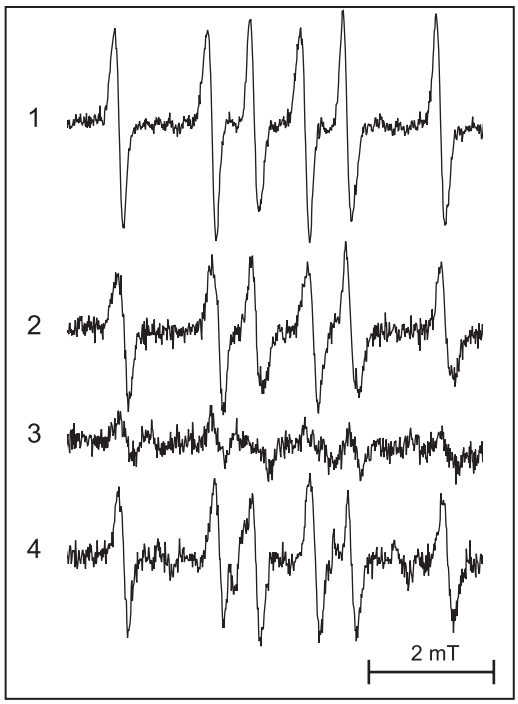

Fig. 2 $O_2^{\bullet-}$ production in solubilized plasma membranes isolated from soybean measured by spin trapping electron paramagnetic resonance (EPR) spectroscopy. (1) Characteristic spectrum of the 2-ethoxycarbonyl-2-methyl-3,4-dihydro-2H-pyrrole-1-oxide (EMPO)/ $O_2^{\bullet-}$ adduct (control), (2) plasma membranes, (3) plasma membranes in the presence of 50 μg ml^{-1} superoxide dismutase (SOD) and (4) plasma membranes in the presence of 1 mM KCN. The samples were incubated for 10 min in 10 mM phosphate buffer, pH 7.5, containing 200 μg of plasma membrane proteins ml^{-1}, 200 μM NADH and 25 mM EMPO. The spectra are representative of at least six measurements.

$O_2^{\bullet-}$ production was shown independently by EPR spectroscopy using the spin trap EMPO (Fig. 2). EMPO reacts with both $O_2^{\bullet-}$ and $^{\bullet}OH$ and gives specific adducts which can be distinguished by their hyperfine splitting pattern (Olive *et al.*, 2000). Spectrum 1 presents the EMPO/$O_2^{\bullet-}$ adduct which was formed by dissolving KO_2 in the assay buffer. Measurements of solubilized plasma membranes incubated with NADH showed the typical spectrum of the EMPO/$O_2^{\bullet-}$ adduct (spectrum 2), which was almost completely abolished in the presence of the $O_2^{\bullet-}$ scavenger SOD (spectrum 3). The signal of the EMPO/$O_2^{\bullet-}$ adduct was unaffected by KCN (spectrum 4), ruling out plasma membrane-bound peroxidases (Mika & Lüthje, 2003) as the source of $O_2^{\bullet-}$. Diphenyleneiodonium chloride (DPI) inhibited $O_2^{\bullet-}$ production at low concentration both in EPR and in XTT reduction measurements (Fig. 3). Fifty per cent inhibition was observed at 1.5 μM DPI, indicating a specific inhibitory effect. DPI is an inhibitor of the mammalian NOX at low micromolar concentrations (< 10 μM; Doussiere & Vignais, 1992).

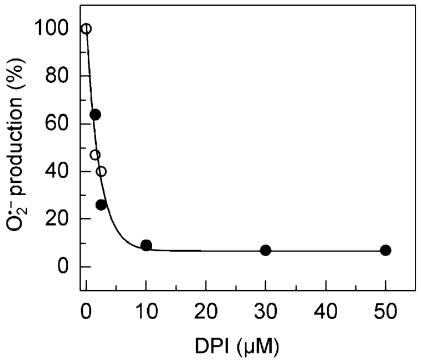

Fig. 3 Effect of diphenyleneiodonium chloride (DPI) on $O_2^{\bullet-}$ production in solubilized plasma membranes isolated from soybean. $O_2^{\bullet-}$ production was measured using electron paramagnetic resonance (EPR) spectroscopy with 2-ethoxycarbonyl-2-methyl-3,4-dihydro-2H-pyrrole-1-oxide (EMPO) as a spin trap (closed circles) and using optical methods, in which it was measured as Na,3′-(1-(phenylaminocarbonyl)-3,4-tetrazolium)-bis(4-methoxy-6-nitro)benzenesulfonic acid hydrate (XTT) reduction (open circles). Maximum activity (100%) corresponds to 31 ± 1 nmol $XTTH_2$ mg^{-1} min^{-1}. The samples were incubated for 10 min in 10 mM phosphate buffer, pH 7.5, containing 200 μg of plasma membrane proteins ml^{-1}, 200 μM NADH and 25 mM EMPO. For the XTT test 0.5 mM XTT was added instead of EMPO. Measurements using XTT were only performed at low diphenyleneiodonium chloride (DPI) concentrations because higher DPI concentrations interfered with the assay.

Effect of $CaCl_2$ or $MgCl_2$ on $O_2^{\bullet-}$ production in solubilized plasma membranes

The inhibition of $O_2^{\bullet-}$ production by DPI (shown in Fig. 3) is in agreement with the assumption that NOX is responsible for the $O_2^{\bullet-}$ production observed in solubilized plasma membranes. To further test this assumption we investigated the effect of Ca^{2+} on $O_2^{\bullet-}$ production. Ca^{2+} is known to bind to the EF-hand motifs of the NOX encoded by the *AtrbohA* gene (Keller *et al.*, 1998) and to stimulate the activity of NOX in tobacco (*Nicotiana tabacum*) and tomato (*Lycopersicon esculentum*) plasma membranes (Sagi & Fluhr, 2001). Indeed, 5 mM Ca^{2+} increased the $O_2^{\bullet-}$ production in solubilized plasma membranes by 30% (Table 2) but it is possible that the plasma membranes used here were not fully depleted of Ca^{2+}. We therefore depleted the solubilized plasma membranes of Ca^{2+} by preincubating them with the Ca^{2+} chelator Chelex 100 or ethylene glycol tetraacetic acid (EGTA). Incubation with Chelex 100 or 1 mM EGTA resulted in a 28 or 77% reduction, respectively, in $O_2^{\bullet-}$ production (Table 2). In the Chelex 100-treated membranes, Ca^{2+} and magnesium (Mg^{2+}) both stimulated the activity. The initial activity was already reached at a concentration of 10 μM. $O_2^{\bullet-}$ production was reduced more efficiently by 1 mM EGTA than by Chelex 100, but Ca^{2+} or Mg^{2+} in the millimolar range was needed to restore the initial activity.

Table 2 Effect of divalent cations and chelators on $O_2^{\bullet-}$-producing activity in solubilized plasma membranes of soybean

Treatment	$O_2^{\bullet-}$ production (%)
No treatment (control)	100
+ 5 mM $CaCl_2$	125 ± 6
+ 5 mM $MgCl_2$	126 ± 4
1 mM EGTA	23 ± 7
Chelex	72 ± 7
+ 10 μM $CaCl_2$	95 ± 4
+ 100 μM $CaCl_2$	97 ± 7
+ 500 μM $CaCl_2$	103 ± 5
+ 10 μM $MgCl_2$	91 ± 9
+ 100 μM $MgCl_2$	104 ± 6
+ 500 μM $MgCl_2$	108 ± 5

$O_2^{\bullet-}$ production was measured as Na,3′-(1-(phenylaminocarbonyl)-3,4-tetrazolium)-bis(4-methoxy-6-nitro)benzenesulfonic (XTT) reduction in the presence of 200 μM NADH. 100% activity corresponds to 31.6 ± 0.9 nmol $XTTH_2$ mg^{-1} protein min^{-1}. EGTA, ethylene glycol tetraacetic acid.

Effect of $CdCl_2$ and $CaCl_2$ on $O_2^{\bullet-}$ production in solubilized plasma membranes

Cd^{2+} is known to cause oxidative stress in the cell and NOX was reported to be involved in this process *in vivo* (Olmos *et al.*, 2003; Garnier *et al.*, 2006). As a potent competitor for Ca^{2+} and an enzyme inactivator (Rivetta *et al.*, 1997; Faller *et al.*, 2005), Cd^{2+} may bind to the EF-hand motifs of the NOX and affect the enzyme activity. We tested the effect of Cd^{2+} on the $O_2^{\bullet-}$ production of plasma membranes. Cd^{2+} inhibited $O_2^{\bullet-}$ production even at the lowest concentration used (100 μM). Concentrations > 1 mM resulted in 85% inhibition (Fig. 4a).

Given that Cd^{2+} often acts on Ca^{2+}-binding sites, we tested the effect of Ca^{2+} on the Cd^{2+}-induced inhibition of $O_2^{\bullet-}$ production. Fig. 4(a) shows that Ca^{2+} and Mg^{2+} competed efficiently with Cd^{2+}: when 5 mM Ca^{2+} or Mg^{2+} was present 300 μM Cd^{2+} had no inhibitory effect. To show the Ca^{2+} dependence, the activity of samples containing 0.3–1 mM Cd^{2+} was measured in the presence of different Ca^{2+} concentrations (Fig. 4b). To determine the inhibition constant (K_i) for Cd^{2+} the data of Fig. 4(b) are presented as a Dixon plot, including the data for 100 μM Cd^{2+} (Fig. 4c). The straight lines intersect at the same value, indicative of Cd^{2+} acting as a competitive inhibitor at the Ca^{2+}-binding site. The intersection of the lines, that is, K_i, is approx. 180 μM. A plot of the slopes obtained from the Dixon plot against the Ca^{2+} concentration (inset, Fig. 4c) resulted in a straight line, a further indication of competitive inhibition. The intercept is not at 0, because the samples were not depleted of Ca^{2+} before the addition of Cd^{2+}. This may explain why the K_i value is relatively high; Ca^{2+} in its binding site has first to be displaced by Cd^{2+}.

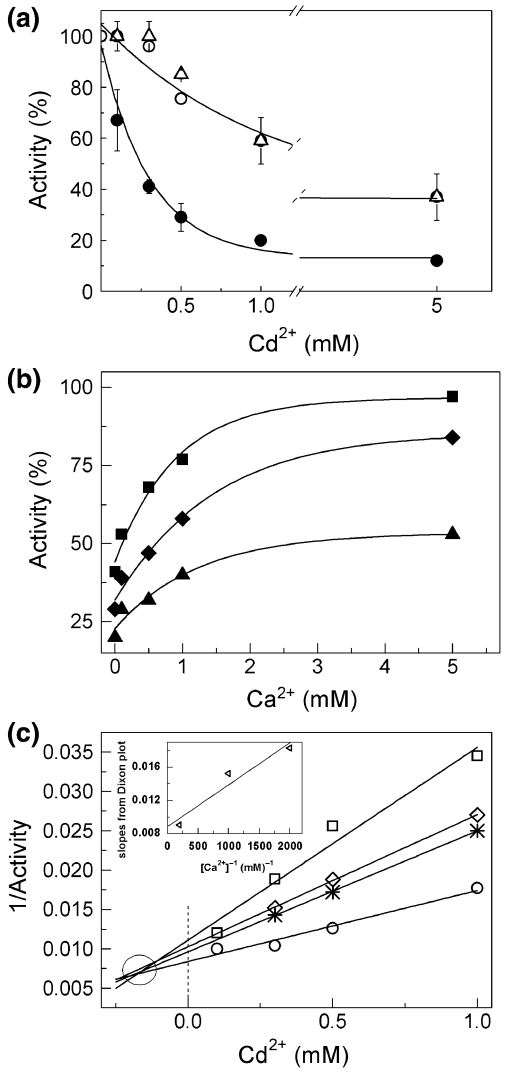

Fig. 4 Effect of $CdCl_2$ and $CaCl_2$ on $O_2^{\bullet-}$ production in solubilized plasma membranes isolated from soybean. $O_2^{\bullet-}$ production was measured as Na,3′-(1-(phenylaminocarbonyl)-3,4-tetrazolium)-bis(4-methoxy-6-nitro)benzenesulfonic acid hydrate (XTT) reduction. (a) Dependence of $O_2^{\bullet-}$ production on the $CdCl_2$ concentration (closed circles), in the presence of 5 mM $CaCl_2$ (open circles) and 5 mM $MgCl_2$ (open triangles). The mean values and SE bars were calculated from at least five measurements. (b) Dependence of $O_2^{\bullet-}$ production on $CaCl_2$ in the presence of 300 μM (closed squares), 500 μM (closed diamonds) and 1 mM (closed triangles) $CdCl_2$. (c) Dixon plot of the data shown in (b); 100 μM (open squares), 500 μM (open diamonds), 1 mM (stars) and 5 mM (open cirlces) $CaCl_2$. The lines were fitted by linear regression. Inset: slopes from the Dixon plot plotted against reciprocal $CaCl_2$ concentration. 100% activity corresponds to 31 ± 1 nmol $XTTH_2$ mg^{-1} protein min^{-1}. Samples contained 25 μg of plasma membrane protein, 0.5 mM XTT and 200 μM NADH. Samples were incubated for 5 min at room temperature with the given divalent cation concentration before starting the reaction by adding NADH.

Effect of $CdCl_2$ on $O_2^{\bullet-}$ and H_2O_2 production in isolated potato tuber mitochondria

Cd^{2+} stimulates $O_2^{\bullet-}$ production in isolated mitochondria from animal tissue (Wang *et al.*, 2004) by inhibiting the electron transfer at respiratory complex III (Miccadei & Floridi, 1993). Antimycin A is a well-known inhibitor of complex III. The binding of antimycin A to complex III results in increased ROS formation (e.g. Boveris *et al.*, 1972) and this is thought to be attributable to the accumulation of semiubiquinone radicals that react with O_2 to form $O_2^{\bullet-}$ (e.g. Cape *et al.*, 2007; Zhang *et al.*, 2007).

To investigate plant mitochondria as a potential source of ROS in response to Cd^{2+}, we monitored $O_2^{\bullet-}$ generation indirectly using the oxygen electrode, measuring the catalase-induced decrease in oxygen consumption. We found that 10–30 μM Cd^{2+} decreased succinate-driven oxygen consumption by 75%, while 2 μM antimycin A decreased it by 50%. (Two molecules of $O_2^{\bullet-}$ are transformed by mitochondrial SOD into H_2O_2 and O_2. Catalase spilts two molecules of H_2O_2 into H_2O and O_2. The evolved O_2 is detected as a further decrease in O_2 consumption.)

$O_2^{\bullet-}$ production could not be measured by XTT. The most likely explanation for this is that it simply does not enter the mitochondria. Instead, we measured $O_2^{\bullet-}$ production in isolated mitochondria by EPR spectroscopy using the EMPO spin trap. Spectra a and f (Fig. 5) show the EMPO/$O_2^{\bullet-}$ and EMPO/$^{\bullet}$OH adducts from KO_2 and the Fenton reaction, respectively. The dashed lines represent the hyperfine splitting pattern of the EMPO/$O_2^{\bullet-}$ adduct. Because of the short lifetime of the EMPO/$O_2^{\bullet-}$ adduct, mitochondria were incubated with the spin trap for only 5 min rather than the 30 min used for H_2O_2 measurements (Fig. 6). In the presence of 30 μM Cd^{2+} or 2 μM antimycin A (spectra b and c), significant production of the EMPO/$O_2^{\bullet-}$ adduct was seen. In the absence of the inhibitors, the EMPO/$O_2^{\bullet-}$ adduct was significantly smaller (spectrum c). SOD abolished the antimycin A-induced EMPO/$O_2^{\bullet-}$ signal (spectrum 5e), indicating that $O_2^{\bullet-}$ caused the hyperfine splitting seen in spectra 5b, c and d. In the presence of SOD, a pure signal of the EMPO/$^{\bullet}$OH adduct was obtained. This signal is also present in spectra b and c, indicating that part of the generated $O_2^{\bullet-}$ is immediately transferred by mitochondrial SOD to H_2O_2. H_2O_2 reacts in the presence of transition metals, which are present in the mitochondria, to form $^{\bullet}$OH. In the presence of SOD and catalase, no EMPO spin trap adduct was detected (not shown). The spectra obtained with mitochondria are much noisier than those obtained with plasma membranes (Fig. 2) because of the more complex composition of the assay medium. High sorbitol concentrations, HEPES and traces of Percoll in the measuring buffer interfere with the spin trapping assay and induce changes in the hyperfine splitting.

H_2O_2 production of the succinate-respiring mitochondria was measured by fluorescence spectroscopy using the scopoletin

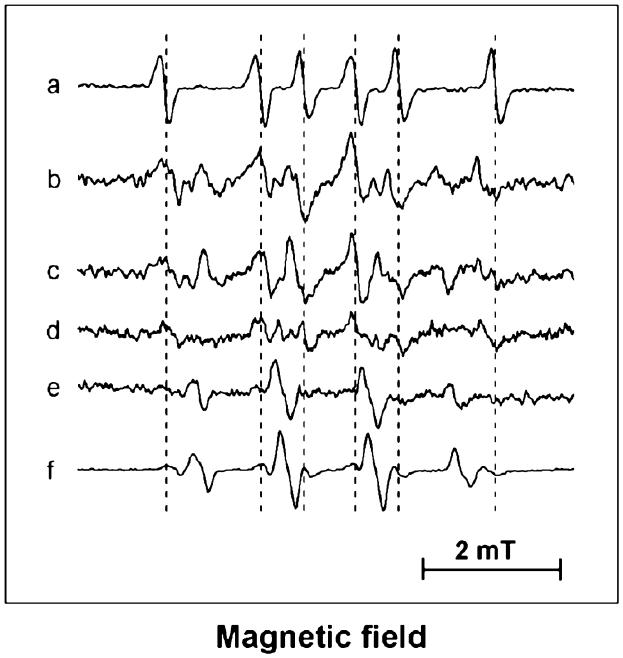

Fig. 5 Effect of $CdCl_2$ and antimycin A on $O_2^{\bullet-}$ production in mitochondria isolated from potato. Mitochondrial $O_2^{\bullet-}$ production was measured by electron paramagnetic resonance (EPR) spectroscopy using the 2-ethoxycarbonyl-2-methyl-3,4-dihydro-2H-pyrrole-1-oxide (EMPO) spin trap. (a) Characteristic spectrum of EMPO/$O_2^{\bullet-}$, (b) mitochondria in the presence of 30 μM $CdCl_2$, (c) mitochondria in the presence of 2 μM antimycin A, (d) mitochondria in control conditions, (e) mitochondria in the presence of 2 μM antimycin A and 50 μg superoxide dismutase (SOD), and (f) characteristic spectrum for the EMPO/•OH adduct produced by the Fenton reaction in 10 mM phosphate buffer, pH 7.5. All measurements with mitochodria (1 mg protein ml^{-1}) were performed in the measuring buffer (see the Materials and Methods) containing 0.5 mM succinate as an electron donor and 0.2 μM mesoxalonitrile 3-chlorophenylhydrazone (CCCP) as an uncoupler. The dashed lines indicate the hyperfine splitting pattern of the EMPO/$O_2^{\bullet-}$ adduct. The spectra are representative of at least three measurements in the indicated conditions.

oxidation assay (Staniek & Noll, 1999) (Fig. 6). The control rate of H_2O_2 production in mitochondria was 0.02 nmol min^{-1} mg^{-1} protein with 0.5 mM succinate as electron donor. The control values were increased twofold by 10 μM Cd^{2+} and almost threefold by 30 μM Cd^{2+}. A fourfold increase in H_2O_2 production was induced by 2 μM antimycin A. Both methods of measuring H_2O_2 (EMPO and scopoletin) showed that ROS production was succinante-dependent and that it could be stimulated by antimycin A. This behavior is specific for mitochondrially generated ROS and would not occur if the ROS originated from any potential contamination from peroxisomes which might be present in our mitochondrial preparation (see Corpas *et al.*, 2001; del Río *et al.*, 2002; Hänsch *et al.*, 2006; Nyathi & Baker, 2006 for evidence of ROS production in peroxisomens).

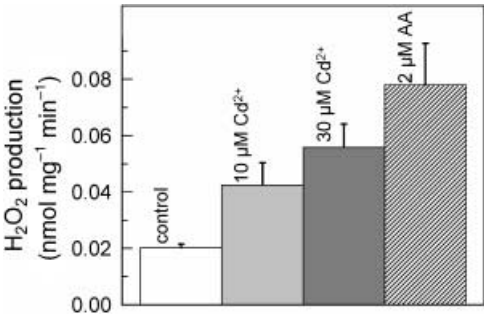

Fig. 6 Effect of $CdCl_2$ and antimycin A (AA) on H_2O_2 production in isolated mitochondria from potato. H_2O_2 production was measured as scopoletin oxidation. Mitochondria were incubated for 30 min in the measuring buffer (see the Materials and Methods) containing 0.5 mM succinate as an electron donor and 0.2 μM mesoxalonitrile 3-chlorophenylhydrazone (CCCP) as an uncoupler, 10 U horseradish peroxidase and 5 μM scopoletin.

Effect of $CdCl_2$ on $O_2^{\bullet-}$ and H_2O_2 production in intact roots

It has been reported that Cd^{2+} stimulates extracellular H_2O_2 generation in tobacco cell cultures upon short-term exposure to the cation (Olmos *et al.*, 2003; Garnier *et al.*, 2006). The question arises as to whether Cd^{2+} affects the activity of the NOX in the plasma membrane or rather stimulates $O_2^{\bullet-}/H_2O_2$ production in the mitochondria. We measured the production of $O_2^{\bullet-}$ and H_2O_2 by intact roots of cucumber and soybean seedlings for 1 h using XTT reduction as a measurement for $O_2^{\bullet-}$ and scopoletin oxidation as a measurement for H_2O_2 (Fig. 7a–d). The rates of $O_2^{\bullet-}$ and H_2O_2 production were uncorrelated. $O_2^{\bullet-}$ production was inhibited by Cd^{2+} (Fig. 7a,c) while H_2O_2 production was stimulated (Fig. 7b,d). As Ca^{2+} reversed the Cd^{2+}-induced inhibition of $O_2^{\bullet-}$ production *in vitro* (Fig. 4), we investigated the effect of Ca^{2+} and Cd^{2+} *in vivo*. When both Cd^{2+} and Ca^{2+} were present, the inhibitory effect of Cd^{2+} on $O_2^{\bullet-}$ production was overridden (Fig. 7a,c). As antimycin A and Cd^{2+} stimulated ROS production in isolated mitochondria, we investigated the effect of antimycin A on H_2O_2 production. In the presence of antimycin A the extracellular concentration of H_2O_2 was increased (Fig. 7b) while $O_2^{\bullet-}$ production was slightly inhibited (*c.* 15%; data not shown). The increase in H_2O_2 production by antimycin A shows that the H_2O_2 originating from mitochondrial electron transport can travel long distances out of the cell to the apoplast and/or out of the roots.

In absolute terms, the effects of Cd^{2+} on $O_2^{\bullet-}$ and H_2O_2 production in cucumber and soybean roots are different but the qualitative effects are the same: $O_2^{\bullet-}$ production is inhibited and H_2O_2 production is stimulated. In soybean the rate of $O_2^{\bullet-}$ production measured by XTT was approximately four to five times lower than in cucumber roots. This may be a result of restricted diffusion of XTT and Cd^{2+} into and out of the apoplast in soybean compared with cucumber roots (see next

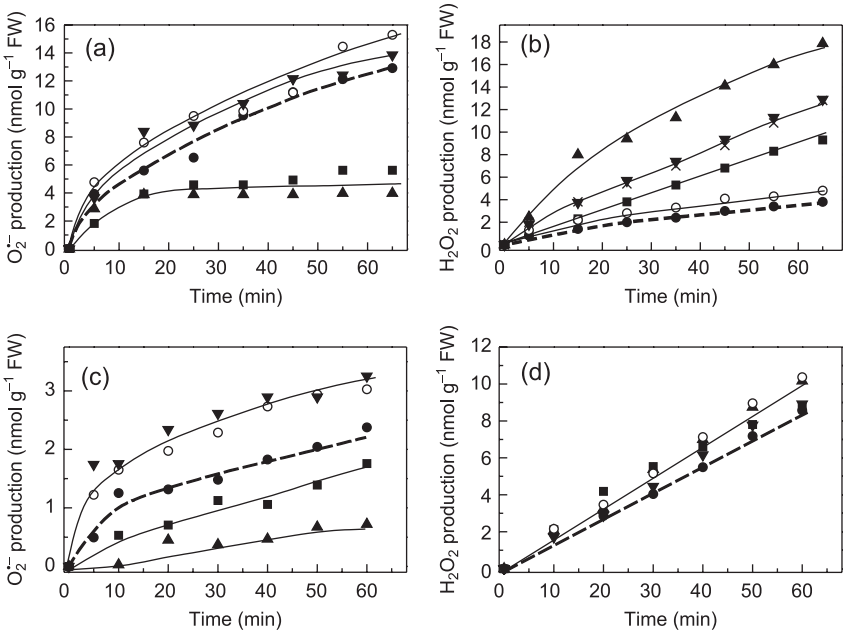

Fig. 7 Effect of $CdCl_2$ and $CaCl_2$ on $O_2^{\bullet-}$ and H_2O_2 production in roots. $O_2^{\bullet-}$ production was measured as Na,3′-(1-(phenylaminocarbonyl)-3,4-tetrazolium)-bis(4-methoxy-6-nitro)benzenesulfonic acid hydrate (XTT) reduction in cucumber (a) and soybean (c), and H_2O_2 production was measured as scopoletin oxidation in cucumber (b) and soybean (d). Symbols: control, dashed line, closed circles; 300 μM $CdCl_2$, closed squares; 3 mM $CdCl_2$, closed triangles, apex up; 5 mM $CaCl_2$, open circles; 5 mM $CaCl_2$ + 300 μM $CdCl_2$, closed triangles, apex down; 2 μM antimycin A, crosses. Roots of intact cucumber (a, b) and soybean seedlings (c, d) were incubated in 10 mM MES, pH 6.5, containing 0.5 mM XTT or 5 μM scopoletin. The results are mean values of at least three independent measurements.

section). In the absence of Cd^{2+} the rate of H_2O_2 production in soybean was higher than in cucumber, while the effects of Cd^{2+} on both $O_2^{\bullet-}$ and H_2O_2 production were lower in soybean than in cucumber.

Effect of $CdCl_2$ on $^{\bullet}OH$ production in intact roots

It has been reported previously that ROS, especially $^{\bullet}OH$, are involved in extension growth (Schopfer *et al.*, 2002). As $^{\bullet}OH$ production in roots has been shown to require both $O_2^{\bullet-}$ and H_2O_2 (Liszkay *et al.*, 2004) the question arises as to whether Cd^{2+} stimulates or inhibits $^{\bullet}OH$ production. We measured $^{\bullet}OH$ production in roots in response to Cd^{2+} and Ca^{2+} by spin trapping EPR spectroscopy using EtOH/POBN as a spin trap (Janzen *et al.*, 1978). After 1 h of incubation without added cations a characteristic EPR spectrum of the stable nitroxide radical was detected (Fig. 8, spectrum 1). The presence of 5 mM Ca^{2+} in the reaction medium increased the signal size by 30% (Fig. 8, spectrum 2). The presence of 300 μM Cd^{2+} decreased the signal size drastically (Fig. 8, spectrum 3). In the presence of both Ca^{2+} (5 mM) and Cd^{2+} (300 μM) the signal size was restored to the same level as seen in the presence of only Ca^{2+} (Fig. 8, spectrum 4).

In Fig. 8, $^{\bullet}OH$ generation was measured with cucumber and soybean roots. Qualitatively the effect of the cations was the same in both species. However, quantitatively the effect differed significantly, being more pronounced in cucumber. This was probably caused by lower penetration of the spin traps and the cations into the soybean roots. (We observed significant differences in the amount of $^{\bullet}OH$ formation in roots from several plant species. The largest signals

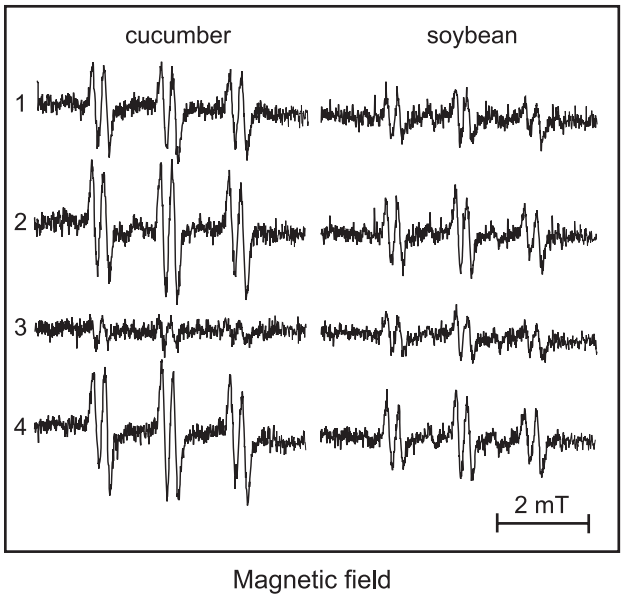

Fig. 8 Effect of $CdCl_2$ and $CaCl_2$ on $^{\bullet}OH$ production in roots. $^{\bullet}OH$ was measured using electron paramagnetic resonance (EPR) as a hydroxyethyl–N-tert-butyl-α-(4-pyridyl)nitrone N′-oxide (4-POBN) adduct. (1) Control, (2) 5 mM $CaCl_2$, (3) 300 μM $CdCl_2$, and (4) 300 μM $CdCl_2$ + 5 mM $CaCl_2$. The roots of 4-d-old intact cucumber seedlings and 3-d-old soybean seedlings were incubated in 10 mM MES, pH 6.5, containing 50 mM 4-POBN and 4% ethanol for 60 min. From the spectra the hyperfine splitting constants were determined to be A_N = 15.61 G and A_H = 2.59 G, similar to values reported in the literature (Finkelstein *et al*., 1982; Ramos *et al*., 1992). The spectra are representative of at least three measurements in indicated conditions.

compared to fresh weights were obtained from *A. thaliana* and cucumber, followed by cress (*Lepidium sativum*), pea (*Pisum sativum*), soybean and maize (*Zea mays*). The access of the spin trap to the apoplast seems to be more restricted in species with more robust roots.)

Comparing the data in Figs 7 and 8, it can be seen that the effects of Cd^{2+} and Ca^{2+} on $^{\bullet}OH$ resemble those observed for $O_2^{\bullet-}$ production. $O_2^{\bullet-}$ production by the Cd^{2+}-sensitive NAD(P)H oxidase seems to be required for this process. H_2O_2 alone, in the absence of $O_2^{\bullet-}$, is not sufficient to generate $^{\bullet}OH$ in the apoplast as H_2O_2 production increases after the addition of Cd^{2+} (Fig. 7b,d) while $^{\bullet}OH$ production decreases (Fig. 8).

Discussion

In the present study, Cd^{2+}-dependent ROS production at the level of the plasma membrane and mitochondrial electron transport chain was investigated *in vitro* and *in vivo*. $O_2^{\bullet-}$ and H_2O_2 production was followed after exposure of isolated plasma membranes, mitochondria or intact roots to Cd^{2+}. $O_2^{\bullet-}$ production by isolated plasma membranes was inhibited by Cd^{2+} competitively to Ca^{2+} (Fig. 4) while the addition of Cd^{2+} stimulated $O_2^{\bullet-}$ and H_2O_2 generation by mitochondria (Figs 5, 6). Upon exposure of intact roots to Cd^{2+}, $O_2^{\bullet-}$ formation was inhibited (Fig. 7a,c) while H_2O_2 formation increased (Fig. 7b,d). Therefore, we conclude that the Cd^{2+}-induced generation of ROS, namely H_2O_2, originates from inside the root cells, mainly from mitochondrial electron transport.

In our work with isolated plasma membranes, at least part of the $O_2^{\bullet-}$ was produced by a plasma membrane NADPH oxidase as this activity was inhibited by low concentrations of DPI (K_i = 1.5 μM) whereas KCN, an inhibitor of peroxidases, had no effect on the activity (Figs 2, 3). Potential $O_2^{\bullet-}$-producing enzymes in the plasma membrane are NOXs (Torres & Dangl, 2005) and quinone oxidoreductases (Schopfer *et al.*, 2008). Furthermore, the activity was stimulated by Ca^{2+} (Table 2) and inhibited by Cd^{2+} in a competitive manner (Fig. 4). The inhibition by low concentrations of DPI and the antagonistic effects of Ca^{2+} and Cd^{2+} indicate that the NADPH oxidase activity investigated in the present study can be attributed to a NOX activity. Sagi & Fluhr (2001) observed a twofold increase of $O_2^{\bullet-}$ production in isolated tobacco and tomato plasma membranes in response to millimolar Ca^{2+} concentrations, while in the present study $O_2^{\bullet-}$ production was only slightly (up to 30%) increased by 1–5 mM Ca^{2+}. The maximum $O_2^{\bullet-}$ production activity obtained in soybean plasma membranes was similar to that reported previously for tobacco plasma membranes (Sagi & Fluhr, 2001). In contrast to the data reported by Sagi & Fluhr (2001), after depletion of the samples of cations using Chelex 100, the activity could be restored to the control level even with micromolar Ca^{2+} concentrations (Table 2). The human EF-hand motif-containing NOX5 was previously shown to be activated at low micromolar Ca^{2+} concentrations (Banfi *et al.*, 2004), in accordance with the data presented here. In the present work, Mg^{2+} had similar effects to Ca^{2+} on $O_2^{\bullet-}$ production. Binding of Mg^{2+} and manganese (Mn^{2+}) to the EF-hand motif of 13-4-4 proteins was reported previously (Athwal & Huber, 2002). It remains to be investigated whether these cations bind to the EF-hand motifs of NADPH oxidase and further whether the effect of Mg^{2+} and Mn^{2+} is restricted to plants, as the EF-hand motifs of the human NOX5 do not bind Mg^{2+} (Banfi *et al.*, 2004).

It has been demonstrated that Cd^{2+} increases ROS formation in mitochondria from animals (Wang *et al.*, 2004). Here, Cd^{2+} and antimycin A stimulated $O_2^{\bullet-}$ and H_2O_2 production in plant mitochondria respiring on succinate (Figs 5, 6). In animal tissue mitochondria are thought to be among the major targets of Cd^{2+} toxicity (Martel *et al.*, 1990). Cd^{2+} and zinc (Zn^{2+}) are well-known inhibitors of electron transport in mitochondria (Skulachev *et al.*, 1967). Cd^{2+} blocks electron transfer between semiquinone and cytochrome b in respiratory complex III (Miccadei & Floridi, 1993) and causes the accumulation of semiquinone radicals, leading to the formation of $O_2^{\bullet-}$ (Wang *et al.*, 2004). The binding site of Cd^{2+} in complex III is likely to be the same as that of Zn^{2+}, that is, blocking a protonable group which is thought to be associated with deprotonation reactions of the quinol oxidation site in complex III (Link & von Jagow, 1995; Giachini *et al.*, 2007).

We attribute most of the $O_2^{\bullet-}$ production measured *in vivo* to NOX activity because it was inhibited by Cd^{2+} and this inhibition was reversed by Ca^{2+} both *in vitro* and *in vivo* (Figs 4, 7a,c, 8). We can exclude the possibility that peroxidases are the source of $O_2^{\bullet-}$ production, because we found that isolated horseradish peroxidase was insensitive to Cd^{2+} at the concentration used here (data not shown). It has been proposed previously that the production of $^{\bullet}OH$ involved in extension growth is initiated by NAD(P)H oxidase-catalyzed formation of $O_2^{\bullet-}$ at the plasma membrane (Schopfer *et al.*, 2002; Liszkay *et al.*, 2004) and involves peroxidases, which are abundant in the cell wall (Dunand *et al.*, 2007). In the presence of $O_2^{\bullet-}$ the catalytic heme in peroxidases is converted into its so-called 'compound III'. In this state peroxidases transform H_2O_2 into ^{-}OH and $^{\bullet}OH$ (Chen & Schopfer, 1999; Schopfer *et al.*, 2002). Thus, in the presence of H_2O_2, a measure of the production of $^{\bullet}OH$ (Fig. 8) reflects the amount of $O_2^{\bullet-}$ produced in the apoplast *in vivo*. The $O_2^{\bullet-}$, generated at the plasma membrane, is needed for the activation of the peroxidase to compound III. $O_2^{\bullet-}$ seems to be necessary in more than just catalytic amounts, because in the presence of Cd^{2+} $O_2^{\bullet-}$ production (Fig. 7a,c) and $^{\bullet}OH$ production (Fig. 8) are strongly inhibited while H_2O_2 increases with time (Fig. 7b,d).

Cd^{2+}-induced H_2O_2 production *in vivo* is likely to originate largely from mitochondrial electron transfer as Cd^{2+} increased ROS production in isolated mitochondria (Figs 5, 6). According to Varga *et al.* (2002), in cucumber, *c.* 70% of the extracellular Cd^{2+} can reach the cytoplasm, implying that a high percentage of the added Cd^{2+} will reach the mitochondria. H_2O_2 produced inside the mitochondria seems to be able to diffuse out

of the cells as in the presence of antimycin A the amount of extracellular H_2O_2 was increased (Fig. 7b). In addition to H_2O_2 of mitochondrial origin, a basal level of peroxisomal H_2O_2 production (Corpas *et al.*, 2001; del Río *et al.*, 2002; Hänsch *et al.*, 2006; Nyathi & Baker, 2006) may affect the total amount of H_2O_2 produced by intact roots.

Increased H_2O_2 production during short-term exposure of tobacco cell cultures to Cd^{2+} has been reported previously (Olmos *et al.*, 2003; Garnier *et al.*, 2006; Ortega-Villasante *et al.*, 2007). Using video microscopy Ortega-Villasante *et al.* (2007) recently observed Cd^{2+}-induced H_2O_2 generation inside and outside of roots, in agreement with our present conclusions. Olmos *et al.* (2003) and Garnier *et al.* (2006), however, concluded that NOX activity is responsible for Cd^{2+}-induced H_2O_2 production, at least during the initial phase of the oxidative burst. Using tobacco cell cultures Olmos *et al.* (2003) measured Cd^{2+}-induced H_2O_2 generation which was strongly inhibited by DPI and interpreted this as evidence for the involvement of a NOX-like enzyme in ROS production. Addition of DPI abolishes the Cd^{2+}-induced generation of H_2O_2 *in vivo* and this is often taken as a sign of the involvement of a plasma membrane NOX-like enzyme in the Cd^{2+}-induced oxidative burst (Olmos *et al.*, 2003; Romero-Puertas *et al.*, 2004; Rodriguez-Serrano *et al.*, 2006). DPI is often regarded as a specific inhibitor of NOX at low micromolar concentrations (< 10 μM; Doussiere & Vignais, 1992) although it also inhibits complex I of the respiratory chain at equally low concentrations (Ragan & Bloxham, 1977). Therefore, DPI also inhibits mitochondrial ROS production *in vivo*. In addition, DPI inhibits other flavin-containing enzymes at higher concentrations (≥ 10 μM; Doussiere *et al.*, 1992) and peroxidases at even higher concentrations (Frahry & Schopfer, 1998). In our hands, DPI inhibited Cd^{2+}-induced H_2O_2 production in roots (data not shown) but because of the different sites of action of this inhibitor it seems to us to be impossible to draw conclusions from this fact.

Garnier *et al.* (2006) identified different phases of Cd^{2+}-induced ROS production using tobacco cell cultures. A transient first wave was linked to the activity of plasma membrane NOX and a second longer lasting wave to $O_2^{\bullet-}$ production in mitochondria, and a third wave was characterized by lipid hydroperoxide accumulation concomitant with cell death. The first wave was completely abolished in an antisense construct of *NtrbohD*, implying that the NOXs of the plasma membrane were responsible for the first wave. We measured Cd^{2+}-induced H_2O_2 production using mutants of *atrbohC* and *atrbohD* defective in NOX activity (Torres *et al.*, 2005). ROS production is decreased in *atrbohC* (Foreman *et al.*, 2003; Renew *et al.*, 2005). In the *atrbohC* mutant, Cd^{2+} stimulated H_2O_2 production to the same extent as in wild type (Supplementary Material Fig. S1), indicating that the Cd^{2+}-dependent H_2O_2 generation was not impaired in this mutant and was therefore not linked to NOX activity. In *atrbohD*, Cd^{2+}-induced H_2O_2 production was abolished, in agreement with Garnier *et al.* (2006). This observation is in contradiction to the results presented here, which clearly indicate that Cd^{2+} induces mitochrondrial ROS production. This seems to indicate that some other processes involved in Cd^{2+} uptake or toxicity are impaired in the *atrbohD* mutant and in *NtrbohD* antisense strains (Garnier *et al.*, 2006). Sagi *et al.* (2004) investigated *Rboh* antisense lines in tomato and reported major pleiotrophic effects on the phenotype of the plant and its reproductive organs. A total of 384 expressed sequence tags (ESTs) were down-regulated and 485 ESTs were up-regulated in the *Rboh* antisense line. According to Sagi *et al.* (2004), Rbohs play a role in redox-related cellular activities and they affect the level of the expression of ROS-dependent genes, signal transduction and developmental processes. Therefore, it seems to be difficult to draw conclusions from *Rboh* antisense lines. Further investigations must be performed on antisense lines to investigate in detail whether the lack of the Cd^{2+}-induced ROS generation is attributable to alterations in the amount of ROS-detoxifying enzymes or to alteration of other metabolic processes.

A short time of exposure to the metal is crucial to study the primary effect of Cd^{2+} toxicity. After a long-term exposure of plants to Cd^{2+} many physiological processes are affected. Higher expression levels of Rbohs have been reported after long-term exposure of plants to Cd^{2+} (Van Belleghem, 2007) and chelation of Cd^{2+} takes place in the cytosol (Schützendübel & Polle, 2002). Furthermore, Cd^{2+} increases the concentration of abscisic acid (ABA) (Hsu & Kao, 2003), which is known to lead to the activation of the NOX (Kwak *et al.*, 2003). Long-term exposure of plants to Cd^{2+} has been reported to activate $O_2^{\bullet-}$ and H_2O_2 production both in the cytoplasm and in the plasma membrane, where NOX is thought to be responsible for the activity (Romero-Puertas *et al.*, 2004; Rodriguez-Serrano *et al.*, 2006).

One problem limiting progress in understanding the biological role of ROS is that it is difficult to attribute an oxidative burst to a well-defined ROS-producing reaction. A new view of the primary sources of ROS produced in response to signaling is developing. Ashtamker *et al.* (2007) using tobacco cell cultures reported a first cryptogein-induced H_2O_2 burst in mitochondria, the endoplasmic reticulum and the nucleus followed by a second burst at the plasma membrane after a few seconds. In a mammalian system, mitochondrial H_2O_2 production in response to a stress signal partially mediated the activation of Nox1 after a lag time of a few hours (Lee *et al.*, 2006). The availability of inhibitors of enzymatic reactions producing ROS in specific cell compartments, as shown here for Cd^{2+}, may elucidate the complex interaction of ROS-producing reactions *in vivo*.

Acknowledgements

We would like to thank Peter Schopfer, Universität Freiburg, and Bill Rutherford, CEA Saclay, for stimulating discussions and critical reading of the manuscript, Katharina Kienzler,

Universität Freiburg, for excellent technical assistance and Francis Haraux, CEA Saclay, and Sébastien Thomine, CNRS Gif sur Yvette, for stimulating scientific discussions. We are grateful to Wolfgang Michalke, Universität Freiburg, Ulrich Schulte, Universität Düsseldorf, and Françoise Simon-Plas, Laboratoire de Phytopharmacie Dijon, for providing us with antibodies against P-ATPase, Rieske and NtrbohD proteins, respectively.

References

Apel K, Hirt H. 2004. Reactive oxygen species: metabolism, oxidative stress, and signal transduction. *Annual Review of Plant Biology* **55**: 373–399.

Ashtamker C, Kiss V, Sagi M, Davydov O, Fluhr R. 2007. Diverse subcellular locations of cryptogein-induced reactive oxygen species production in tobacco bright yellow-2 cells. *Plant Physiology* **143**: 1817–1826.

Athwal GS, Huber SC. 2002. Divalent cations and polyamines bind to loop 8 of 14-3-3 proteins, modulating their interaction with phosphorylated nitrate reductase. *Plant Journal* **29**: 119–129.

Banfi B, Tirone F, Durussel I, Knisz J, Moskwa P, Molnar GZ, Krause KH, Cox JA. 2004. Mechanism of Ca^{2+} activation of the NADPH oxidase 5 (NOX5). *Journal of Biological Chemistry* **279**: 18583–18591.

Bienert GP, Møller AL, Kristiansen KA, Schulz A, Møller IM, Schjoerring JK, Jahn TP. 2007. Specific aquaporins facilitate the diffusion of hydrogen peroxide across membranes. *Journal of Biological Chemistry* **282**: 1183–1192.

Boveris A, Chance B. 1973. Mitochondrial generation of hydrogen peroxide – general properties and effect of hyperbaric-oxygen. *Biochemical Journal* **134**: 707–716.

Boveris A, Oshino N, Chance B. 1972. The cellular production of hydrogen peroxide. *Biochemical Journal* **128**: 617–630.

Bradford MM. 1976. A rapid and sensitive method for the quantitation of microgram quantities of protein utilizing the principle of protein-dye binding. *Analytical Biochemistry* **72**: 248–254.

Brightman AO, Barr R, Crane FL, Morré DJ. 1988. Auxin-stimulated NADH oxidase purified from plasma membrane of soybean. *Plant Physiology* **86**: 1264–1269.

Cape JL, Bowman MK, Kramer DM. 2007. A semiquonone intermediate generated at the Qo site of the cytochrome bc_1 complex: importance for the Q-cycle and superoxide production. *Proceedings of the National Academy of Sciences, USA* **104**: 7887–7892.

Chen SX, Schopfer P. 1999. Hydroxyl-radical production in physiological reactions. A novel function of peroxidase. *European Journal of Biochemistry* **260**: 726–735.

Corpas FJ, Barroso JB, Del Río LA. 2001. Peroxisomes as a source of reactive oxygen species and nitric oxide signal molecules in plant cells. *Trends in Plant Science* **6**: 145–150.

DeHahn T, Barr E, Morré JM. 1997. NADH oxidase activity present on both the external and internal surfaces of soybean plasma membranes. *Biochimica et Biophysica Acta* **1328**: 99–108

Del Río LA, Corpas J, Sandalio LM, Palma JM, Gómez M, Barroso JB. 2002. Reactive oxygen species, antioxidant systems and nitric oxide in peroxisomes. *Journal of Experimental Botany* **53**: 1255–1272.

Douce R, Bourguignon J, Brouquisse R, Neuburger M. 1987. Isolation of plant mitochondria: general principles and criteria of integrity. *Methods in Enzymology* **48**: 403–420.

Doussiere J, Gaillard J, Vignais PV. 1999. The heme component of the neutrophil NADPH oxidase complex is a target for aryliodonium compounds. *Biochemistry* **38**: 3694–3703.

Doussiere J, Vignais PV. 1992. Diphenylene iodonium as an inhibitor of the NADPH oxidase complex of bovine neutrophils. Factors controlling the inhibitory potency of diphenylene iodonium in a cell-free system of oxidase activation. *European Journal of Biochemistry* **208**: 61–71.

Dunand C, Crevecoeur M, Penel C. 2007. Distribution of superoxide and hydrogen peroxide in Arabidopsis root and their influence on root development: possible interaction with peroxidases. *New Phytologist* **174**: 332–341.

Faller P, Kienzler K, Krieger-Liszkay A. 2005. Mechanism of Cd^{2+} toxicity: Cd^{2+} inhibits photoactivation of photosystem II by competitive binding to the essential Ca^{2+} site. *Biochimica et Biophysica Acta* **1706**: 158–164.

Finkelstein E, Rosen GM, Raukman EJ. 1982. Production of hydroxyl radicals by decomposition of superoxide spin trapped adducts. *Molecular Pharmacology* **21**: 262–265.

Foreman J, Demidchik V, Bothwell JH, Mylona P, Miedema H, Torres MA, Linstead P, Costa S, Brownlee C, Jones JD *et al.* 2003. Reactive oxygen species produced by NADPH oxidase regulate plant cell growth. *Nature* **422**: 442–446.

Frahry G, Schopfer P. 1998. Inhibition of O_2-reducing activity of horseradish peroxidase by diphenyleneiodonium. *Phytochemistry* **48**: 223–227.

Garnier L, Simon-Plas F, Thuleau P, Agnel JP, Blein JP, Ranjeva R, Montillet JL. 2006. Cadmium affects tobacco cells by a series of three waves of reactive oxygen species that contribute to cytotoxicity. *Plant, Cell & Environment* **29**: 1956–1969.

Giachini L, Francia F, Veronesi G, Lee DW, Daldal F, Huang LS, Berry EA, Cocco T, Papa S, Boscherini F *et al.* 2007. X-ray absorption studies of Zn^{2+} binding sites in bacterial, avian and bovine cytochrome bc1 complexes. *Biophysical Journal* **93**: 2934–2951.

Halliwell B, Gutteridge JMC. 1999. *Free radicals in biology and medicine*. Oxford, UK: Oxford University Press.

Hänsch R, Lang C, Riebeseel E, Lindigkeit R, Gessler A, Rennenberg H, Mendel RR. 2006. Plant sulphite oxidase as novel producer of H_2O_2. *Journal of Biological Chemistry* **281**: 6884–6888.

Henderson LM, Chappel JB, Jones OTG. 1988. Internal pH changes associated with the activity of NADPH oxidase of human neutrophils. *Biochemical Journal* **251**: 563–567.

Hsu YT, Kao CH. 2003. Role of abscisic acid in cadmium tolerance of rice (*Oryza sativa* L.) seedlings. *Plant, Cell & Environment* **26**: 867–874.

Janzen EG, Wang YY, Shetty RV. 1978. Spin trapping with a-pyridyl 1-oxide N-tert-butyl nitrones in aequous solutions. A unique electron spin resonance spectrum for the hydroxyl radical adduct. *Journal of the American Chemical Society* **100**: 2923–2925.

Kabała K, Janicka-Russak M, Burzyński M, Kłobus G. 2008. Comparison of heavy metal effect on the proton pumps of plasma membrane and tonoplast in cucumber root cells. *Journal of Plant Physiology* **165**: 278–288.

Kashino Y, Satoh K, Katoh S. 1986. A simple procedure to determine Ca^{2+} in oxygen-evolving preparations from *Synechococcus* sp. *FEBS Letters* **205**: 150–154.

Keller T, Damude HG, Werner D, Doerner D, Dixon RA, Lamb C. 1998. A plant homolog of the neutrophil NADPH oxidase $gp91^{phox}$ subunit gene encodes a plasma membrane protein with Ca^{2+} binding motifs. *Plant Cell* **10**: 255–266.

Kwak JM, Mori IC, Pei ZM, Leonhardt N, Torres MA, Dangl JL, Bloom RE, Bodde S, Jones JD, Schroeder JI. 2003. NADPH oxidase AtrbohD and AtrbohF genes function in ROS-dependent ABA signaling in Arabidopsis. *EMBO Journal* **22**: 2623–2633.

Larsson C, Sommarin M, Widell S. 1994. Isolation of highly purified plant plasma membranes and separation of inside-out and right-side-out vesicles. *Methods in Enzymology* **228**: 451–469.

Lee SB, Bae IH, Bae YS, Um HD. 2006. Link between mitochondria and NADPH oxidase 1 isozyme for the sustained production of reactive oxygen species and cell death. *Journal of Biological Chemistry* **281**: 36228–36235.

Link TA, von Jagow G. 1995. Zinc ions inhibit the Q_p center of bovine heart mitochondrial bc_1 complex by blocking a protonatable group. *Journal of Biological Chemistry* **270**: 25001–25006.

Liszkay A, van der Zalm E, Schopfer P. 2004. Production of reactive oxygen intermediates O_2^-, H_2O_2, and OH by maize roots and their role in wall loosening and elongation growth. *Plant Physiology* **1362**: 3114–3123.

Martel E, Marion M, Denizeau M. 1990. Effect of cadmium on membrane potential in isolated rat hepatocytes. *Toxicology* **60**: 161–172.

Miccadei S., Floridi A. 1993. Sites of inhibition of mitochondrial electron transport by cadmium. *Chemical and Biological Interactions* **89**: 159–167.

Michalke W, Schmieder M. 1979. Fractionation of particulate material from maize coleoptile homogenates with polyethylene glycol. *Planta* **145**: 129–135.

Mika A, Lüthje S. 2003. Properties of guaiacol peroxidase activities isolated from corn root plasma membranes. *Plant Physiology* **132**: 1489–1498.

Nyathi Y, Baker A. 2006. Plant peroxisomes as a source of signalling molecules. *Biochimica et Biophysica Acta* **1763**: 1478–1495.

Olive G, Mercier A, Le Moigne F, Rockenbauer A, Tordo P. 2000. 2-ethoxycarbonyl-2-methyl-3,4-dihydro-2H-pyrrole-1-oxide: evaluation of the spin trapping properties. *Free Radicals in Biology and Medicine* **28**: 403–408.

Olmos E, Martinez-Solano JR, Piqueras A, Hellin E. 2003. Early steps in the oxidative burst induced by cadmium in cultured tobacco cells (BY-2 line). *Journal of Experimental Botany* **54**: 291–301.

Ortega-Villasante C, Hernández LE, Rellán-Álvarez R, Del Campo FF, Carpena-Ruiz RO. 2007. Rapid change of cellular redox homeostasis upon exposure to cadmium and mercury in alfalfa seedlings. *New Phytologist* **176**: 96–107.

Potocký M, Jones MA, Bezvoda R, Smirnoff N, Zárský V. 2007. Reactive oxygen species produced by NADPH oxidase are involved in pollen tube growth. *New Phytologist* **174**: 742–751.

Ragan CI, Bloxham DP. 1977. Specific labelling of a constituent polypeptide of bovine heart mitochondrial reduced nicotin-adenine dinucleotide-ubiquinone reductase by the inhibitor diphenyleneiodonium. *Biochemical Journal* **163**: 605–615.

Ramos CL, Pou S, Britigan BE, Cohen MS, Rosen GM. 1992. Spin trapping evidence for myeloperoxidase-dependent hydroxyl radical formation by human neutrophils and monocytes. *Journal of Biological Chemistry* **267**: 8307–8312.

Ravanel P, Tissut M, Douce R. 1984. Effects of rotenoids on isolated plant mitochondria. *Plant Physiology* **75**: 414–420.

Renew S, Heyno E, Schopfer P, Liszkay A. 2005. Sensitive detection and localization of hydroxyl radical production in cucumber roots and Arabidopsis seedlings by spin trapping electron paramagnetic resonance spectroscopy. *Plant Journal* **44**: 342–347.

Rivetta A, Negrini N, Cocucci M. 1997. Involvement of Cd^{2+} toxicity during the early phases of radish (*Raphanus sativus* L.) seed germination. *Plant, Cell & Environment* **20**: 600–608.

Rodríguez-Serrano M, Romero-Puertas MC, Zabalza A, Corpas FJ, Gómez M, Del Río LA, Sandalio LM. 2006. Cadmium effect on oxidative metabolism of pea (*Pisum sativum* L.) roots. Imaging of reactive oxygen species and nitric oxide accumulation in vivo. *Plant, Cell & Environment* **29**: 1532–1544.

Romero-Puertas MC, Rodríguez-Serrano M, Corpas FJ, Gómez M, Del Río LA, Sandalio LM. 2004. Cadmium-induced subcellular accumulation of $O_2^{\bullet-}$ and H_2O_2 in pea leaves. *Plant, Cell & Environment* **27**: 1122–1134.

Sagi M, Davydov O, Orazova S, Yesbergenova Z, Ophir R, Stratmann JW, Fluhr R. 2004. Plant respiratory burst oxidase homologs impinge on wound responsiveness and development in *Lycopersicon esculentum*. *Plant Cell* **16**: 616–628.

Sagi M, Fluhr R. 2001. Superoxide production by plant homologues of the gp91(phox) NADPH oxidase. Modulation of activity by calcium and by tobacco mosaic virus infection. *Plant Physiology* **126**: 1281–1290.

Scandalios JG. 2002. The rise of ROS. *Trends in Biochemical Sciences* **27**: 483–486.

Schaffner W, Weissmann C. 1973. A rapid, sensitive, and specific method for the determination of protein in dilute solution. *Analytical Biochemistry* **56**: 502–514.

Schopfer P, Heyno E, Drepper F, Krieger-Liszkay A. 2008. Naphthoquinone-dependent generation of superoxide radicals by quinone reductase isolated from the plasma membrane of soybean. *Plant Physiology* **147**: 1–15.

Schopfer P, Liszkay A, Bechthold M, Fahry G, Wagner A. 2002. Hydroxyl radicals mediate cell-wall loosening and extension growth in plants. *Planta* **214**: 821–828.

Schützendübel A, Polle A. 2002. Plant responses to abiotic stresses: heavy metal-induced oxidative stress and protection by mycorrhization. *Journal of Experimental Botany* **53**: 1351–1365.

Simon-Plas F, Elmayan T, Blein JP. 2002. The plasma membrane oxidase NtrbohD is responsible for AOS production in elicited tobacco cells. *Plant Journal* **31**: 137–147.

Skulachev VP, Chistyakov VV, Jasaitis AA, Smirnova EG. 1967. Inhibition of the respiratory chain by zinc ions. *Biochemical and Biophysical Research Communication* **26**: 1–6.

Staniek K, Nohl H. 1999. H_2O_2 detection from intact mitochondria as a measure for one-electron reduction of dioxygen requires a noninvasive assay system. *Biochimica et Biophysica Acta* **1413**: 70–80.

Sutherland MW, Learmonth BA. 1997. The tetrazolium dyes MTS and XTT provide new quantitative assays for superoxide and superoxide dismutase. *Free Radical Research* **27**: 283–289.

Torres MA, Dangl JL. 2005. Functions of the respiratory burst oxidase in biotic interactions, abiotic stress and development. *Current Opinion in Plant Biology* **8**:397–403.

Torres MA, Jones JDG, Dangl JL. 2005. Pathogen-induced, NADPH oxidase-derived reactive oxygen intermediates suppress spread of cell death in *Arabidopsis thaliana*. *Nature Genetics* **37**: 1130–1134.

Van Assche F, Clijsters H. 1990. Effects of metals on enzyme activity in plants. *Plant, Cell & Environment* **13**: 195–206.

Van Belleghem F. 2007. Cadmium responses in *Arabidopsis thaliana*: a study focusing on subcellular localisation, effects on the cellular ultra structure and photosynthesis in relation to oxidative stress. PhD thesis. Hasselt, Belgium: University of Hasselt.

Van Gestelen P, Asard H, Caubergs RJ. 1997. Solubilization and separation of a plant plasma membrane NADPH- O_2^- synthase from other NAD(P)H oxidoreductases. *Plant Physiology* **115**: 543–550.

Varga A, Záray G, Fodor F. 2002. Determination of element distribution between the symplasm and apoplasm of cucumber plant parts by total reflection X-ray fluorescence spectrometry. *Journal of Inorganic Biochemistry* **89**: 149–154.

Wang Y, Fang J, Leonard SS, Rao KM. 2004. Cadmium inhibits the electron transfer chain and induces reactive oxygen species. *Free Radicals in Biology and Medicine* **36**: 1434–1443.

Zhang H, Osyczka A, Dutton PL, Moser CC. 2007. Exposing the complex III Qo semiquinone radical. *Biochimica et Biophysica Acta* **1767**: 383–387.

Supplementary Material

The following supplementary material is available for this article online:

Fig. S1 Effect of 300 μM $CdCl_2$ on H_2O_2 production in *Atrboh* mutants.

This material is available as part of the online article from:
http://www.blackwell-synergy.com/doi/abs/10.1111/j.1469-8137.2008.02512.x
(This link will take you to the article abstract.)

Please note: Blackwell Publishing are not responsible for the content or functionality of any supplementary materials supplied by the authors. Any queries (other than about missing material) should be directed to the journal at *New Phytologist* Central Office.

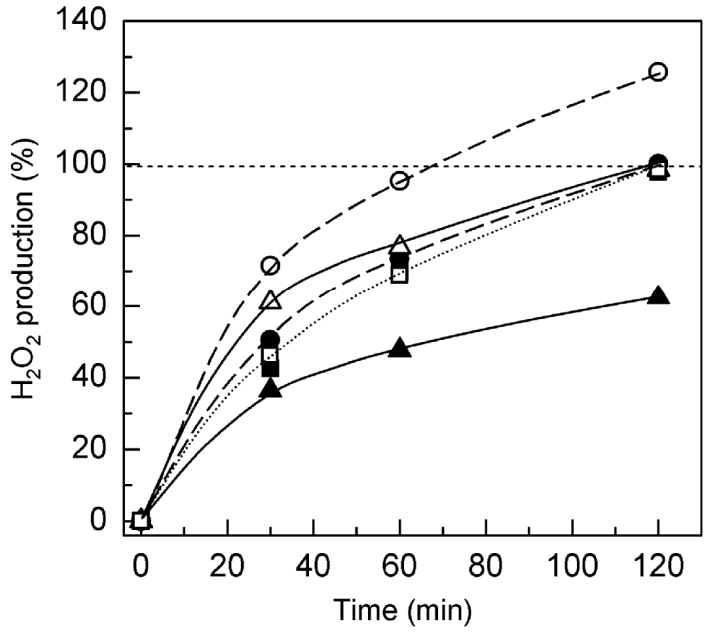

Fig.S1 Effect of 300 µM $CdCl_2$ on H_2O_2 production in *Atrboh* mutants. Closed symbols, absence of $CdCl_2$; open symbols, presence of $CdCl_2$; circles, dashed line, wt; squares, dotted line, *AtrbohD* mutant; triangles, solid line, *AtrbohC* mutant. Twenty-day-old seedlings were incubated for the given time in the assay medium.

2.3 Manuscript in preparation:

Superoxide generating enzymes in isolated plant plasma membranes

Abstract

In the present study we investigated superoxide producing enzymes of plasma membranes isolated from etiolated soybean seedlings. Evidence is presented that quinone reductases and NAD(P)H oxidases are involved in the production reactive oxygen species (ROS) in plasma membranes. We used the XTT reduction assay for detecting superoxide generation and spin-trapping EPR spectroscopy for detecting hydroxyl radical generation in PMs. The quinone reductase activity could be distinguished from background superoxide-generating NAD(P)H oxidases by differences in substrate requirements and different sensitivities to inhibitors. Peroxidase activities, also leading to ROS production, were not observed in the PM. Similarly, no hydroxyl radical-generating activity was observed in the absence of Fe^{2+}. Regulation of the activity of superoxide-producing enzymes by phosphorylation and end-product inhibition was tested. Finally, evidence for a naphtoquinone species in the plasma membranes is presented by Fourier transform infrared spectroscopy and high field EPR spectroscopy.

Abbreviations: CDPK, Calcium-dependent protein kinase; MD, menadione; NOX, NADPH oxidase; $O_2^{\bullet-}$, superoxide; $^{\bullet}OH$, hydroxyl radical; OST-1, open stomata-1; PM, plasma membrane; PRX, peroxidase; QR, quinone reductase; SnRK2, sucrose non-fermenting related kinase 2; XO, xanthin oxidase

Introduction

The plant plasma membrane (PM) contains at least two classes of enzymes able to reduce O_2 to the superoxide radical ($O_2^{\bullet-}$) using NAD(P)H as electron donor: 1) Phagocyte-type NADPH oxidases (NOXs), also called Rboh enzymes (respiratory burst oxidase homolog), which are trans-membrane enzymes that catalyse the oxidation of intracellular NADPH reducing apoplastic O_2 (Torres and Dangl, 2005) and 2) PM-associated quinone reductases (QRs) which indirectly produce $O_2^{\bullet-}$ when their end-products, dihydroquinones, deprotonate and react with O_2 (Schopfer et al., 2008). In addition it has been reported that peroxidases are located in plant plasma membranes of roots (Mika and Lüthje, 2003; Mika et al., 2008).

The presence of a phagocyte-type NOX in plant PMs is well accepted - at the genetic level - and its involvement in many plant responses has been elucidated during the last decade (Torres and Dangl, 2005). However its biochemistry is still poorly understood. Many regulatory mechanisms of plant NOXs have been found with the help of mutant studies and the knowledge from the mammalian NOXs (Torres and Dangl., 2005; Sumimoto, 2008). There is evidence of the regulation of NOX by phosphorylation *in vivo*. Proteomic studies have revealed phosphorylation of serine-residues in *A. thaliana*, potato and tobacco Rboh proteins in response

to elicitor treatment (Benschop et al., 2007; Nühse et al., 2007; Kobayashi et al., 2008). Similarly, the addition of a phosphatase inhibitor led to phosphorylation and activation of AtrbohD (Ogasawara et al., 2008). It is yet to be shown if PM $O_2^{\bullet-}$ production can be regulated by phosphorylation.

End product inhibition of $O_2^{\bullet-}$-producing enzymes in PMs was suggested recently by our group. We found a mismatch in the stoichiometry of $O_2^{\bullet-}$ production and NAD(P)H oxidation of PMs. This effect was eliminated by the addition of SOD which highly stimulated NAD(P)H oxidation (Heyno et al., 2008). Low NAD(P)H oxidation rates by isolated PMs in the absence of artificial electron acceptors have been reported earlier (Buckhout and Hrubec, 1986; Askerlund et al., 1988), but at the time it was concluded that O_2 was not a viable acceptor in PM redox reactions.

QRs catalyse the 2-electron reduction of quinones to dihydroquinones and are found in the cytosol (Sparla et al., 1996; 1998; 1999; Trost et al., 1995) and PMs (Guerrini et al., 1987; Luster and Buckhout, 1989; Pupillo et al., 1986; Serrano et al., 1994, Schopfer et al., 2008) in plants. Given the lack of information on NOX and the indirect generation of ROS by QRs, the latter are sometimes regarded as an alternative source of ROS in the PMs (Schopfer et al., 2008). Although QRs mediate ROS production *in vitro*, it is not known if these enzymes can serve as a source of ROS *in vivo*. A quinone substrate in the PM is a crucial point for this activity. Evidence for PM electron transfer reactions involving vitamin K1 in cultured carrot cells was presented by Barr et al. (1992) and a vitamin K-type quinone was extracted from isolated PMs of *Zea mays* roots (Lüthje et al.,1998) Unfortunately, there are no further studies on the nature of plant PM quinones, e.g. amounts or biochemical properties. On the contrary, evidence for ubiquinones (UQ) in mammalian PMs is solid (Kalén et al., 1987). Furthermore, depleting rat liver PMs of UQ led to decreased ferricyanide reduction rates which were recovered after re-introducing UQ but not vitamin K to the membranes (Sun et al., 1992).

Peroxidases (PRXs) generate $O_2^{\bullet-}$ via the 1-electron oxidation of NADH (Halliwell and Gutteridge, 2003). PRXs are thought to reside mainly in the cell wall but there is evidence for low abundances of PM-bound PRXs in PM isolated from maize roots (Mika and Lüthje, 2003; Mika et al., 2008). In the presence of $O_2^{\bullet-}$ and H_2O_2 the heme protein PRX can give rise to hydroxyl radical ($^{\bullet}OH$) in a Fenton-type reaction, effectively replacing the Fenton catalyst Fe^{2+}/Fe^{3+} (Chen and Schopfer, 1999):

$$Fe^{3+} + O_2^{\bullet-} \rightarrow Fe^{2+} + O_2$$
$$H_2O_2 + Fe^{2+} \rightarrow {}^{\bullet}OH + {}^{-}OH + Fe^{3+}$$

Given this scenario, the formation of $O_2^{\bullet-}$ by the PM, which also serves as the source of H_2O_2 via spontaneous or SOD-catalyzed $O_2^{\bullet-}$ dismutation, can theoretically initiate the generation of $^{\bullet}OH$.

The production of $^{\bullet}OH$ by living plant tissues presumably involving PM enzyme activities has been demonstrated with the help of electron paramagnetic resonance (EPR) spectroscopy using ethanol/α-(4-pyridyl-1-oxide)-*N*-*tert*-butylnitrone (POBN) as a specific spin-trapping system (Kuchitsu et al., 1995; Schopfer et al., 2002; Liszkay et al., 2003; 2004; Renew et al., 2005). However, it has not yet been clearly established whether the apoplastic generation of $^{\bullet}OH$ *in vivo* represents an intrinsic property of the PM or an accessory function catalysed by cell wall PRXs supplied with $O_2^{\bullet-}$ and H_2O_2 originating from the PM. Spatially separated production of $O_2^{\bullet-}$ (by the PM) and $^{\bullet}OH$ (within the cell wall) has been proposed as a central feature of a hypothesis in which PRX-generated $^{\bullet}OH$ functions as a wall-loosening agent in cell growth (Schopfer et al., 2002; Liszkay et al., 2004; Schopfer and Liszkay, 2006). On the other hand, NADH-dependent but $O_2^{\bullet-}$-independent $^{\bullet}OH$ production by PMs was reported by Mojović et al (2004), which seems to be a PRX-independent mechanism.

Many of the mechanistic constraints of these three enzymes are unknown. In the present work we investigated the substrate preference and regulation of the NAD(P)H-dependent ROS-producing activities NOX and QR. We distinguished between these two activities in PMs based on sensitivities to inhibitors. Furthermore we studied the presence of quinones in the PM by specific spectroscopic approaches. The electronic/chemical structure of quinones and their corresponding reduced forms (semiquinone and quinol) are readily detectable using optical/vibrational and magnetic resonance spectroscopies. We have used high field electron paramagnetic resonance (HFEPR) and Fourier transform infrared (FTIR) spectroscopies to detect and characterise a quinone species in isolated PMs. In addition, we investigated the presence of PRXs in PMs and the ability of PMs to generate $^{\bullet}OH$. To clarify the biochemical relationship between $O_2^{\bullet-}$ and $^{\bullet}OH$ generation, we have investigated the formation of these radicals in isolated PMs and critically addressed the question whether PRXs are present in PMs isolated form soybean hypocotyl. Last, we applied for the first time a phosphorylation assay on isolated PM and followed changes in $O_2^{\bullet-}$-generation. In addition, we investigated the regulation mechanism of $O_2^{\bullet-}$-producing enzymes by end product inhibition in more detail.

Materials and methods

Plant material

Seedlings of *Glycine max* L. (cv Jutro) were grown on wet vermiculite in darkness for 4.5 days

at 25°C. The top 2 cm of the hypocotyl were excised and used for plasma membrane preparation.

Isolation of plasma membranes from etiolated soybean hypocotyls

The PMs were isolated according to Thein and Michalke (1988) with some modifications. The top 1 cm of the hypocotyls were excised and incubated for 10 min in four-fold volume (fresh weight/volume) of isolation buffer (10 mM Tris/HCl pH 8.0, 20 mM Na_2EDTA, 300 mM NaCl) to which 0.1% BSA and 0.5 mM phenylmethylsulfonyl fluoride (PMSF) were added prior to use. The hypocotyls were homogenised in a blender (Waring), filtered through a nylon cloth, and centrifuged (30 min at 1300 g, 4°C). The supernatant (raw fraction) was centrifuged (45 min at 91 000 g, 4°C) to separate soluble proteins and membranes. The pellet was resuspended in isolation buffer and homogenised in a glass potter. The homogenate was diluted two-fold with isolation buffer. Polyethylene glycol (PEG) 6000 was added (4.3 g/100 ml), and the mixture was stirred on ice for 30 min, followed by centrifugation (30 min at 1300 g, 4°C) to sediment the intracellular membranes. The supernatant, containing the PMs, was centrifuged (45 min at 91 000 g, 4°C). If washed, the pellet was resuspended in two-fold volume of 1.5 M KCl, centrifuged (45 min at 91 000 g, 4°C), and the pellet was resuspensed in 20 mM HEPES buffer (pH 7.8) and stored in -70 °C. Otherwise, the final pellet of the isolation procedure was resuspended directly in HEPES buffer.

The isolated PMs were solubilised by adding 4 % Tween-20 and incubating for 30 min at 30 °C, after which the membranes were placed on ice. Perforation of the membranes was done by adding 0.025% Triton-X100 and incubating for 30 min on ice. The intactness of the isolated membranes was determined by comparing the rates of $O_2^{\bullet-}$ production (XTT reduction) and $^{\bullet}OH$ production (spin trapping EPR with 4-POBN) by the plasma membrane in the absence and presence of detergents.

Measurements of NADH oxidation

NADH oxidation was measured at 340 nm (ε_{340} =6.21 mM^{-1} cm^{-1}). The reaction mixture contained 200 µM NADH and 10-100 µg PM ml^{-1} H in 20 mM HEPES buffer, pH 7.5 (25°C). The reaction was followed for 5-20 min.

Measurements of $O_2^{\bullet-}$ production by XTT

$O_2^{\bullet-}$ production was measured by the reduction of Na,3'-[1- [(phenylamino)-carbonyl]-3,4-tetrazolium]-bis(4-methoxy-6-nitro)benzenesulfonic acid hydrate) at 470 nm (ε_{470} = 21.6

mM^{-1} cm^{-1}). XTT is apparently a 2-electron acceptor, therefore $O_2^{\bullet-}$ reacts with it in the stoichiometry of 2:1. The reaction mixture contained 10-30 µg PM ml^{-1}, 200 µM NAD(P)H, 500 µM XTT and, when mentioned, 100 µM menadione in 20 mM HEPES buffer, pH 7.5 (25°C).

Measurements of $^{\bullet}OH$

$^{\bullet}OH$ production was measured by electron paramagnetic resonance (EPR) spectroscopy using 4-POBN [α-(4-Pyridyl N-oxide)-N-tert-butylnitrone] as the spin trap. The reaction mixture contained 10-50 µg PM ml^{-1}, 50 mM POBN, 4% EtOH, Fe^{2+}-EDTA, 200 µM NAD(P)H and, when mentioned, 100 µM menadione in 20 mM HEPES (pH 7.5). EPR spectra were recorded at room temperature with a Bruker 300 X-band spectrometer at 9.69 GHz microwave frequency, 63 mW microwave power and 100 kHz modulation frequency.

Phosphorylation assay

PMs were phosphorylated according to Vlad et al. (2008). PMs were incubated for 1-3 h with 20 mM $MgCl_2$, 10 mM NaF, 200 µM ATP and 0,5-1 mM DTT in 20 mM HEPES (pH 7.5). When mentioned, 200 ng OST-1, CDPK and SnRK2-10 kinases were added (kinases provided by dr. Sylvain Merlot, CNRS Gif sur Yvette, France). The $O_2^{\bullet-}$ production of 10-30 µg ml^{-1} of incubated PMs was measured in the presence of 500 µM XTT, 200 µM NAD(P)H. The rates of DTT-mediated XTT reduction before addition of NAD(P)H were subtracted from the final rates.

FTIR spectroscopy

Isolated PMs were washed twice with the measuring buffer (10 mM MES, 10 mM $MgCl_2$, pH 5.6) followed by centrifugation at 40 000g for 15 min. The final pellet was resuspended in a small volume of the measuring buffer and ultrasonicated. A Bruker IFS88 FTIR equipped with a KBr beam splitter was used for the measurements. A PM sample of 8-10 µl was loaded on the prism and allowed to dry into a film. After verifying the stability of the film, differential spectra were recorded. Typically, the experiment started with the oxidation of the sample by 1 mM $K_3[Fe(CN)_6]$ for 5 min. 5x500 interferograms were recorded and averaged and the acquired spectrum was set as the background prior to reduction of the sample with 1 mM NADH (5 min). 5x500 interferograms were recorded, averaged and set as the background. These oxidation-reduction cycles were performed several times. Between the oxidative and reductive treatments the film was washed briefly with the measuring buffer.

HFEPR spectroscopy

Freshly isolated and solubilised PMs in 20 mM HEPES (pH 7.5) were incubated with 12 mM NADH for 10 min under light shaking and frozen in liquid nitrogen. The HFEPR spectra of 400 ul samples were measured at 4.2 K, under non-saturating conditions. Typically more than 30 scans were required. The spectrometer used for these studies has been previous described (Un et al., 2001).

Results

General characteristics of the isolated PM

We have used an isolation method in which PMs were separated from the total membrane fraction by precipitation of the intracellular membranes in PEG 6000 at low centrifugation speed. This procedure is based on the same principle as the aquaeous Dextran-PEG (two-phase) system of Larsson et al. (1994) the only difference being the absence of dextran and sucrose. The purity of the isolated PMs was of the same high level with both methods (Schopfer et al., 2008 Supplementary 1). As the majority of research on isolated PMs has been performed with membranes obtained by the method of Larsson et al. (1994), we report here the characteristics of our PM preparations that are important for the present work and its comparison with the literature. These are the intactness of the PM vesicles, the activity of ROS-producing enzymes with NADH and NADPH, and the localisation of the NOX in the PM.

Intactness of plasma membrane preparations

NADH and NADPH are intracellular electron carriers. Extracellular NAD(P)H is thought to play a role as a signalling molecule (Billington et al., 2006) but its participation in redox reactions outside the PM is questionable. It has been shown that solubilisation of isolated right-side-out PMs leads to higher rates of reduction of membrane impermeable electron acceptors such as ferricyanide and cytochrome C by NAD(P)H (Askerlund et al., 1988; Palmgren et al., 1990). This is taken as evidence for a cytoplasmic location of the NAD(P)H binding sites in membrane proteins, and therefore it can be used to estimate the intactness of isolated PMs. In the present study $O_2^{\bullet-}$ production of washed PMs was measured by XTT reduction or indirectly via EPR spectroscopy using POBN/EtOH as a spin trap (Janzen et al., 1978). $O_2^{\bullet-}$ dismutates to H_2O_2 which forms in the presence of Fe^{2+} $^{\bullet}OH$ radicals that are detected by the spin trap.

We isolated up to 90% intact PMs, but freezing and thawing of the samples decreased

the intactness to 60%. When the membranes were washed with salt (1.5 M KCl) to remove unspecifically bound proteins from the membrane surface, the intactness was decreased to 40% as seen by measuring the Fe^{2+}-catalysed $^{\bullet}OH$ production (Fig. 1). The enzyme activity (XTT reduction in the presence of NADH) was decreased by 15-25% after salt-washing. Intact PM produced 31 and 6 nmol $XTTH_2$ mg^{-1} min^{-1} with NADH and NADPH as the substrate, respectively. Table 1 shows the stimulating effects of detergents on the $O_2^{\bullet-}$-producing activities of the salt-washed PMs. Solubilisation with 4% Tween led to approximately 2-fold rate with both substrates. Perforation of the membranes by 0.025% Triton X-100 was slightly less stimulating. Menadione (MD), an artificial quinone substrate used to study QRs, led to 5- and 30-fold activity with NADH and NADPH, respectively. The MD-driven activity was almost the same with NADH and NADPH, 166 and 172 nmol $XTTH_2$ mg^{-1} min^{-1}, respectively. Treatment with detergents stimulated these rates approximately by 10-15%. Because salt-washing led to leaky membranes (Fig 1.), it is not possible to define on which side of the PM QRs are located.

In EPR spin-trapping measurements of PMs a signal attributable to POBN/$^{\bullet}OH$ was detectable in the presence of Fe^{2+}. NADPH gave signal sizes of approximately 30-40% of those with NADH. Table 2 shows the stimulating effects of detergents on the POBN/$^{\bullet}OH$ signal sizes from the salt-washed PMs. Solubilisation with 4% Tween led to a 3.6-fold and 2.5-fold rate with NADH and NADPH, respectively. Perforation of the membranes by 0.025% Triton X-100 was less effective than solubilisation with Tween. In the presence of MD a 10-fold and 24-fold increase in signal size was observed in non-treated PMs with NADH and NADPH, respectively. The MD-driven activity was almost the same with both substrates and treatment with detergents led to ~ 50% higher rates.

In our spin trapping assays Fe^{2+}-EDTA was present to allow the Fenton reaction. However, Mojović et al. (2004) reported direct $^{\bullet}OH$ generation by PMs. PRXs would be likely candidates for $^{\bullet}OH$ generation from $O_2^{\bullet-}$ and H_2O_2. There is evidence of PM-bound PRXs (Mika and Lüthje, 2003; Mika et al., 2008). However, according to our previous data, no PRX activity was found in the PM preparations from soybean hypocotyl (Schopfer et al., 2008). In the present work with the same material we did not detect EPR signals in the absence of either Fe^{2+}-EDTA, PM, or NADH (Fig. 2, spectra 2-4). Therefore, the detected $^{\bullet}OH$ radical formation in the presence Fe^{2+}-EDTA was derived from H_2O_2 generated by PMs. These PMs do not generate directly $^{\bullet}OH$ radicals in contrast to the findings reported by Mojović et al. (2004). These authors used EPR spectroscopy with 5-diethoxyphosphoryl-5-methyl-1-pyrroline-*N*-oxide (DEPMPO) as a spin-trap that forms adducts with both $O_2^{\bullet-}$ and $^{\bullet}OH$. The lifetime of the superoxide adduct is about 15 min while the hydroxyl radical adduct is longer stable (Ramos et

al., 1992). Thus, reactions in which $O_2^{\bullet-}$ serves as a precursor of $^{\bullet}OH$ are compromised in this method.

Preference of NADH- and NADPH-dependent ROS-producing enzymes in the plasma membrane

In the literature conflicting results have been reported with respect to the substrate of the $O_2^{\bullet-}$-producing NAD(P)H oxidase (Berczí and Møller, 2000). Therefore, we determined the $O_2^{\bullet-}$-production in perforated un-washed PMs in the presence of NADPH and NADH. The absolute majority of the preparations showed approximately 5-fold higher rates with NADH in comparison with NADPH. Perforated PMs gave XTT reduction rates of 82 ± 25 and 19 ± 11 nmol $XTTH_2$ mg^{-1} min^{-1} with NADH and NADPH, respectively. Figure 3 shows the XTT reduction activity of perforated PMs as a function of the NAD(P)H concentration. Two K_m values for NADH and NADPH were determined. The high affinity values were 8 and 6 µM with NADH and NADPH, respectively. The low affinity values were 200 and 167 µM. The low affinity values may reflect an unspecific enzyme activity not related to the NADH or NADPH oxidase, since the cytosolic NAD(P)H concentration is estimated to be 0.3-0.6 mM and the $NAD(P)^+$:NAD(P)H ratio 600-1000 (leaf cell cytosol: Noctor et al., 2006). The V_{max} is five times higher with NADH compared to NADPH. However, it has to be noted that we obtained also preparations with two fold higher rates with NADH in comparison with NADPH, and, very rarely, the preparations showed similar rates with both electron donors, with only a slight preference for NADH. This variation in enzyme activity within preparations suggests that the PM might be isolated in different states of activity.

Localisation of NOX

There is evidence that NOX is located in the lipid rafts in both animals and plants. The recruitment and activation of the phagocytic NOX was shown to be dependent of its localisation in the lipid rafts (Vilhardt and van Deurs, 2004). In a proteomics study on plant PM, *AtrbohD*-encoded NOX was found in the detergent-insoluble membranes after elicitation with cryptogein (Mongrand et al., 2004). Liu et al. (2009) reported the lipid raft-mediated concentration of the NOX into the tips of growing pollen tubes. In the present study, the sub-localisation of NOX in the detergent-soluble and -insoluble PM fractions was addressed.

Soluble cytosolic proteins, total membranes, intracellular membranes and the detergent-soluble and -insoluble PM fractions were separated by SDS-PAGE, immunoblotted and the presence of PM-ATPase, mitochondrial Rieske protein and NOX was verified (Fig. 4). The NOX was detected only in detergent-insoluble fraction while PM-ATPase was detected in both

fractions. There was no major contamination of PM by mitochondrial membranes, only a very weak signal from anti-Rieske was seen in the detergent-insoluble PM fraction. While the PM-ATPase and mitochondrial Rieske proteins were detected at sites of correct molecular weight (100 kDa and 29 kDa, respectively), the protein recognised by the $gp91^{phox}$-antibodies did not enter the resolving gel at all and stayed in the stacking gel. This results likely from the heavy glycosylation of the protein. Good results have been gained by de-glycosylation of the human $gp91^{phox}$ protein but these assays were ineffective in the present study (data not shown).

Pharmacological study of ROS production in isolated KCl-washed plasma membranes

The effects of known activators and inhibitors of redox enzymes on the XTT reduction of PMs was tested using NADH as the substrate (Fig. 5 a,b). Such an approach should help to identify different distinct enzymes which are capable to generate $O_2^{\bullet-}$.

Ca^{2+} is known to activate the NOX by binding to its EF-hand structures (Keller et al., 1998; Sagi and Fluhr, 2001; Heyno et al., 2008; Ogasawara et al., 2008). $CaCl_2$ stimulated XTT reduction of intact membranes only slightly. In the presence of detergent the effect was stronger. The same is seen when ROS was measured by spin trapping EPR spectroscopy (Fig. 6 a, b). Cd^{2+}, an antagonist of Ca^{2+} and an inhibitor of the NAD(P)H oxidase (Heyno et al., 2008), inhibited XTT reduction and $^{\bullet}OH$ generation by 50% in non-treated membranes and by 25% in detergent-treated membranes, $^{\bullet}OH$ generation was inhibited by 50% in both conditions. Cibacron blue 3G-A, a dye mimicking adenine nucleotides and an efficient inhibitor of QRs (Prochaska, 1988; Schopfer et al., 2008), inhibited the activities by 50% in all conditions. KCN, an inhibitor of PRXs and other heme-containing enzymes, slightly stimulated the activities. SOD (100 µg/ml) led to the disappearance of a measurable rate of XTT-reduction, indicating that only $O_2^{\bullet-}$ reacted with XTT. Diphenyleneiodonium (DPI), an inhibitor of NOXs but not of QRs, inhibited the NADPH-dependent $O_2^{\bullet-}$ production stronger than the NADH-dependent rates. The concentration-dependent effect of DPI is shown in Figure 7. 5 µM DPI led to a plateau with both substrates which corresponded to a maximal inhibition of 40 % and 80 % with NADH and NADPH, respectively. Treatment of the membranes with Triton-X-100 led to more pronounced inhibition with NADH than with NADPH. Triton likely made NADPH available to cytosolic binding sites of enzymes insensitive to DPI, while it made NADH available to DPI-sensitive activities. Indeed, if the activities in the presence of 5 µM DPI are considered 100% inhibited, the K_I of DPI is lower in the presence of Triton for both substrates; 0.2 and 0.4 µM with NADH and 0.1 and 0.2 µM with NADPH in the presence and absence of Triton, respectively. DPI could not be used in the spin trapping assays, because it leads to distorted EPR signals.

In the presence of MD XTT reduction was strongly inhibited only by Cibacron Blue while Ca^{2+} and DPI had little effect on the activity (Fig. 5 c,d). SOD decreased the XTT reduction rates by 50%, indicating that $MD^{\bullet-}$ is responsible for half of the XTT reduction (Schopfer et al., 2008). When the $^{\bullet}OH$ production was measured in the presence of MD (Fig 6 c), a clear inhibition was seen in the presence of Cd^{2+} and Cibacron Blue. Ca^{2+} had no significant effect on the $^{\bullet}OH$ production while KCN had a strong stimulating effect on both XTT reduction and $^{\bullet}OH$ production, indicating that PRXs can be excluded to contribute to the ROS production by the PM used here.

Our PM preparations contain clearly a QR, a NOX and probably other not further characterised $O_2^{\bullet-}$ generating enzymes.

Detection of quinones in isolated plasma membranes

There is little evidence for quinones in plant PMs in the literature although enzymes requiring a quinone substrate reside in PMs. We studied the presence of quinones in PM by FTIR and HFEPR spectroscopies. Figure 8 shows the FTIR difference spectra of the reduced - oxidised and oxidised - reduced PMs and the double difference spectrum of these (red. - ox.). The double difference spectrum has similar characteristics as reported previously for quinones in the literature. Positive bands corresponding to C=O vibrations of a semiquinone are expected in the range of 1640-1650 cm^{-1}, negative bands corresponding to C=C vibrations of the oxidised quinone in the range of 1585-1618 cm^{-1} (Breton et al., 1994; Breton and Nabedryk, 1996). We observed a positive band at 1648 cm^{-1} and a negative band at 1618 cm^{-1}. Positive bands corresponding to C–C and C–O vibrations of the semiquinone forms are expected in the range of 1400-1490 cm^{-1}. We observed two positive bands in this region at 1483 and 1425 cm^{-1}. No bands characteristic for free quinols in the membrane, as reported by Mezzetti et al. (2003), were detected. To conclude, similarity of the spectra in the range of C=C and C=O vibrations and, especially, the observed bands in the range typical for semiquinones, suggest protein bound quinones in the PM. However, the quality of the obtained spectra is not sufficient to determine if the quinone is a benzo- or naphthoquinone. For this purpose, HFEPR spectroscopy was applied.

The HFEPR spectrum of the PM clearly indicated the presence of an organic radical (Figure 9, black trace). The overall shape and position of the spectrum was consistent with a semiquinone radical (Un et al., 2001). Furthermore, the relative positions of the three characteristic values of the spectra (denoted gx, gy and gz) suggested that the radical was indeed a naphthosemiquinone radical that was in a relative non-polar environment. For comparison, the vitamin K_1 radical generated in ethanol (green) and in photosystem I (red) are

also shown in Figure 9. The former is in strongly polar environment while latter is in a weakly polar environment. It is well known that the magnet field values corresponding to the gx and gy positions decrease with decreasing polarity (see Un et al., 2001). The relatively low values for the PM radical would be consistent with non-polar lipid environment. For the purposes of comparison, the spectrum of the plastosemiquinone (Q_A) from plant photosystem II is also shown in Figure 9 (blue trace).

Regulation of ROS production by plasma membranes

In the present work we have observed a variation in NADH- and NADPH-dependent $O_2^{\bullet-}$-producing activities between individual preparations. A variation in redox activities with these substrates between PM preparations was mentioned also by Buckhout and Rhubec (1986). This led us to consider different regulatory mechanisms that could explain the observed differences. Potential regulatory mechanisms include phosphorylation of $O_2^{\bullet-}$-producing enzymes, and the inhibition of $O_2^{\bullet-}$ producing enzymes by $O_2^{\bullet-}$, the end-product.

Phosphorylation of the AtrbohD-encoded NOX protein has been shown by mass spectrometry (Benschop et al., 2007; Nühse et al., 2007) and evidence for the stimulation of the NOX activity by CDPK-mediated phosphorylation has also been demonstrated (Kobayashi et al., 2007; Ogasawara et al., 2008). Here preliminary results of the effect of phosphorylation of PM are shown. The effect of ATP on NAD(P)H-dependent $O_2^{\bullet-}$ production in the PM was studied. PMs in the absence or presence of Triton X-100 were incubated in the phosphorylation assay in the absence or presence of recombinant kinases OST1, SnRK2-10 (Sn-related protein kinase 2, a kinase related to OST1) and CDPK32. The effect of detergent was analysed to determine on which side of the membrane phosphorylation takes place. As described before in Table 1 and 2, solubilisation increased the rates by 40-50 % of both NADH- and NADPH-dependent activities. In the absence of detergent, incubation for 3 h in the phosphorylation assay decreased the enzyme activity while in the presence of detergent it was stimulated (Fig. 10). This seems to indicate that phosphorylation on the cytosolic side is responsible for the stimulation of the enzyme activity. The inhibitory effect of ATP on the XTT-reducing activity of intact membranes is not clear. It may be just due to the long incubation (3 h) of PM at room temperature. ATP had a stimulating effect on both, NADPH- and NADH-dependent rates and the presence of recombinant kinases had no effect on the rates (data not shown). It was also tested if the DTT concentration given in the original assay could be lowered, because it interferes with XTT reduction. The effects of ATP on the activies were seen even at the lowest DTT concentration (10 µM). The rates were slightly lower at high DTT concentrations. To conclude, in the presence of detergent, ATP had a stimulating effect on the XTT-reducing

activity of PMs.

We have previously observed a mismatch in the stoichiometries of NADH oxidation and XTT reduction, which was corrected by the addition of SOD to the NADH oxidation assay (Fig. 11; Heyno et al., 2008). The effect of SOD indicates that $O_2^{\bullet-}$ inhibits the $O_2^{\bullet-}$ production of PMs. To study this effect in more detail, we determined the rate of NADH oxidation at different SOD concentrations, the pH dependency of the inhibition of the activity by $O_2^{\bullet-}$ and the effect of externally produced $O_2^{\bullet-}$ on NADH oxidation. NADH oxidation by PM was measured at different concentrations of SOD (Fig. 12). Maximal NADH oxidation, approximately 33 nmol $mg^{-1}min^{-1}$, was reached in the presence of 25 µg ml^{-1} SOD. The removal of $O_2^{\bullet-}$ was tested next by studying the effect of pH on the NADH oxidation of the PMs (Fig. 13). $O_2^{\bullet-}$ is a short-lived molecule whose stability is pH-dependent. Spontaneous dismutation to H_2O_2 and O_2 is facilitated by the protonation of $O_2^{\bullet-}$ at acidic pH. The pK of $O_2^{\bullet-}$ is 4.8, thus the pH of the medium can be utilised to study the degree of inhibition of NADH oxidation by $O_2^{\bullet-}$. The XTT reduction rates of PM were very low at pH 4-5 because XTT is an effective electron acceptor only at alkaline pH (data not shown; Ukeda et al., 1997). Therefore, the initial rates of NADH oxidation were measured at pH 5-7.5. At pH 5.0, initial rates (0-30 s) of NADH oxidation were 10 nmol and decreased to rapidly to 2-3 nmol $mg^{-1}min^{-1}$ (Fig. 13 inset). At pH 7.5, no changes were observed in the rates over the time. At this pH the rates were approximately 3 nmol mg^{-1} min^{-1} throughout the measurement. The pH dependency of NADH oxidation suggests that the inhibiting species is $O_2^{\bullet-}$ and not H_2O_2, which is readily formed by the dismutation of $O_2^{\bullet-}$ at acidic pH. In the presence of ferricyanide no pH-dependency of NADH oxidation was observed. The reduction of ferricyanide does not involve protonation reactions. Ferricyanide seems to accept electrons prior to the site of $O_2^{\bullet-}$ inhibition. Finally, the effect of added $O_2^{\bullet-}$ on NADH oxidation was tested. $O_2^{\bullet-}$ was produced by the xanthine/xanthine oxidase (X/XO) system (Fig. 15). $O_2^{\bullet-}$ production by the X/XO system was quantified by the XTT reduction assay up to 0.1 XO units at pH 7.5 (Fig. 14 inset). The NADH oxidation of samples from two separate PM preparations, showing initial rates of 2.3 and 0.5 nmol mg^{-1} min^{-1}, was almost complete inhibited by XO concentration as low as 0.01 U, corresponding to 20 nmol $O_2^{\bullet-}$ ml^{-1} min^{-1} produced in the assay medium.

Discussion

Plant PMs contain a number of redox enzymes (Berczí and Møller, 2000) of which some are able to reduce O_2 at the expenses of NAD(P)H. We could exclude PRX-derived ROS generation in our PM preparations based on the inefficiency of KCN as an inhibitor and the lack of $^{\bullet}OH$ production in the absence of Fe^{2+}. Thus, a PRX-mediated $^{\bullet}OH$ generation which is

dependent of $O_2^{\bullet-}$ and H_2O_2 (Chen and Schopfer, 1999) can be ruled out. PM-bound or -associated PRXs have been found in material isolated from maize roots (Mika and Lüthje, 2003; Mika et al., 2008). However, PMs isolated from rose cells showed very weak PRX activities (Murphy and Auh, 1996). It is thus possible that PM PRXs are present only in PM of root tissues or that they are present in monocotyledons but not in dicotyledons.

We could resolve the QR activity from other $O_2^{\bullet-}$-producing enzymes based on the similar activities seen with NADH and NADPH, inhibition by Cibacron Blue and its insensitivity to Ca^{2+}, Cd^{2+} and DPI. Isolated QRs reported by others showed similar rates with NADPH and NADH or a slight preference for the former, depending on the quinone substrate (Pupillo et al., 1986; Guerrini et al., 1987; Luster and Buckhout, 1989, Serrano et al., 1994; Trost et al. 1995; Sparla et al., 1999, Schopfer et al., 2008). Cibacron is known to inhibit isolated QRs from several species (Deller et al., 2008). The question arises if a quinone is present in the plasma membrane. A phylloquinone has been extracted in hexane from PM (Lüthje et al., 1998). However, this extraction could not be reproduced by other groups (P. Trost, personal communication, and own assays). Here, evidence for the presence of a quinone is presented by FTIR and HFEPR spectroscopy (Figs 8 and 9). However, the quality of the spectra is not sufficient to allow a satisfying attribution to a naphthoquinone.

In the absence of menadione the activity of $O_2^{\bullet-}$-producing enzymes was stimulated by Ca^{2+} and strongly inhibited by Cd^{2+} (Fig. 5). This puts in favour a NOX being partially responsible for the observed $O_2^{\bullet-}$ production. NOX is known for the regulation of its activity by Ca^{2+} binding to its EF-hand structures. The activity is also strongly inhibited by very low concentrations of DPI while in the presence of MD DPI has no or a very small effect on the activity. DPI is used commonly as a specific inhibitor for NOX, but one should be aware of the fact that DPI inhibits in general flavin-containing enzymes in case of the participation of the semi-reduced flavin in the catalysis (O'Donnell et al., 1994).

ROS production in the absence of menadione was clearly higher with NADH than NADPH. We observed that the $O_2^{\bullet-}$ production by isolated PMs was five-fold higher with NADH than with NADPH (Figs. 3, 5, 6). This seems to be a general characteristic of plant PMs (Hassidim et al., 1987; Murphy and Auh, 1996). The same holds true for the reduction of artificial electron acceptors by isolated PMs (Buckhout and Hrubec, 1986; Luster and Buckhout, 1986; Hassidim et al., 1987). This is confusing with respect to the activity of plant NOX which is homologous to the human phagocytic NOX, showing 30-40 % identity/60-70 % similarity to the carboxy terminus (i.e. NADPH- and flavin-binding sites and the membrane-spanning regions) (Groom et al., 1996; Keller et al;, 1998;Torres et al., 1998). The isolated phagocytic NOX utilises NADPH about 30 times more efficiently than NADH (Bellavite et al.,

1983). Furthermore, a cell-free system of granulocytes and isolated granules produce more $O_2^{\bullet-}$ with NADPH than with NADH as substrate even in the dormant state of the cells (Babior et al., 1975; Iverson et al., 1977). There is some indirect evidence that the Rboh-encoded NOX utilises NADPH as the substrate. The inactivation or stimulation of the hexose monophosphate shunt, the source for cytosolic NADPH, abolished or stimulated NOX activity during pathogen challenge, respectively (Pugin et al., 1997; Scharte et al., 2009). Furthermore, DPI, an efficient inhibitor of the isolated phagocytic NOX, inhibits NADPH-dependent $O_2^{\bullet-}$ production in plant PMs more effectively than the NADH-dependent activity (Fig. 7; Murphy and Auh, 1996). It should be noted that Van Gestelen et al. (1997; 1998) separated an NADPH-dependent $O_2^{\bullet-}$-producing activity from three other activities: one NADH-dependent and two NAD(P)H-dependent activities which were stimulated by artificial quinones. However, no molecular weight was given for the separated NADPH-dependent $O_2^{\bullet-}$-producing enzyme and the activity was only weakly inhibited by DPI (I_{50}=60 µM). NOX enzymes have been detected in isolated PMs by antibodies (Keller et al., 1996; Sagi and Fluhr, 2001). We detected the NOX exclusively in detergent-insoluble fraction of PMs (Fig. 4 b). Murphy and Auh (1996) reported the sedimentation of NADH-dependent activity after solubilisation while the NADPH-dependent activity stayed in the supernatant. The possibility thus remains that the plant NOXs utilise preferentially NADH.

In the present work we showed that a phosphorylation assay stimulated the $O_2^{\bullet-}$ producing activity in isolated PM in the presence of detergent. This implies that the site of action of ATP and/or the binding site of the substrate of the phosphorylated enzyme(s) were intracellular. Addition of external kinases had no further stimulating effect on the activities. It is thus possible that a kinase present in the PMs was responsible for this effect. Several receptor kinases are located in plant PMs (Walker, 1994). It is also possible that the kinases tested in the present work, the *A. thaliana* CDPK-32, OST-1 and a SnrK2-10, are not capable to phosphorylate soybean enzymes. There is strong evidence for the requirement of cytosolic kinases in the activation of plant NOX. Doke and Miura (1995) reported an elicitor-driven activation of the NADPH-driven $O_2^{\bullet-}$ production in isolated PMs which was dependent on both ATP and cytosolic proteins. Kobayashi et al. (2007) succeeded to phosphorylate a tobacco RbohD protein with a CDPK of potato and simultaneously to enhance RbohD-derived $O_2^{\bullet-}$ production *in vivo*. A kinase of the SnrK family has been demonstrated to act up-stream of PM ROS production in ABA-dependent signalling. The OST1 kinase gene (open stomata 1) was found in mutant screens of plants that fail to close their stomata (Mustilli et al. 2002). Very recently the direct interaction with and phosphorylation of the AtrbohF protein by OST1 was

shown (Sirichandra et al., 2009).

The mammalian NOXs are also regulated by phosphorylation but there are differences in the sites of phosphorylation and the kinases involved in this process between plants and animals. Plant NOXs have been reported to be phosphorylated exclusively on the cytosolic EF-hands. The phagocytic NOX2 complex is known to be regulated by the phosphorylation of the cytosolic subunits which are absent in plants. However, Raad et al. (2009) reported the phosphorylation of the C-terminus in phagocytic $gp91^{phox}$ by protein kinase C (PKC). Phosphorylation increased the diaphorase activity of a truncated $gp91^{phox}$ C-terminus (containing the NADPH-binding site and FAD). The mammalian NOX5 has four Ca^{2+}-binding EF-hands in the N-terminal region and does not have cytosolic subunits and is, therefore, the closest homolog of the plant NOXs. There is evidence of its regulation by phosphorylation by PKC-family of kinases in the vicinity of the C-terminal FAD-binding site (Jagnandan et al., 2007; Serrander et al., 2007). Also a redox-dependent activation of the NOX5 by the c-Abl tyrosine kinase was demonstrated by El Jamali et al. (2008).

We reported the inhibition of the NADH oxidation by PMs by $O_2^{\bullet-}$ (Heyno et al., 2008). Very slow rates of NAD(P)H oxidation in the absence of artificial electron acceptors have been reported before (Buckhout and Hrubec, 1986; Askerlund et al., 1988). To the best of our knowledge, the inhibition of NOX or other professional ROS producers by $O_2^{\bullet-}$ has not been reported before in plants nor in animals. Although we always observed the incorrect stoichiometry between the rates of NADH oxidation and $O_2^{\bullet-}$ production, in some PM preparations the effect of SOD was very high, weak or absent. Yet the $O_2^{\bullet-}$ production was relatively constant in all PM preparations. The reason for the heterogeneity of the PM preparations with respect to this effect is unclear. However, it allows us to hypothesise that the inhibition of NADH oxidation by $O_2^{\bullet-}$ is reversible and may turn into an irreversible mode if $O_2^{\bullet-}$ is present for a too long time or is bound too tightly. In NOX O_2 reduction takes place at the second heme at the apoplastic side of the PM (Cross and Segal, 2004). Irreversible inhibition could occur if $O_2^{\bullet-}$ can not leave this site and the SOD does not have access to it. The relatively stable XTT reduction rates in the PM preparations can still occur because XTT gets close enough to this site and removes the $O_2^{\bullet-}$. It remains to be studied if a total inactivation by $O_2^{\bullet-}$ takes place in NOXs and if also other redox activities in PMs are inhibited by $O_2^{\bullet-}$. We propose that a different level of $O_2^{\bullet-}$-mediated inhibition may play a role in the fluctuating properties of our PM preparations and of those reported by others. End-product inhibition seems to be an attractive strategy for the regulation of $O_2^{\bullet-}$ producing enzymes *in vivo*. $O_2^{\bullet-}$ is the precursor of potentially very harmful ROS like $^{\bullet}OH$ and therefore its production has to be

controlled at several levels. It remains to be studied if such end-product inhibition occurs *in vivo*. This will be a difficult task since many simultaneous signalling events and sinks for ROS are present in a living system. It is likely that this kind of regulation takes place within very short time scales, contributing to the $O_2^{\bullet -}$ production rates observed *in vivo*.

Table 1. Effect of detergents and menadione (MD) on XTT reduction in salt-washed plasma membranes (PMs). The increase in activity is indicated as a fold value with respect to the untreated PM. The effect of detergent on the rates in the presence of MD is given in brackets. The activity of the untreated PM was 31 ± 2 nmol and 6 ± 2 $XTTH_2$ mg^{-1} min^{-1} with 200 µM NADH (n= 9) and NADPH (n=6), respectively. All samples were frozen and thawed once.

	XTT reduction rate	
Sample	***NADH***	***NADPH***
PM (untreated)	**1**	**1**
PM + Triton X-100	1.4	2
PM + Tween	1.8	2.3
PM (untreated) + MD	5.5 (1)	28 (1)
PM + Triton X-100 + MD	6.6 (1.2)	31 (1.1)
PM + Tween + MD	6.8 (1.2)	41 (1.5)

Table 2. Effect of detergents and menadione (MD) on Fe^{2+}-catalysed $^{\bullet}OH$ generation in salt-washed PMs. The increase in activity is indicated as a fold value with respect to the the untreated PM. The effect of detergent on the signal sizes in the presence of MD is given in brackets. All samples were frozen and thawed once.

	POBN/OH signal size	
Sample	***NADH***	***NADPH***
PM (untreated)	**1**	**1**
PM + Triton X-100	1.5	1,3
PM + Tween	3.5	2.5
PM (untreated) + MD	10 (1)	24 (1)
PM + Triton X-100 + MD	14 (1.4)	36 (1.5)
PM + Tween + MD	n.d.	n.d.

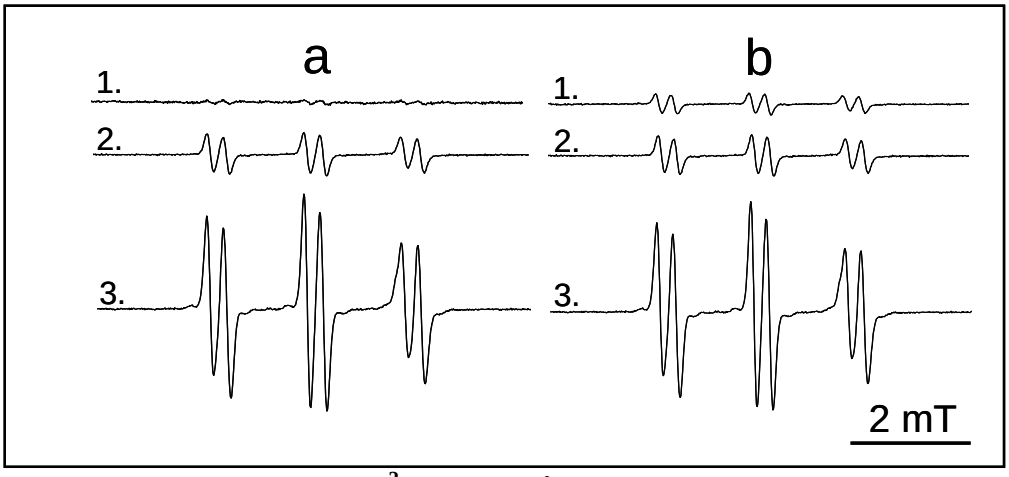

Figure 1. Comparison of Fe^{2}-catalysed $^{\bullet}OH$ generation in a) control and b) salt-washed plasma membranes (PMs). 1. Untreated PMs, 2. Triton-treated PMs and 3. Triton-treated PM in the presence of 100 µM menadione. A reaction mixture contained 50 mM POBN, 4% EtOH, 50 µM Fe^{2+} -EDTA, 10-14 µg ml^{-1} PM proteins and 200µM NADH.

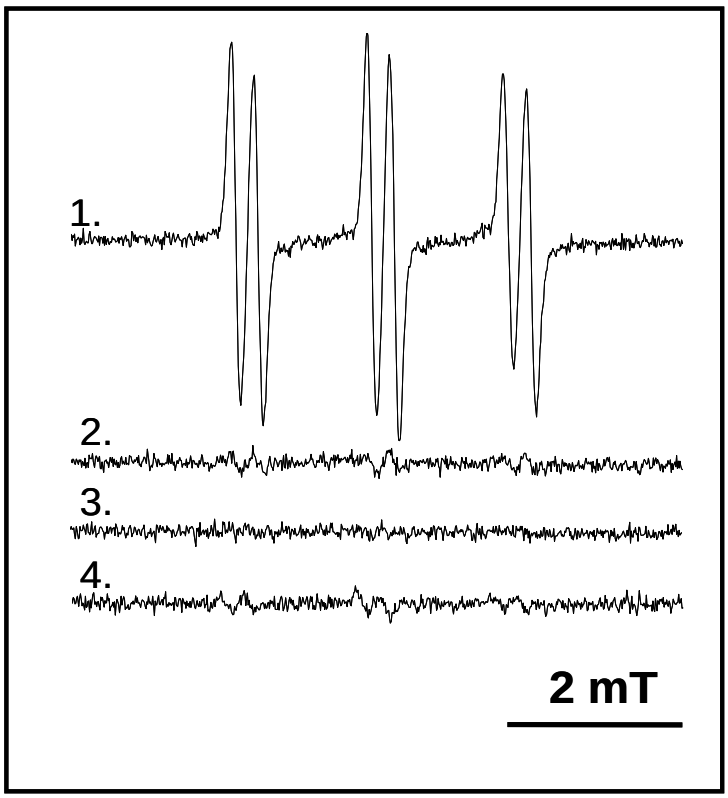

Figure 2. The EPR signal size of POBN-spintrap in $^{\bullet}OH$-generating assays of PM. A reaction mixture contained 50 mM POBN, 4% EtOH, 50 µg ml^{-1} PM proteins, 200µM NADH and 50 µM Fe^{2+}-EDTA (1.). The assay was also performed without Fe^{2+}-EDTA (2.), without NADH (3.), or without both Fe^{2+}-EDTA and NADH (4.).

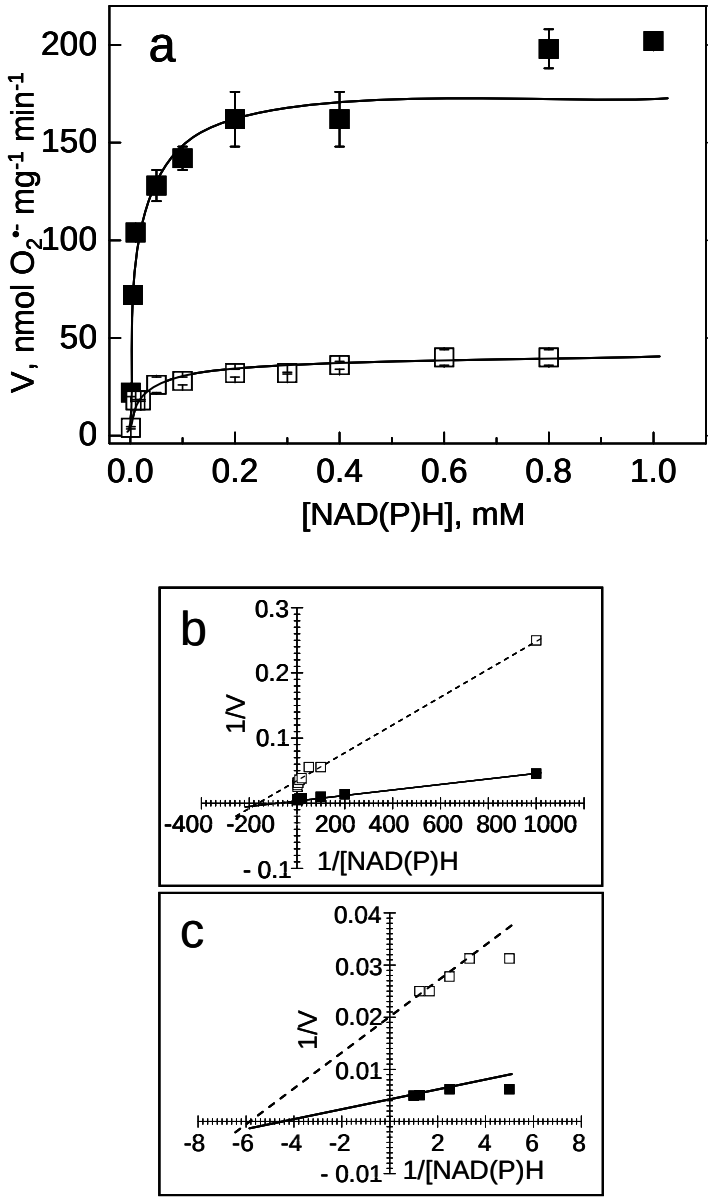

Figure 3. $O_2^{\bullet-}$ production of Triton-treated plasma membranes. a) Michaelis-Menten representation of the initial rates with NADH (■) and NADPH (□). b) Lineweaver-Burk plot of data at 1-50 µM NAD(P)H concentration (the Km value is 8 for NADH and 6 µM for NADPH). b) Lineweaver-Burk blot of data at 0.2-1 mM NAD(P)H concentrations (the Km value is 200 for NADH and 167 µM for NADPH). The reaction mixture contained 30 µg PMs ml^{-1}, 500 µM XTT and 1-1000 µM NAD(P)H in 20 mM HEPES (pH 7.5).

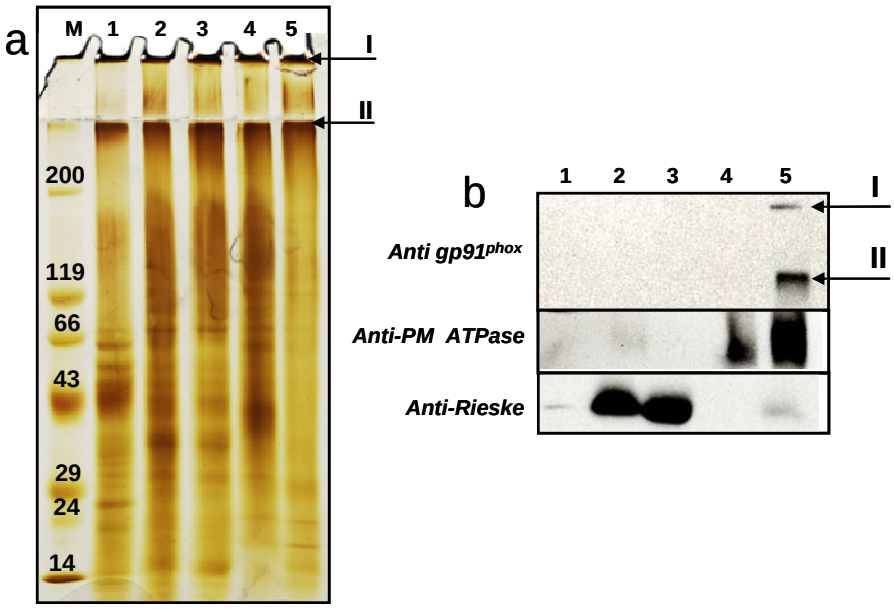

Figure 4. SDS-PAGE and immunoblots of soluble protein and membrane protein fractions obtained from soybeans. a) The following samples were loaded on gel: M= marker, 1=soluble proteins, 2= total membranes, 3= intracellular membranes, 4= Tween-soluble plasma membranes and 5= Tween-insoluble plasma membranes. b) immunoblot was decorated with antibodies against the human $gp91^{phox}$ (NOX), PM-ATPase and mitochondrial Rieske protein. I and II stand for start of stacking and resolving gel, respectively, indicating the poor entrance of the NOX into the gel. 20 µg protein was loaded on a 12-8% polyacrylamide gel.

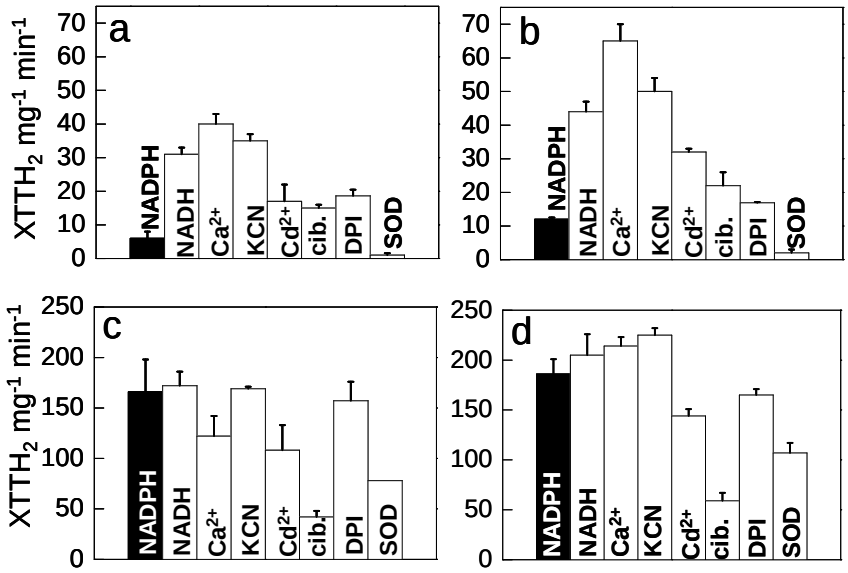

Figure 5. Effect of Ca^{2+} and different inhibitors on XTT reduction of plasma membranes. Intact PMs (a,c) and Triton-treated PMs (b,d). In c and d 100µM menadione was present. A reaction mixture contained 10 µg PM ml^{-1}, 200 µM NAD(PH) and 500 µM XTT in 20 mM HEPES (pH 7.5). Other concentrations: 5 mM $CaCl_2$, 1mM KCN, 0.3mM $CdCl_2$, 20 µM Cibacron Blue, 5 µM DPI and 100 µg SOD.

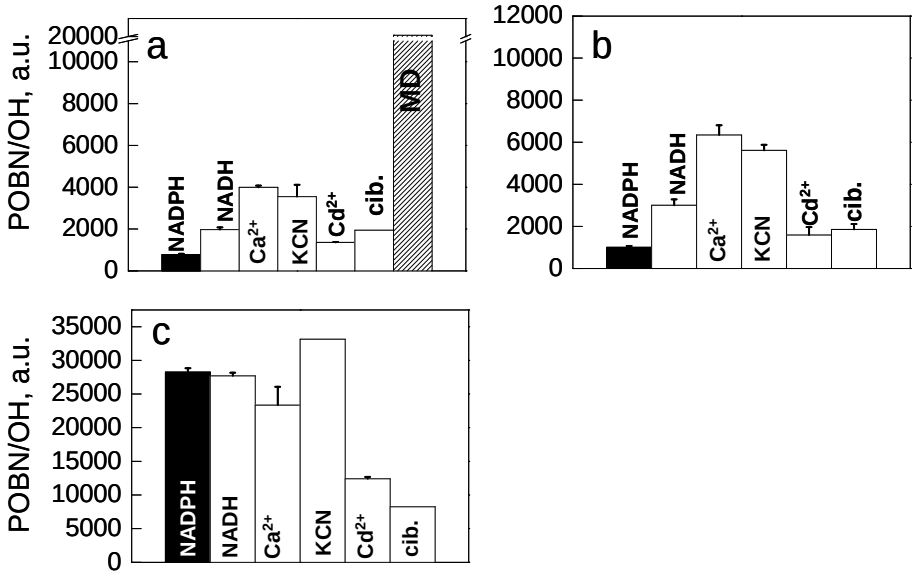

Figure 6. Effect of Ca^{2+} and different inhibitors on Fe^{2+}-catalysed $^{\bullet}OH$-formation of plasma membranes. Intact PMs (a), Triton-treated PMs (b,c). In c) and in the striped column in a) 100µM menadione was present. A reaction mixture contained 15 µg PM ml^{-1}, 200 µM NAD(P)H, 50 mM 4-POBN, 4% EtOH and 50 µM Fe^{2+}-EDTA in 20 mM HEPES (pH 7.5). Other concentrations: 5 mM $CaCl_2$, 1mM KCN, 0.3 mM $CdCl_2$ and 20 µM Cibacron Blue. The arbitrary units were calculated from the signal sizes of the EPR spectra.

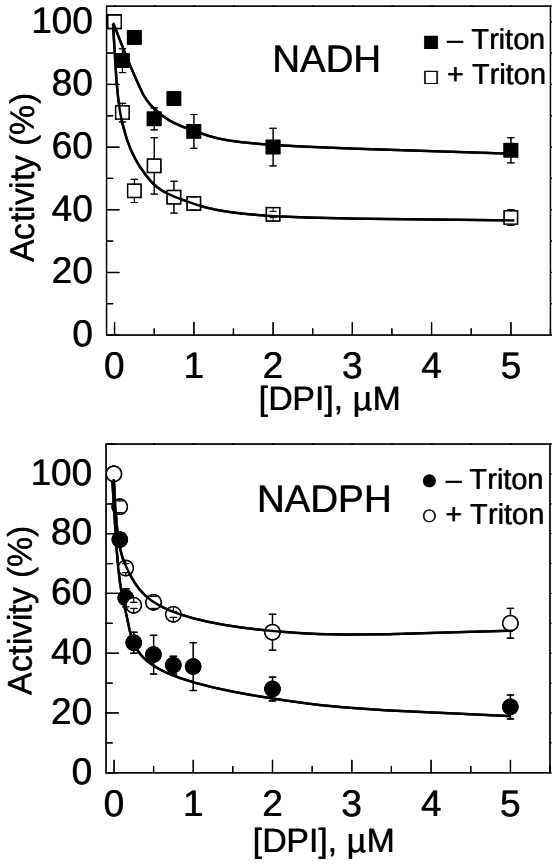

Figure 7. Effect of diphenyleneiodonium (DPI) on plasma membrane $O_2^{\bullet-}$ production. The reaction mixture contained 30 µg PMs ml^{-1}, 500 µM XTT, 200 µM NAD(P)H and 0.125-5 µM DPI.

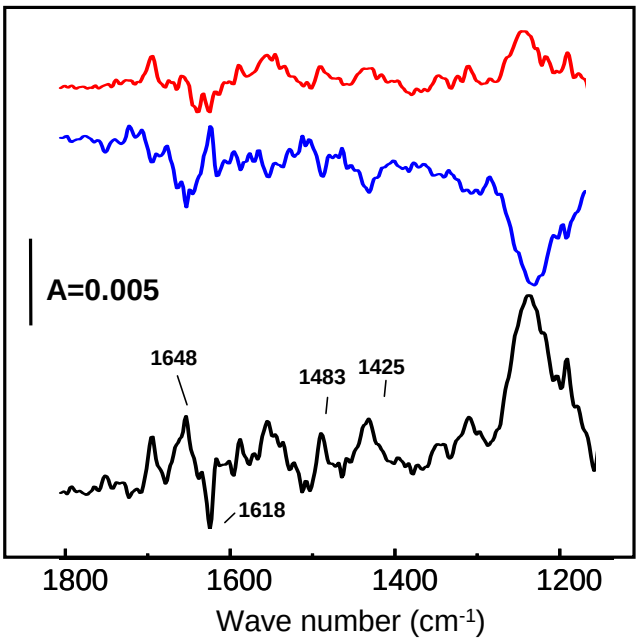

Figure 8. FTIR difference spectra of plasma membranes in the presence of NADH and ferricyanide. Reduced-oxidised spectra are shown in red and oxidised-reduced spectra in blue. The double difference spectrum of red-blue is shown in black. Putative bands correspoding to quinone species are indicated at 1600-1650 cm^{-1} and at 1400-1500 cm^{-1}.

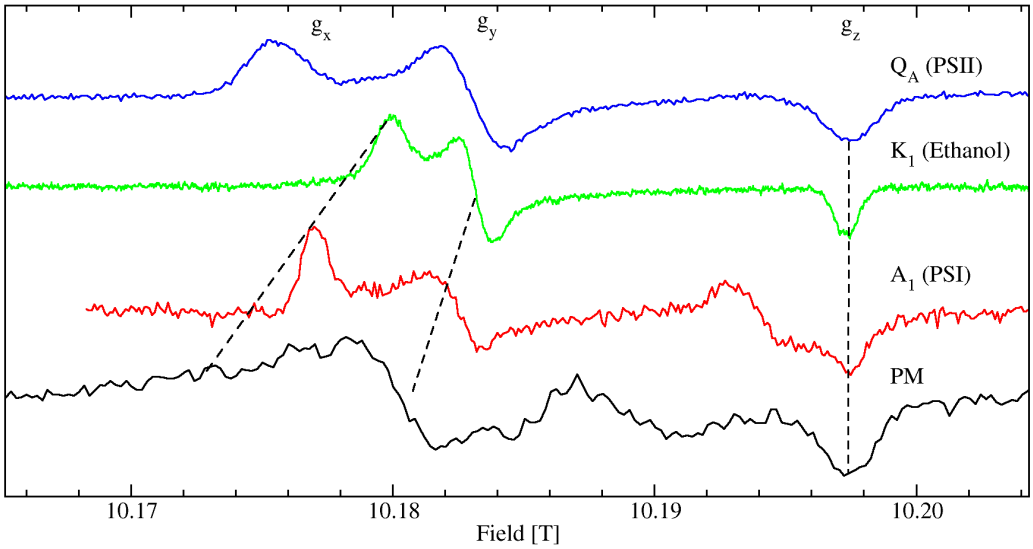

Figure 9. HFEPR spectra of solubilised plasma membranes (black). As a comparison vitamin K_1 radical generated in ethanol (green) and in photosystem I (red), and the plastosemiquinone (Q_A) from plant photosystem II are also presented. The g-tensors gx, gy and gz are depicted with dashed lines. The spectra were taken at 4.2 K.

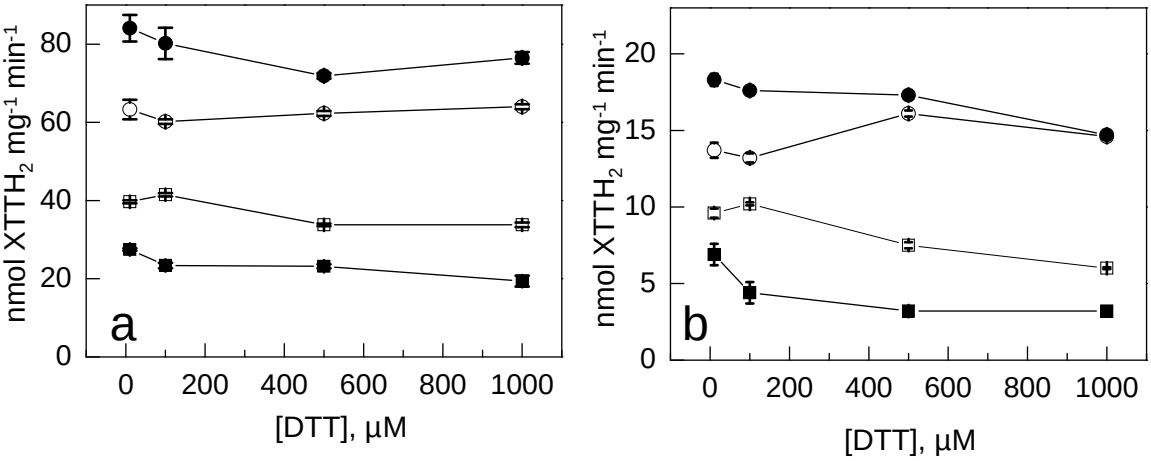

Figure 10. Effect of ATP on plasma membrane $O_2^{\bullet-}$ production. PMs were incubated for 2h in 10-1000 µM DTT. (a) NADH- and (b) NADPH-dependent XTT reduction was measured in control PMs (□), PMs incubated with ATP (■), detergent-treated PMs (○), and in detergent-treated PMs incubated with ATP (●). The rates of Triton-treated PM before the assay were 77 and 16 nmol $XTTH_2$ $mg^{-1}min^{-1}$ with NADH and NADPH respectively. The rates of non-treated membranes were of 42 and 9 nmol $XTTH_2$ $mg^{-1}min^{-1}$ with NADH and NADPH, respectively. A reaction mixture contained 30 µg PM ml^{-1}, 200 µM NAD(P)H, 500 µM XTT and 200 uM ATP.

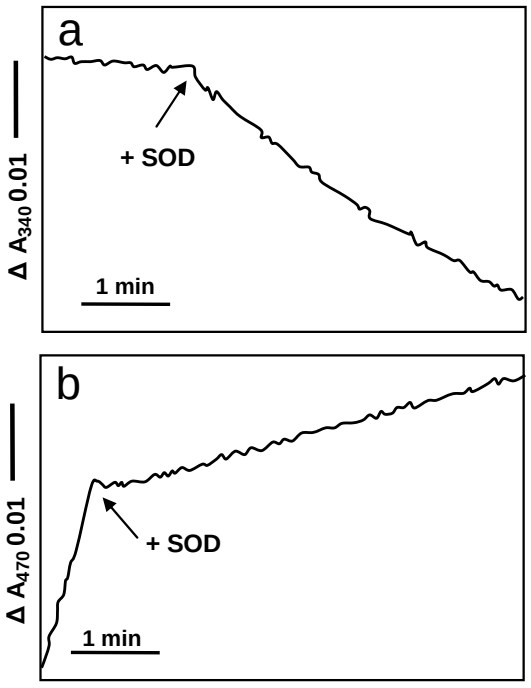

Figure 11. Effect of SOD on NADH oxidation and XTT reduction of Triton-treated plasma membranes. a) The NADH oxidation rate without SOD was 2.7 and after addition of SOD 69.8, decreasing to 37.6, nmol mg^{-1} mg^{-1}. b) The XTT reduction rate was 36.4 before and 2.9 nmol $XTTH_2$ mg^{-1} min^{-1}. A reaction mixture contained 30-50 µg PM ml^{-1}, 200 µM NADH and, in XTT reduction assay 500µM XTT in 20 mM HEPES pH 7.5. 50 µg SOD was added.

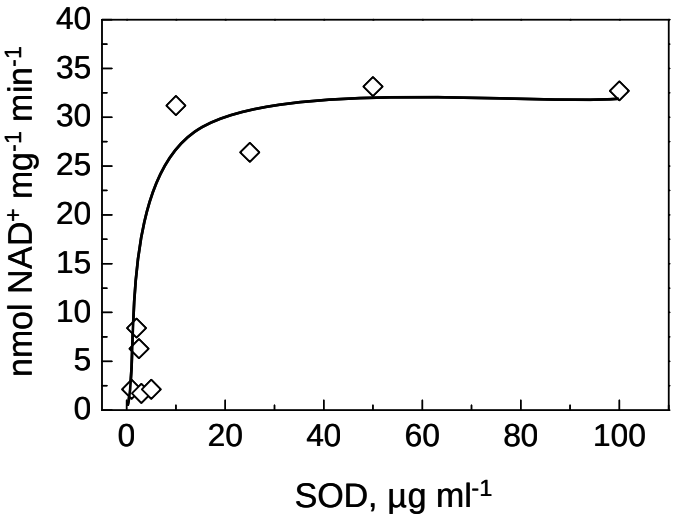

Figure 12. Effect of SOD on NADH oxidation by Triton-treated plasma membranes. A reaction mixture contained 50 µg PMs ml^{-1} and 200 µM NADH in 20 mM HEPES, pH 7.5.

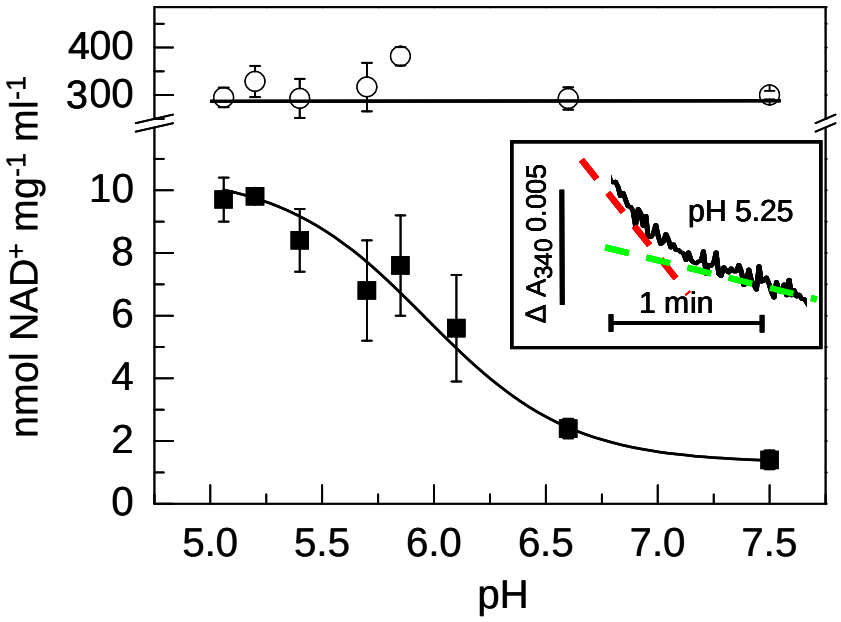

Figure 13. Effect of pH on NADH oxidation of detergent-treated plasma membranes. The rate of NADH oxidation as the function of time at pH 5.25 is shown in the inset (red dashed line = initial rate 10 nmol mg^{-1} min^{-1}, green dashed line = inhibited rate of 3 nmol mg^{-1} min^{-1}). In the principle figure the initial rates, corresponding to the red dashed line, are presented. NADH oxidation was measured in the absence of added electron acceptors (■) and in the presence of ferricyanide (○). The rates are averages of at least four measurements performed in 50 mM phosphate buffer. A reaction mixture contained 100 µg PM, 200 µM NADH and, when added, 5 mM $K_3[Fe(CN)_6]$.

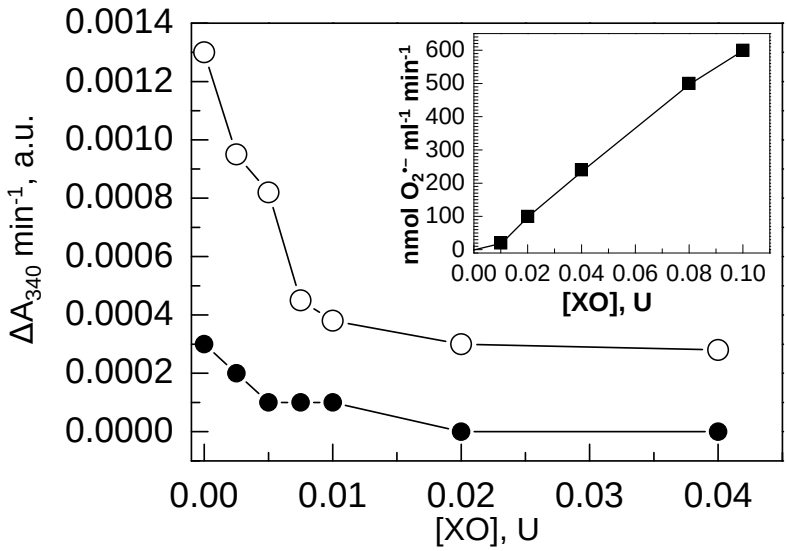

Figure 14. Effect of external $O_2^{\bullet-}$ on NADH oxidation of detergent-treated plasma membranes. External $O_2^{\bullet-}$ was produced by the XO/X system (inset: $O_2^{\bullet-}$ production as the function of XO concentration in the presence of 500 µM xanthine). The decrease in the NADH oxidation activity of two PM preparations (○ and ●) is shown as the function of XO concentration. The initial NADH oxidation rates were 2.1 and 0.5 nmol mg^{-1} min^{-1} for ○ and ●, respectively. The reaction mixture contained 100 µg PM ml^{-1}, 200 µM NADH, 500 µM xanthine and 0.0025-0.04 U XO in 20 mM HEPES (pH 7.5).

2.4 Manuscript in preparation:

The biological role of quinone reductases

Abstract

Quinone reductases may either produce ROS or prevent ROS-forming reactions to occur. To understand the biological role of quinone reductases in plants, we studied insertion knock-out lines of two genes encoding for quinone reductases in *Arabidopsis thaliana*, NQR (At3g27890) and FQR1 (At5g54500). In addition, the subcellular localisation of these two quinone reductases in roots were studied by immunolocalisation by confocal fluorescence microscopy using specific antibodies. Preliminary data are presented. The quinone reductase mutants showed stunted root growth, chlorophyll bleaching and increased ROS-production. Both quinone reductases showed similar localisation which was cytosolic in the root meristem zone and mainly restricted plasma membrane in the elongation zone and root hairs.

Introduction

Quinone reductases (QRs) catalyse the reduction of quinones using NAD(P)H as electron donor. The biological role of QRs in plants is not clear. They are hypothesised to participate in PM electron and H^+ transfer reactions providing a substrate to quinol oxidases (Morré, 2004) or to cyt b_{561} (Preger et al., 2001). Additionally, QRs may generate ROS by producing redox-labile dihydroquinones (Schopfer et al., 2008) or reducing free flavins (Gaudu et al., 1994). Both membrane-associated (Guerrini et al., 1987; Luster and Buckhout, 1989; Pupillo et al., 1986; Serrano et al., 1994, Schopfer et al., 2008) and soluble (Sparla et al., 1996; 1998; 1999; Trost et al., 1995) QR activities are present in plants.

Because of the reaction mechanism (2-electron reduction of quinones to dihydroquinones) of QRs, they are regarded as detoxifying enzymes that prevent the formation of ROS via semiquinones, generated by e.g. cytochrome P450. However, the experimental evidence for a *bona fide* detoxifying role of QRs is ambiguous. First, QR KO or over-expressing lines do not have a phenotype in control conditions (Radjendirane et al., 1998; Laskowski et al., 2002). Second, in quinone stress experiments, it is both the nature of the added quinone and the reducing enzyme that determines the viability of the organism. Although QR1 KO mice were sensitive to menadione (Radjendirane et al., 1998), bacteria challenged with benzo-α-pyrene 3,6-quinone showed increased mutation rates with distinct nucleotide targets depending on whether QR1 or cyt P-450 reduced the added quinone (Joseph and Jaiswal, 1998; Joseph et al., 1998). The toxicity of the benzo-α-pyrene 3,6-quinone was due to the ROS that are formed during the cyt P-450 reaction cycle and due to dihydroquinones that are formed during the QR reaction cycle. Third, redox-labile dihydroquinones, formed by QRs, generate ROS during autoxidation (Schopfer et al., 2008). Because the action of QRs may have so many effects, there is a need for a careful analysis of functions of QRs *in vivo*.

Mutants offer a good starting point for studying the role of QRs *in vivo*. There are two gene families encoding QRs in plants. An NAD(P)H:quinone oxidoreductase, NQR, was identified from the cytosolic fraction of tobacco leaves which showed limited homology to the mammalian DT-diaphorase (later renamed to QR1 in humans) and plant monodehydroascorbate reductase (Sparla et al. 1996, 1998). The peptide sequences obtained from this protein showed homology to one gene in *A. thaliana* (Sparla et al. 1999). The QR of soybean plasma membranes is likewise homologous to this QR (Schopfer et al. 2008). On the other hand, a gene found in a screen of early auxin-response genes in *A. thaliana* showed homology to bacterial QR genes and was named *Fqr1* for flavin-dependent quinone reductase (Laskowski et al., 2002). The FQR1 was found in the soluble protein fraction in soybean (Schopfer et al., 2008). We have started to analyse insertion knock-out (KO) lines of two the *Fqr1* and *Nqr* genes in *A. thaliana*. Preliminary results of the mutant geno- and phenotypes and immunolocalisation of QR proteins by confocal fluorescence microscopy are presented.

Materials and methods

Plant material

A. thaliana insertion knock-out lines (Alonso et al., 2003) were ordered from the Nottingham Arabidopsis Stock Centre (NASC). Plants were grown on soil, vermiculite or plates (plates contained ½ Murashige Skoog medium in 10 mM MES, pH 6.1 and 0.5 % Phytoagar, Sigma) in the green house or in a growth chamber under 100-300 µmol photons m^{-2} s^{-1} irradiation in a 12 h light 12 h dark rhythm. Prior to placing on plates, the *A. thaliana* seedlings were sterilised (96 % EtOH 2 min, 70 % EtOH 2 min, sterilised destilled H_2O 3x5 min). The seeds were stratificated for 2-3 days in dark at 6 °C.

Primers and PCR reactions

Four NQR and two FQR insertion lines of At3g27890 and At5g54500 genes, respectively, were tested for homogeneity. DNA was isolated from a leaf sample using alcohol precipitation. The following genomic primer pairs were chosen by the Signal SALK T-DNA Primer Design tool:

NQR lines 1 and 5 (SALK):

Right primer (rp) 5'-GGAGACCAGTATGGAAGGAGG-3'

Left primer (lp) 5'-GAAACATCACAACCCAAGGTG-3',

NQR line 2 (CSHL):

rp 5’-CCTTCCATACTGGTCTCCTCC-3’

lp 5’-CATCGACAAGGTTTCCTTCTG-3’

NQR line 6 (SAIL):

rp 5’-TCTTGTAGCAAATCAAGAAACCTC-3’

lp 5’-GCTCTTTGCCTTTTATTCAGC-3’

FQR line 3 (SALK):

rp 5’-CATGATGATGATGAGCGTGAC-3’

lp 5’-CACCTTCAACAGAAGCAGCTC-3’

FQR line 4 (SAIL):

rp 5’-TTGATTTTGGATTCTTGGCTG-3’

lp 5’.CAAGAATAATGACGACGCATC-3’.

The primers for the inserts were:

SALK (LBb1.3) 5’-ATTTTGCCGATTTCGGAAC-3’

SAIL (modified left border 3) 5’-TAGCATCTGAATTTCATAACCAATCT-3’

CSHL Ds 3’-primer 5’-CCGTCCCGCAAGTTAAATAT-3’ and

Ds 5’-primer 5’-TACGATAACGGTCGGTACG-3'.

The PCR reactions were started with a denaturation at 94 °C for 3 min. The PCR program consisted of 35 cycles of denaturation at 94 °C for 15 s, annealing at 60 °C for 30 s and extension 72 °C for 90 s.

Western blotting

Proteins were isolated from leaves and roots of appr. 4-week-old *A. thaliana* plants. Root material was homogenised by mortle and pestle in the presence of liquid nitrogen followed by addition of a small amount of isolation buffer (10 mM Tris/HCl pH 8.0, 20 mM Na_2EDTA, 300 mM NaCl). Leaf material was homogenised in a blender with a small amount of isolation buffer. The homogenate was filtered through a cheese cloth and centrifuged (30 min at 1300 g, 4°C). The supernatant (raw fraction) was centrifuged (45 min at 91 000 g, 4°C) to separate soluble proteins and membranes. The pellet was resuspended in a small volume of isolation buffer and homogenised in a glass potter. After determining protein concentration with Bradford or Aminoblack assay the samples were separated by SDS-PAGE on 10% polyacrylamide gels. The separated proteins were transferred by semi-dry blotting on PVDF membranes. The membranes were decorated with specific polyclonal antibodies directed against the *A. thaliana* NQR (provided by Drs. F. Sparla and P. Trost, Università di Bologna)and FQR1 proteins (provided by Dr. M. Laskowski, Oberlin College).

Measurements of $^{\bullet}OH$

$^{\bullet}OH$ production was measured by EPR spectroscopy using 4-POBN [α-(4-Pyridyl N-oxide)-N-tert-butylnitrone]/ethanol as the spin trap. Seedlings (20-30) were incubated in 20 mM HEPES buffer (pH 7.5) containing 50 mM POBN, 4% EtOH and, when mentioned, 50 µM Fe^{2+}-EDTA. EPR spectra of the incubation medium were recorded at room temperature with a Bruker 300 X-band spectrometer at 9.69 GHz microwave frequency, 63 mW microwave power and 100 kHz modulation frequency.

Immunolocalisation

For immunolocalisation of NQR proteins and FQR1 proteins specific antibodies were used. The primary antibodies were used in 1:500 and 1:200 dilutions. Alexa488 Fluor (goat anti-rabbit IgG, Invitrogen) was used as the secondary antibody in a 1:500 dilution. The diluted secondary antibody was centrifuged lightly (2 min 200 g) before use to remove precipitates.

The *A. thaliana* seeds were grown on Phytoagar (Sigma) plates for four days under 100 µmol photons m_2^{-1} s^{-1} irradiation in a 12h light 12 h dark rhythm. Plantlets were fixed in 3% paraformaldehyde under vacuum for 45 min followed by 15 min washing in 0.1 M glycine, 15 min washing in 0.1 M NH_4Cl, and finally 5x 5 min rinsing in microtubule stabilising buffer (MTSB; 50 mM PIPES, 5 mM EGTA, 5 mM $MgSO_4$, pH adjusted to 6.9 with KOH).

The seedlings were placed into the baskets of the liquid handling robot system. The following incubation steps were performed by the robot at room temperature: 10 x 12 min MTBS buffer in which 0.1 % Triton was added (MTSBT), 30 min 2 % Driselase, 5 x 12 min MTSBT, 2 x 30 min nonidet P40/DMSO (30%/10%), 5 x 12 min MTSBT, 1h 3% BSA in MTSBT (blocking). The following steps were performed by the robot at 37 °C: 6 h primary antibodies in MTSBT/BSA, 8 x 12 min MTSBT, 3 h secondary antibody in MTSBT/BSA, 10 x 12 min MTSBT.

The seedlings were placed on object slides, VECTASHIELD® Hard_Set™ Mounting Medium with DAPI was added and the coverslip placed. The slides were kept in dark and cold over night. Slides were observed and images were collected with an upright laser scanning confocal microscope TCS SP2 (Leica Microsystems, Mannheim, Germany) using an HC PL APO 10.0x0.40 COMBI or HCX PL APO 40.0x1.25 OIL. FITC images were detected using the 488 nm argon laser line at 493-581 nm. Images were processed using Image J (Rasband, 1997-2009).

Results

An un-rooted phylogenetic tree was constructed of a set of known QRs from multiple phyla, proteins showing homology to them and, additionally, two bacterial flavodoxins (Fig. 1). QRs are found in a wide variety of organisms and more than two families seem to have divided in the course of evolution. Although distant at the level of sequence homology, these enzymes are very similar when structure, substrate spectrum and reaction mechanism are compared (Agarwal et al., 2006; Carey et al., 2007; Deller et al., 2008). Tentative sub-families showing at least 50 % identity to *A. thaliana* NQR and FQR protein sequences are shown in Figure 1.

There are five genes encoding QRs in *A. thaliana*: four *Fqr1* homologs and one *Nqr* gene. At the level of amino acid sequence, the *Fqr1* (At5g54500)-gene product is almost identical to that of At4g27270 (91 % identity, 96 % similarity). The two other *Fqr*-genes are less homologous but have still >50 % identity and >60 % similarity with *Fqr1*. The *Fqr* genes and *Nqr* genes are not homologous, there is only 20 % identity and 30% similarity between them. A phylogram with distances of the *A. thaliana Nqr*- and *Fqr*-genes is presented in Figure 2.

Insertion lines of *Nqr*- and *Fqr1*- genes

T-DNA insertion lines of *Nqr* and *Fqr1* genes were from SALK and SAIL (T-DNA mutagenesis by *Agrobacterium tumefaciens*) and in one case a CSHL collection (transposon mutagenesis). Gene structure and the sites and orientation of the inserts according to Signal Salk, are shown in Figure 3. Lines were tested by PCR with primers specific for the insertion site (Fig. 4a) and homozygous lines were selected. For two lines the absence of the protein was verified by western blotting (Fig 4b). Interestingly in the mutant plants the absence of the NQR protein led to an increase in the FQR1 protein and vice versa. In WT plants the NQR protein was detected in the membrane fraction of leaves and both in the membrane and the soluble fraction of roots. In the WT plants the FQR1 protein was detected in the membrane fraction of both leaves and roots.

When the lines were grown on plates under irradiation of 300 µM photons m^{-2} s^{-1}, they showed stunted root growth after four days. This phenotype was more pronounced in *fqr1* than in *nqr* mutant lines (Fig. 5). This phenotype was transient. The roots of *nqr* lines, but not those of *fqr1* lines, reached lengths resembling the wt within two weeks. Additionally, *fqr1* lines had bleached leaves. When the lines were grown on soil, no phenotype could be detected in the surface parts, except early flowering in NQR line 2. When the plants were grown on vermiculite, the root system of the mutants did not differ from the wild type. According to the sequence information in Signal Salk, three of the *nqr* KO lines (nqr lines 1,5 and 6) have

insertions elsewhere in the genome. The early flowering phenotype of a group of the offspring in the fourth *nqr* l line 2 (data not shown) speaks for it, too, having multiple insertions in the genome. Therefore, the phenotypes presented in Figure 5. should be analysed with caution in the case of *nqr*-lines. The exact location of the inserts will be verified by sequencing and, if needed, the mutants will be back-crossed with wt to obtain true homozygous QR KO lines.

$^{\bullet}$OH production by QR mutant lines

To know if altered ROS production caused delayed root growth of the mutant lines, we measured their $^{\bullet}$OH production by spin-trapping EPR spectroscopy. Figures 6 and 7 clearly show that $^{\bullet}$OH production in mutants was increased. In the absence of Fe^{2+}, the difference between the WT and the mutants was more pronounced than in the presence of it (Fig. 6). The signal sizes were larger in vermiculite-grown than in plate-grown plants (arbitrary units in Fig. 6 vs. Fig. 7), which might reflect the age of the plants. Vermiculite-grown plants were 4 weeks old, while the plate grown plants were 6 days old.

Immunolocalisation of NQR and FQR1 proteins in wt plants

According to the biochemical characterisation of plant PM and cytosolic proteins, both membrane-attached as well as soluble QRs exist. In our previous work, the NQR protein was found exclusively in the PMs of etiolated soybean hypocotyls (Schopfer et al., 2008), while its homolog was found in the soluble fraction of tobacco leaf preparations (Sparla et al., 1996). Additionally, we previously found a soybean FQR1 homolog in the cytosolic fraction (Schopfer et al., 2008) while in *A. thaliana* it was found in the PM (Marmagne et al., 2004). To get a better insight on the localisation of the QR proteins in plants, immunolocalisation with confocal fluorescence microscopy was performed with *A. thaliana* seedlings using specific antibodies against the NQR and FQR1 proteins of this species.

The NQR localisation in the meristem and elongation zone of a 4-day-old *A. thaliana* root is shown in Figure 8. The signal is saturated in the root meristem zone showing no clear subcellular localisation while it is restricted to peripheral areas of the cell, likely to the PMs. The localisations of NQR and FQR1 were similar (Fig 9 a and e). Larger magnification shows a diffuse signal in the cells of root meristem (Fig. 9 b and f) and a strongly localised signal in the PMs of the elongation zone (Fig. 9 c,d and g). Both antibodies showed a comparable localisation in the meristem, but in the elongation zone the FQR1 signal was slightly more diffuse than that of NQR. In the elongation zone NQR was detected mainly in the epidermal cells while the conducting tissue showed a weaker signal (Fig. 9 c and d).

Both proteins were detected in the root hairs and they seemed to be located to the PM

(Fig. 10). A homogenous signal was detected in the whole root hair cell (Fig. 10 a, e and f). However, we observed also root hairs in which the tip showed no signal (Fig. 10 b) or in which the middle part showed an inhomogeneous localisation (Fig. 10 c and g). This suggests a dynamic behaviour of the QRs in the root hair cells.

To conclude, the QRs showed a PM localisation in the elongation zone and the localisation was diffuse in the meristem. It has to be verified with co-localisation experiments whether these seemingly differential root zone-dependent localisations are true and if other subcellular compartments are targets for QR action.

Discussion

We have chosen several insertion KO lines of *fqr1* and *nqr* lines to study the biological role of the encoded enzymes. Also an immunolocalisation of the corresponding proteins was performed. Unfortunately, three of the four *nqr* lines were found to have additional insertions elsewhere in the genome. The clean lines, one *nqr* (Line 2) and two *fqr1*s (Lines 3 and 4), allowed us to make some preliminary observations. Both gene products led to a transient delay in the growth of roots, which was not evident in later development. To determine if the root phenotype is related to decreased or increased ROS production, we measured $^{\bullet}OH$ production of these plantlets by spin trapping EPR spectroscopy. $^{\bullet}OH$ production was 2-20 fold higher in the mutants than in wt. This difference could be detected even in 4-week old seedling grown in soil, although there were no visible differences between the WT and mutants. Therefore, QRs probably function as a protective enzymes avoiding increased ROS production.

QR1 and Lot6p KO mice and yeast, respectively, showed signs of oxidative stress only in the presence of added quinones (Radjendirane et al., 1998; Sollner et al., 2007). In these works ROS production was not measured. Over-expression of Lot6p led to an enhanced tolerance towards quinones (Sollner et al., 2007). The KO mutant of the MdaB QR in *Helicobacter hepaticus*, a microaerophilic bacterium, was sensitive towards O_2 and peroxide-reagents. A gene encoding for SOD was up-regulated in this mutant (Hong et al., 2008). From these reports it can be seen that stress reveals a visible phenotype in QR KOs. This could explain the lack of strong phenotypes in the QR KOs in the present work in which the plants were grown under optimal non-stressing conditions.

The question arises why QR KO lines show an increased ROS production. QRs may avoid ROS formation by participating in conjugation reactions of quinones with glucuronic acid or sulfate removing them from the cellular quinone pool (Shangari et al., 2005). This makes quinones unavailable to enzymes that catalyse one-electron reduction and therefore reduces ROS production. Alternatively, QRs have been shown to interact with the proteasome

and transcription factors in a redox-dependent manner which regulates the transcription of genes (Sollner and Macheroux, 2009). In animals and yeast the target genes of the transcription factors, protected by QRs, regulate genes whose action lead to growth arrest and apoptosis (mammalian p53) and other stress-related genes (yeast Yap4p) (Sollner and Macheroux, 2009). It remains to be studied if plant QRs have interaction partners. Interaction of a soluble plant quinone reductase with PM proteins was discussed by Trost and coworkers (1997). The same group recently purified an ascorbate-reducible b-type cytochrome (Preger et al., 2009), which is transcribed by an early auxin-responsive gene similarly to FQR1 (Laskowski et al., 2002). It will be interesting to study if these two proteins interact. It is also possible that QRs function in both ways; detoxifying quinones and regulating the stability and localisation of transcription factors involved in stress-signalling. However, ROS production and growth of plant QR mutants and the effect of various stresses on these plants has to be tested again with reliable material.

Immunolocalisation of NQR and FQR1 proteins in the roots of *A. thaliana* seedlings did not differ from each other. The localisation was diffuse in the root meristem zone, while it became restricted in the PMs in elongated cells and root hair cells. Proteomic approaches have revealed four of the QRs in *A. thaliana* in PMs, two of which were predicted to have a trans-membrane domain (Marmagne et al. 2004). It has to be determined with markers specific to subcellular membranes if QRs reside in PMs, cytosol or both. It is also possible that plant QRs interact with other membrane compartments, such as the vacuole (Szponarski et al., 2004).

It is tempting to envisage QRs capable of transiently interacting with membranes. Evidence for such interaction has been provided in bacterial QRs based on structural features (Carey et al., 2007; Jonas et al., 2006). In our previous work with isolated material, NQR was detected in the PMs and FQR exclusively in the cytosolic fraction (Schopfer et al., 2008). However, the homologous protein in tobacco was isolated from the cytosolic fraction (Sparla et al., 1998) and the recombinant *A. thaliana* homolog was likewise soluble (1999). Interestingly, hydrophilic and -phobic forms of apparently the same QR were isolated from the cytosolic fraction of mice (Prochaska and Talalay, 1986). There are, thus, indications that QRs have an affinity to membranes. The structure of plant QRs has to be determined and, also, whether there is a change in the conformation, e.g. in response to environmental queues, exposing parts interacting with membranes.

In yeast, the GFP-fused Lot6p QR was detected as a diffuse signal in the cytosol and nuclei (Sollner et al., 2007). In the same study, using antibodies the Lot6p protein was detected in cytosol and vacuolar membranes, although the latter was thought to be a contamination.

Marmagne et al. (2004) reported the construction of a GFP-fusion of the FQR1-homolog encoded by At4g27270. This construct showed a strong labelling of the PM and a fluorescence back-ground from the cytosol of *A. thaliana* protoplasts. In the present work performed with antibodies, we observed diffuse signals only in the root meristemal zone. It will yet to be determined if GFP-fusions of QRs affect their tertiary structure, a homotetramer in plants.

In this work the QRs in root hair PMs suggested a dynamic pattern as their localisation was homogenious in some root hairs and restricted to the subapical regions in others. Oscillating patterns of ROS production and pH changes has been shown an important factor in the regulation of root hair growth (Monshausen et al., 2007). QRs may be involved in these patterns, but whether their role is to prevent ROS formation (Figures 5 and 6) or produce ROS in a pH-dependent manner (Schopfer et al., 2008) has yet to be confirmed.

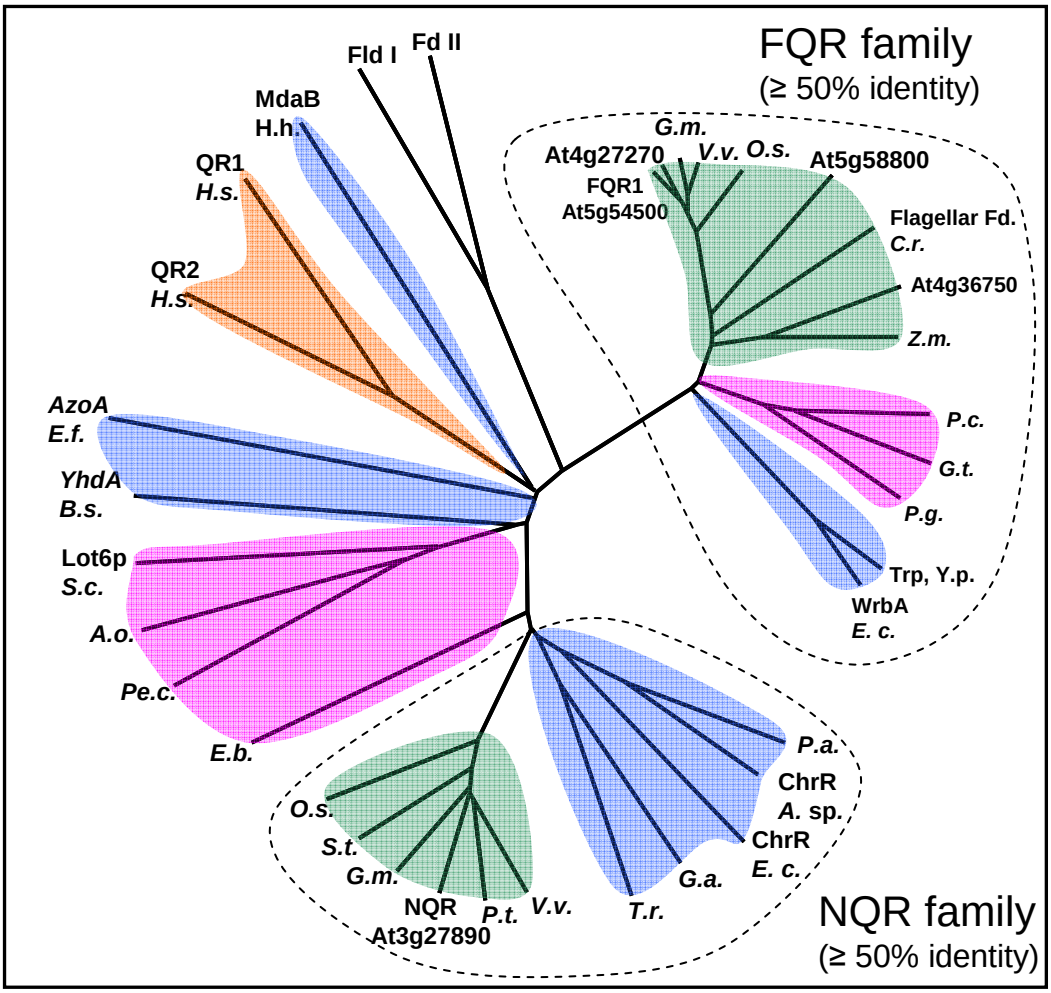

Figure 1. Phylogenetic tree of quinone reductases in plants, fungi, bacteria and humans. The un-rooted tree was constructed with the ClustalX2 program. The abbreviations and full names of species of 1) **the plant QRs (in green)***: C.r. Chlamydomonas reinhardtii, G.m. Glycine max, O.s. Oryza sativa, P.P. Populus trichocarpa, S.t. Solanum tuberosum, V.v. Vitis vinifera, Z.m. Zea mays; 2)* **the fungal QRs (in red)***: A.O. Aspergillus oryzae, E.b. Enterocytozoon bieneusi, G.t. Gloeophyllum trabeum, Pe.c. Penicillium chrysogenum P.c. Phanerochaete chrysosporium, P.g. Pichia guilliermondii, S.c. Saccharomyces cerevisiae; 3)* **the bacterial QRs (in blue)**: *A. sp. Azoarcus* sp., *B.s. Bacillus subtilis subsp. subtilis str. 168, E.f. Enterococcus faecalis, E.c. Escherichia coli, G.a. Gemmatimonas aurantiaca, H.h. Helicobacter hepaticus,ATCC 51449, P.a. Pseudomonas aeruginosa, T.r. Thermomicrobium roseum,* Y.p. *Yersinia pestis, and* **the human QRs (in orange**): *H.s. Homo sapiens.*

Abbreviations for the gene names and enzymes*: AzoA= Azoredcutase, ChrR=Chromate reductase, Fld= flavodoxin, FQR= flavin-dependent quinone reductase,* MdaB= modulator of drug activity, Lot6p= LOw Temperature Responsive, NQR=NAD(P)H:quinone oxidoreductase, QR1= quinone oxidoreductase, QR2= NRH:quinone oxidoreductase (dihydronicotinamide), Yhda (gene name, ferric ion reductase activity).

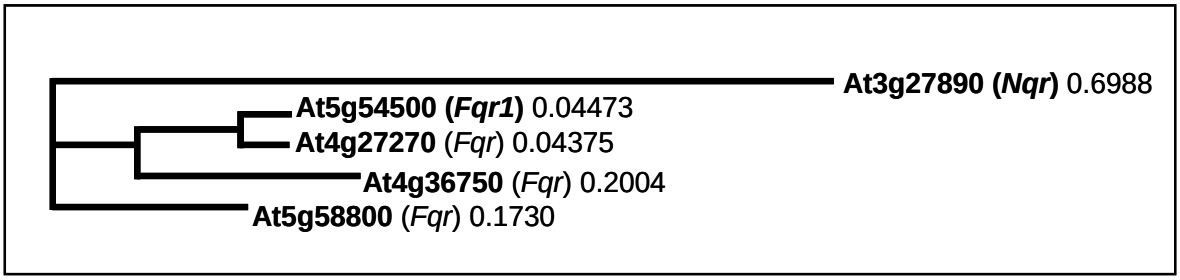

Figure 2. A phylogram of quinone reductase genes in *Arabidopsis thaliana* with distances constructed with the ClustalW alignment analysis. Flavin-dependent quinone reductases form a four-member family. *Nqr* sequence (At3g27890) shows only 16% identity and 30% similarity to *Fqr1* (At5g54500).

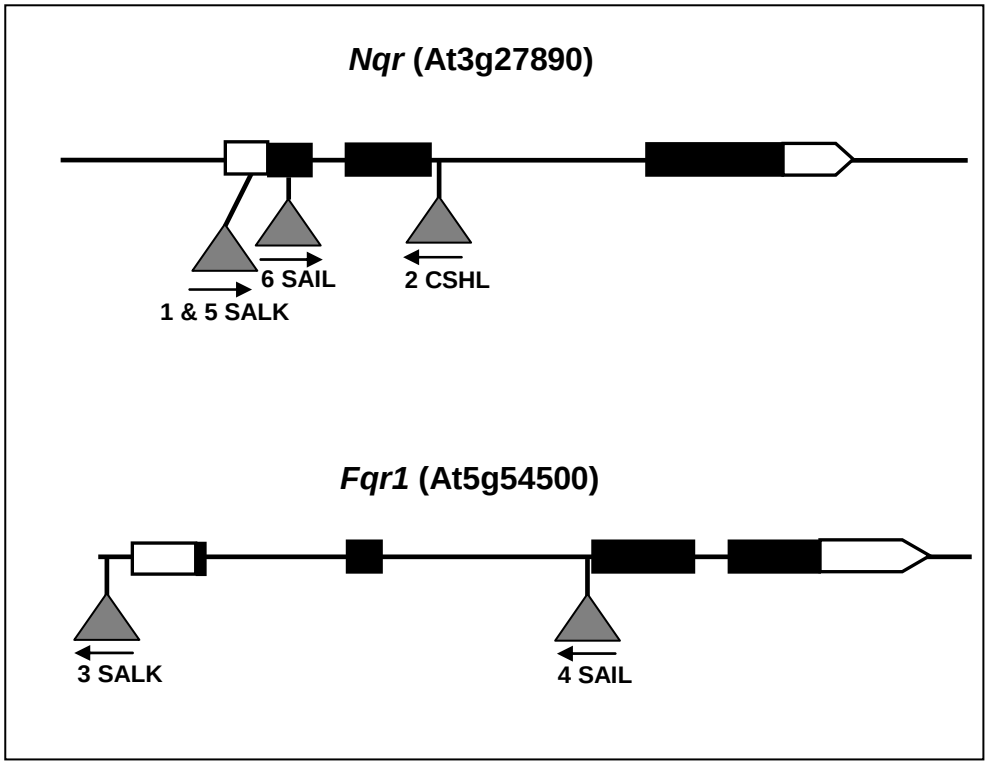

Figure 3. The intron-exon organisation of *Nqr* and *Fqr1* genes. Protein-coding regions are shown in black and untranslated regions in white. The triangles depict the sites of T-DNA insertions and the arrows their direction. The NQR lines are numbered 1,2,5,6 and the FQR lines 3,4. In the SALK lines the T-DNA insert contains the *nptII* gene conferring resistance to kanamycin. In the SAIL lines the insert contains a BASTA resistance cassette and ampicillin resistance gene. In CSHL lines the insert contains the *GUS* gene.

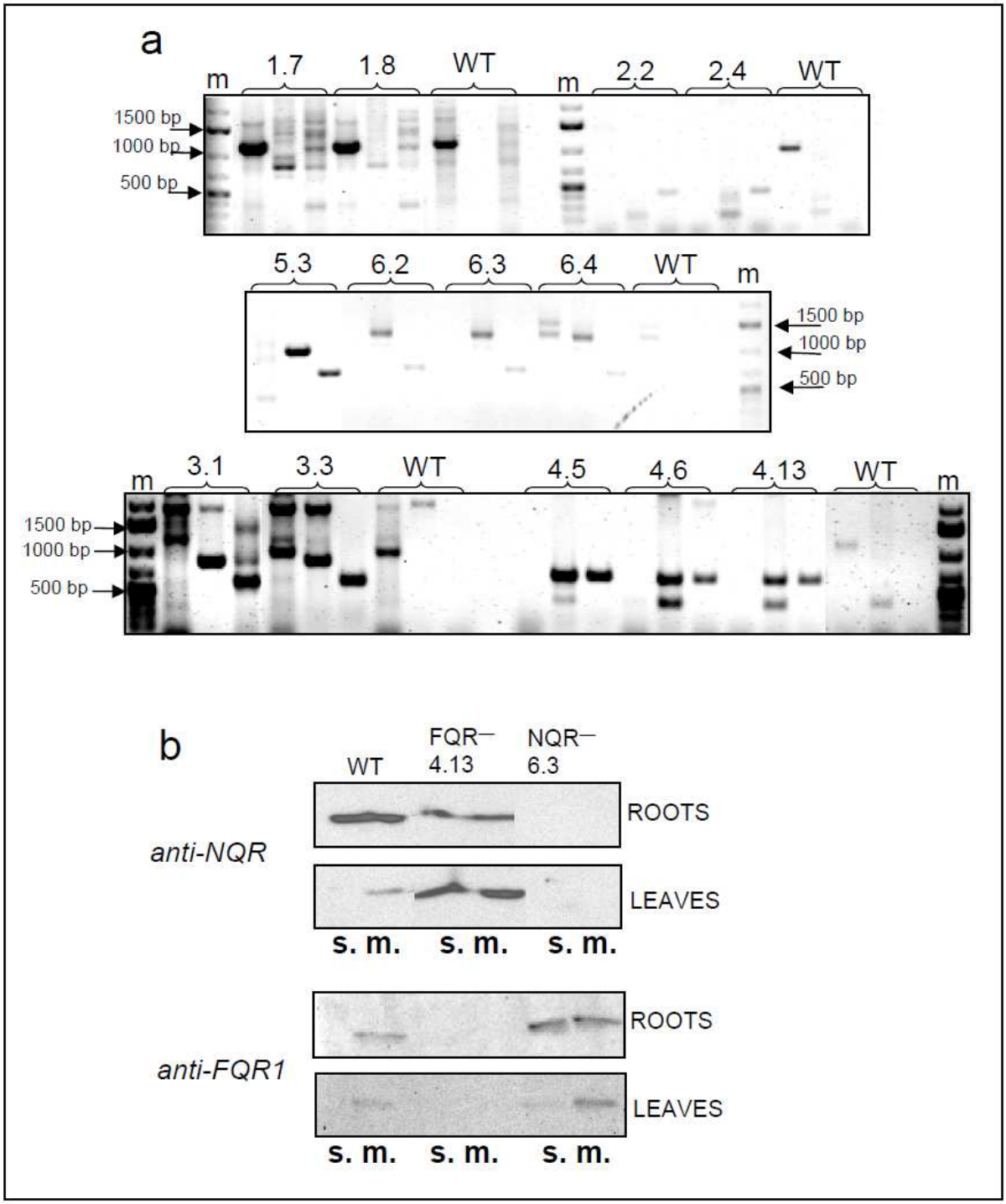

Figure 4. (a) PCR products of the DNA from the WT and knock-out lines obtained with specific primers for the QR genes and the inserts, (b) levels of FQR1 and NQR protein in the leaves and roots of *A. thaliana* WT and two QR insertion knock-out mutants. The PCR products of individual lines were obtained with the following primer combinations: first lane genomic rb and lb, second lane genomic rb and insertion-specific primer, third lane genomic lb and insertion-specific primer. In the case of line 2. the ds5 primer was used. WT product was 1000-1200 bp (first lane) and the insert-containing product 400-800 bp. For the immunoblot 50 µg soluble (s.) and total membrane proteins (m.) were separated by SDS-PAGE. The immunoblot was decorated with polyclonal antibodies against *A. thaliana* NQR and FQR1 proteins.

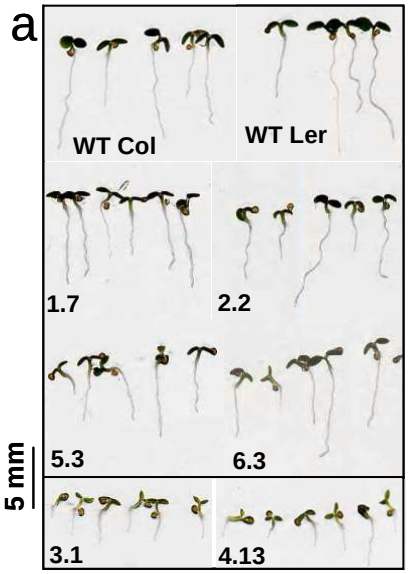

Figure 5. 4-day-old seedlings of WT and *nqr* and *fqr1* insertion knock-out lines. (a) Root length of the WT and mutant seedlings. Lines 1, 2, 5 and 6 are *nqr* and lines 3 and 4 *fqr1*. (b). Lines 1.7 and 1.8 were offspring of heterozygous plants. Lines 2.2 and 2.4 were homozygous. Line 5.3 was homozygous. Lines 6.2 and 6.4 were heterozygous, line 6.3 homozygous. All the *Fqr1*-lines were homozygous.

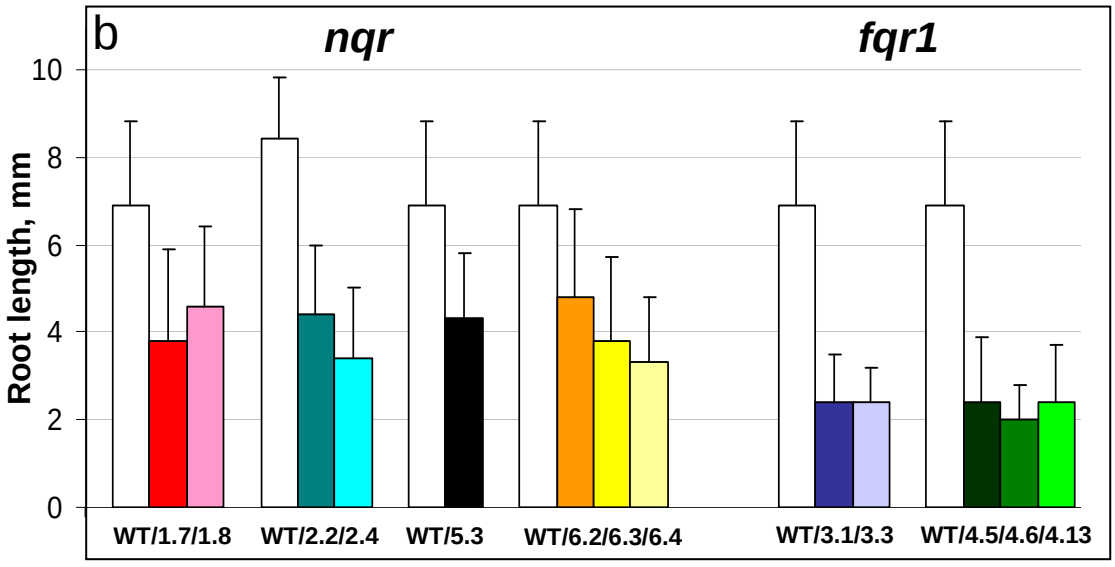

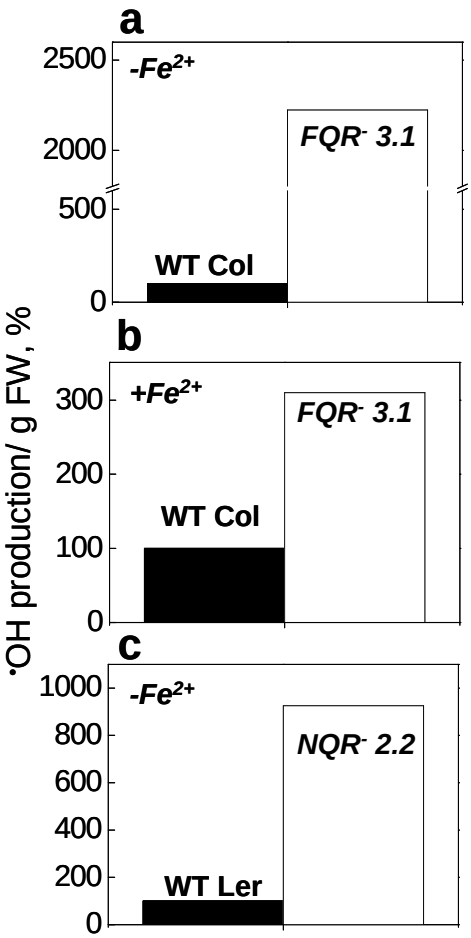

Figure 6. •OH production in WT and QR mutant lines grown in vermiculite. The figure shows the relative EPR signal sizes from appr. 25 seedlings. Signal size from the wt was set as 100 %. The corresponding arbitrary units of the signals, expressed with respect to the fresh weight, are as follows:
a) 0.63 for the WT Col and 13.9 for *fqr1*,
b) 25.3 for WT Col and 78.5 for *fqr1*,
c) 3.4 for WT Ler and 31.7 for *nqr*,
$(FW\ g)^{-1} \times 10^{-4}$.
The seedlings were incubated for 1 h in the reaction mixture (50 mM POBN, 4% EtOH and, when mentioned, 50 µM Fe^{2+}-EDTA in 20 mM HEPES pH 7.5) which was measured.

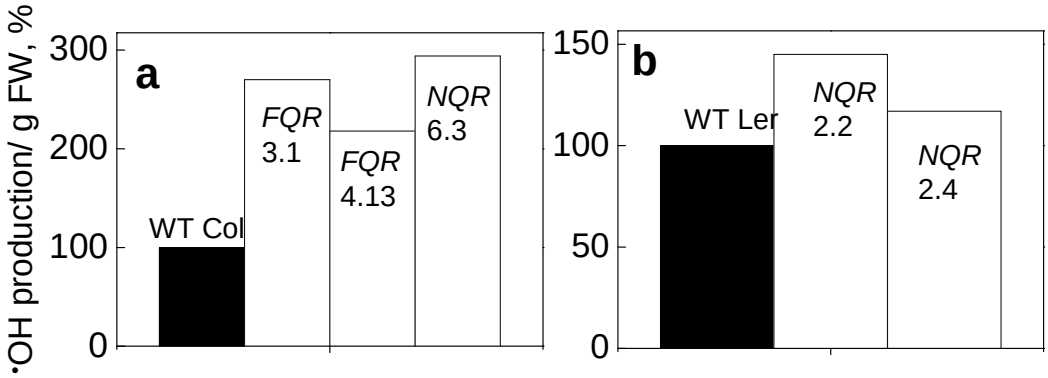

Figure 7. •OH production in WT and QR mutant lines grown on agar plates. The figure shows the relative EPR signal sizes from appr. 30 seedlings. The measurements were performed in the presence of Fe^{2+}-EDTA. The corresponding arbitrary units of the signals, expressed with respect to the fresh weight, are as follows:
a) 4.2 for WT Col, 11.2 for *fqr1* (3.1), 9.1 for *fqr1* (4.13), 12.3 for *nqr* 6.3,
b) 15.6 for WT Ler, 22.6 for *nqr* 2.2 and 18.2 for *nqr* 2.4,
$(FW\ g)^{-1} \times 10^{-4}$.
The 6-day-old seedlings (12-20 mg FW) were incubated for 1h in the reaction mixture (50 mM POBN, 4% EtOH and 50 µM Fe^{2+}-EDTA in 20 mM HEPES pH 7.5) which was measured.

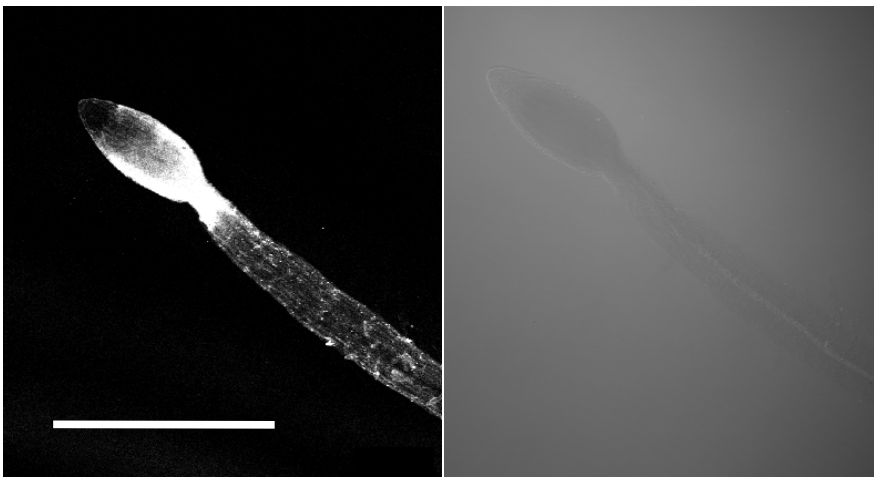

Figure 8. Immunolocalisation of NQR proteins by confocal fluorescence microscopy. The left figure presents the fluorescence image and the right figure the bright field image of a 4-day-old *A. thaliana* root. Scale bar 500 µm.

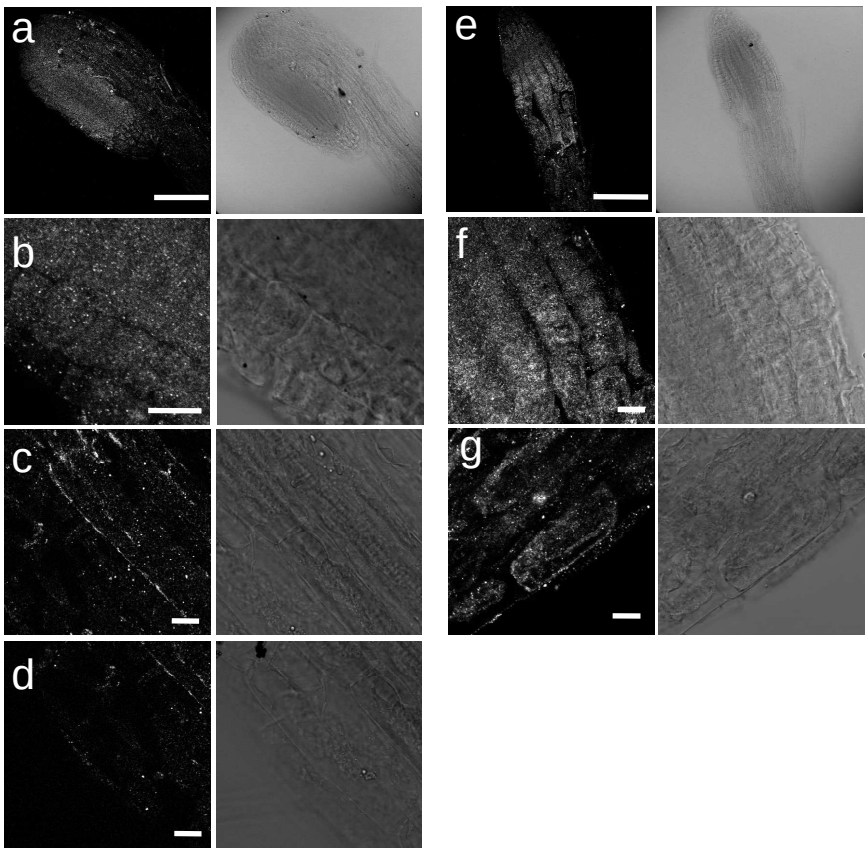

Figure 9. Immunolocalisation of NQR proteins (a-d) and FQR1 proteins (e-g) in 4-day-old *A. thaliana* seedlings by confocal fluorescence microscopy. In a column the fluorescence image is presented on the left and the bright field image on the right. First panel (a and e): root tip. Second panel (b and f): magnification on root meristem zone. Third panel (c and g): magnification of the root growth zone, epidermis. Fourth panel: root growth zone conductive tissue (NQR). Scale bars in (a) and (e) 100 µm, in other figures 10 µm.

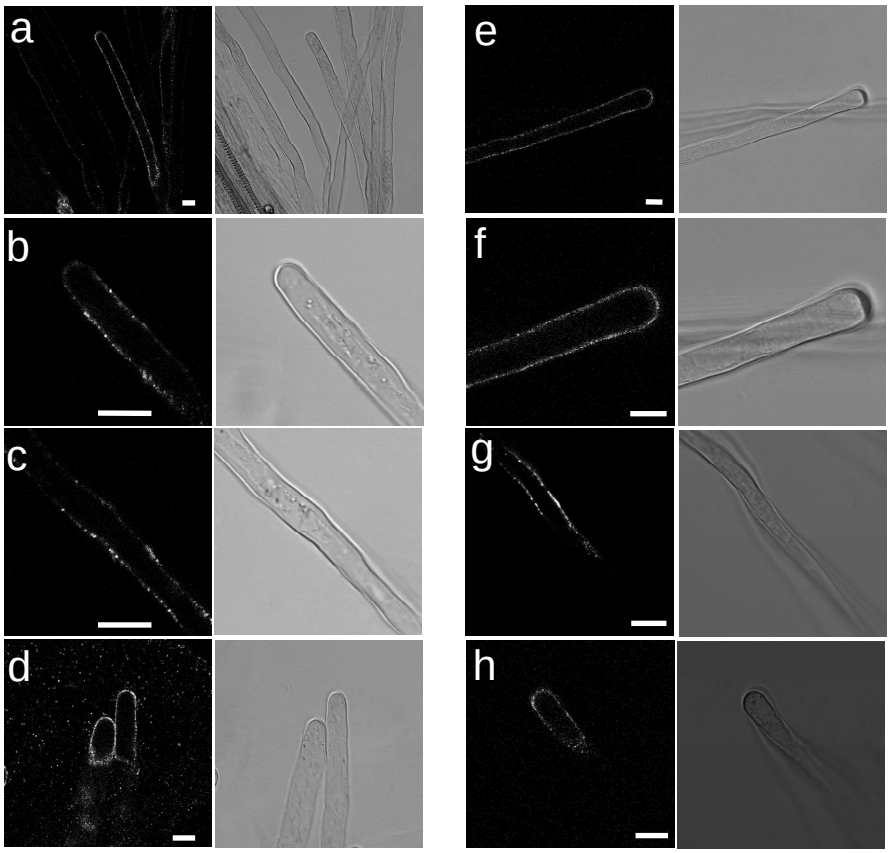

Figure 10. Immunolocalisation of NQR proteins (a-d) and FQR1 proteins (e-h) in the root hairs of 4-day-old *A. thaliana* plantlets by confocal fluorescence microscopy. In a column the fluorescence image is presented on the left and the bright field image on the right. Scale bar 10 µm.

2.5. Plastid alternative oxidase (PTOX) promotes oxidative stress when overexpressed in tobacco

Presented with publishers permission

THE JOURNAL OF BIOLOGICAL CHEMISTRY VOL. 284, NO. 45, pp. 31174–31180, November 6, 2009

Plastid Alternative Oxidase (PTOX) Promotes Oxidative Stress When Overexpressed in Tobacco

Received for publication, May 15, 2009, and in revised form, September 1, 2009 Published, JBC Papers in Press, September 9, 2009, DOI 10.1074/jbc.M109.021667

Eiri Heyno[‡], Christine M. Gross[‡], Constance Laureau[§], Marcel Culcasi[¶], Sylvia Pietri[¶], and Anja Krieger-Liszkay[‡1]

From the [‡]Commissariat à l'Energie Atomique (CEA), iBiTecS, CNRS URA 2096, Service de Bioénergétique Biologie Structurale et Mécanisme, 91191 Gif-sur-Yvette Cedex, the [§]Laboratoire d'Ecologie, Systématique et Evolution, CNRS-UMR 8079-IFR 87, Université Paris XI, 91405 Orsay Cedex, and the [¶]Sondes Moléculaires en Biologie-Laboratoire Chimie Provence, CNRS UMR 6264, 13397 Marseille Cedex 20, France

Photoinhibition and production of reactive oxygen species were studied in tobacco plants overexpressing the plastid terminal oxidase (PTOX). In high light, these plants was more susceptible to photoinhibition than wild-type plants. Also oxygen-evolving activity of isolated thylakoid membranes from the PTOX-overexpressing plants was more strongly inhibited in high light than in thylakoids from wild-type plants. In contrast in low light, in the PTOX overexpressor, the thylakoids were protected against photoinhibition while in wild type they were significantly damaged. The production of superoxide and hydroxyl radicals was shown by EPR spin-trapping techniques in the different samples. Superoxide and hydroxyl radical production was stimulated in the overexpressor. Two-thirds of the superoxide production was maintained in the presence of DNP-INT, an inhibitor of the cytochrome b_6f complex. No increase of the SOD content was observed in the overexpressor compared with the wild type. We propose that superoxide is produced by PTOX in a side reaction and that PTOX can only act as a safety valve under stress conditions when the generated superoxide is detoxified by an efficient antioxidant system.

The plastid terminal oxidase (PTOX[2] or IMMUTANS) is a plastid-located plastoquinol:oxygen oxidoreductase (1–3). It is distantly related to the alternative oxidase (AOX) of the mitochondrial inner membrane. The active site of both oxidases, PTOX and AOX, comprises a non-heme di-iron center (4, 5). PTOX is a minor component (~1% of PSII levels *in Arabidopsis thaliana*) of the thylakoid membrane and is located in the stroma lamellae (6, 7). PTOX plays an important role in carotenoid biosynthesis and seems to be involved in phytoene desaturation reactions (8–13).

The physiological importance of the role of PTOX as plastoquinol oxidase in alternative photosynthetic electron transport pathways is unclear. Evidence that PTOX acts as a plastoquinol oxidase was shown in tobacco plants, which constitutively expressed the *A. thaliana* PTOX gene (14). It has been suggested that PTOX may serve to keep the photosynthetic electron transport chain relatively oxidized. Exposure of plants to excess light may result in over-reduction of the plastoquinol pool and may lead to photoinhibition (15). However, no major role for PTOX in oxidizing the PQ pool was found in chlorophyll fluorescence assays when thylakoids from wt *A. thaliana* and the immutans mutant lacking PTOX were compared (16).

Recently, several groups reported that the PTOX level increased under natural stress conditions in several species specialized to harsh environmental conditions. This was the case in *Ranunculus glacialis*, an alpine plant, when it was acclimated to high light and low temperature (17); in the halophyte *Thellungiella halophila* when it was exposed to salt stress (18); and in *Brassica fruticulosa* when it was exposed to elevated temperature and high light (19). Although these findings support the hypothesis that PTOX may serve as a safety valve under stress conditions, they are in direct conflict with the data of Rosso *et al.* (20). These authors have shown that overexpression of PTOX in *A. thaliana* did not result in an increased capacity to keep the plastoquinone pool oxidized and did not provide any significant photoprotection. A more detailed study of photoinhibition and the generation of reactive oxygen species (ROS) under photoinhibitory illumination seems to be required to answer the question if and under which conditions PTOX can contribute to photoprotection. Using wt and PTOX$^+$ plants that overexpress PTOX (14), we investigated the susceptibility to light by measuring the loss of variable chlorophyll fluorescence in leaves and oxygen evolution in isolated thylakoids. Furthermore, we followed the light-induced generation of ROS by spin trapping EPR spectroscopy. We suggest, based on Western blots, that PTOX can only act as a safety valve and protect against photoinhibition when the level of SOD is adjusted to the actual level of PTOX.

EXPERIMENTAL PROCEDURES

Chemicals—All chemicals were of the highest grade from commercial suppliers. The spin trap α-(4-pyridyl-1-oxide)-*N*-tert-butyl nitrone (4-POBN) was obtained from Sigma. The nitrone 5-diethoxyphosphoryl-5-methyl-1-pyrroline *N*-oxide (DEPMPO) was synthesized according to Ref. 21. Commercial antibodies directed against D1, Cu/Zn-SOD, and Fe-SOD were obtained from Agrisera (Sweden).

Plant Material—Tobacco wild-type plants (*Nicotiana tabacum* var. petit Havana) and the plants overexpressing PTOX (14) were grown for 3 months on soil in a growth cabinet

[1] To whom correspondence should be addressed: CEA Saclay, iBiTec-S, Bât. 532, 91191 Gif-sur-Yvette, France. Fax: 33169088717; E-mail: anja.krieger-liszkay@cea.fr.

[2] The abbreviations used are: PTOX, plastid alternative oxidase; AOX, alternative oxidase; wt, wild type; ROS, reactive oxygen species; DEPMPO, 5-diethoxyphosphoryl-5-methyl-1-pyrroline *N*-oxide; SOD, superoxide dismutase; DNP-INT, 2′iodo-6-isopropyl-3-methyl-2′,4,4′-trinitrodiphenylether.

(24 °C day/18 °C night) under an irradiance of 150 or 450 μmol quanta m^{-2} s^{-1}.

Escherichia coli Expressing PTOX—E. coli cells expressing *Arabidopsis* PTOX (22) were grown in M9/glycerol medium until D_{600} = 0.3. Isopropyl thio-β-D-galactoside was then added (final concentration 40 μM) to induce the expression of the recombinant gene during 12 h. The control strain was grown in parallel. *E. coli* membranes were prepared according to Ref. 22.

Chloroplast Preparation—Intact chloroplasts were prepared according to Ref. 23. $MnCl_2$ was omitted from the medium because it interfered with EPR measurements. Intact chloroplasts (20–50 μg of Chl ml^{-1}) were shocked for 20 s in 5 mM $MgCl_2$, 25 mM HEPES, pH 7.5. Then an equal volume of 0.6 M sorbitol, 5 mM $MgCl_2$, 25 mM HEPES, pH 7.5, was added. The intactness of the chloroplasts was determined as the ratio of light-driven reduction of the membrane impermeable K_3-[Fe(CN)$_6$] measured with intact and osmotically shocked chloroplasts. The intactness of the chloroplasts was 70–80%.

Photoinhibition Treatment Leaves—The leaves were first kept at low light (8 μmol quanta m^{-2} s^{-1}) for 4 h with the petioles in lincomycin solution (1 g/liter). The photoinhibitory illumination was done in a growth cabinet with controlled temperature (22 °C), and the temperature of the illuminated leaves was around 28 °C. The petioles were kept in the lincomycin solution during the whole illumination period. During the illumination, samples were taken from the leaves for measurements of fluorescence.

Thylakoids—Prior to the photoinhibitory treatment, the chloroplasts were shocked. Thylakoids were illuminated with white light (120 or 1500 μmol quanta m^{-2} s^{-1}), stirred, and kept at 20–22 °C.

Fluorescence Measurements—The initial (F_o) and maximum (F_m) fluorescence levels were measured with a pulse amplitude modulated fluorometer (PAM 101; Heinz Walz, Effeltrich, Germany), using a saturating flash (7000 μmol quanta m^{-2} s^{-1}; duration, 1 s) for F_m. The variable fluorescence ($F_v = F_m - F_o$) was calculated. The samples were dark adapted for 30 min before each measurement to allow most of the reversible light-induced fluorescence quenching to relax.

Measurements of Electron Transport Activity—Light-saturated electron transport activity was measured as the rate of oxygen evolution in shocked chloroplasts using 1 mM K_3-[Fe(CN)$_6$] (ferricyanide) or 2,6-dichloro-1,4-benzoquinone (DCBQ) as electron acceptor and 0.5 mM NH_4Cl as uncoupler using an oxygen electrode.

EPR Measurements—Spin-trapping assays with 4-POBN were carried out using freshly shocked chloroplasts at a concentration of 10 μg of Chl ml^{-1}. Samples were illuminated for 5 min with white light (120 or 1500 μmol quanta m^{-2} s^{-1}) in the presence of 50 mM 4-POBN, 4% ethanol, 50 μM Fe-EDTA, and buffer (25 mM Hepes, pH 7.5, 5 mM $MgCl_2$, 0.3 M sorbitol).

When *E. coli* membranes were used, sonicated membranes (0.4 mg protein ml^{-1}) were incubated for 5 min in 20 mM Tris/HCl pH 7.5, 10 mM KCl, 5 mM $MgCl_2$ with 5 mM succinate as electron donor in the presence of 50 mM 4-POBN, 4% ethanol, 50 μM Fe-EDTA.

Spin-trapping assays with DEPMPO were carried out with thoroughly washed thylakoids (washing buffer contained 25 mM HEPES, pH 7.5, and 5 mM $MgCl_2$) at a concentration of 50 μg of Chl ml^{-1}. Samples were illuminated for 5 min with white light (1500 μmol quanta m^{-2} s^{-1}) in the presence of 50 mM DEPMPO, 1 mM DTPA and buffer (25 mM Hepes, pH 7.5, 5 mM $MgCl_2$).

EPR spectra were recorded at room temperature in a standard quartz flat cell using an ESP-300 X-band (9.73 GHz) spectrometer (Bruker, Rheinstetten, Germany). The following parameters were used: microwave frequency 9.73 GHz, modulation frequency 100 kHz, modulation amplitude: 1G, microwave power: 63 milliwatt in DEPMPO assays, or 6.3 milliwatt in 4-POBN assays, receiver gain: 2×10^4, time constant: 40.96 ms; number of scans: 4.

SDS-PAGE and Western Blotting—SDS-PAGE was carried out in 12% polyacrylamide gel. Western blotting was performed using nitrocellulose membrane and a Multiphor II Novablot unit (Amersham Biosciences). For detection, the enhanced chemoluminescence (ECL) system (Amersham Biosciences) was used according to the manufacturer's protocol.

RESULTS

Influence of High Amounts of PTOX on Photoinhibition—In this study, tobacco plants ($PTOX^+$) overexpressing the plastid terminal oxidase from *A. thaliana* (14) were used. $PTOX^+$ and wt plants were grown at 450 μmol quanta m^{-2} s^{-1}. When attached leaves were exposed to photoinhibitory light (1500 μmol quanta m^{-2} s^{-1}) a similar loss of variable fluorescence was observed for both, wt and $PTOX^+$ plants. The recovery of variable fluorescence in low light (8 μmol quanta m^{-2} s^{-1}) was significantly faster in the wild type than in $PTOX^+$ plants (Fig. 1*A*). To investigate whether the $PTOX^+$ plants were more susceptible to photoinhibition, leaves of wt and $PTOX^+$ were incubated for 4 h in lincomycin to block the synthesis of D1 and thereby the repair of damaged PSII centers. Leaves were illuminated for up to 4 h with 850 μmol quanta m^{-2} s^{-1} and the ratio of F_v/F_m, a measure of the maximum quantum yield of photosynthesis, was determined. Prior to high light exposure, F_v/F_m was 0.81 for wt and $PTOX^+$, consistent with measurements on a wide range of unstressed higher plants (24). During high light exposure, the loss of variable fluorescence was considerably higher in $PTOX^+$ than in wt (Fig. 1*B*). When plants grown at 150 μmol quanta m^{-2} s^{-1} were illuminated with 400 μmol quanta m^{-2} s^{-1}, a much lower loss of F_v/F_m was observed and no significant difference between $PTOX^+$ and wt was found (data not shown).

In addition to measurements of chlorophyll fluorescence in leaves, photoinhibition was measured as loss of the activity of the electron transfer chain in isolated thylakoids from wt and $PTOX^+$ (Fig. 2). Thylakoids from $PTOX^+$ illuminated with low light (120 μmol quanta m^{-2} s^{-1}) showed almost no loss of activity while in wt thylakoids 20% of oxygen evolution was lost after 20 min of illumination. However, when thylakoids were illuminated with high light (1500 μmol quanta m^{-2} s^{-1}) just the opposite effect was observed (Fig. 2*B*). Thylakoids from $PTOX^+$ were more susceptible to illumination with high light intensities than those from wt (Fig. 2*A*). The loss of electron transport activity was about 10% higher than in wt thylakoids. To distinguish between

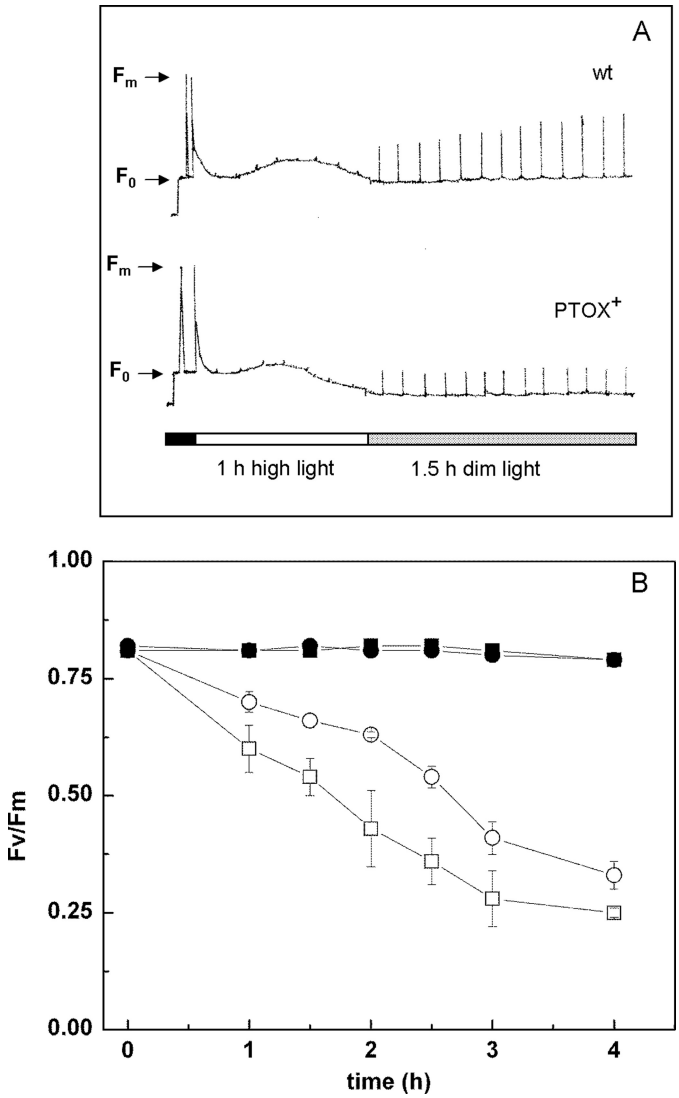

FIGURE 1. **Effect of high light on chlorophyll fluorescence in wt and PTOX$^+$ leaves.** *A*, fluorescence measurements on attached leaves of wild-type and PTOX$^+$ plants. Plants were dark-adapted for 30 min prior to the measurements. Segments of the leaves were illuminated for 1 h with white light (1500 μmol quanta m^{-2} s^{-1}) and then transferred to dim light (8 μmol quanta m^{-2} s^{-1}) for 1.5 h. *B*, detached leaves were incubated with lincomycin. *Circles*, wt; *squares*, PTOX$^+$ leaves, *filled symbols*, incubated at low light (8 μmol quanta m^{-2} s^{-1}), *open symbols*, incubated at high light (850 μmol quanta m^{-2} s^{-1}). Error bars represent S.D. (nine independent experiments).

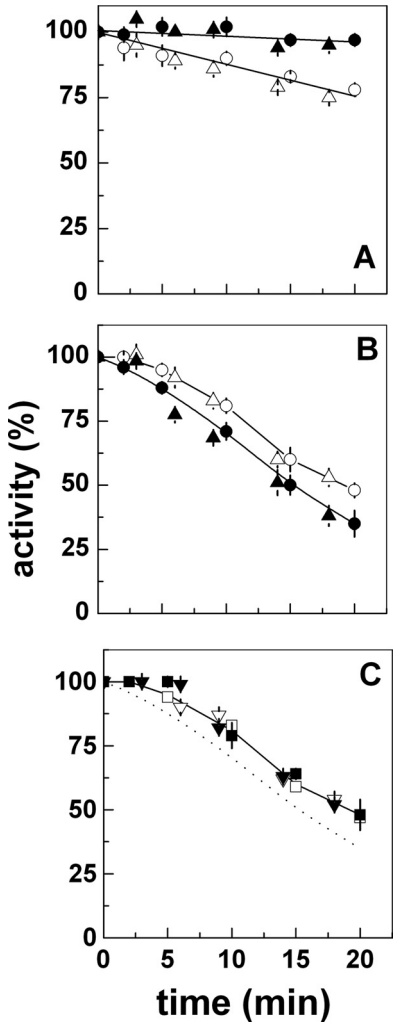

FIGURE 2. **Photoinhibition assays on wt and PTOX$^+$ thylakoids in low and high light.** Freshly shocked thylakoids were incubated: (*A*) at low light (120 μmol quanta m^{-2} s^{-1}), wt with ferricyanide (○), and DCBQ (△), and PTOX$^+$ with ferricyanide (●), and DCBQ (▲); *B*, same as *A* but at high light (1500 μmol quanta m^{-2} s^{-1}); *C*, high light (1500 μmol quanta m^{-2} s^{-1}) in the presence of SOD, wt with ferricyanide (□), and DCBQ (▽), and PTOX$^+$ with ferricyanide (■), and DCBQ (▼). 50 μg SOD/ml were added prior to the photoinhibitory illumination. The *dotted line* is the same as the *lower line* in *panel B*, and the difference between it and the *solid line* shows the protective effect of SOD. The maximum activity was between 270–290 μmol of O_2 mg Chl^{-1} h^{-1} for both wt and PTOX$^+$ thylakoids in the presence of ferricyanide and 400–425 μmol O_2 mg Chl^{-1} h^{-1} in the presence of DCBQ as electron acceptor. Error bars represent S.D. (3–4 independent experiments).

damage of the total electron transport chain and damage of PSII, the activity was measured by using ferricyanide as electron acceptor to determine the activity of the total linear electron transport and by using DCBQ as electron acceptor for PSII. The data show that the most susceptible part of the electron transport chain is PSII. Addition of SOD rescued the electron transfer activity of PTOX$^+$ thylakoids to a level comparable with the wt (Fig. 2*C*). The addition of SOD had no effect on the light-induced damage of photosynthetic electron transport in wt thylakoids (Fig. 2*C*). These photoinhibition experiments were performed in the absence of an uncoupler. No external electron acceptor was present during the photoinhibition treatment leaving oxygen as the only available electron acceptor.

Influence of High Amounts of PTOX on ROS Production—ROS, including superoxide ($O_2^{\cdot-}$), hydrogen peroxide (H_2O_2), and hydroxyl radicals ($HO^{\bullet}$), can be generated by the reduction of oxygen in photosynthetic electron transfer in a number of different reactions: O_2 can act as terminal acceptor in the so-called Mehler reaction at the acceptor side of PSI, it can be reduced by plastosemiquinones in the membrane (25), it can be reduced at the acceptor side of PSII (26–30), and it is the electron acceptor of the plastid terminal oxidase, which uses two plastoquinol molecules as electron donor (4, 5, 31). We investigated the light-induced formation of ROS by EPR spectroscopy using either ethanol/4-POBN or DEPMPO as the spin traps. Performing 4-POBN spin trapping in the presence of ethanol is a general procedure to indirectly prove the formation of

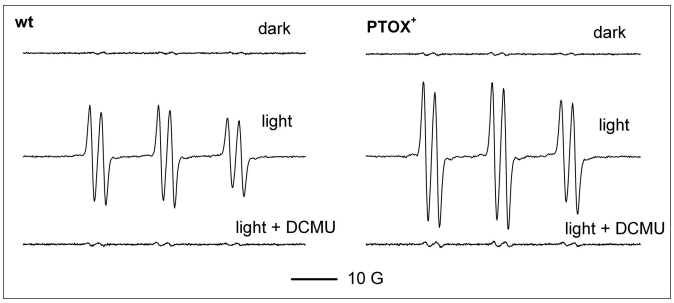

FIGURE 3. **Light-induced hydroxyl radical formation in wt and PTOX$^+$ thylakoids.** Generation of hydroxyl radicals is shown by indirect spin trapping with 4-POBN/ethanol. Typical EPR spectra of the 4-POBN/α-hydroxyethyl adduct are shown. Samples were illuminated for 5 min at high light (1500 μmol quanta m^{-2} s^{-1}). Where indicated, 10 μM DCMU was added prior to the illumination.

TABLE 1

ROS production in wt and PTOX$^+$ thylakoids

Thylakoids were illuminated for 5 min at high light (1500 μmol quanta m^{-2} s^{-1}) in the presence of the spin traps 4-POBN (50 mM)/ethanol or DEPMPO (50 mM). Where indicated 10 μM DCMU, 10 μM DNP-INT, or 50 μg of SOD/ml were added prior to the illumination. The double integral of the total signal obtained with wt thylakoids after illumination was set to unity. If not stated otherwise four spectra of different preparations were used to calculate the mean and the standard deviation.

	EPR signal size	
	wt	PTOX$^+$
4-POBN/EtOH		
Light	1.00 ± 0.10	1.56 ± 0.15
Light + DCMU	0.03 ± 0.01	0.04 ± 0.01
Dark	0.02 ± 0.01	0.02 ± 0.01
DEPMPO		
Light	1.00 ± 0.15 (n = 4)	1.55 ± 0.23 (n = 9)
Light + DNP-INT	0.31 ± 0.10 (n = 9)	0.63 ± 0.09 (n = 5)
Light + DCMU	Not detectable	Not detectable
Light + SOD	0.07 ± 0.02 (n = 4)	Not detectable
Dark	Not detectable	Not detectable

HO$^\bullet$ through the detection of the secondary 4-POBN/α-hydroxyethyl spin adduct (32). The cyclic nitrone DEPMPO was used because it forms characteristic, non-exchangeable adducts with OH$^\bullet$ and $O_2^{\bullet-}$, and the EPR signal patterns are easily distinguishable (21).

Whereas little or no signal was observed when samples were maintained in the dark in the presence of ethanol/4-POBN, illumination of thylakoids resulted in strong EPR signals as sextets of lines (a_N = 15.61 G; $a_{H\beta}$ = 2.55 G) characteristic of 4-POBN/α-hydroxyethyl aminoxyl (Fig. 3). Representative spectra are shown in Fig. 3. PTOX$^+$ thylakoids produced a signal that was ~50% larger than the signal obtained from wt thylakoids after 5 min of illumination with 1500 μmol quanta m^{-2} s^{-1} white light (Table 1). Addition of DCMU, an inhibitor of electron transfer in PSII, almost completely inhibited spin adduct formation. Taken altogether, the data of Fig. 3 show that OH$^\bullet$ radicals were generated by photosynthetic electron transfer reactions and not by excitation of chlorophylls in disordered reaction centers or antenna systems.

In our system, HO$^\bullet$ could result from a metal ion-assisted Fenton mechanism involving H_2O_2, the disproportionation product of $O_2^{\bullet-}$. To investigate whether $O_2^{\bullet-}$ was the primary radical species formed experiments were carried out in the presence of DEPMPO instead of 4-POBN/ethanol (Fig. 4). Again no EPR signal was detected in the dark while a complex signal was observed upon illumination. A satisfactory simulation of the

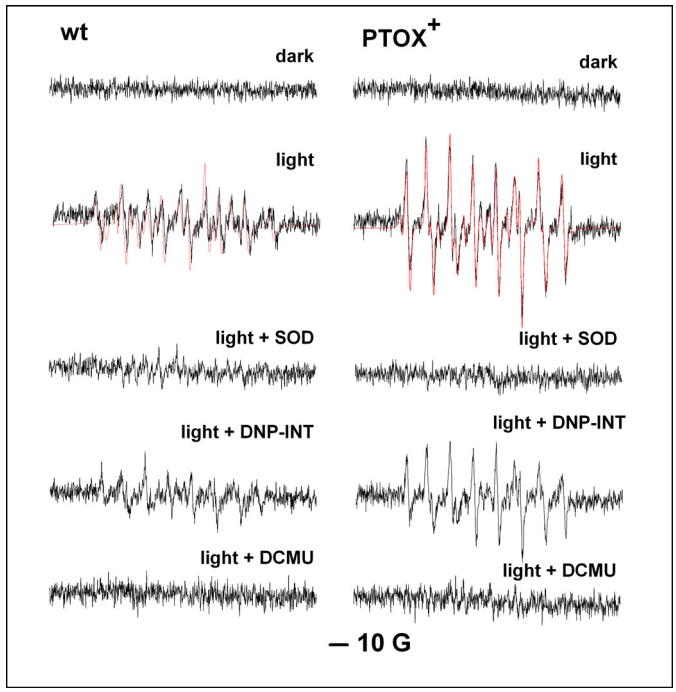

FIGURE 4. **Light-induced superoxide formation in wt and PTOX$^+$ thylakoids.** Typical EPR spectra of the DEPMPO-OOH adduct are shown. Thylakoid samples were illuminated as described in Fig. 4 in the presence of 50 mM DEPMPO. Typical EPR spectra are mixtures of superoxide (~70%), hydroxyl and carbon-centered DEPMPO adducts (*red lines*, simulated spectra). DEPMPO-OOH is generated as a relatively stable radical after DEPMPO reacts with $O_2^{\bullet-}$. Samples were illuminated for 5 min at high light (1500 μmol quanta m^{-2} s^{-1}). Where indicated, 50 μg SOD/ml, 10 μM DNP-INT, or 10 μM DCMU was added prior to the illumination.

signals in Fig. 4 was obtained assuming a mixture of DEPMPO/$O_2^{\bullet-}$ (DEPMPO-OOH; the asymmetrical signal of which could be simulated by the 1:1 mixture of two species having the coupling constants: a_N = 13.1 (13.2); a_P = 50.7 (49.9) and $a_{H\beta}$ = 11.7 (10.5) G), DEPMPO/HO$^\bullet$ (DEPMPO-OH: a_N = 13.0; a_P = 47.4 and $a_{H\beta}$ = 15.2 G) and a carbon-centered/DEPMPO spin adduct (DEPMPO-R; a_N = 14.4; a_P = 45.5 and $a_{H\beta}$ = 21.3 G). In all spectra, DEPMPO-OOH was the dominant species (~70%) while the remaining DEPMPO-OH and DEPMPO-R appeared in approximately 1:1 mixtures.

PTOX$^+$ thylakoids produced an EPR signal which was ~60% larger than the signal obtained from wt thylakoids after 5 min illumination with 1500 μmol quanta m^{-2} s^{-1} white light (Fig. 4 and Table 1). In the presence of SOD, the signal in PTOX$^+$ thylakoids was completely suppressed while in wt thylakoids a small signal was still observed (Fig. 4). These data indicate that $O_2^{\bullet-}$, which was primarily generated by illumination, partially decomposed into HO$^\bullet$, which could in turn undergo hydrogen abstraction from a series of cellular targets to form carbon-centered radicals. The higher level of $O_2^{\bullet-}$ production in the overexpressor suggests that PTOX is responsible for the additional $O_2^{\bullet-}$ generation. However, the Mehler reaction will also contribute to $O_2^{\bullet-}$ generation in thylakoids. To measure electron transport to oxygen in the absence of that reaction, the cytochrome b_6f inhibitor DNP-INT, a specific inhibitor of the Q_o binding site (33), was added prior to the illumination. In the presence of DNP-INT, the EPR signal size in DEPMPO experiments was reduced by ~30% in PTOX$^+$ thylakoids. In wt thy-

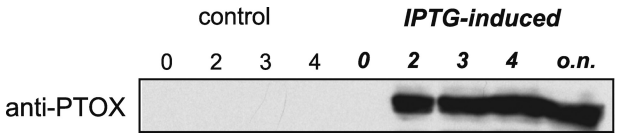

FIGURE 5. **Expression of PTOX in *E. coli*.** The immunoblot was decorated with polyclonal antibodies directed against PTOX. 250 μl of culture was taken as a sample at given times after induction by isopropyl-1-thio-β-D-galactopyranoside (0–4 h and overnight, *o.n.*), centrifuged, and the pellet was resuspended in 50 μl of SDS loading buffer. 10 μl were loaded.

TABLE 2

ROS production in control and PTOX-containing *E. coli* membranes

Membranes (0.4 mg protein ml^{-1}) were incubated for 5 min with 5 mM succinate and, when indicated, 0.2 mM decyl-plastoquinone in the presence of the spin trap 4-POBN (50 mM)/ethanol. The double integral of the total signal obtained with control membranes in the presence of decyl-plastoquinone was set to unity. Five spectra were used to calculate the mean and the standard deviation.

	EPR signal size	
	Control membranes	PTOX-containing membranes
No decyl-PQ	Not detectable	0.6 ± 0.05
+decyl-PQ	1.0 ± 0.1	1.6 ± 0.1

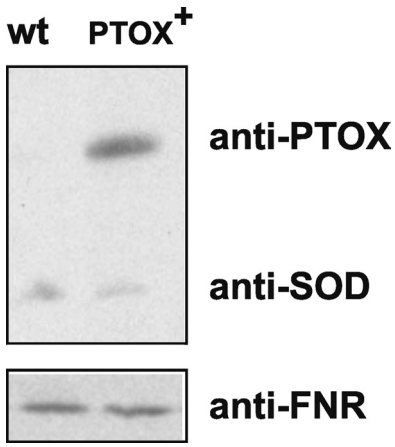

FIGURE 6. **PTOX and Cu/Zn-SOD protein levels in wt and PTOX$^+$ chloroplasts.** The immunoblot was decorated with polyclonal antibodies directed against PTOX and Cu/Zn-SOD. FNR antibodies were used for a loading control. 10 μg of chlorophyll were loaded.

lakoids, the signal size decreased by about 60% in comparison to the signal size measured in the absence of the inhibitor. The data obtained in the presence of DNP-INT show that the Mehler reaction counts for about two-thirds of the $O_2^{\cdot-}$ generation in wt thylakoids. Unfortunately, DEPMPO could only detect $O_2^{\cdot-}$ in thoroughly washed thylakoids while 4-POBN could be used with freshly shocked intact chloroplasts. Although DEPMPO-OOH does not significantly self-decompose into DEPMPO-OH (21), at least two reductive mechanisms occurring in cells can alter the DEPMPO-OOH EPR signal, *i.e.* conversion into DEPMPO-OH by certain enzymes such as glutathione peroxidase (21, 34) or formation of EPR-silent hydroxylamines such as with ascorbate (35, 36). Intense washing did not damage the thylakoids as can be seen by the complete inhibition of the signal in the presence of DCMU.

To test whether the presence of PTOX leads in general to an increase in ROS generation, PTOX was expressed in *E. coli* (Fig. 5), and ROS generation was measured by the spin trap EtOH/POBN in the presence of succinate as electron donor to complex II of the respiratory chain. In the presence of 1 mM KCN a significant level of ROS was formed in control membranes while this ROS generation was reduced by about 50% in PTOX-containing membranes (data not shown). This shows that PTOX functions as an alternative oxidase in this system. PTOX-containing membranes generated a small, but significant, amount of ROS while ROS production in control membranes was hardly detectable (Table 2). Decyl-plastoquinone was added to obtain higher rates of electron flow to PTOX (22). Under these conditions, ROS generation was detectable in control membranes and to a 1.6-fold higher level in PTOX-containing membranes. This result clearly shows that PTOX forms ROS when the quinone pool is over-reduced.

SOD Protein Level in PTOX$^+$ and Wt—The question arises why PTOX$^+$ thylakoids were more susceptible to photoinhibition in strong light while they were protected in low light compared with wt thylakoids. One possibility is that the antioxidant system in PTOX$^+$ cannot cope with the heavier burden of $O_2^{\cdot-}$ generation in high light conditions while it is sufficient to detoxify the amount of $O_2^{\cdot-}$ under low light illumination. The antioxidant system of the chloroplast consists of SODs and several forms of ascorbate peroxidases. We focused here on SODs, which detoxify $O_2^{\cdot-}$. The presence of a Cu/Zn-SOD and an Fe-SOD in chloroplasts of *A. thaliana* has been shown (37). In tobacco, one Cu/Zn-SOD is present in the chloroplast and there is evidence for a Fe-SOD on the transcript level (Data Bank Uniprot/Swiss-Prot). To show amounts of SOD, we performed immunoblots of the proteins of intact chloroplasts of wt and PTOX$^+$ using polyclonal antibodies directed against PTOX, plastid Cu/Zn-SOD, and Fe-SOD (Fig. 6). Wt and PTOX$^+$ chloroplasts contained about the same amount of Cu/Zn-SOD as shown by the reaction with the specific anti-Cu/Zn-SOD antibody. No protein was detected with the anti-Fe-SOD antibody.

DISCUSSION

In the literature it has been shown that PTOX is involved in plastoquinol oxidation (14), and it has been suggested that it plays an important role as a stress-induced safety valve (15, 38) and helps the plants to adapt to stress conditions like salt stress (18), extreme temperatures and high light (17, 19, 39). However, PTOX overexpression did not protect PSII against photoinhibition in either tobacco (14) or *Arabidopsis* plants (20). It is likely that PTOX has a minimal impact on electron transport between PSII and PSI in mature leaves (3, 16, 20) but that it plays an important role in keeping the PQ pool oxidized during chloroplast biogenesis and assembly of the photosynthetic apparatus (20).

In the present study, the susceptibility to light was studied in wt and PTOX$^+$ tobacco plants. In high light, PTOX$^+$ plants were more damaged than the wt (Figs. 1 and 2) and higher levels of $O_2^{\cdot-}$ (Fig. 4) and other ROS (H_2O_2 and $OH^{\bullet}$, Fig. 3) were produced in these plants than in wt. In low light, thylakoids from PTOX$^+$ plants were protected against photoinhibition. In low light, in the presence of oxygen as the only available electron acceptor, the reduction state of the PQ pool will be high in wt plants. Under these conditions, the acceptor side of PSII becomes easily reduced and charge recombination reactions

occur between the reduced semiquinones at the acceptor side of PSII and oxidized states of the donor side. Charge recombination reactions in PSII can lead to the formation of triplet chlorophyll in the reaction center which reacts with O_2 to $^1O_2$. $^1O_2$ is likely to be the main responsible species for photoinhibition in low light (40–42). In PTOX$^+$ plants, the PQ pool will be less reduced and, therefore, $^1O_2$-triggered damage of PSII will be lower. The protein level of SOD will be sufficient to detoxify O_2^- under low light illumination.

In high light, O_2^- produced by the Mehler reaction and other alternative pathways plays an important role in photoinhibition in addition to $^1O_2$. The photoinhibition treatment was performed in the absence of an uncoupler so that the presence of a high proton gradient (photosynthetic control) limits oxygen reduction at the level of PSI. We attribute most of the O_2^- production measured in thylakoids to PTOX activity since O_2^- generation was largely increased in PTOX$^+$ plants and since it was only partially inhibited by DNP-INT (Fig. 4). Overexpression of PTOX does clearly not protect the photosynthetic electron transport chain from ROS generation but is just doing the opposite. The question arises which process causes the increase in O_2^- production in PTOX$^+$ thylakoids and plants. One possibility is that the overexpressed protein is either not correctly assembled or not well integrated into the membrane and produces therefore more O_2^-. This seems to be rather unlikely, because Joët *et al.* (14) have shown that the PQ pool was much faster oxidized in PTOX$^+$ plants by measuring chlorophyll fluorescence curves during dark to light transitions.

A second possibility is that the plastoquinol oxidation by PTOX itself produces O_2^- in a side reaction. PTOX is a plastoquinol oxidase that catalyzes the four-electron reduction of oxygen to water. PTOX is distantly related to the AOX of the mitochondrial inner membrane. The active site of both oxidases, PTOX and AOX, comprises a non-heme di-iron center. The molecular mechanism of the reduction of oxygen to water by these oxidases is not known. In analogy to a side reaction of the methane monooxygenase, which contains a non-heme di-iron center and is capable of fully reducing oxygen to water, it was proposed that peroxide intermediates are formed in AOX and PTOX (4, 43). Alternatively it has been proposed that instead of a peroxide intermediate a diferryl center or a divalent ferric-ferryl or differic iron site together with a protein-derived radical is formed in analogy to the reaction intermediates of the R2 subunit of the class I ribonucleotide reductase (see (43) for a discussion of the different mechanisms). The reaction intermediates of oxidases with non-heme di-iron centers are likely to be sensitive to oxidation. This may lead to the generation of ROS like superoxide. In methane monooxygenase and also in Δ^9-desaturase, reactivity toward oxygen is controlled to prevent potential side reactions which lead to ROS formation (4). In both enzymes, special mechanisms are employed to ensure the presence of both substrates before the reaction starts. It is an open question if the alternative oxidases, AOX and PTOX, use a similar strategy to ensure that the second quinol is already bound before oxygen binds and thereby allow the timely delivery of the two last electrons needed for the full reduction of oxygen to water. If this is the case, a coupling protein might be needed to avoid O_2^- generation like in the methane monooxygenase. In such a case, it might be that the expression of such an enzyme is not up-regulated in the PTOX overexpressor.

Alternatively, it could also be envisaged that a tight coupling between the level of SOD and PTOX is needed for an efficient detoxification of the produced O_2^-. As can be seen in Fig. 6, the amount of Cu/Zn-SOD is the same in chloroplasts from PTOX$^+$ and wt. Under low light conditions, the amount of SOD seems to be sufficient to detoxify the produced O_2^- while in high light the SOD is limiting and the O_2^- may cause the observed higher damage to PSII in PTOX$^+$ thylakoids and leaves (Figs. 1 and 2). In a tobacco mutant lacking complex I of the respiratory chain a higher amount of AOX was found and, at the same time, the level of Mn-SOD (localized in the mitochondria) was increased (44). Plants completely lacking PTOX are more susceptible to photoinhibition (12), while plants which are exposed to an environmental stress that promotes photoinhibition have increased protein levels of PTOX (17–19). Further investigations are needed to show whether there is a correlation between PTOX and SOD levels in alpine plants at high light and cold temperatures (17), in halophytes under salt stress (18) and in oat and *B. fruticulosa* at high light and elevated temperatures (19, 39). Furthermore, a putative functional relationship between PTOX and SOD has to be established in plants which have increased protein levels of both, PTOX and SOD. If this is the case, PTOX could act as a safety valve even under high light conditions in which the PQ pool is highly reduced when the O_2^- level is controlled by SODs.

Acknowledgments—We thank Bernard Genty, CEA Cadarache, for providing us with seeds of PTOX$^+$. We would like to thank Sun Un, CEA Saclay, and Peter Streb, Université Paris-Sud, for stimulating discussions. We are grateful to Marcel Kuntz, Université Grenoble, who provided the E. coli strain expressing PTOX and antibodies against PTOX and to R. J. Berzborn, Ruhr-Universität Bochum, who provided the antibodies against FNR.

REFERENCES

1. Berthold, D. A., and Stenmark, P. (2003) *Annu. Rev. Plant Biol.* **54,** 497–517
2. Kuntz, M. (2004) *Planta* **218,** 896–899
3. Rumeau, D., Peltier, G., and Cournac, L. (2007) *Plant Cell Environ.* **30,** 1041–1051
4. Berthold, D. A., Andersson, M. E., and Nordlund, P. (2000) *Biochim. Biophys. Acta* **1460,** 241–254
5. Fu, A., Park, S., and Rodermel, S. (2005) *J. Biol. Chem.* **280,** 42489–42496
6. Andersson, M. E., and Nordlund, P. (1999) *FEBS Lett.* **449,** 17–22
7. Lennon, A. M., Prommeenate, P., and Nixon, P. J. (2003) *Planta* **218,** 254–260
8. Wetzel, C. M., Jiang, C. Z., Meehan, L. J., Voytas, D. F., and Rodermel, S. R. (1994) *Plant J.* **6,** 161–175
9. Carol, P., Stevenson, D., Bisanz, C., Breitenbach, J., Sandmann, G., Mache, R., Coupland, G., and Kuntz, M. (1999) *Plant Cell* **11,** 57–68
10. Wu, D., Wright, D. A., Wetzel, C., Voytas, D. F., and Rodermel, S. (1999) *Plant Cell* **11,** 43–55
11. Carol, P., and Kuntz, M. (2001) *Trends Plant Sci.* **6,** 31–36
12. Shahbazi, M., Gilbert, M., Labouré, A. M., and Kuntz, M. (2007) *Plant Physiol.* **145,** 691–702
13. Aluru, M. R., and Rodermel, S. R. (2004) *Physiol. Plant.* **120,** 4–11
14. Joët, T., Genty, B., Josse, E. M., Kuntz, M., Cournac, L., and Peltier, G. (2002) *J. Biol. Chem.* **277,** 31623–31630

15. Niyogi, K. K. (2000) *Curr. Opin. Plant Biol.* **3,** 455–460
16. Nixon, P. J., and Rich, P. R. (2006) *The Structure and Function of Plastids* (Wise, R. R., and Hoober, J. K., eds) pp. 237–251, Springer, The Netherlands
17. Streb, P., Josse, E. M., Gallouët, E., Baptist, F., Kuntz, M., and Cornic, G. (2005) *Plant Cell Environ.* **28,** 1123–1135
18. Stepien, P., and Johnson, G. N. (2009) *Plant Physiol.* **149,** 1154–1165
19. Díaz, M., De Haro, V., Muñoz, R., and Quiles, M. J. (2007) *Plant Cell Environ.* **30,** 1578–1585
20. Rosso, D., Ivanov, A. G., Fu, A., Geisler-Lee, J., Hendrickson, L., Geisler, M., Stewart, G., Krol, M., Hurry, V., Rodermel, S. R., Maxwell, D. P., and Hüner, N. P. (2006) *Plant Physiol.* **142,** 574–585
21. Frejaville, C., Karoui, H., Tuccio, B., Le Moigne, F., Culcasi, M., Pietri, S., Lauricella, R., and Tordo, P. (1995) J. *Med. Chem.* **38,** 258–265
22. Josse, E. M., Alcaraz, J. P., Labouré, A. M., and Kuntz, M. (2003) *Eur. J. Biochem.* **270,** 3787–3794
23. Laasch, H. (1987) *Planta* **171,** 220–226
24. Bjorkman, O., and Demmig, B. (1987) *Planta* **170,** 489–504
25. Ivanov, B., Mubarakshina, M., and Khorobrykh, S. (2007) *FEBS Lett.* **581,** 1342–1346
26. Ananyev, G., Renger, G., Wacker, U., and Klimov, V. (1994) *Photosynth. Res.* **41,** 327–338
27. Pospísil, P., Arató, A., Krieger-Liszkay, A., and Rutherford, A. W. (2004) *Biochemistry* **43,** 6783–6792
28. Arató, A., Bondarava, N., and Krieger-Liszkay, A. (2004) *Biochim. Biophys. Acta* **1608,** 171–180
29. Kruk, J., and Strzalka, K. (1999) *Photosynth. Res.* **62,** 273–279
30. Kruk, J., and Strzalka, K. (2001) *J. Biol. Chem.* **276,** 86–91
31. Cournac, L., Josse, E. M., Joët, T., Rumeau, D., Redding, K., Kuntz, M., and Peltier, G. (2000) *Philos. Trans. R. Soc. Lond. B Biol. Sci.* **355,** 1447–1454
32. Ramos, C. L., Pou, S., Britigan, B. E., Cohen, M. S., and Rosen, G. M. (1992) *J. Biol. Chem.* **267,** 8307–8312
33. Trebst, A., Wietoska, H., Draber, W., and Knops, H. J. (1978) *Z. Naturforsch., C: J. Biosci.* **33,** 919–927
34. Culcasi, M., Rockenbauer, A., Mercier, A., Clément, J. L., and Pietri, S. (2006) *Free Radic. Biol. Med.* **40,** 1524–1538
35. Berliner, J., Khramtsov, V., Fujii, H., and Clanton, T. L. (2001) *Free Radic. Biol. Med.* **30,** 489–499
36. Karoui, H., Rockenbauer, A., Pietri, S., and Tordo, P. (2002) *Chem. Commun.* (*Camb*) **24,** 3030–3031
37. Kliebenstein, D. J., and Monde, R. A. (1998) *Plant Physiol.* **118,** 637–650
38. Peltier, G., and Cournac, L. (2002) *Annu. Rev. Plant Biol.* **53,** 523–550
39. Quiles, M. J. (2006) *Plant Cell Environ.* **29,** 1463–1470
40. Keren, N., Gong, H., and Ohad, I. (1995) *J. Biol. Chem.* **270,** 806–814
41. Keren, N., Berg, A., van Kan, P. J., Levanon, H., and Ohad, I. (1997) *Proc. Natl. Acad. Sci. U.S.A.* **94,** 1579–1584
42. Krieger-Liszkay, A. (2005) *J. Exp. Bot.* **56,** 337–346
43. Affourtit, C., Albury, M. S., Crichton, P. G., and Moore, A. L. (2002) *FEBS Lett.* **510,** 121–126
44. Dutilleul, C., Garmier, M., Noctor, G., Mathieu, C., Chétrit, P., Foyer, C. H., and de Paepe, R. (2003) *Plant Cell* **15,** 1212–1226

3. Summary

In this chapter the main results of the thesis are summarised and general conclusion are drawn (Fig. 1). ROS-producing enzymes were studied in the PM, in mitochondria and chloroplasts to get an insight into different enzymatic activities leading to superoxide generation.

The main focus on the work was the characterisation of $O_2^{\bullet-}$-producing enzymes in the PMs. Such enzymes are important sources of apoplastic $O_2^{\bullet-}$ and H_2O_2 involved in PRX-catalysed $^{\bullet}OH$ formation that mediates elongation growth. A quinone reductase (QR) was isolated from PMs showing homology to the NQR of *A. thaliana*. The isolated QR mediated ROS production by the reduction of certain naphthoquinones that were susceptible to deprotonation at pH ≥7. A potential naphthoquinone species in PMs was detected which might serve as a QR substrate *in vivo*. A tentative model of the QR activity in the PMs is shown in Figure 1a. At pH < 7, the quinols reduced by QR take part in redox reactions with e.g. quinol oxidases and ascorbate reductases. At pH > 7, the deprotonation of the quinols would lead to ROS formation. The question arises whether such a model could be valid *in vivo*. According to the preliminary studies on QR knock-out mutants (chapter 2.4), ROS generation was stimulated in the mutants while the growth was retarded. The QR mutants showed stunted root growth, chlorophyll bleaching and increased ROS production. The source of ROS might be a 1-electron reduction of quinones by a different enzyme, such as cyt P-450 (Iyanagi and Yamazaki, 1969). The NADPH oxidase (NOX) might also reduce a quinone, as it has singly-reduced cofactors in or near the PM. The resulting semiquinone radicals readily reduce O_2. QRs have been reported to protect against oxidative stress. The observation that the QR knockout mutants produce more ROS seems to point towards such a role for QR. It has also been reported that QRs have other functions in the cell in addition to the reduction of quinones. For instance, they regulate the proteosomal degradation of transcription factors (Sollner and Macheroux, 2009). Moreover, the QR substrate spectrum is very wide and QRs have been found both in the cytosol and PMs, underlining the present incomplete understanding of the biological function of these enzymes. Therefore, the cellular homeostasis might be disturbed in a larger scale in the QR mutants masking their proposed role as mediators of ROS formation.

Figure 1b illustrates the three regulatory mechanisms of the PM NOX that were studied in this thesis. Cd^{2+} was shown to be a competitive inhibitor of the NOX activity in PMs. The targets of Cd^{2+} are likely the calcium binding EF-hands of NOX because Ca^{2+} efficiently competed with Cd^{2+} restoring the NOX activity. In intact plants Cd^{2+} inhibited the

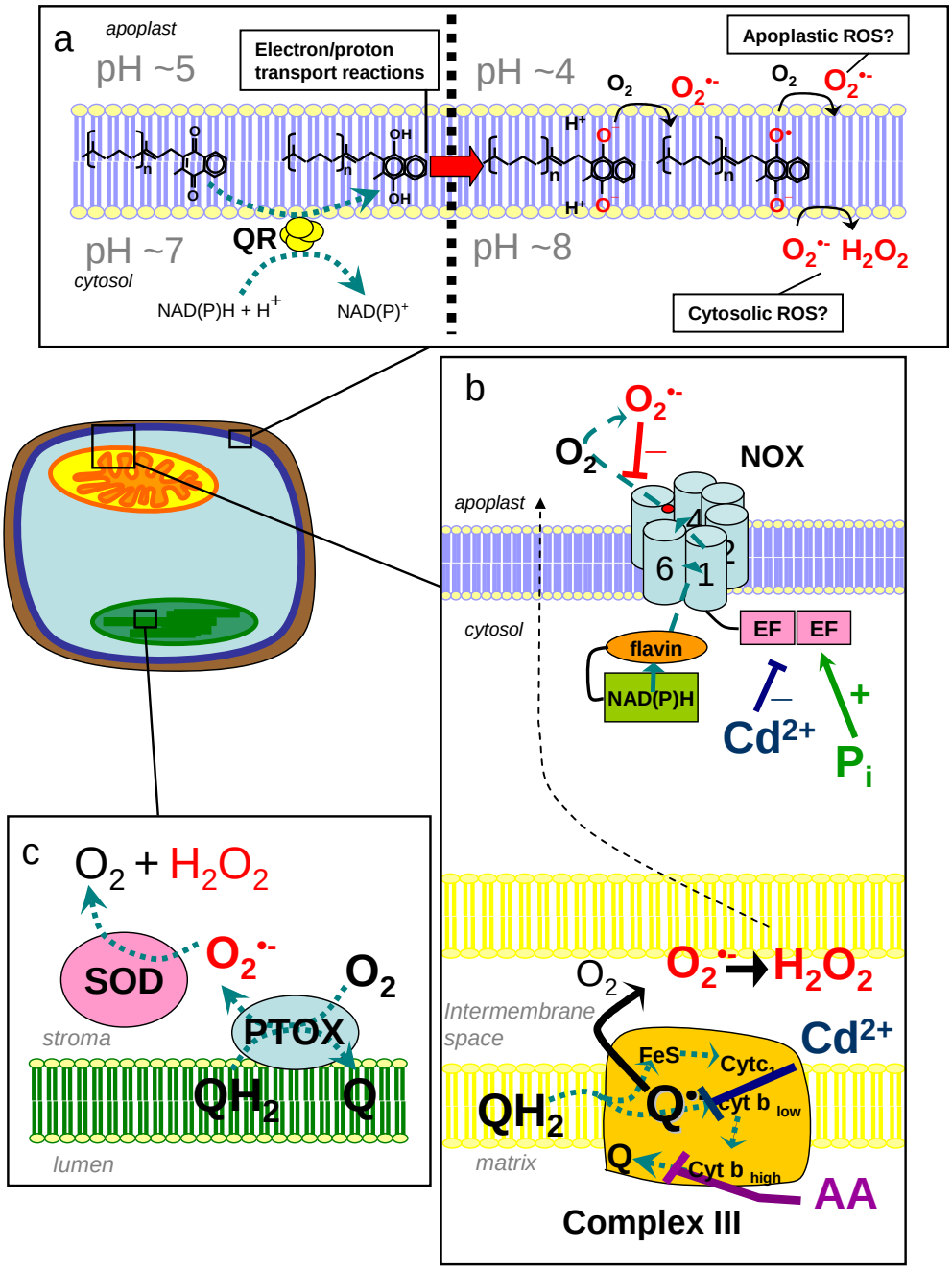

Figure 4.1. Summary of ROS production in the plasma membranes, mitochondria and chloroplasts. a) Quinone reductases (QR) reduce quinones in the plasma membrane using cytosolic NAD(P)H. At pH < 7 the quinols may participate in electron transfer reactions in the plasma membrane. At pH > 7 the quinol deprotonates and the resulting unstable intermediates reduce O_2 to ROS. b) The plasma membrane NADPH oxidase (NOX) reduces apoplastic O_2 to $O_2^{\bullet-}$ using cytosolic NAD(P)H. NOX is inhibited by the end product $O_2^{\bullet-}$ (in red) and by Cd^{2+} (blue), while it is stimulated by phosphorylation (green). The mitochondrial respiratory complex III is inhibited by Cd^{2+} (blue) and by AA (purple). Both of these inhibitors result in the stabilisation of the semiquinone species which is involved in the reaction cycle of complex III. The semiquinone reduces O_2 to ROS. H_2O_2 that is produced in the mitochondria can diffuse to the apoplast (black dotted arrow). c) Plastid alternative oxidase (PTOX) produces $O_2^{\bullet-}$ which is metabolised by a superoxide dismutase (SOD). Electron transfer reactions catalysed by the enzymes and leading to $O_2^{\bullet-}$ in a side reaction are shown in turquoise dotted arrows.

apoplastic $O_2^{\bullet-}$ production but stimulated the H_2O_2 production. Because H_2O_2 usually originates from $O_2^{\bullet-}$ dismutation and because it can pass membranes, it was reasoned that the source of H_2O_2 must be intracellular. Isolated plant mitochondria showed increased production of $O_2^{\bullet-}$ and H_2O_2 in a manner similar to antimycin A (AA), the specific inhibitor of respiratory complex III of mitochondria. Accordingly, the addition of AA to intact plants increased apoplastic H_2O_2 production but had no effect on apoplastic $O_2^{\bullet-}$ production. Figure 1b illustrates the ROS production in the PM and mitochondria in response to Cd^{2+}.

Inhibition of NOX by its end-product $O_2^{\bullet-}$ was found when the rates of NAD(P)H oxidation and $O_2^{\bullet-}$ production were compared. An end-product inhibition of the NOX appears to be an attractive mechanism to avoid uncontrolled ROS production (Fig. 1b). The human NOXs contribute in many diseases resulting from over-production of ROS (Lambeth, 2007). In the majority of these diseases the regulation of the $O_2^{\bullet-}$ production by NOX is disturbed at the level of its transcription or of the cytosolic subunits, while the catalytic subunit is unaffected. Interestingly, the phagocytic NOX is not inhibited by $O_2^{\bullet-}$ (Bellavite et al. 1983). It is possible that the end-product regulation NOXs is unique to plants or to NOX enzymes lacking cytosolic subunits, such as the human NOX5. The site of inhibition in NOX by $O_2^{\bullet-}$ remains to be studied.

Stimulation of the NAD(P)H oxidase activity was achieved by phosphorylation and seemed to occur in the cytosolic side of the enzyme (Fig. 1b) which is in accordance with the previously reported phosphorylation sites in the EF-hands of the plant NOXs (Benschop et al., 2007; Nühse et al., 2007; Kobayashi et al., 2008).

Finally, the function of PTOX in chloroplastic electron transfer chain was studied using PTOX-overexpressing plants ($PTOX^+$). In high light conditions, when the plastoquinone pool is reduced, $PTOX^+$ plants produced more $O_2^{\bullet-}$ than the wild type plants. In the presence of added SOD isolated thylakoid membranes from $PTOX^+$ showed similar characteristics as thylakoid membranes of WT plants. To explain the role of PTOX in the chloroplast and to hypothesize on its catalytic mechanism, it was proposed that PTOX produces $O_2^{\bullet-}$ in a side reaction and that it is coupled to an SOD. Figure 1c shows a model of the PTOX function which is dependent of SOD. In artificially constructed $PTOX^+$ plants the amount of chloroplastic SOD was not elevated. Under low light conditions the $PTOX^+$ plants were more protected against photoinhibition than the wild type. Under these conditions, only a slightly reduced plastoquinone pool, the amount of SOD in the chloroplast was enough to detoxify the $O_2^{\bullet-}$ produced by PTOX and other sources, e.g. PSI.

4. References

Adams, M.A. and Jia, Z. (2005). Structural and biochemical evidence for an enzymatic quinone redox cycle in Escherichia coli: identification of a novel quinol monooxygenase. *J Biol Chem* **280**: 8358-63.

Adams, M.A. and Jia, Z. (2006). Modulator of drug activity B from Escherichia coli: crystal structure of a prokaryotic homologue of DT-diaphorase. *J Mol Biol* **359**: 455-65.

Affourtit, C., Albury, M.S., Crichton, P.G. and Moore, A.L. (2002). Exploring the molecular nature of alternative oxidase regulation and catalysis. *FEBS Lett* **510**: 121-6.

Agarwal, R., Bonanno, J.B., Burley, S.K. and Swaminathan, S. (2006). Structure determination of an FMN reductase from Pseudomonas aeruginosa PA01 using sulfur anomalous signal. *Acta Crystallogr D Biol Crystallogr* **62**: 383-91.

Alonso, J.M., Stepanova, A.N., Leisse, T.J., Kim, C.J., Chen, H., Shinn, P., Stevenson, D.K.,Zimmerman, J., Barajas, P., Cheuk, R., Gadrinab, C., Heller, C., Jeske, A., Koesema, E., Meyers, C.C., Parker, H., Prednis, L., Ansari, Y., Choy, N., Deen, H., Geralt, M., Hazari, N., Hom, E., Karnes, M., Mulholland, C., Ndubaku, R., Schmidt, I., Guzman, P., Aguilar-Henonin, L., Schmid, M., Weigel, D., Carter, D.E., Marchand, T., Risseeuw, E., Brogden, D., Zeko, A., Crosby, W.L., Berry, C.C. and Ecker, J.R. (2003). Genome-wide insertional mutagenesis of Arabidopsis thaliana. *Science* **301**: 653-7.

Andrade, S.L., Patridge, E.V., Ferry, J.G. and Einsle, O. (2007). Crystal structure of the NADH:quinone oxidoreductase WrbA from Escherichia coli. *J Bacteriol* **189**: 9101-7.

Asada, K. (1999). THE WATER-WATER CYCLE IN CHLOROPLASTS: Scavenging of Active Oxygens and Dissipation of Excess Photons. *Annu Rev Plant Physiol Plant Mol Biol* **50**: 601-639.

Askerlund, P., Larsson, C. and Widell, S. (1988). Localization of donor and acceptor sites of NADH dehydrogenase activities using inside-out and right-side-out plasma membrane vesicles from plants. *FEBS Lett* **239**: 23-28.

Babior, B.M., Curnutte, J.T. and Kipnes, B.S. (1975). Pyridine nucleotide-dependent superoxide production by a cell-free system from human granulocytes. *J Clin Invest* **56**: 1035-42.

Babior, B. M., Kipnes, R. S. and Curnutte, J. T. (1973). Biological defense mechanisms. The production by leukocytes of superoxide, a potential bactericidal agent. *J Clin Invest* **52**: 741-4.

Baldridge, C.W. and Gerard, R.W. (1932). The extra respiration of phagocytosis. *Am J Physiol* **103**: 235-6.

Badger, M. R., von Caemmerer, S., Ruuska, S. and Nakano, H. (2000). Electron flow to oxygen in higher plants and algae: rates and control of direct photoreduction (Mehler reaction) and rubisco oxygenase. *Philos Trans R Soc Lond B Biol Sci* **355**: 1433-46.

Barceló, A.R. (2005). Xylem parenchyma cells deliver the H2O2 necessary for lignification in differentiating xylem vessels. *Planta* **220**: 747-56.

Barr, R., Pan, R.S., Crane, F. L., Brightman, A.O. and Morre, D.J. (1992). Destruction of vitamin K1 of cultured carrot cells by ultraviolet radiation and its effect on plasma membrane electron transport reactions. *Biochem Int* **27**: 449-56.

Benschop, J.J., Mohammed, S., O'Flaherty, M., Heck, A. J., Slijper, M. and Menke, F.L. (2007). Quantitative phosphoproteomics of early elicitor signaling in Arabidopsis. *Mol Cell Proteomics* **6**: 1198-214.

Bérczi A. and Møller, I.M. (2000). Redox enzymes in the plant plasma membrane and their possible roles. *Plant Cell Environ* **23**:1287-1302.

Billington, R.A., Bruzzone, S., De Flora, A., Genazzani, A.A., Koch-Nolte, F., Ziegler, M. and Zocchi, E. (2006). Emerging functions of extracellular pyridine nucleotides. *Mol Med* **12**: 324-7.

Bright, J., Desikan, R., Hancock, J.T., Weir, I.S. and Neill, S.J. (2006). ABA-induced NO generation and stomatal closure in Arabidopsis are dependent on H2O2 synthesis. *Plant J* **45**: 113-22.

Brock, B.J. and Gold, M.H. (1996). 1,4-Benzoquinone reductase from basidiomycete Phanerochaete chrysosporium: spectral and kinetic analysis. *Arch Biochem Biophys* **331**: 31-40.

Brock, B.J., Rieble, S. and Gold, M.H. (1995). Purification and Characterization of a 1,4-Benzoquinone Reductase from the Basidiomycete Phanerochaete chrysosporium. *Appl Environ Microbiol* **61**: 3076-3081.

Buchanan, B.B., Gruissem, W. and Russell, L.J. (2000). Biochemistry and molecular biology of plants. *American. Society of Plant Physiologist, Rockville, Maryland.* p. 720.

Buckhout, T.J. and Hrubec, T.C. (1986). Pyridine nucleotide-dependent ferricyanide reduction associated with isolated plasma membranes of maize (*Zea mays* L.) roots. *Protoplasma* **135**: 144-54.

Cape, J.L., Bowman, M.K. and Kramer, D.M. (2007). A semiquinone intermediate generated at the Qo site of the cytochrome bc1 complex: importance for the Q-cycle and superoxide production. *Proc Natl Acad Sci U S A* **104**: 7887-92.

Cardenas, L. (2009). New findings in the mechanisms regulating polar growth in root hair cells. *Plant Signal Behav* **4**: 4-8.

Carey, J., Brynda, J., Wolfova, J., Grandori, R., Gustavsson, T., Ettrich, R. and Smatanova, I.K. (2007). WrbA bridges bacterial flavodoxins and eukaryotic NAD(P)H:quinone oxidoreductases. *Protein Sci* **16**: 2301-5.

Carol, P. and Kuntz, M. (2001). A plastid terminal oxidase comes to light: implications for carotenoid biosynthesis and chlororespiration. *Trends Plant Sci* **6**: 31-6.

Chen, S.X. and Schopfer, P. (1999). Hydroxyl-radical production in physiological reactions. A novel function of peroxidase. *Eur J Biochem* **260**: 726-35.

Cona, A., Rea, G., Angelini, R., Federico, R. and Tavladoraki, P. (2006). Functions of amine oxidases in plant development and defence. *Trends Plant Sci* **11**: 80-8.

Cross, A.R. and Segal, A.W. (2004). The NADPH oxidase of professional phagocytes-prototype of the NOX electron transport chain systems. *Biochim Biophys Acta* **1657**: 1-22.

Deller, S., Macheroux, P. and Sollner, S. (2008). Flavin-dependent quinone reductases. *Cell Mol Life Sci* **65**: 141-60.

Diaz, M., de Haro, V., Munoz, R. and Quiles, M. J. (2007). Chlororespiration is involved in the adaptation of Brassica plants to heat and high light intensity. *Plant Cell Environ* **30**: 1578-85.

Dinauer, M.C., Orkin, S.H., Brown, R., Jesaitis, A J. and Parkos, C.A. (1987). The glycoprotein encoded by the X-linked chronic granulomatous disease locus is a component of the neutrophil cytochrome b complex. *Nature* **327**: 717-20.

Doke, N. (1983). Involvement of superoxide anion generation in hypersensitive response of potato tuber tissues to infection with an incompatible race of *Phytophthora infestans. Physiol. Plant Pathol* **23**: 345-57.

Doke, N. and Miura, Y. (1995). *In vitro* activation of NADPH-dependent O_2^- generating system in a plasma membrane-rich fraction of potato tuber tissues by treatment with an elicitor from *Phytophthora infestans* or with digitonin. *Physiol Mol Plant Pathol*. **46:** 17-28.

Doring, O. and Luthje, S. (1996). Molecular components and biochemistry of electron transport in plant plasma membranes (review). *Mol Membr Biol* **13**: 127-42.

Dunand, C., Crèvecoeur, M. and Penel, C. (2007). Distribution of superoxide and hydrogen peroxide in *Arabidopsis* root and their influence on root development: possible interaction with peroxidases. *New Phyt* **174**: 332-41.

El Jamali, A., Valente, A.J., Lechleiter, J.D., Gamez, M.J., Pearson, D.W., Nauseef, W.M. and Clark, R.A. (2008). Novel redox-dependent regulation of NOX5 by the tyrosine kinase c-Abl. *Free Radic Biol Med* **44**: 868-81.

Ernster, L. and Navazio, F. (1958). Soluble diaphorase in animal tissues. *Acta Chem Scand* **12**: 595-5.

Ernster, L., Danielson, L. and Ljunggren, M. (1962). DT diaphorase. I. Purification from the soluble fraction of rat-liver cytoplasm, and properties. *Biochim Biophys Acta* **58**: 171-88.

Foreman, J., Demidchik, V., Bothwell, J.H., Mylona, P., Miedema, H., Torres, M.A., Linstead, P., Costa, S., Brownlee, C., Jones, J.D., Davies, J.M. and Dolan, L. (2003). Reactive oxygen species produced by NADPH oxidase regulate plant cell growth. *Nature* **422**: 442-6.

Fridovich, I. (1978). The biology of oxygen radicals. *Science* **201**: 875-80.

Fry, S.C., Dumville, J.C. and Miller, J.G. (2001). Fingerprinting of polysaccharides attacked by hydroxyl radicals in vitro and in the cell walls of ripening pear fruit. *Biochem J* **357**: 729-37.

Gaudu, P., Touati, D., Niviere, V. and Fontecave, M. (1994). The NAD(P)H:flavin oxidoreductase from Escherichia coli as a source of superoxide radicals. *J Biol Chem* **269**: 8182-8.

Gong, X., Gutala, R. and Jaiswal, A.K. (2008). Quinone oxidoreductases and vitamin K metabolism. *Vitam Horm* **78**: 85-101.

Greenshields, D.L., Liu, G., Selvaraj, G. and Wei, Y. (2005). Differential regulation of wheat quinone reductases in response to powdery mildew infection. *Planta* **222**: 867-75.

Groom, Q.J., Torres, M.A., Fordham-Skelton, A.P., Hammond-Kosack, K.E., Robinson, N.J. and Jones, J.D. (1996). rbohA, a rice homologue of the mammalian gp91phox respiratory burst oxidase gene. *Plant J* **10**: 515-22.

Guerrini, F., Valenti, V. and Pupillo, P. (1987). Solubilization and Purification of NAD(P)H Dehydrogenase of Cucurbita Microsomes. *Plant Physiol* **85**: 828-834.

Hall, J.L. and Sexton, R. (1972). Cytochemical localization of peroxidase activity in root cells. *Planta* **108**: 103-20.

Halliwell, B and Gutteridge, J.M.C. (2003). Free radicals in biology and medicine. *Oxford Science publications*

Hassidim, M., Rubinstein, B., Lerner, H.R. and Reinhold, L. (1987). Generation of a Membrane Potential by Electron Transport in Plasmalemma-Enriched Vesicles of Cotton and Radish. *Plant Physiol* **85**: 872-875.

Heyno, E., Klose, C. and Krieger-Liszkay, A. (2008). Origin of cadmium-induced reactive oxygen species production: mitochondrial electron transfer versus plasma membrane NADPH oxidase. *New Phytol* **179**: 687-99.

Hong, Y., Wang, G. and Maier, R.J. (2008). The NADPH quinone reductase MdaB confers oxidative stress resistance to Helicobacter hepaticus. *Microb Pathog* **44**: 169-74.

Horton, P., Ruban, A.V. and Walters, R.G. (1996). Regulation Of Light Harvesting In Green Plants. *Annu Rev Plant Physiol Plant Mol Biol* **47**: 655-684.

Ivanov, B., Mubarakshina, M. and Khorobrykh, S. (2007). Kinetics of the plastoquinone pool oxidation following illumination Oxygen incorporation into photosynthetic electron transport chain. *FEBS Lett* **581**: 1342-6.

Iverson, D., DeChatelet, L.R., Spitznagel, J.K. and Wang, P. (1977). Comparison of NADH and NADPH oxidase activities in granules isolated from human polymorphonuclear leukocytes with a fluorometric assay. *J Clin Invest* **59**: 282-90.

Iyanagi, T. and Yamazaki, I. (1970). One-electron-transfer reactions in biochemical systems. V. Difference in the mechanism of quinone reduction by the NADH dehydrogenase and the NAD(P)H dehydrogenase (DT-diaphorase). *Biochim Biophys Acta* **216**: 282-94.

Iyanagi, T. and Yamazaki, I. (1969). One-electron-transfer reactions in biochemical systems. 3. One-electron reduction of quinones by microsomal flavin enzymes. *Biochim Biophys Acta* **172**: 370-81.

Jagnandan, D., Church, J.E., Banfi, B., Stuehr, D.J., Marrero, M.B. and Fulton, D.J. (2007). Novel mechanism of activation of NADPH oxidase 5. calcium sensitization via phosphorylation. *J Biol Chem* **282**: 6494-507.

Janzen, E.G., Wang, Y.Y. and Shetty, R.V. (1978). Spin trapping with alpha-pyridyl 1-oxide N-tert-butyl nitrones in aqueous solutions. A unique electron spin resonance spectrum for the hydroxyl radical adduct. *J Am Chem Soc* **100**: 2923–25.

Jiang, Y., Yang, B., Harris, N.S. and Deyholos, M.K. (2007). Comparative proteomic analysis of NaCl stress-responsive proteins in Arabidopsis roots. *J Exp Bot* **58**: 3591-607.

Jonas, K., Tomenius, H., Romling, U., Georgellis, D. and Melefors, O. (2006). Identification of YhdA as a regulator of the Escherichia coli carbon storage regulation system. *FEMS Microbiol Lett* **264**: 232-7.

Joseph, P. and Jaiswal, A.K. (1998). NAD(P)H:quinone oxidoreductase 1 reduces the mutagenicity of DNA caused by NADPH:P450 reductase-activated metabolites of benzo(a)pyrene quinones. *Br J Cancer* **77**: 709-19.

Joseph, P., Klein-Szanto, A.J. and Jaiswal, A.K. (1998). Hydroquinones cause specific mutations and lead to cellular transformation and in vivo tumorigenesis. *Br J Cancer* **78**: 312-20.

Kalen, A., Norling, B., Appelkvist, E.L. and Dallner, G. (1987). Ubiquinone biosynthesis by the microsomal fraction from rat liver. *Biochim Biophys Acta* **926**: 70-8.

Kärkönen, A., Warinowski, T., Teeri, T. H., Simola, L.K. and Fry, S.C. (2009). On the mechanism of apoplastic H2O2 production during lignin formation and elicitation in cultured spruce cells--peroxidases after elicitation. *Planta* **230**: 553-67.

Keller, T., Damude, H.G., Werner, D., Doerner, P., Dixon, R.A. and Lamb, C. (1998). A plant homolog of the neutrophil NADPH oxidase gp91phox subunit gene encodes a plasma membrane protein with Ca2+ binding motifs. *Plant Cell* **10**: 255-66.

Kobayashi, M., Ohura, I., Kawakita, K., Yokota, N., Fujiwara, M., Shimamoto, K., Doke, N. and Yoshioka, H. (2007). Calcium-dependent protein kinases regulate the production of reactive oxygen species by potato NADPH oxidase. *Plant Cell* **19**: 1065-80.

Kozaki, A and Takeba, G. (1996). Photorespiration protects C3 plants from protooxidation. *Nature* **384**: 557-60.

Krieger-Liszkay, A., Fufezan, C. and Trebst, A. (2008). Singlet oxygen production in photosystem II and related protection mechanism. *Photosynth Res* **98**: 551-64.

Kwak, J.M., Mori, I.C., Pei, Z.M., Leonhardt, N., Torres, M.A., Dangl, J.L., Bloom, R.E., Bodde, S., Jones, J.D. and Schroeder, J.I. (2003). NADPH oxidase AtrbohD and AtrbohF genes function in ROS-dependent ABA signaling in Arabidopsis. *Embo J* **22**: 2623-33.

Lamb, C. and Dixon, R.A. (1997). The Oxidative Burst In Plant Disease Resistance. *Annu Rev Plant Physiol Plant Mol Biol* **48**: 251-275.

Lambeth, J.D. (2007). Nox enzymes, ROS, and chronic disease: an example of antagonistic pleiotropy. *Free Radic Biol Med* **43**: 332-47.

Larsson, C., Sommarin, M. and Widell, S. (1994). Isolation of highly purified plant plasma membranes and separation of inside-out and right-side-out vesicles. *Methods Enzymol* **228**: 451-69.

Laskowski, M.J., Dreher, K.A., Gehring, M.A., Abel, S., Gensler, A.L. and Sussex, I.M. (2002). FQR1, a novel primary auxin-response gene, encodes a flavin mononucleotide-binding quinone reductase. *Plant Physiol* **128**: 578-90.

Li, R., Bianchet, M.A., Talalay, P. and Amzel, L.M. (1995). The three-dimensional structure of NAD(P)H:quinone reductase, a flavoprotein involved in cancer chemoprotection and chemotherapy: mechanism of the two-electron reduction. *Proc Natl Acad Sci U S A* **92**: 8846-50.

Link, T.A. and von Jagow, G. (1995). Zinc ions inhibit the QP center of bovine heart mitochondrial bc1 complex by blocking a protonatable group. *J Biol Chem* **270**: 25001-6.

Liszkay, A., Kenk, B. and Schopfer, P. (2003). Evidence for the involvement of cell wall peroxidase in the generation of hydroxyl radicals mediating extension growth. *Planta* **217**: 658-67.

Liszkay, A., van der Zalm, E. and Schopfer, P. (2004). Production of reactive oxygen intermediates (O(2)(-), H(2)O(2), and OH) by maize roots and their role in wall loosening and elongation growth. *Plant Physiol* **136**: 3114-23.

Liu, P., Li, R.L., Zhang, L., Wang, Q. L., Niehaus, K., Baluska, F., Samaj, J. and Lin, J.X. (2009). Lipid microdomain polarization is required for NADPH oxidase-dependent ROS signaling in Picea meyeri pollen tube tip growth. *Plant J.*

Luster, D.G. and Buckhout, T.J. (1989). Purification and Identification of a Plasma Membrane Associated Electron Transport Protein from Maize (Zea mays L.) Roots. *Plant Physiol* **91**: 1014-1019.

Lüthje, S. (2008). Plasma membrane redox systems: Lipid rafts and protein assemblies. In UE Lüttge, W Beyschlag, J Murata, eds, Springer-Verlag, Berlin. *Progress in Bot* **69**: 169-200.

Lüthje, S., Van Gestelen, P., Córdoba-Pedregosa, M.C., González-Reyes, J.A., Asard, H., Villalba, J.M. and Böttger, M. (1998). Quinones in plant plasma membranes - a missing link? *Protoplasma* **205**: 43-51.

Maerki, F. and Martius, C. (1961). Vitamin K reductase, from cattle and ratliver. *Biochem Z* **334**: 293-303.

Mezzetti, A., Leibl, W., Breton, J. and Nabedryk, E. (2003). Photoreduction of the quinone pool in the bacterial photosynthetic membrane: identification of infrared marker bands for quinol formation. *FEBS Lett* **537**: 161-5.

Mika, A., Buck, F. and Luthje, S. (2008). Membrane-bound class III peroxidases: identification, biochemical properties and sequence analysis of isoenzymes purified from maize (Zea mays L.) roots. *J Proteomics* **71**: 412-24.

Mika, A. and Luthje, S. (2003). Properties of guaiacol peroxidase activities isolated from corn root plasma membranes. *Plant Physiol* **132**: 1489-98.

Miller, J.G. and Fry, S.C. (2001). Characteristics of xyloglucan after attack by hydroxyl radicals. *Carbohydr Res* **332**: 389-403.

Mittler, R., Vanderauwera, S., Gollery, M. and Van Breusegem, F. (2004). Reactive oxygen gene network of plants. *Trends Plant Sci* **9**: 490-8.

Mojovic, M., Vuletic, M., Bacic, G.G. and Vucinic, Z. (2004). Oxygen radicals produced by plant plasma membranes: an EPR spin-trap study. *J Exp Bot* **55**: 2523-31.

Mongrand, S., Morel, J., Laroche, J., Claverol, S., Carde, J. P., Hartmann, M.A., Bonneu, M., Simon-Plas, F., Lessire, R. and Bessoule, J.J. (2004). Lipid rafts in higher plant cells: purification and characterization of Triton X-100-insoluble microdomains from tobacco plasma membrane. *J Biol Chem* **279**: 36277-86.

Monshausen, G.B., Bibikova, T.N., Messerli, M.A., Shi, C. and Gilroy, S. (2007). Oscillations in extracellular pH and reactive oxygen species modulate tip growth of Arabidopsis root hairs. *Proc Natl Acad Sci U S A* **104**: 20996-1001.

Morel, F., Doussiere, J. and Vignais, P.V. (1991). The superoxide-generating oxidase of phagocytic cells. Physiological, molecular and pathological aspects. *Eur J Biochem* **201**: 523-46.

Morré, J.D. (2004). Quinone oxidoreductases of the plasma membrane. *Methods Enzymol* **378**: 179-99.

Müller, K., Carstens, A.C., Linkies, A., Torres, M.A. and Leubner-Metzger, G. (2009). The NADPH-oxidase AtrbohB plays a role in Arabidopsis seed after-ripening. *New Phytol*.

Müller, K., Linkies, A., Vreeburg, R. A., Fry, S. C., Krieger-Liszkay, A. and Leubner-Metzger, G. (2009). In vivo cell wall loosening by hydroxyl radicals during cress seed germination and elongation growth. *Plant Physiol* **150**: 1855-65.

Murphy, M.P. (2009). How mitochondria produce reactive oxygen species. *Biochem J* **417**: 1-13.

Murphy, T.M. and Auh, C.K. (1996). The Superoxide Synthases of Plasma Membrane Preparations from Cultured Rose Cells. *Plant Physiol* **110**: 621-629.

Mustilli, A.C., Merlot, S., Vavasseur, A., Fenzi, F. and Giraudat, J. (2002). Arabidopsis OST1 protein kinase mediates the regulation of stomatal aperture by abscisic acid and acts upstream of reactive oxygen species production. *Plant Cell* **14**: 3089-99.

Nohzadeh Malakshah, S., Habibi Rezaei, M., Heidari, M. and Salekdeh, G.H. (2007). Proteomics reveals new salt responsive proteins associated with rice plasma membrane. *Biosci Biotechnol Biochem* **71**: 2144-54.

Nuhse, T.S., Bottrill, A.R., Jones, A.M. and Peck, S.C. (2007). Quantitative phosphoproteomic analysis of plasma membrane proteins reveals regulatory mechanisms of plant innate immune responses. *Plant J* **51**: 931-40.

O'Donnell, V.B., Smith G.C.M. and Jones, O.T.G. (1994). Involvement of phenyl radicals in iodonium compound inhibition of flavoenzymes. *Mol Pharmacol* **46**: 778-85.

Ogasawara, Y., Kaya, H., Hiraoka, G., Yumoto, F., Kimura, S., Kadota, Y., Hishinuma, H., Senzaki, E., Yamagoe, S., Nagata, K., Nara, M., Suzuki, K., Tanokura, M. and Kuchitsu, K. (2008). Synergistic activation of the Arabidopsis NADPH oxidase AtrbohD by Ca2+ and phosphorylation. *J Biol Chem* **283**: 8885-92.

Palmgren, M.G., Askerlund, P., Fredrikson, K., Widell, S., Sommarin, M. and Larsson, C. (1990). Sealed Inside-Out and Right-Side-Out Plasma Membrane Vesicles: Optimal Conditions for Formation and Separation. *Plant Physiol* **92**: 871-880.

Paul, B.B., Strauss, R.R., Jacobs, A.A. and Sbarra, A.J. (1970). Function of H(2)O(2), Myeloperoxidase, and Hexose Monophosphate Shunt Enzymes in Phagocytizing Cells from Different Species. *Infect Immun* **1**: 338-344.

Pospíšil, P. (2009). Production of reactive oxygen species by photosystem II. *Biochim Biophys Acta* **1787**: 1151-60.

Potocky, M., Jones, M.A., Bezvoda, R., Smirnoff, N. and Zarsky, V. (2007). Reactive oxygen species produced by NADPH oxidase are involved in pollen tube growth. *New Phytol* **174**: 742-51.

Preger, V., Pesaresi, A., Pupillo, P. and Trost, P. (2001). Ascorbate-independent electron transfer between cytochrome b561 and a 27 kDa ascorbate peroxidase of bean hypocotyls. *Protoplasma* **217**: 137-45.

Preger, V., Tango, N., Marchand, C., Lemaire, S.D., Carbonera, D., Di Valentin, M., Costa, A., Pupillo, P. and Trost, P. (2009). Auxin-responsive genes AIR12 code for a new family of plasma membrane b-type cytochromes specific to flowering plants. *Plant Physiol* **150**: 606-20.

Prochaska, H.J. (1988). Purification and crystallization of rat liver NAD(P)H:(quinone-acceptor) oxidoreductase by cibacron blue affinity chromatography: identification of a new and potent inhibitor. *Arch Biochem Biophys* **267**: 529-38.

Prochaska, H.J. and Talalay, P. (1986). Purification and characterization of two isofunctional forms of NAD(P)H: quinone reductase from mouse liver. *J Biol Chem* **261**: 1372-8.

Pugin, A., Frachisse, J.M., Tavernier, E., Bligny, R., Gout, E., Douce, R. and Guern, J. (1997). Early Events Induced by the Elicitor Cryptogein in Tobacco Cells: Involvement of a Plasma Membrane NADPH Oxidase and Activation of Glycolysis and the Pentose Phosphate Pathway. *Plant Cell* **9**: 2077-2091.

Pupillo, P., Valenti, V., De Luca, L. and Hertel, R. (1986). Kinetic Characterization of Reduced Pyridine Nucleotide Dehydrogenases (Duroquinone-Dependent) in Cucurbita Microsomes. *Plant Physiol* **80**: 384-389.

Raad, H., Paclet, M.H., Boussetta, T., Kroviarski, Y., Morel, F., Quinn, M.T., Gougerot-Pocidalo, M.A., Dang, P.M. and El-Benna, J. (2009). Regulation of the phagocyte NADPH oxidase activity: phosphorylation of gp91phox/NOX2 by protein kinase C enhances its diaphorase activity and binding to Rac2, p67phox, and p47phox. *Faseb J* **23**: 1011-22.

Radjendirane, V., Joseph, P., Lee, Y. H., Kimura, S., Klein-Szanto, A.J., Gonzalez, F.J. and Jaiswal, A.K. (1998). Disruption of the DT diaphorase (NQO1) gene in mice leads to increased menadione toxicity. *J Biol Chem* **273**: 7382-9.

Ramos, C.L., Pou, S., Brittigan, B.E., Cohen, M.S. ans Rosen, G.M. (1992). Spin trapping evidence for myeloperoxidase-dependent hydroxyl radical formation by human neutophils and monocysts. *J Biol Chem* **267**: 8307-8312.

Rasband, W.S. (1997–2006) ImageJ. US National Institutes of Health, Bethesda, MD, U.S.A. http://rsb.info.nih.gov.gate1.inist.fr/ij/

Renew, S., Heyno, E., Schopfer, P. and Liszkay, A. (2005). Sensitive detection and localization of hydroxyl radical production in cucumber roots and Arabidopsis seedlings by spin trapping electron paramagnetic resonance spectroscopy. *Plant J* **44**: 342-7.

Rodriguez, A.A., Grunberg, K.A. and Taleisnik, E.L. (2002). Reactive oxygen species in the elongation zone of maize leaves are necessary for leaf extension. *Plant Physiol* **129**: 1627-32.

Rosso, D., Ivanov, A.G., Fu, A., Geisler-Lee, J., Hendrickson, L., Geisler, M., Stewart, G., Krol, M., Hurry, V., Rodermel, S.R., Maxwell, D.P. and Huner, N.P. (2006). IMMUTANS does not act as a stress-induced safety valve in the protection of the photosynthetic apparatus of Arabidopsis during steady-state photosynthesis. *Plant Physiol* **142**: 574-85.

Royer-Pokora, B., Kunkel, L.M., Monaco, A.P., Goff, S.C., Newburger, P.E., Baehner, R.L., Cole, F.S., Curnutte, J.T. and Orkin, S.H. (1986). Cloning the gene for an inherited human disorder chronic granulomatous disease on the basis of its chromosomal location. *Nature* **322**: 32-8.

Sagi, M. and Fluhr, R. (2001). Superoxide production by plant homologues of the gp91(phox) NADPH oxidase. Modulation of activity by calcium and by tobacco mosaic virus infection. *Plant Physiol* **126**: 1281-90.

Sagi, M. and Fluhr, R. (2006). Production of reactive oxygen species by plant NADPH oxidases. *Plant Physiol* **141**: 336-40.

Sbarra, A.J. and Karnovsky, M.L. (1959). The biochemical basis of phagocytosis. I. Metabolic changes during the ingestion of particles by polymorphonuclear leukocytes. *J Biol Chem* **234**: 1355-62.

Scharte, J., Schon, H., Tjaden, Z., Weis, E. and von Schaewen, A. (2009). Isoenzyme replacement of glucose-6-phosphate dehydrogenase in the cytosol improves stress tolerance in plants. *Proc Natl Acad Sci U S A* **106**: 8061-6.

Schopfer, P. (2001). Hydroxyl radical-induced cell-wall loosening in vitro and in vivo: implications for the control of elongation growth. *Plant J* **28**: 679-88.

Schopfer, P., Heyno, E., Drepper, F. and Krieger-Liszkay, A. (2008). Naphthoquinone-dependent generation of superoxide radicals by quinone reductase isolated from the plasma membrane of soybean. *Plant Physiol* **147**: 864-78.

Schopfer, P. and Liszkay, A. (2006). Plasma membrane-generated reactive oxygen intermediates and their role in cell growth of plants. *Biofactors* **28**: 73-81.

Schopfer, P., Liszkay, A., Bechtold, M., Frahry, G. and Wagner, A. (2002). Evidence that hydroxyl radicals mediate auxin-induced extension growth. *Planta* **214**: 821-8.

Schutzendubel, A. and Polle, A. (2002). Plant responses to abiotic stresses: heavy metal-induced oxidative stress and protection by mycorrhization. *J Exp Bot* **53**: 1351-65.

Segal, A.W., Cross, A.R., Garcia, R.C., Borregaard, N., Valerius, N.H., Soothill, J.F. and Jones, O.T. (1983). Absence of cytochrome b-245 in chronic granulomatous disease. A multicenter European evaluation of its incidence and relevance. *N Engl J Med* **308**: 245-51.

Serrander, L., Jaquet, V., Bedard, K., Plastre, O., Hartley, O., Arnaudeau, S., Demaurex, N., Schlegel, W. and Krause, K.H. (2007). NOX5 is expressed at the plasma membrane and generates superoxide in response to protein kinase C activation. *Biochimie* **89**: 1159-67.

Serrano, A., Cordoba, F., Gonzalez-Reyes, J.A., Navas, P. and Villalba, J.M. (1994). Purification and Characterization of Two Distinct NAD(P)H Dehydrogenases from Onion (Allium cepa L.) Root Plasma Membrane. *Plant Physiol* **106**: 87-96.

Shangari, N., Chan, T.S. and O'Brien, P.J. (2005). Sulfation and glucuronidation of phenols: implications in coenyzme Q metabolism. *Methods Enzymol* **400**: 342-59.

Sirichandra, C., Gu, D., Hu, H. C., Davanture, M., Lee, S., Djaoui, M., Valot, B., Zivy, M., Leung, J., Merlot, S. and Kwak, J. M. (2009). Phosphorylation of the Arabidopsis AtrbohF NADPH oxidase by OST1 protein kinase. *FEBS Lett* **583**: 2982-6.

Slater, E. C. (1973). The mechanism of action of the respiratory inhibitor, antimycin. *Biochim Biophys Acta* **301**: 129-54.

Smith, M. T. (1999). Benzene, NQO1, and genetic susceptibility to cancer. *Proc Natl Acad Sci U S A* **96**: 7624-6.

Sollner, S. and Macheroux, P. (2009). New roles of flavoproteins in molecular cell biology: an unexpected role for quinone reductases as regulators of proteasomal degradation. *Febs J* **276**: 4313-24.

Sollner, S., Nebauer, R., Ehammer, H., Prem, A., Deller, S., Palfey, B.A., Daum, G. and Macheroux, P. (2007). Lot6p from Saccharomyces cerevisiae is a FMN-dependent reductase with a potential role in quinone detoxification. *Febs J* **274**: 1328-39.

Sparla, F., Tedeschi, G., Pupillo, R. and Trost, P. (1998). Molecular characterization of NAD(P)H:quinone oxidoreductase of tobacco leaves. *Protoplasma* **205**: 52-8.

Sparla, F., Tedeschi, G., Pupillo, P. and Trost, P. (1999). Cloning and heterologous expression of NAD(P)H:quinone reductase of Arabidopsis thaliana, a functional homologue of animal DT-diaphorase. *FEBS Lett* **463**: 382-6.

Sparla, F., Tedeschi, G. and Trost, P. (1996). NAD(P)H:(Quinone-Acceptor) Oxidoreductase of Tobacco Leaves Is a Flavin Mononucleotide-Containing Flavoenzyme. *Plant Physiol* **112**: 249-258.

Stepien, P. and Johnson, G.N. (2009). Contrasting responses of photosynthesis to salt stress in the glycophyte Arabidopsis and the halophyte thellungiella: role of the plastid terminal oxidase as an alternative electron sink. *Plant Physiol* **149**: 1154-65.

Streb, P., Josse, E.M., Gallouët, E., Baptist, F., Kuntz, M., and Cornic, G. (2005). Evidence for alternative electron sinks to photosynthetic carbon assimilation in the high mountain plant species *Ranunculus glacialis. Plant cell Environ* **28**:1123-35.

Suh, H.J., Kim, C.S. and Jung, J. (2000). Cytochrome b6/f complex as an indigenous photodynamic generator of singlet oxygen in thylakoid membranes. *Photochem Photobiol* **71**: 103-9.

Sumimoto, H. (2008). Structure, regulation and evolution of Nox-family NADPH oxidases that produce reactive oxygen species. *Febs J* **275**: 3249-77.

Sun, I.L., Sun, E.E., Crane, F. L., Morre, D.J., Lindgren, A. and Low, H. (1992). Requirement for coenzyme Q in plasma membrane electron transport. *Proc Natl Acad Sci U S A* **89**: 11126-30.

Szponarski, W., Sommerer, N., Boyer, J. C., Rossignol, M. and Gibrat, R. (2004). Large-scale characterization of integral proteins from Arabidopsis vacuolar membrane by two-dimensional liquid chromatography. *Proteomics* **4**: 397-406.

Teahan, C., Rowe, P., Parker, P., Totty, N. and Segal, A.W. (1987). The X-linked chronic granulomatous disease gene codes for the beta-chain of cytochrome b-245. *Nature* **327**: 720-1.

Tenhaken R. and Rübel, C. (1999). Cloning of putative subunits of the soybean plasma membrane NADPH oxidase involved in the oxidative burst by antibody expression screening. *Protoplasma* **205**: 21–8.

Thein, M. and Michalke, W. (1988). Bisulfite interacts with binding sites of the auxin-transport inhibitor N-l-naphthylphthalamic acid. *Planta* **176**: 343-50.

Torres, M. A. and Dangl, J.L. (2005). Functions of the respiratory burst oxidase in biotic interactions, abiotic stress and development. *Curr Opin Plant Biol* **8**: 397-403.

Torres, M.A., Dangl, J.L. and Jones, J.D. (2002). Arabidopsis gp91phox homologues AtrbohD and AtrbohF are required for accumulation of reactive oxygen intermediates in the plant defense response. *Proc Natl Acad Sci U S A* **99**: 517-22.

Torres, M.A., Jones, J.D. and Dangl, J.L. (2005). Pathogen-induced, NADPH oxidase-derived reactive oxygen intermediates suppress spread of cell death in Arabidopsis thaliana. *Nat Genet* **37**: 1130-4.

Torres, M.A., Onouchi, H., Hamada, S., Machida, C., Hammond-Kosack, K.E. and Jones, J.D. (1998). Six Arabidopsis thaliana homologues of the human respiratory burst oxidase (gp91phox). *Plant J* **14**: 365-70.

Trost, P., Bonora, P., Scagliarini, S. and Pupillo, P. (1995). Purification and properties of NAD(P)H: (quinone-acceptor) oxidoreductase of sugarbeet cells. *Eur J Biochem* **234**: 452-8.

Trost, P., Foscarini, S., Preger, V., Bonora, P., Vitale, L. and Pupillo, P. (1997). Dissecting the Diphenylene Iodonium-Sensitive NAD(P)H:Quinone Oxidoreductase of Zucchini Plasma Membrane. *Plant Physiol* 114: 737-746.

Ukeda, H., Maeda, M., Ishii, T. and Sawamura, M. (1997). Spectrophotometric assay for superoxide dismutase based on tetrazolium salt 3′-{1-[(Phenylamino)-carbonyl]-3,4-tetrazolium}-bis(4-methoxy-6-nitro)benzenesulfonic acid hydrate reduction by xanthine-xanthine oxidase. *Anal Biochem* **251** :206-209.

Un, S., Dorlet, P, Rutherford, A.W. (2001). A high-field EPR tour of radicals in photosystems I and II. *Appl Magn Res* **21**: 341-61.

Van Gestelen, P., Asard, H. and Caubergs, R.J. (1997). Solubilization and Separation of a Plant Plasma Membrane NADPH-O2- Synthase from Other NAD(P)H Oxidoreductases. *Plant Physiol* **115**: 543-550.

Van Gestelen, P., Asard, H., Horemans, N. and Caubergs, R.J. (1998). Superoxide-producing NAD(P)H oxidases in plasma membrane vesicles from elicitor-responsive bean plants. *Physiol Plant* **104**: 653-60.

Vilhardt, F. and van Deurs, B. (2004). The phagocyte NADPH oxidase depends on cholesterol-enriched membrane microdomains for assembly. *Embo J* **23**: 739-48.

Vlad, F., Turk, B.E., Peynot, P., Leung, J. and Merlot, S. (2008). A versatile strategy to define the phosphorylation preferences of plant protein kinases and screen for putative substrates. *Plant J* **55**: 104-17.

Walker, J. C. (1980). Atmospheric constraints on the evolution of metabolism. *Orig Life* **10**: 93-104.

Walker, J. C. (1994). Structure and function of the receptor-like protein kinases of higher plants. *Plant Mol Biol* **26**: 1599-609.

Wang, Y., Fang, J., Leonard, S.S. and Rao, K.M. (2004). Cadmium inhibits the electron transfer chain and induces reactive oxygen species. *Free Radic Biol Med* **36**: 1434-43.

Yoshioka, H., Numata, N., Nakajima, K., Katou, S., Kawakita, K., Rowland, O., Jones, J.D. and Doke, N. (2003). Nicotiana benthamiana gp91phox homologs NbrbohA and NbrbohB participate in H2O2 accumulation and resistance to Phytophthora infestans. *Plant Cell* **15**: 706-18.

Zhang, H., Osyczka, A., Dutton, P.L. and Moser, C.C. (2007). Exposing the complex III Qo semiquinone radical. *Biochim Biophys Acta* **1767**: 883-7.

5. Abbreviations

A_0 = acceptor chlorophyll in PSI
A_1 = vitK in PSI
AA = antomycin A
ABA = abscissic acid
ATP = adenosine triphosphate
BQ = benzoquinone
CDPK = calcium-dependent protein kinase
CGD = chronic granulomatous syndrome
CSHL lines = insertion mutants from Cold Spring Harbour Laboratories
cyt = cytochrome
DPI = diphenylene iodonium
DT-diaphorase = DPNH/TPNH-diaphorase = diphosphopyridine nucleotide/triphosphopyridine nucleotide diaphorase
DUOX = dual oxidase
bp = base pair
EPR = electron paramagnetic resonance
FAD = flavin adenine dinucleotide, oxidised
$FADH_2$ = flavin adenine dinucleotide, reduced
Fd = ferredoxin
FeS = iron sulphur (cluster)
FMN = flavin mononucleotide
FQR = flavin-dependent quinone reductase
FTIR = Fourier transform infrared
$gp91^{phox}$ = glycoprotein, 91 kDa, phagocyte oxidase
H_2O_2 = hydrogen peroxide
$heme_{low/high}$ = low/high potential heme
HFEPR = high field EPR
$HO_2^{\bullet}$ = protonated superoxide radical
$HQ^{\bullet}$ = protonated semiquinone
KO = knock-out
MD = menadione
NAD^+ = nicotineamide adenine dinucleotide, oxidised
NADH = nicotineamide adenine dinucleotide, reduced
$NADP^+$ = nicotineamide adenine dinucleotide phosphate, oxidised
NADPH = nicotineamide adenine dinucleotide phosphate, reduced
NOX = NADPH oxidase
NQ = naphthoquinone
NQR = NAD(P)H:quinone oxidoreductase
$O_2^{\bullet-}$ = superoxide radical
$^1O_2$ = singlet oxygen
$^{\bullet}OH$ = hydroxyl radical
OEC = oxygen evolving complex
OST-1 = open stomata 1
P_{680} = central chlorophyll of PSII
P_{700} = central chlorophyll of PSI
Pheo = pheophytin
PKC = protein kinase C
PM = plasma membrane
POBN = α-(4-pyridyl-1-oxide)-*N*-tert-butylnitrone
PRX = peroxidase
PSI = photosystem one
PSII = photosystem two

PTOX = plastid alternative oxidase
Q = quinone, oxidised
$Q^{\bullet-}$ = semiquinone radical
Q^{2-} = double reduced deprotonated quinone
Q_A = first quinone acceptor in PSII, oxidised
Q_B = second quinone acceptor in PSII, oxidised
QH_2 = dihydroquinone, quinol
QR = quinone reductase
rboh = respiratory burst oxidase
ROS = reactive oxygen species
SAIL lines = insertion mutants from Syngenta *Arabidopsis* Insertion Library
SALK lines = insertion mutants from SALK institute
SnRK = sucrose non-fermenting related kinase
SOD = superoxide dismutase
UQ = ubiquinone
vitK = vitamin K
WT = wild type
X/XO = xanthine/xanthine oxidase
XTT = Na,3'-[(phenylamino)-carbonyl]-3,4-tetrazolium]-bis(4-methoxy-6-nitro)benzenesulfonic acid hydrate